The studies on Momordica charantia fruits and the synthesis of pyrazolyl substituted benzylidene indanone derivatives as dengue virus type-2 NS2B/NS3 protease inhibitor

Nadirah Zawani Mohd Nesfu

Ecole Doctorale C2MP (Chimie - Mécanique - Matériaux- Physique)

<u>Thèse</u> en cotutelle entre
l'Université de Lorraine et l'Universiti Sains malaysia

Présentée et soutenue publiquement pour l'obtention du titre de

DOCTEUR DE l'UNIVERSITE DE LORRAINE en Chimie

par **Nadirah Zawani BINTI MOHD NESFU**

Les études sur les fruits de Momordica charantia et la synthèse de dérivés de benzylidène indanone pyrazolyl substitués comme inhibiteurs de la protéase NS2B/NS3 du virus de la dengue de type 2

Le 01 Septembre 2020

Président du Jury: Anne-Claire OFFER	Professeur, Université de Bourgogne Franche-Comté, France
Rapporteurs: Ahmad Sazali HAMZAH	Professeur, Universiti Teknologi MARA, Selangor, Malaysia
Examinateurs: Melati KHAIRUDDEAN	Assistant Professeur, Universiti Sains Malaysia, Penang, Malaysia
Vikneswaran MURUGAIYAH	Maitre, Universiti Sains Malaysia, Penang, Malaysia
Membres invités: Dominique LAURAIN-MATTAR	Professeur, Université de Lorraine, France Directeur de these
Hasnah OSMAN	Professeur, Universiti Sains Malaysia, Penang, Malaysia, Directeur de these
Nicolas BROSSE	Professeur, Université de Lorraine, France Co-directeur de these
Ezatul E. KAMARULZAMAN	Maitre, Universiti Sains Malaysia, Penang, Malaysia. Co-directeur de these

Laboratoire L2CM, UMR 7053, Faculté des Sciences et Technologies, Boulevard des Aiguillettes, BP 70239,54506 Vandoeuvre-lès-Nancy,France
School of Chemical Sciences, Universiti Sains Malaysia, 11800 Gelugor Penang, Malaysia

THE STUDIES ON *MOMORDICA CHARANTIA* FRUITS AND THE SYNTHESIS OF PYRAZOLYL SUBSTITUTED BENZYLIDENE INDANONE DERIVATIVES AS DENGUE VIRUS TYPE-2 NS2B/NS3 PROTEASE INHIBITOR

NADIRAH ZAWANI BINTI MOHD NESFU

UNIVERSITI SAINS MALAYSIA

2020

THE STUDIES ON *MOMORDICA CHARANTIA* FRUITS AND THE SYNTHESIS OF PYRAZOLYL SUBSTITUTED BENZYLIDENE INDANONE DERIVATIVES AS DENGUE VIRUS TYPE-2 NS2B/NS3 PROTEASE INHIBITOR

by

NADIRAH ZAWANI BINTI MOHD NESFU

Thesis submitted in fulfillment of the requirements
for the degree of
Doctor of Philosophy

October 2020

DEDICATION

Alhamdulillah.

I would like to dedicate my thesis to:

IBU, my mother, my backbone, my strength.
ABAH, you're gone but your words of wisdom are not forgotten.
ARIFFUDIN, a shoulder to cry on, a good listener, and my supporter.
KAK DIAH & IEAH, sisters, best friends, my everything.

Thank you for being by my side thru thick and thin.
I am so blessed to have all of you.
May Allah bless all of you.

ACKNOWLEDGEMENT

All praise, glory and thanks give to Allah s.w.t for His amazing grace and generous that helps me throughout the whole process of completing this research

I would like to take this opportunity to express my gratitude to my beloved supervisor, Prof. Dato' Dr. Hasnah Osman, for her guidance, knowledge, support and advice along the way of finishing this research.

I want to thank my supervisor from the University of Lorraine, France, Prof. Dr. Dominique Laurain-Mattar and Prof. Dr. Nicolas Brosse for their mentorship, guidance, trust, and patience during my work in their lab (CNRS and LERMAB), in administrative work in France as well as in writing my report and thesis. The experiences obtained during my stay in France will not be forgotten.

I wish to take this chance to thank Prof. Dr. Afidah and Dr. Hazwan for their guidance and help in path a way for my dual PhD program and administrative works. Besides, I would like to thank all the School of Chemical Sciences lecturers and staff, the Institute of Postgraduate Studies (IPS) staff, the staff of Malaysian Institute of Pharmaceuticals and Nutraceuticals (IPharm), as well as University of Lorraine, France staff for their hospitality, supports, assistances and helps.

Special thanks to the France Embassy in Malaysia, Minister of Foreign Affair France, Campus France and Ministry of Education Malaysia under MyPhD program for the scholarship and financial support.

Last but not the least, I would like to thank my parent (Abah & Mak) and family members (especially; Kak Diah, Ieah & Ariffudin) for their patience, encouragement, understanding and care during the hardship and the difficult times.

Thank you so much and I am so grateful for your support and help.

TABLE OF CONTENTS

LIST OF TABLES

Page

LIST OF FIGURES

Page

LIST OF SCHEMES

Page

LIST OF SYMBOLS

%	Percent
Å	Angstrom unit
J	Coupling constant
m	Multiplet
º	degree
ºC	Degree Celsius
s	Singlet
V_{max}	Maximum velocity
β	Beta; second letter Greek alphabet
δ	Delta, chemical shift scale

LIST OF ABBREVIATIONS

^{13}C	Carbon Nuclear Magnetic Resonance
1D-NMR	One-Dimensional Magnetic Resonance
^{1}H	Proton Nuclear Magnetic Resonance
^{1}H-^{1}H COSY	Correlation Spectroscopy
2D-NMR	Two-Dimensional Magnetic Resonance
Asn	Asparagine
Asp	Aspartic acid
ATR	Attenuated Total Reflection
Boc	tert-butoxycarbonyl
CHN	Carbon, hydrogen and nitrogen (Elemental analysis)
d	doublet
DENV-2	Dengue virus type-2
DEPT	Distortionless enhancement by polarization transfer
DF	Dengue fever
DMSO	Dimethyl sulfoxide
DMSO-d_6	Deuterated dimethyl sulfoxide
EtOAc	Ethyl acetate
EtOH	Ethanol
FEB	Free energy of binding
FTIR	Fourier Transform Infrared
Gly	Glycine
His	Histidine
HMBC	Heteronuclear multiple bond correlation
IC_{50}	Half-maximal inhibitory concentration
IR	Infra-red
kcal/mol	kilocalorie per mole

MHz	Mega Hertz
MIC	Minimum concentration inhibition
m.p.	Melting point
NaOH	Sodium hydroxide
NMR	Nuclear Magnetic Resonance spectroscopy
Phe	Phenylaniline
Pro	Proline
Ser	Serine
SEC	Size exclusion chromatography
TLC	Thin-layer chromatography
UV	Ultra-violet

KAJIAN KE ATAS BUAH *MOMORDICA CHARANTIA* DAN SINTESIS TERBITAN PIRAZOLIL TERTUKARGANTI BENZILIDEN INDANON SEBAGAI PERENCAT PROTEASE NS2B/NS3 VIRUS DENGGI JENIS-2

ABSTRAK

Tiada terapi penyembuhan atau pencegahan bagi demam denggi (DF). Hanya rawatan perubatan tambahan dan terapi cecair disediakan untuk melawan DF. Sesetengah pesakit memilih untuk menggunakan kaedah mencegah dan merawat yang digunakan oleh orang-orang purba atau ubat tradisional. Salah satu ubat tradisional yang digunakan dalam kalangan pesakit DF di hospital Malaysia adalah memakan sup daging katak bersama peria katak (*M. charantia*). Isi buah dan biji *Momordica charantia* (*M. charantia*) digunakan dalam kajian ini. Minyak biji *M. charantia* diekstrak melalui pengekstrakan akueus enzim (AEE) dan hasil minyak meningkat dengan keadaan optimum untuk mengekstrak minyak biji adalah dengan menggunakan HEL1: X7 (5:1.25). Kandungan minyak biji serta lignin, hemiselullosa, gula larut, dan asid uronik berbeza mengikut jenis nisbah koktail enzim yang digunakan. Sementara itu,, ekstrak etil asetat isi buah *M. charantia* didapati merencat protease NS2B/NS3 DENV-2 sebanyak 38.11 ± 1.06 %. Berdasarkan analisis GC-MS, asid galik dapat dikesan dan dipilih sebagai rangka struktur asas bagi sintesis perencat protease NS2B/NS3 DENV-2. Terbitan pirazolil tertukarganti benziliden indanon, **90a-t** disintesis dan dicirikan menggunakan analisis FTIR, NMR, dan LC-MS. Peratusan hasil sebatian yang sesuai diperoleh. Sebatian **90a-t** menjalani kajian *in siliko* menggunakan AutoDock4.2 bagi mengenalpasti mod pengikatan dan pengesahan bersama struktur kristal homologi protein Wichapong. Lima sebatian

didapati memperoleh tenaga pengikatan bebas (FEB) kurang dari -7.55 kkal/mol. Sebatian **90p** menunjukkan lapan interaksi ikatan hidrogen, satu interaksi susunan π-π, dan satu interaksi π-alkil dengan residu asid amino dalam protease NS2B/NS3 DENV-2. Akhir sekali, lima sebatian utama telah menjalani kajian *in vitro* terhadap protease NS2B/NS3 DENV-2 dengan menggunakan substrat peptida florogenik Boc-Gly-Arg-7-amino-4-metilkumarin telah. Panduratin A digunakan sebagai kawalan positif. Sebatian **90p** menunjukkan aktiviti perencat protease NS2B/NS3 DENV-2 yang tinggi (65.61 ± 0.98%), sementara panduratin A (47.59 ± 1.03%), dan asid gallic (25.11 ± 1.11%). Nilai IC_{50} bagi sebatian **90p** diperhatikan 78.87 μM yang lebih rendah berbanding panduratin A, 290.27 μM. Dapat disimpulkan bahawa sebatian **90p** berpontensi menjadi sebatian *hit-to-led* dalam pembangunan perencat protease NS2B/NS3 DENV-2.

THE STUDIES ON *MOMORDICA CHARANTIA* FRUITS AND THE SYNTHESIS OF PYRAZOLYL SUBSTITUTED BENZYLIDENE INDANONE DERIVATIVES AS DENGUE VIRUS TYPE-2 NS2B/NS3 PROTEASE INHIBITOR

ABSTRACT

There are neither curative nor preventive therapies of dengue fever (DF). Only supplemental medical care and fluid therapy are available to fight DF. Some patients opt for prevention and treatment measure used by the ancient people or folk remedy to treat sickness. One of folk remedy used among patients with dengue fever in the Malaysia hospital is consumption of frog meat soup with bitter melon (*Momordica charantia*). The fruits flesh and seeds of *Momordica charantia* (*M. charantia)* were utilized in this study. The oil of *M. charantia* seeds were extracted via aqueous enzymatic extraction (AEE) and the oil yield increased with optimum condition to extract the seed oil was to use HEL1:X7 (5:1.25). The seeds oil as well as the lignin, hemicelullose, soluble sugars, and uronic acids content were different accordance to the type of enzyme cocktail ratio. On the other hand, the *M. charantia* fruits flesh ethyl acetate extract was found to inhibit 38.11 ± 1.06 % of the DENV-2 NS2B/NS3 protease. Based on the GC-MS analysis the trace of gallic acid was found and was selected the basic structural frameworks for synthesis of the DENV-2 NS2B/NS3 protease inhibitor. The pyrazolyl substituted indanone derivatives, **90a-t** were synthesized and characterized using FTIR, NMR, and LC-MS analysis. An appropriate percentage of yield of the compounds were obtained. The compounds **90a-t** underwent *in silico* study using AutoDock4.2 to identify the binding mode and conformation with

the Wichapong homology protein crystal structure. Five compounds were found to obtained free energy of binding (FEB) less than -7.55 kcal/mol. Compound **90p** showed eight hydrogen bond interactions, one π-π stacking interaction, and one π-alkyl interaction with the amino acid residue in the DENV-2 NS2B/NS3 protease. Lastly, the *in vitro* studies of top five docked synthesized compound towards DENV-2 NS2B/NS3 protease by using fluorogenic peptide substrate Boc-Gly-Arg-7-amino-4-methylcoumarin were conducted. The panduratin A was used as the positive control. Compound **90p** showed a high DENV-2 NS2B/NS3 protease inhibitor activity (65.61 ± 0.98 %), while panduratin A (47.59 ± 1.03 %), and gallic acid (25.11 ± 1.11 %). The IC_{50} value for compound **90p** was observed to be 78.87 μM which is lower compared to the panduratin A, 290.27 μM. The compound **90p** is concluded to be a potent hit-to-led compound in the development of DENV-2 NS2B/NS3 protease inhibitor.

LES ÉTUDES SUR LES FRUITS DE *MOMORDICA CHARANTIA* ET LA SYNTHÈSE DE DÉRIVÉS DE BENZYLIDÈNE INDANONE PYRAZOLYL SUBSTITUÉS COMME INHIBITEURS DE LA PROTÉASE NS2B/NS3 DU VIRUS DE LA DENGUE DE TYPE 2

RÉSUMÉ

Il n'existe pas de thérapies curatives ou préventives de la dengue (DF). Seuls des soins médicaux complémentaires et une thérapie par les fluides sont disponibles pour lutter contre la dengue. Certains patients optent pour des mesures de prévention et de traitement utilisées par les peuples anciens ou des remèdes populaires pour traiter la maladie. L'un des remèdes populaires utilisés par les patients atteints de dengue à l'hôpital de Malaisie est la consommation de soupe de viande de grenouille au melon amer (*Momordica charantia*). La chair des fruits et les graines du *Momordica charantia* (*M. charantia*) ont été utilisées dans cette étude. L'huile des graines de *M. charantia* a été extraite par extraction enzymatique aqueuse (AEE) et le rendement en huile a augmenté avec la condition optimale pour extraire l'huile de graines était d'utiliser HEL1:X7 (5:1.25). L'huile de graines ainsi que la teneur en lignine, hémicelullose, sucres solubles et acides uroniques étaient différentes selon le type de cocktail enzymatique. D'autre part, l'extrait d'acétate d'éthyle de la chair du fruit de *M. charantia* a inhibé 38.11±1.06 % de la DENV-2 protéase NS2B/NS3. Sur la base de l'analyse GC-MS, on a trouvé la trace d'acide gallique et on a sélectionné les cadres structurels de base pour la synthèse de l'inhibiteur de protéase DENV-2 NS2B/NS3. Les dérivés de l'indanone substituée par le pyrazolyle, **90a-t**, ont été synthétisés et caractérisés par analyse FTIR, RMN et LC-MS. Un pourcentage approprié de

rendement des composés a été obtenu. Les composés **90a-t** ont été soumis à une étude *in silico* en utilisant AutoDock4.2 pour identifier le mode de liaison et la conformation avec la structure cristalline de la protéine d'homologie de Wichapong. Cinq composés ont obtenu une énergie libre de liaison (FEB) inférieure à -7.55 kcal/mol. Le composé **90p** a montré huit interactions de liaison hydrogène, une interaction d'empilement π-π, et une interaction π-alkyle avec le résidu d'acide aminé dans la DENV-2protéase NS2B/NS3. Enfin, les études in vitro des cinq principaux composés synthétisés par ancrage vers la DENV-2 protéase NS2B/NS3 en utilisant le substrat peptidique fluorogène Boc-Gly-Arg-7-amino-4-méthylcoumarine ont été menées. La panduratine A a été utilisée comme témoin positif. Le composé **90p** a montré une forte activité d'inhibiteur de la DENV-2 protéase NS2B/NS3 (65.61±0.98 %), tandis que la panduratine A (47.59±1.03 %) et l'acide gallique (25.11±1.11 %) ont été utilisés comme témoins positifs. La valeur de la CI_{50} pour le composé **90p** a été observée à 78.87 μM, ce qui est inférieur à la valeur de 290.27 μM pour la panduratine A. Le composé **90p** est considéré comme un puissant composé de type *"hit-to-led"* dans le développement de l'inhibiteur de DENV-2 protéase NS2B/NS3.

CHAPTER 1

INTRODUCTION

1.1 Background of the study

Dengue fever (DF), a mosquito-borne viral infection increased from 2.2 million in 2010 to over 3.34 million in 2016 worldwide (WHO, 2019). The infected female mosquitoes of *Aedes aegypti* and *Aedes albopictus* (Figure 1.1) transmitted the dengue virus to humans through the bites. The dengue viruses can be categorized into four serotypes based on the antigens on the surface of the virus, which are dengue virus type 1, 2, 3 and 4 (Guzman & Kouri, 2003; Lindenbach *et al.*, 2007; Lanciotti *et al.*, 1992).

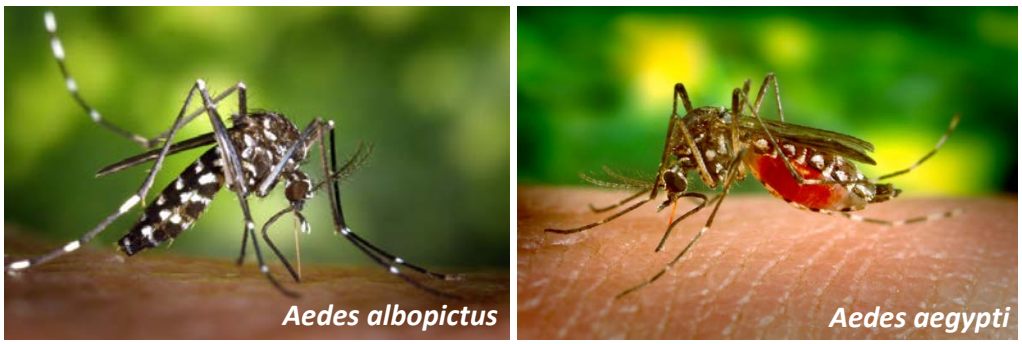

Figure 1.1: Images of the two predominant arthropod vectors of dengue virus, *Aedes albopictus* and *Aedes aegypti* (Wikimedia commons, 2010 & 2005).

There are no exact symptoms of DF have been identified. However, the high fever ranging from 39.5 to 41 ºC than usually continues for 2–7 days accompanied by muscle and joint pain could be a sign. The DF may occur within 3 to 14 days after a bite from an infected mosquito. The infected human felt a loss of appetite and

vomiting. Some infected human experienced swollen glands or rashes (WHO, 2009 & MoHM, 2015).

Approximately, 72,356 dengue cases were reported in Malaysia from January to July 2019, showing 89.5 % increment from the same period on 2018, including 138 death cases (Bernama, 2019 & BKP, 2019). In Malaysia, all four dengue serotypes can be isolated at a time. However, the main dengue serotypes found in Malaysia were dengue virus type 1 (DENV-1) and dengue virus type 2 (DENV-2) (Suppiah *et al.*, 2018 & Rahman *et al.*, 2012). The treatment of DF available nowadays is limited to supplemental medical care and fluid replacement, as there is no specific treatment.

1.2 Problem statement

As there is neither curative nor preventive therapies of DF and only one licensed dengue vaccine, Dengvaxia by Sanofi Pasteur was approved by regulatory authorities for trial use in a highly endemic area (WHO, 2017). Apart from that, only supportive measure and judicious fluid therapy are available for DF (Rajapakse *et al.*, 2012).

Some patients opt for a traditional folks' remedy to cure DF by improving their platelet count. In Pakistan, a dengue patient was treated with 25 mL aqueous extract of *Carica papaya (C. papaya)* leave, twice per day and found that in short time, it of increased the platelet count (Ahmad *et al.*, 2011). The studies showed that *C. papaya* leaves contained some active compounds that can enhance hemopoiesis and thrombopoiesis (Dharmarathna *et al.*, 2013).

People in Philippines used *Euphorbia hirta (E. hirta)* to treat dengue as it is believed to have anti-viral properties which will speed up the recovery process and

prevent the DF to develop into critical phase (Perera *et al.*, 2018; de Guzman *et al.*, 2016). The *E. hirta* contained phenolics and flavonoids that are well-known compounds able to increase the platelet.

The traditional Chinese practician, Dr. Yong Kian Fui said that there is no cure for dengue fever in Traditional Chinese Medicine (TCM). However, a herbal concoction called *"qin wen bai tu san"* a soup made by slow cooking of *Momordica charantia L. (M. charantia)* and frog meat or any type of meat for two hours can be consumed as one dose a day for three consecutive days. The *M. charantia* is used to detox the body by removing the heat, while the meat will neutralises the *M. charantia,* so that it does not become too cooling (Tan, 2014).

With the absence of promising anti-dengue drugs or vaccine options, there are ongoing needs to seek other prevention and treatment measures. As lots of researcher focus on the use of *C. papaya* leaves and *E. hirta*, this study focused on the anti-dengue activity of *M. charantia* fruits or also known as bitter melon, balsam pear, bitter squash or bitter gourd. The local Malay name for this plant is "peria katak" (Ong & Azliza, 2015). *M. charantia* plant from the family of *Cucurbitaceae*, possess a thin climbing vine with a long-stalked leaf and oblong fusiform-cylindrical, irregularly warty, shaped fruit (Figure 1.2). The classification of *M. charantia* are as follow:

Kingdom: *Plantae*
Division: *Magnoliophyta*
Class: *Magnoliopsida*
Order: *Cucurbitales*
Family: *Cucurbitaceae*
Genus: *Momordica*
Species: *M. charantia*

Figure 1.2: (a) *M. charantia* plant and fruit (b) Cross section of *M. charantia* fruit (Komakech, 2018).

M. charantia is well-known for its anti-diabetic activities (Joseph & Jini, 2013), anti-tumor activities (Yun *et al.*, 2016), anti-inflammatory activities (Shivanagoudra *et al.*, 2019), and wound healing promoter (Alippilakkotte *et al.*, 2017). *M. charantia* contains biologically active compounds that include glycosides, saponins, alkaloids, fixed oils, triterpenes, proteins, phenolic acid, and steroids (Sharma, 2019 & Dandawate *et al.*, 2016). However, there are lack of studies on the lignocellulosic biomass of *M. charantia* seeds.

M. charantia is worldwide known for its effectiveness in treating diabetes. As its chemically contains a compound that is very much similar to insulin (Omokhua-Uyi & Van Staden, 2020). Researchers have shown that when it is taken continuously for some period has the ability to substitute the insulin in the body. It also contains steroidal saponins called charantin, peptides similar to that of peptides and certain alkaloids that effectively control sugar level in blood (Kumar & Bhowmik, 2010).

In addition, the *M. charantia* is rich in supportive bioactive molecules in the treatment of cardiovascular diseases through inhibition of proliferation of vascular smooth muscle cells. *M. charantia* has high level of fatty acids. It contains fatty acids, that reduce the risk of developing cardiovascular disease such as omega- 3. Besides,

the MAP30, a 30 kDa protein isolated from seeds, has been proposed as the agent responsible for antiviral and antineoplastic properties (Aydin & Kaya, 2020).

As plants provide a wealth of small molecules with drug-like properties and can be used a proven template for the development of new scaffolds of drugs that might be helpful in the optimization of the drugs discovery process (Verpoorte, 1998; Atanasov, 2015).

1.3 Rationale of the study

The only available licensed dengue vaccine, Dengvaxia efficacy varied by serotype. The vaccine efficacy was higher against serotype 3 and 4 (71.6 % and 76.9 % respectively) than for serotype 1 and 2 (54.7 % and 43.0%) (WHO, 2018). Besides, a warning was released by Sanofi on Nov 29, 2017, that Dengvaxia could increase the risk of severe dengue in particular circumstances, following a review of the data from the clinical trials (The, 2018). This led to a suspension of the dengue vaccination programme in the Philippines.

As DENV-1 and DENV-2 are the most domain dengue virus serotypes in Malaysia, it is crucial to find an anti-dengue drug or vaccine which is suitable for both DENV-1 and DENV-2. The knowledge of the virus infection mechanisms is crucial to facilitate the search and development of the most effective drugs from potential anti-dengue plants or compounds. The use of *M. charantia* and other anti-dengue compound based on literature may speed up the quest in searching for a hit-to-led compound.

The use of fruits in the extraction process will lead to a production of waste. Approximately 122.80 hectares of farmland is planted with *M. charantia* that can

produce a total of 1372.46 metric tonnes of *M. charantia* fruits every year. In accordance, about 548.984 metric tonnes of *M. charantia* seed that can be used to produce seed oil are being discarded every year in Malaysia (DoA, 2014). These are a waste of natural resources as the extraction of oil from the seed can easily be carried. Hence, the study on seed oil as well as the lignocellulosic biomass of *M. charantia* seeds will be an added value in picking a right material for the development of a sustainable product using natural resources.

1.4 Hypothesis of the study

The hypothesis of the study was listed below:

The seed part:

1. The AEE will increase the *M. charantia* seed oil percentage of yield.
2. The AEE will extract oil with a slightly modification in the biochemical properties.
3. The AEE will change the biochemical properties of the seed lignocellulosic biomass.

The fruit flesh part:

1. *M. charantia* extract have an inhibitory activity towards DENV-2 NS2B/NS3 protease.
2. The pyrazolyl substituted benzylidene indanone derivatives will have a higher inhibitory activity towards DENV-2 NS2B/NS3 protease than the *M. charantia* extract.

1.5 Objectives of the study

The objectives of the study were consists of the seed part and the fruit flesh part. The objective were as follow:

The seed part:

1. To extract the seeds oil of *M. charantia* and study the composition of the seed lignocellulosic biomass.

The fruit flesh part:

1. To test the activity of *M. charantia* fruits extract (methanol, ethyl acetate and *n*-hexane) towards DENV-2 NS2B/NS3 protease.
2. To identify the chemical composition of active extract
3. To synthesize and characterize the pyrazolyl substituted indanone derivatives derivatize from small molecule present in the selected *M. charantia* fruit extract.
4. To conduct *in silico* molecular docking screening of the synthesized compounds.
5. To perform *in vitro* studies towards DENV-2 NS2B/NS3 protease of synthesized compounds.

1.6 Scope of the study

The research was conducted at Universiti Sains Malaysia, Penang, Malaysia and Université de Lorraine, Nancy, France. Therefore, only available instruments within the research facilities in both universities were used in this research.

The specific scopes of studies were:

The seed part (at Université de Lorraine, Nancy, France)

1. To extract the seeds oil of *M. charantia*, using aqueous enzymatic extraction method, in order to study effect of aqueous enzymatic extraction using a different ratio of enzyme cocktails HEL1 and X7 towards the production of *M. charantia* seed oil using gas chromatography (GC) and gas chromatography-mass spectroscopy (GC-MS).
2. To study the biochemical properties, and identification of the seed lignocellulosic biomass using high-performance anion-exchange chromatography with pulsed amperometry detection (HPAEC-PAD), Fourier-transform infrared (FTIR) spectroscopy and size exclusion chromatography (SEC).

The fruit flesh part (at Universiti Sains Malaysia, Penang, Malaysia):

1. To obtain methanolic, ethyl acetate, and *n*-hexane extracts of *M. charantia* fruits.
2. To screen the methanolic, ethyl acetate, and *n*-hexane extracts of *M. charantia* fruits towards DENV-2 NS2B/NS3 protease by using fluorogenic peptide substrate Boc-Gly-Arg-7-amino-4-methyl coumarin at Malaysian Institute of Pharmaceuticals and Nutraceuticals (IPharm), Penang, Malaysia

3. To identify the chemical constituents of the most active anti-dengue *M. charantia* fruits extract using gas chromatography (GC) and gas chromatography-mass spectroscopy (GC-MS).
4. To synthesize and characterize the pyrazolyl substituted benzylidene indanone derivatives derivatized from small molecule present in the *M. charantia* fruit extract.
5. To conduct *in silico* molecular docking screening of the synthesized compounds towards dengue virus 2 (DENV-2) NS2B/NS3 protease using Wichapong homology crystal model using AutoDock4.2 programme.
6. To perform *in vitro* studies of synthesized compounds towards DENV-2 NS2B/NS3 protease by using fluorogenic peptide substrate Boc-Gly-Arg-7-amino-4-methyl coumarin at Malaysian Institute of Pharmaceuticals and Nutraceuticals (IPharm), Penang, Malaysia

1.7 Study flowchart

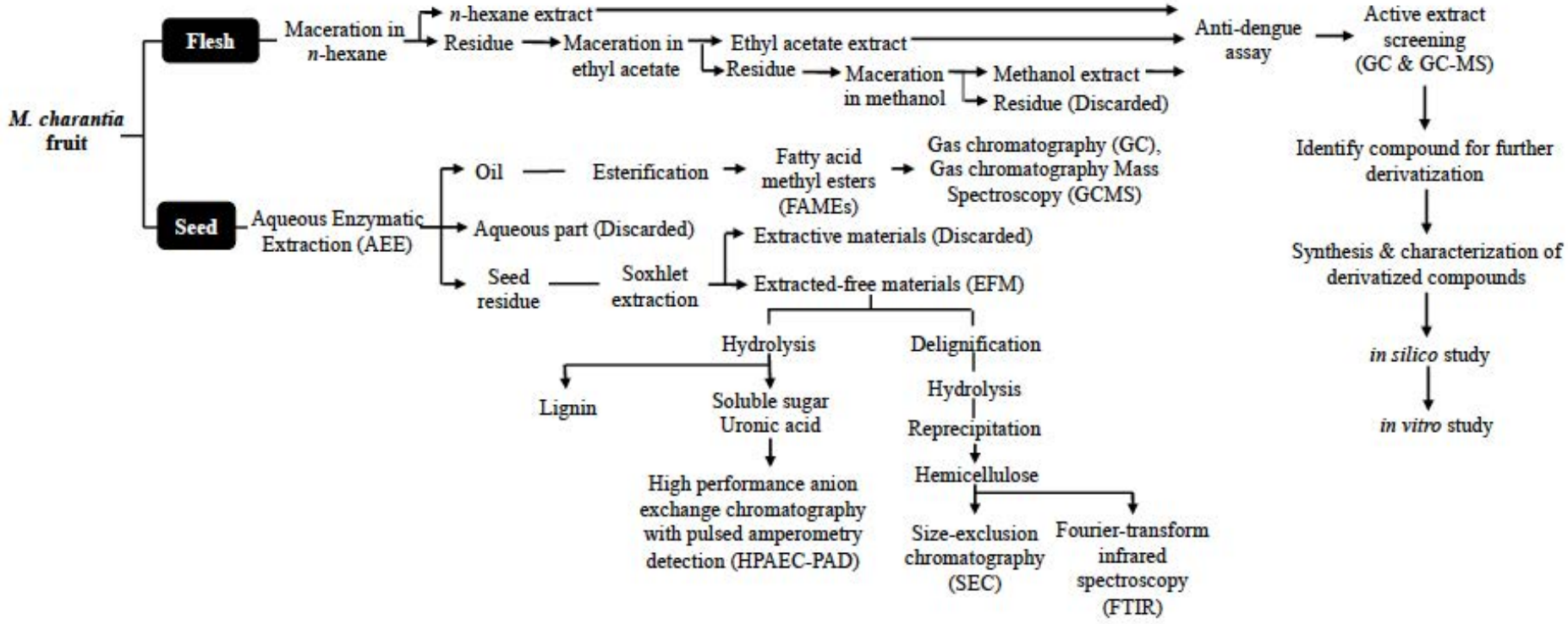

Figure 1.3: The studies of *M. charantia* fruits and seed flowchart.

CHAPTER 2

LITERATURE REVIEW

2.1 *M. charantia* overview

A megadiverse tropical rainforest of Malaysia which cover around 59.5 % of Malaysia's land area is recognized as one of the most productive types of forest in the world (WWF-Malaysia, 2019). About 10 % or approximately 2000 species from 20,000 species of vascular plants in Malaysia are classified as plants with medicinal qualities, and the number is expected to increase (Foster, 2009; Maarten & James, 2016; Ali *et al.*, 2014).

One of the frequently use tropical plant is "peria katak" or *M. charantia* . This tropical plant is growing wildly in tropical and subtropical Africa, Asia, America and the Caribbean and cultivated for edible fruits (Purnima & Harshani, 1999). The traditional uses of *M. charantia* vary widely by region throughout the world, but typically included the use as a digestive aid, anti-viral, antibacterial, parasiticide, blood sugar regulator, blood pressure regulator and hormonal balancer (Kumar & Bhowmik, 2010; Ahmad *et al.*, 2016; Grover & Yadav, 2004; Beloin *et al.*, 2005).

A study conducted by Ali and co-worker (2012) at Kangkar Pulai Region, Johor Bahru, Malaysia showed that the fruit of *M. charantia* are consumed as a juice to cure diabetes as well as to treat high blood pressure. In addition, a limited study among patients with diabetes mellitus found that 7.9 % patient consumed *M. charantia* as a complementary alternative medicine (Ching *et al.*, 2013).

The estimations of nutritional composition of *M. charantia* are 90.00 % water, 0.200 % fat, 4.20 % carbohydrates, 1.60 % protein, 0.03 % calcium, 2.57 % vitamins, and 1.4% fibres (Saeed *et al.*, 2018). Scientific research on *M. charantia* has been continuously performed since 1962 and from there onwards various chemical constituents as well as new health benefits are being revealed.

2.1.1 The phytochemical studies on of *M. charantia* fruit

M. charantia fruits have been studied chemically and were found to contain biologically active compounds that include glycosides, saponins, alkaloids, fixed oils, triterpenes, proteins, phenolic acid, and steroids (Sharma, 2019 & Dandawate *et al.*, 2016).

Cucurbitane type triterpene was identified as the major chemical constituent of *M. charantia* (Figure 2.1). The reported structures of cucurbitane type triterpenoids isolated from *M. charantia* are found to have a basic tetracyclic nucleus with substitutions of methyl, hydroxy, or sugar moieties (Perez *et al.*, 2014). The first compound isolated from *M. charantia* was cucurbitane type triterpenoids namely momordicoside A **[1]** and momordicoside B **[2]** (Okabe *et al.*, 1980).

Fatope and co-worker isolated six cucurbitane type triterpene from *M. charantia* fruits namely, 3,7-bis(acetyloxy)-25-methoxy-(3β,7β,9β,10α,23*E*)-19-norlanosta-5,23-diene-9-carboxaldehyde **[3]**, 3,7-dihydroxy-25-methoxy (3β,7β,9β, 10α,23*E*)-19-norlanosta-5,23-diene-9-carboxaldehyde **[4]**, (+)-Momordicin I **[5]**, Momordicin II **[6]**, 3,7-bis(acetyloxy)-25-hydroxy-(3β,7β,9β,10α,23*E*)-19-norla nosta-5,23-diene-9-carboxaldehyde **[7]**, 3β,7β,25-trihydroxycucurbita-5,23(*E*)-dien-19-al **[8a]** (Fatope *et al.*, 1990).

Other cucurbitane type triterpene isolated and identified from *M. charantia* were 5β,19-epoxycucurbita-6,23-diene-3β,19,25-triol **[9]**, momordicoside P **[10]** (Yan *et al.*, 2007), (19*R*,23*E*)-5β,19-epoxy-19-methoxycucurbita-6,23,25-trien-3β-ol **[11]**, (23*E*)-3β-hydroxy-7β-methoxycucurbita-5,23,25-trien-19-al **[12a],** (23*E*)-3β-hydroxy-7β,25-dimethoxycucurbita-5,23-dien-19-al **[12b]** (Kimura *et al.*, 2005). In addition, 9-methyl-(9β,10α,23*E*)-19-norlanosta-5,23,25-triene-3,7-dione **[14b]**, 25-hydroxy-9-methyl-(9β,10*α*,23*E*)-19-norlanosta-5,23-diene-3,7-dione **[8c]**, (3β,7β,9β,10*α*,23*E*)-9-methyl-19-norlanosta-5,23,25-triene-3,7-diol **[8d]**, and (3β,7β,9β, 10*α*,23*E*)-25-methoxy-9-methyl-19-norlanosta-5,23-diene-3,7-diol **[8e]** were isolated and elucidated by Chang and co-worker (Chang *et al.*, 2006) believed to be the antidiabetic components of Taiwanese *M. charantia* fruits.

Akihisa *et al.* (2007) tested the cancer chemo preventive effects of cucurbitane-type triterpenoids namely (19*R*,23*E*)-5β,19-epoxy-19-methoxycucurbita-6,23,25-trien-3β-ol **[13a]** and (23*E*)-3β-Hydroxy-7β,25-dimethoxycucurbita-5,23-dien-19-al **[14]** from the methanolic extract of *M. charantia* fruits. The isolated compounds exhibited a moderate inhibitory activity in mouse skin carcinogenesis tests. Other two cucurbitane type triterpenoids were isolated and identified as 5β,19-epoxy-cucurbita-6,22E,24-trien-3β-ol **[13b]** and cucurbita-6,22(E),24-trien-3β-ol-19,5β-olide **[13c]** from the acid hydrolysed ethanol extract of *M. charantia* seeds (Cao *et al.*, 2013).

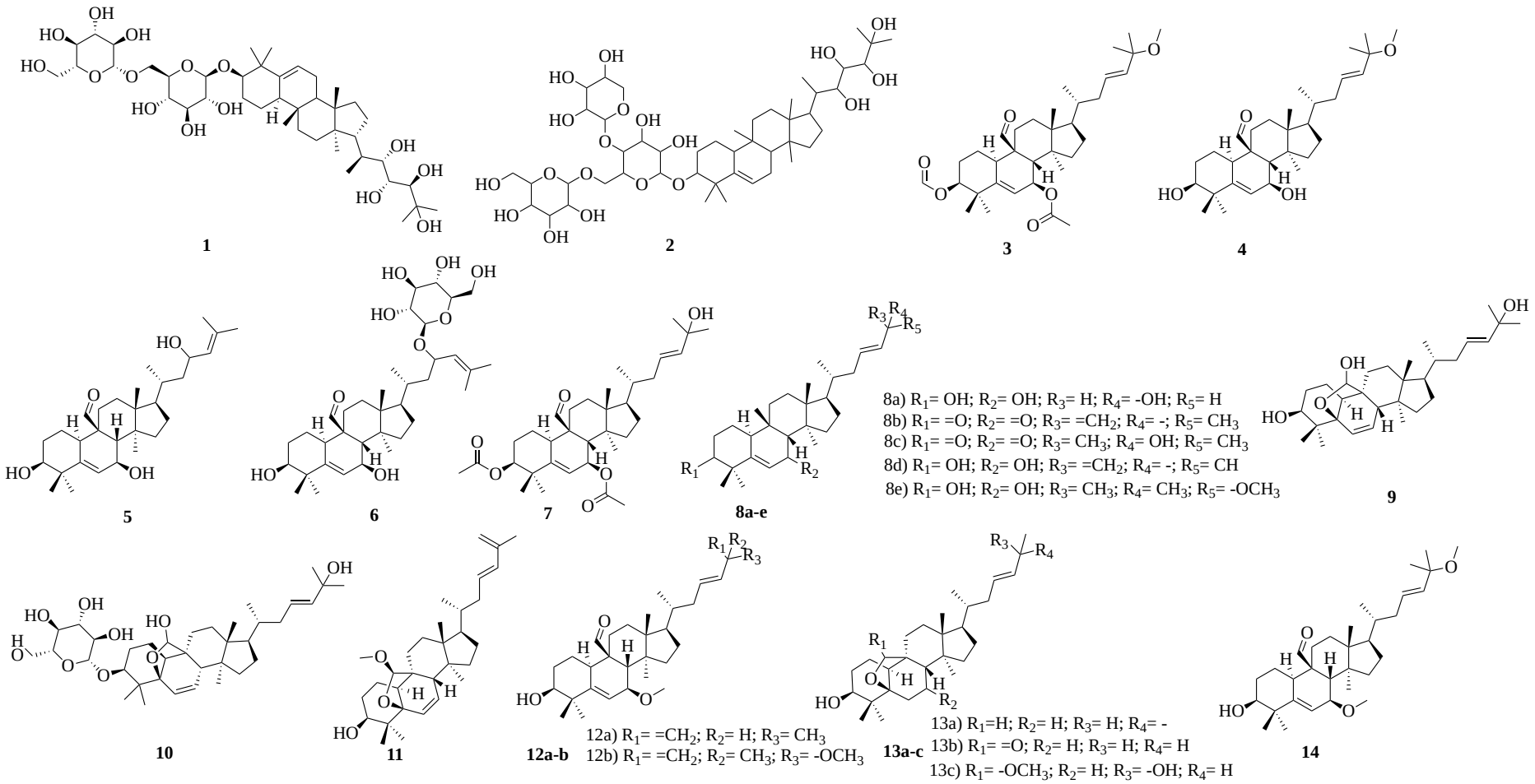

Figure 2.1: Some cucurbitane type triterpene isolated and identified from *M. charantia*.

Total phenol contents of 42.36 ± 0.75 mg per gram from *M. charantia* fruits extract was determined using the Folin–Ciocalteu method was reported by by Ibrahim and co-worker (2010). The phenolic acid fraction analysis of 100 g *M. charantia* dry sample using high performance liquid chromatography (HPLC) showed that gallic acid **[15]** (26.7 ± 0.73 mg) was the major phenolic acid followed by caffeic acid **[16]** (5.73 ± 0.89 mg) and *o*-coumaric acid **[17]** (9.93 ± 1.20 mg). Other phenolic acids presents in *M. charantia* were quinic acid **[18]**, protocatechuic acid **[19]**, ascorbic acid **[20]**, chlorogenic acid **[21]**, syringic acid **[22]**, 4-coumaric acid **[23]**, gentisic acid **[24]**, vanillic acid **[25]**, *t*-cinnamic acid **[26]**, and *p*-methoxy-benzoic acid **[27]** (Harinantenaina *et al.*, 2006; Horax *et al.*, 2010; Kenny *et al.*, 2013). Figure 2.2 showed the structures of phenolic acids found in *M. charantia.*

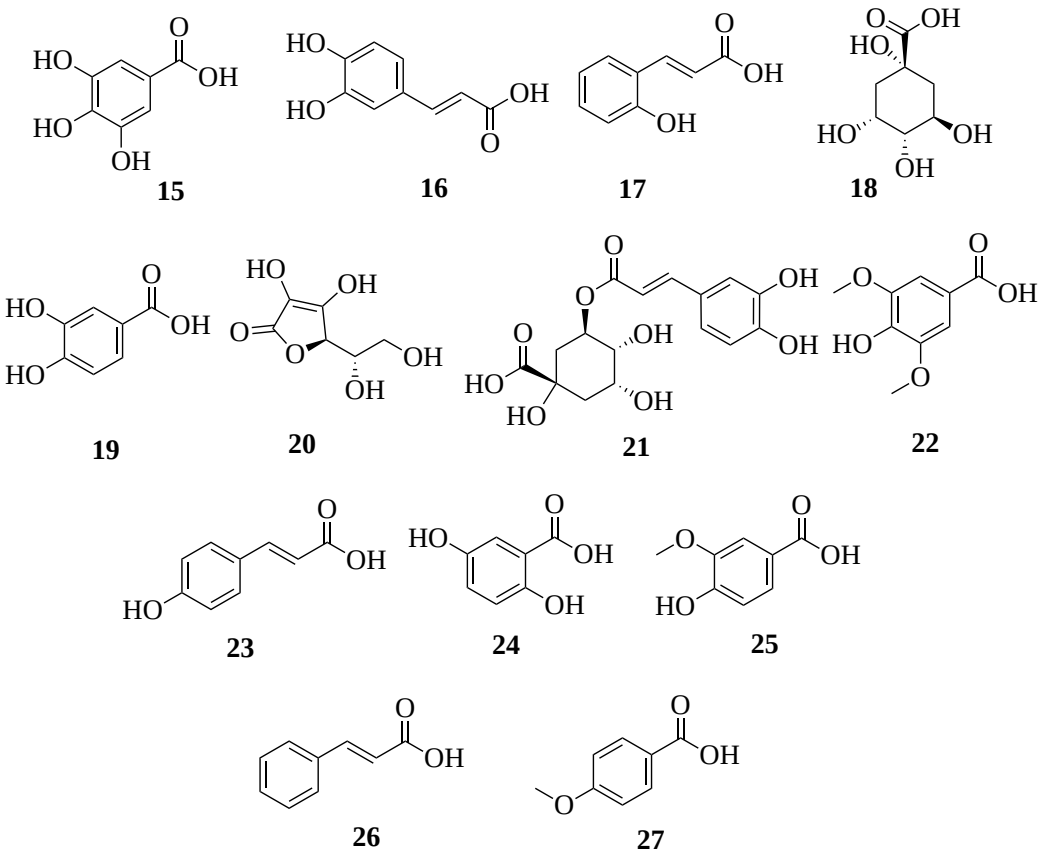

Figure 2.2: Phenolic acids found in *M. charantia*.

Gallic acid could be used as the structure along of this synthesis it is the major phenolic compound of *M. charantia* fruit extract. Apart from that, some researchers reported on the anti-viral activity of gallic acid and its derivatives.

2.1.2 The phytochemical studies of *M. charantia* seeds

The seeds of *M. charantia* are usually discarded without any further uses. Few studies have shown that the seeds of *M. charantia* contained high content of omega-3 polyunsaturated fatty acids such as α-linolenic acid **[28]**, eicosapentaenoic acid **[29]**, and stearidonic acid **[30]** (Liu *et al.*, 1998; Yasui *et al.*, 2005). In the study of biodiesel mixture of fatty acid methyl esters (FAMEs) with methanol, Škrbić and co-worker (2015) stated that some of the major FAMEs such as, palmitic acid **[31]**, linoleic acid **[32]**, oleic acid **[33]**, arachidic acid **[34]**, and stearic acid **[35]** were found in *M. charantia* seed oil. According to Chen *et al.*, the α-eleostearic acid **[36]** present in bitter melon seed oil could reduce hepatic triglyceride accumulation (Chen *et al.*, 2016). Figure 2.3 showed some of the chemical constituents found in *M. charantia* seed.

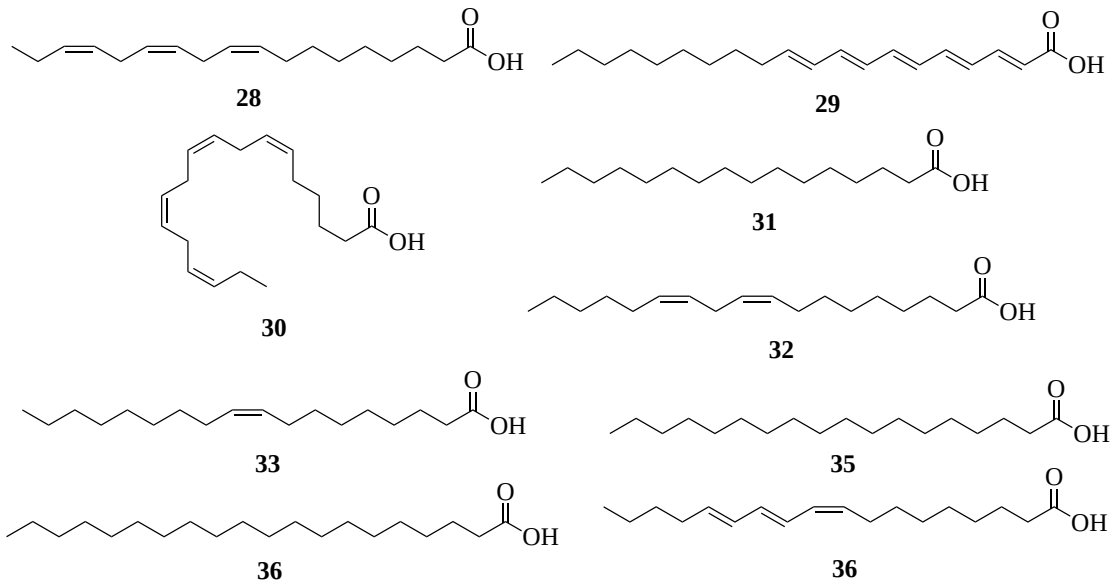

Figure 2.3: The chemical constituents found in *M. charantia* seed.

Apart from that, the essential oil containing α-pinene **[37]**, β-pinene **[38]**, octanal **[39]**, 1,8-cineole **[40]**, β-phellandrene **[41]**, dihydrocarveol **[42]**, *trans*-dihydrocarveol **[43]**, carvone **[44]**, *(E)*-anethole **[45]**, safrole **[46]**, methyl-eugenol **[47]**, germacrene D **[48]**, β-selinene **[49]**, α-selinene **[50]**, myristicin **[51]**, δ-cadinene **[52]**, trans-nerolidol **[53]**, spathulenol **[54]**, cedrol **[55]**, β-bisabolol **[56]**, and apiol **[57]** (Figure 2.4) from *M. charantia* seed has been isolated and tested for its anti-bacterial and antifungal activities (Braca *et al.*, 2008).

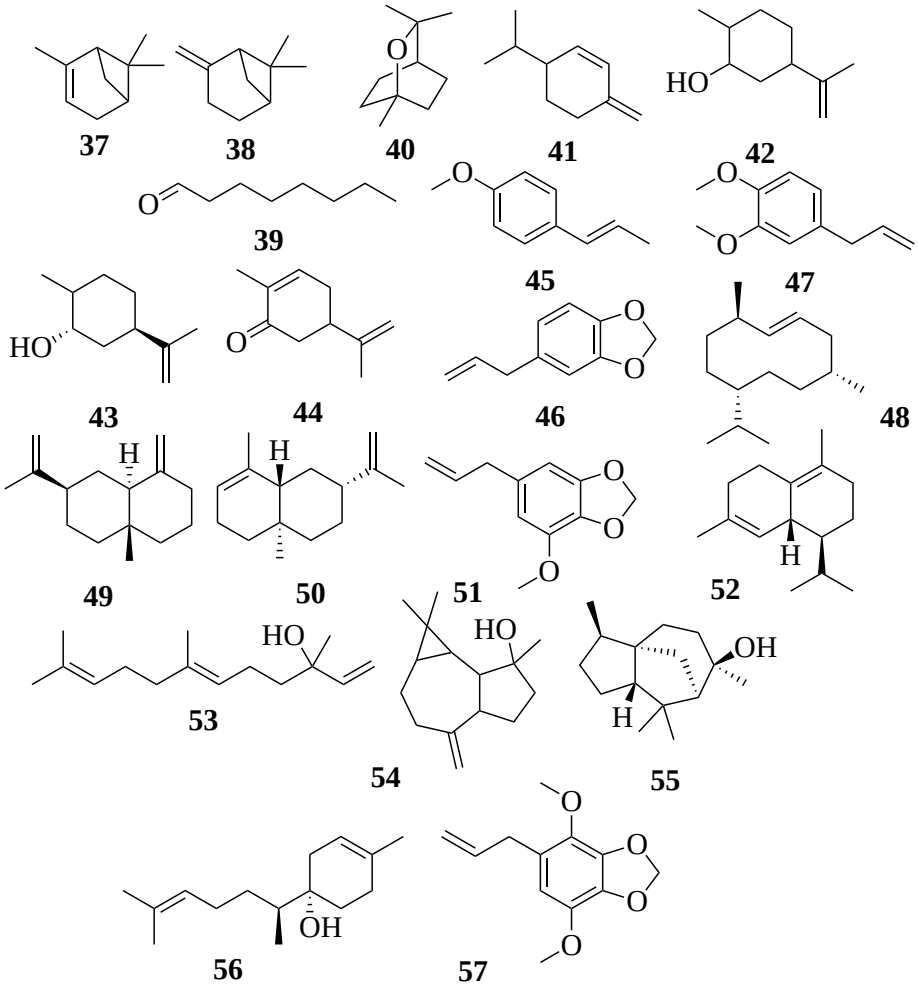

Figure 2.4: The chemical constituents present in *M. charantia* seeds essential oil.

2.2 The extraction method of *M. charantia*

2.2.1 The fruits flesh extraction via maceration method

Maceration is an extractive technique that is conducted at room temperature. It consists of immersing a plant in a liquid (water, oil, alcohol, or solvent) inside an airtight container, for a variable time based on the plant material and liquid used. The solvent must be chosen based upon the chemical nature of the compounds contained within the plant.

The study on antioxidation activity of *M. charantia* fruit extracts under different maceration periods of 6, 12, 24 and 48 h in different organic solvent was conducted. The result indicated that nitric oxide scavenging activity of antioxidation test was higher using ethanolic extract followed by aqueous, acetone, ethyl acetate, petroleum ether and hexane extracts at 12 h (Malik *et al.*, 2019). Kaneria and co-worker worked on identifying the metabolome pattern and study the biological efficacy of almond (*Terminalia catappa L.*) peels found that the methanolic maceration extraction method proved to be the best extraction method for the extraction of antioxidant (Kaneria *et al*., 2018).

In addition, Yeo and co-worker (2014) revealed the importance of appropriate maceration periods in combination with different extraction solvents on the anti-microbial activity of *M. charantia* fruit extract. Thus, the results revealed that the active anti-microbial compounds from fruit of *M. charantia* are mostly extracted in the non-polar to intermediate polarity solvent. The Tukey's multiple comparison tests proven that findings as *n*-hexane, petroleum ether and ethyl acetate demonstrated better anti-microbial activity as compared to other solvents used. Hence, the semi to non-polar solvent showed a better potency in extracting the active compounds from *M. charantia*.

2.2.2 The *M. charantia* seed oil extraction method

Various methods have been used to extract oil from *M. charantia* seeds. The traditional method of oil extraction from the seeds was the maceration of the seed with a non-polar solvent. Verma and Aggarwal (1956), obtained a clear reddish-brown oil yielding of 26.5 % by extracting the fresh seeds with petroleum ether. On the other hand, very little quantity of essential oil was obtained (yield: 0.012%) by hydro distillation of dried seeds using the Clevenger-type apparatus (Braca *et al.*, 2008).

Two methods were used by Yoshime and co-workers (2016) to extract the *M. charantia* seed oil. The research concluded that the Soxhlet extraction method (40 % *w*/*w*) resulted in higher yield than the Folch extraction method (16 % *w*/*w*). An adequate amount of seed oil yielding of 36.89 % was obtained by using the supercritical CO_2 extraction method (Liu *et al.*, 2010b).

With the increasing demand for oilseed from agricultural plants, oil extraction technology has become more advance such as the alternative solvent extraction methods including supercritical fluids (Sodeifian *et al.*, 2018), enzyme-assisted aqueous extraction (AEE) (Yusoff *et al.*, 2016), and microwave-assisted extraction (Kumar *et al.*, 2018).

2.2.2(a) The enzyme-assisted aqueous extraction (AEE) oil extraction method

The AEE is getting some attention nowadays due to its efficient, sustainable, and eco-friendly characteristics. This extraction process depends on the specific properties of the enzyme itself. The enzyme, acting as a catalyst under optimum experimental conditions, disrupts the plant cell wall by hydrolysation to release the intracellular components (Sheldon *et al.*, 2013). As the plant cell walls are a complex

structure which mainly made of cellulose, hemicellulose, lignin and protein in addition to pectin (Waldron *et al.*, 2003; Carpita, & Gibeaut, 1993).

Rosenthal reported that the cell wall degradation enzyme for rapeseed consists of a combination of pectinase, cellulase, and hemicellulase (Rosenthal *et al.*, 1196). In a previous study, Latif and Anwar reported that the active mechanism of enzyme cocktail (Alcalase 2.4L, Viscozyme L, Protex 7L, Natuzyme, and Kemzyme.) during AEE was the degradation of cellulose, pectin, and protein. Thus, the destructing of structural cell wall integrity led to higher sesame oil recovery; 16.5–24.8% for the AEE was observed compared to only 12.3% for the control (without enzyme treatment) (Latif & Anwar, 2011). The deployment of AEE in this study could resulting in a higher quality *M. charantia* seeds oil.

2.3 The indanone with gallic acid moieties derivatives

2.3.1 Gallic acid

Gallic acid is a phenolic compound that is easily found in various plants and is a primary phenolic compound present in *M. charantia* (Ibrahim *et al.*, 2010). Gallic acid is extensively used in medicine and chemical research as well as pharmaceutical, cosmetic, and food industries (Brewer, 2011). The three hydroxyl groups and a carboxylic acid group attached to a benzene ring are the two functional groups that make up a gallic acid compound as presented in Figure 2.5.

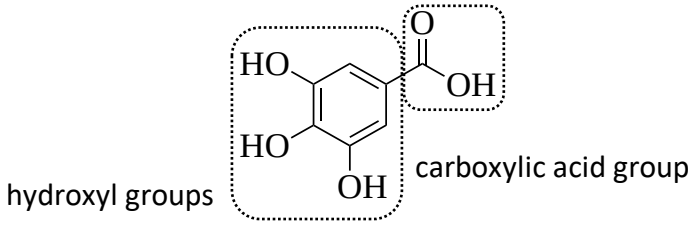

Figure 2.5: The gallic acid structure.

The ortho position of the hydroxyl groups resulted in a coplanar bent configuration make it prone to antioxidative activities (Badhani *et al.*, 2015). The coplanar backbones enable the formation of π–π stacks that facilitate the intermolecular bonding (Zhan & Yao, 2016). The presence of polyphenolic functionality in gallic acid is induced by the high oxygen derived free radical scavenging moieties present in the compound and make it capable of acting as a Bronsted acid with carboxylic group shows the highest acidity value compared to the three hydroxyl groups (Singh *et al.*, 2016; Škorňa *et al.*, 2016).

2.3.2 The indanone

1-indanone **[58]** is a polynuclear hydrocarbon with an unstable five-membered ring cyclopentanone fused to benzene ring (Figure 2.6). The two-active sites in 1-indanone reacted according to a specific reaction condition. The ionic reaction condition resulted in the substituent at the α carbon, while the reaction in a radical condition happen at the ß carbon (Fatma Yelda, 2009).

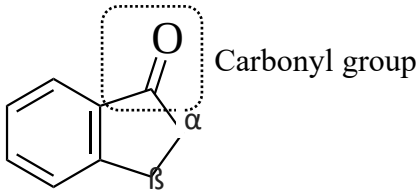

Figure 2.6: The 1-indanone structure.

The indanone possess structural motifs that are frequently found in various types of natural compounds and act as one of the essential classes in organic chemistry as it can be an intermediate in the synthesis of a variety of molecules.

2.3.3 The synthesis of indanone-based derivatives and its pharmacological studies

Several synthetic strategies have been developed inspired by the useful moiety of gallic acid and indanone. These compounds have been studied mainly for their anti-Alzheimer' activity (Cho *et al.*, 2011; Patil *et al.*, 2017; Sugimoto *et al.*, 2000; Huang *et al.*, 2012) and anti-cancer activity(Saxena *et al.*, 2008; Chanda *et al.*, 2012), monoamine oxidase inhibitor (Nel *et al.*, 2016), efflux pump inhibition (Dwivedi *et al.*, 2016), and anti-tumor (Garcia-Rivera *et al.*, 2011).

The anti-cancer compound synthesized by Saxena and co-worker (2008) was depicted in Scheme 2.1. The synthetic strategies involved the methylation process of gallic acid **[15]** using dimethyl sulphate in 20% aqueous alkali to form a 3,4,5-trimethyl gallic acid methyl ester **[59]**, which further underwent Grignard reaction with methyl magnesium iodide to yield the desired substrate 3,4,5-trimethoxyacetophenone **[60]** and 2-(3,4,5-trimethoxyphenyl)propan-2-ol **[61]** as the minor compound. The acetophenone **[60]** and **[62]** were reacted and condensed in 3% aqueous methanolic sodium hydroxide to get a compound **[63]**. The compound **[63]** underwent reflux in trifluoroacetic acid to obtain desired compound 4,5,6-trimethoxy-3-(3,4,5-trimethoxyphenyl)-2,3-dihydro-1*H*-inden-1-one **[64]**.

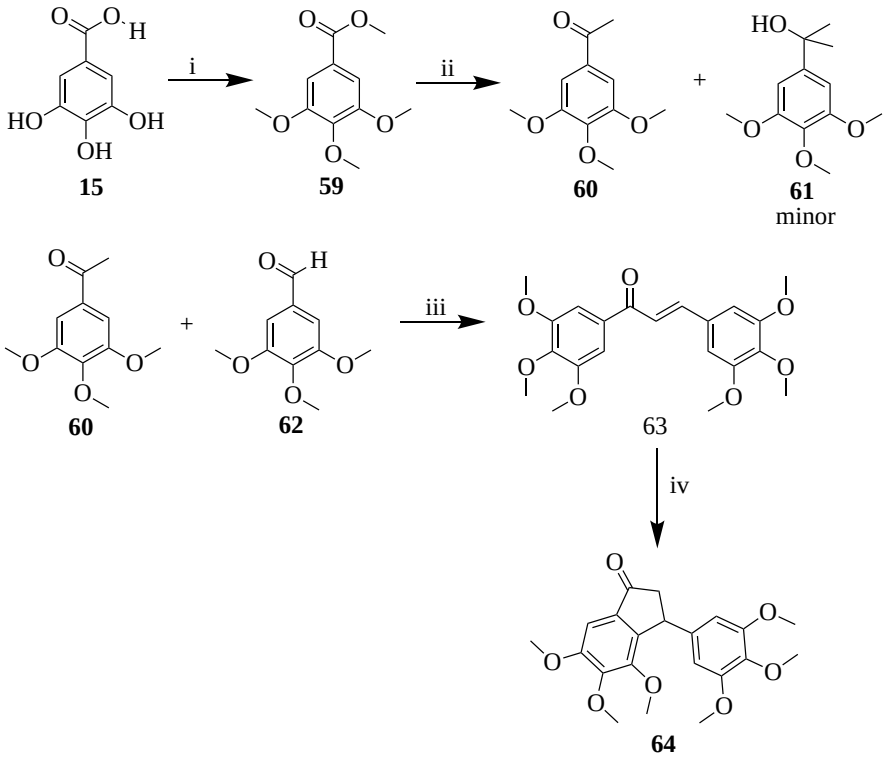

Scheme 2.1: Synthesis of 4,5,6-trimethoxy-3-(3,4,5-trimethoxyphenyl)-2,3-dihydro-1*H*-inden-1-one**.** *Reagents and conditions: (i) 20% aq alkali, dimethyl sulphate, refluxed for 3 h, 60%; (ii) CH_3I, Mg turnings, THF, 20 min at RT then reflux for 1 h, 42%; (iii) 3% aq methanolic NaOH, RT, overnight 16–18 h, 62–84% respective acetophenones and aldehydes used; (iv) TFA, refluxed in a sealed tube, 3–4 h, 28–52% (Saxena *et al.*, 2008).

The synthesized gallic acid-based indanone derivative, 4,5,6-trimethoxy-3-(3,4,5-trimethoxyphenyl)-2,3-dihydro-1*H*-inden-1-one **[64]** showed potent anti-cancer activity against hormone-dependent breast cancer, oral and liver cancer cell lines. The *in vitro* study of compound **64** towards MCF-7 hormone-dependent breast cancer cell lines showed a promising activity with IC_{50} = 2.2. The trimethoxyphenyl units identical to gallic acid in both the rings in the compound **64** suggested to have a potent anticancer activity which increased the activity towards MCF-7, HEPG2 and WRL68 human cancer cell line (Saxena *et al.*, 2008).

The widely used Claisen-Schmidt condensation method has been utilized by Xiao and co-worker (2018) to synthesize an anti-inflammatory agent for the treatment of acute lung injury. As showed in Scheme 2.2, the commercially available 6-hydroxy-

1-indanone **[65]** was protected with tetrahydropyranyl (THP) resulted in 6-[(tetrahydro-2*H*-pyran-2-yl)oxy]-1-indanone **[66]** and further reacted with various benzaldehyde to obtain THP protected 2-benzylidene-1-indanone intermediates **[67a-b, 68e-t]** via Claisen-Schmidt condensation in the presence of ethanolic sodium hydroxide. The deprotection process was carried out by using hydrochloric acid in ethanol resulting in the formation of the desired 2-benzylidene-1-indanone derivatives **[68a-b, 68e-t]**. Whilst, the single step synthesis of the compound **65** with 3,4-dihydroxybenzaldehyde and 4-hydroxy-3-methoxybenzaldehyde with the present of HCl gas and ethanol as the solvent yielding compound **68c** and **68d** respectively.

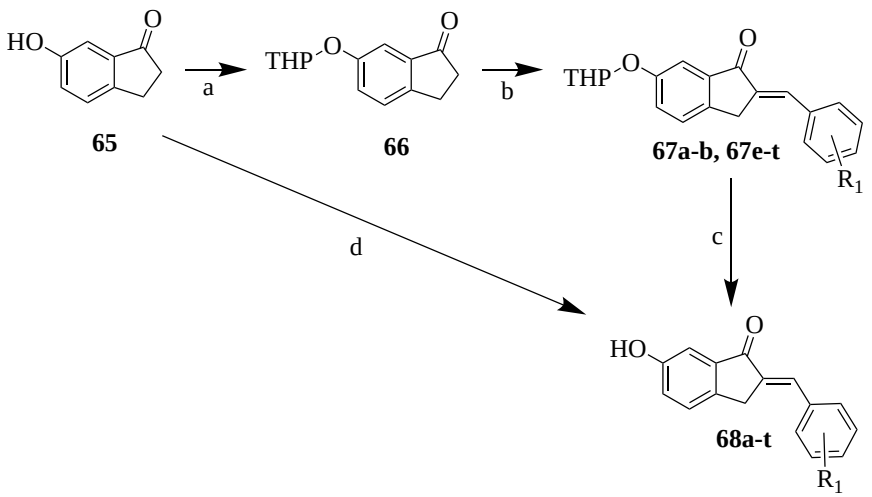

68a:4′-OMe	**68k** :2′-F
68b:4′-OEt	**68l** :2′-Cl
68c:3′,4′-OH	**68m**:2′-Br
68d:3′-OMe, 4′-OH	**68n** :3′-Br
68e:2′,3′-OMe	**68o** :4′-Br
68f :2′,4′-OMe	**68p** :4′-F
68g:3′,4′,5′-OMe	**68q** :4′-CF3
68h:2′,3′,4′-OMe	**68r** :3′,4′-F
68i :2′,4′,6′-OMe	**68s** :3′,4′-Cl
68j :2′,4′,5′-OMe	**68t** :3′-NO_2, 4′-Cl

Scheme 2.2: General synthetic method for 6-hydroxyl-2-benzylidene-1-indanone derivatives **68a-t**. *Reagents and conditions: (a) 3,4-dihydro-2H-pyran, PPTS, 4 h, CH_2Cl_2, 40°C; (b) various benzaldehydes, EtOH, 20% (w/v) NaOH, room temperature, overnight; (c) 1.0 mol/L HCl, EtOH, room temperature, 5 h; (d) HCl (gas), EtOH, room temperature, overnight (Xiao *et al.*, 2018).

The anti-inflammatory activity was measured as inhibition of lipopolysaccharide, LPS induced interleukin-6, IL-6 and tumour necrosis factor-α, TNF-α. The cytokine-inhibitory effects of the 6-hydroxyl-2-benzylidene-1-indanone derivatives **68a-t** was determined and found that compound **68d** had the highest percentage inhibition of 69.28 ± 1.58 and 83.73 ± 4.05 towards lipopolysaccharide respectively. The structure activities relationship of synthesized compounds was determined and illustrated as presented in Figure 2.7.

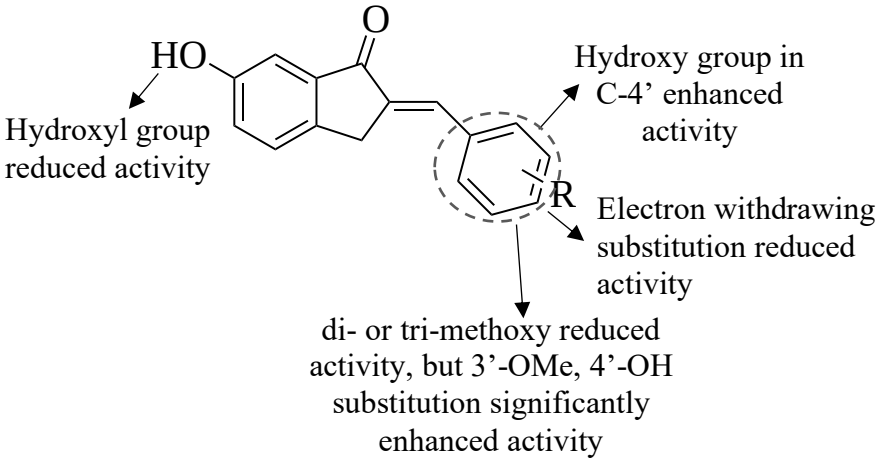

Figure 2.7: The structure activity relationship of 6-hydroxyl-2-benzylidene-1-indanone derivatives **68a-t** (Xiao *et al.*, 2018).

A most famous indanone compound called donepezil **[69]** is the most effective AChE inhibitor in Alzheimer's disease that is currently available on the market. Figure 2.8 showed the structure of donepezil.

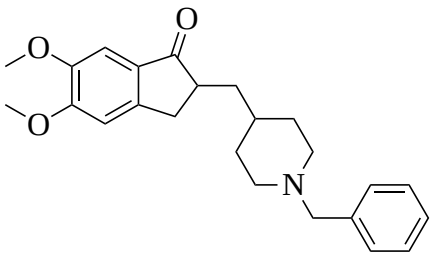

Figure 2.8: The structure of called donepezil **[69]**.

The attempt to synthesize compounds with dual activity on AChE and BACE-1 of Alzheimer's disease was reported by modifying the donepezil analogue by introducing a double bond on the indanone moiety (Costanzo *et al.*, 2016). The general eco-friendly synthetic pathway for the synthesis of donepezil analogues is described in Scheme 2.3.

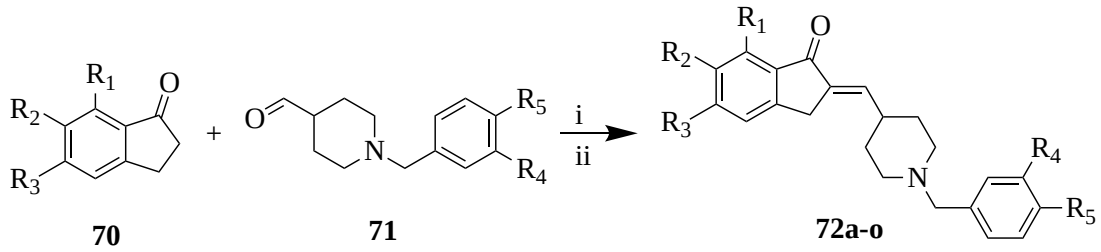

70 **71** **72a-o**

72a:R_1= R_4=R_5=H; R_2=OH; R_3=OCH_3

72b:R_1= R_4=R_5=H; R_2= OCH_3; R_3=OH

72c:R_1= R_3= R_4=R_5=H; R_2=OH

72d:R_1= OH; R_2=R_3= R_4=R_5=H

72e:R_1= R_2= R_4=R_5=H; R_3=OH

72f:R_1= R_4=R_5=H; R_2= R_3=OCH_3

72g:R_1= R_3=R_4=R_5=H; R_2=OCH_3

72h:R_2= R_3=R_4=R_5=H; R_1=OCH_3

72i :R_1= R_3=R_4=R_5=H; R_2=OCH_3

72j :R_1= R_2=R_4=R_5=H; R_3=OCH_2O-

72k :R_1= R_2= R_5=H; R_3= R_4=OCH_3

72l :R_1= R_3= R_5=H; R_2= R_4=OCH_3

72m:R_1= R_4=OCH_3: R_2= R_3=R_5= H

72n :R_1=R_3=H; R_2= OCH_3; R_4= R_5=OCH_2O-

72o :R_1= OCH_3; R_2=R_3=H; R_4= R_5=OCH_2O-

Scheme 2.3: The synthesis of donepezil analogues.
*Reagents and conditions: i) Amberlyst A-26, Methanol, 40–50°C,))) 250W;
ii) dry DMF, iodocyclohexane, reflux (Costanzo *et al.*, 2016).

In method development phase, Costanzo and co-worker (2016) found about 20 % of the hydroxyl impurities in the synthesis of compound **72f** when using homogeneous catalyst, alkali metal hydroxides or alkoxides in methanol which required additional purification steps. Hence, the homogeneous catalyst was changed to Amberlyst A-26, a commercially available heterogenous catalyst. The synthesized compounds were tested against both AChE and BACE-1 enzymes. Compounds **72f**

and **72i** displayed promising dual activity and lower IC_{50} value compared to the significantly low activities of compounds **72n** and **72o**, which suggested due to an unfavourable hindrance from the *N*-benzyl piperidine moiety for the compound to reach the active site of the enzymes.

Some of indanone-based chalcone derivatives have also been constructed based on the basic structure of donepezil **[69]**. The *(E)*-2-(4-ethoxybenzylidene)-2,3-dihydro-1*H*-inden-1-one **[73]** with a maximal relaxation (R_{max}) value of 38.34 ± 8.90% for its vasorelaxant properties have been synthesized by Sabri and co-worker (2018). The compound **73** was synthesized by reacting 0.01 mol of 1-indanone **[58]** with 0.01 mol 4-ethoxybenzaldehyde in 10 mL methanol. Piperidine was added as a catalyst and the reaction was refluxed at 75°C–85 °C for 12 h. The reaction mixture was then cooled to a room temperature and the precipitated formed was filtered and washed with a cold methanol, before being recrystallized using hot ethanol. The reaction was depicted as in Scheme 2.4.

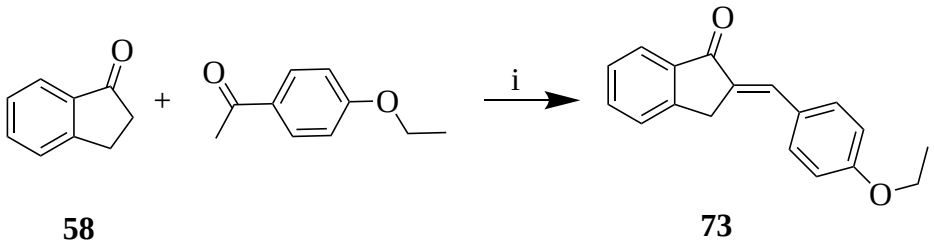

58 **73**

Scheme 2.4: The synthesis of indanone-based chalcone compound.
*Reagents and conditions: i) Piperidine, 75°C–85°C, reflux, 12 h (Costanzo *et al.*, 2016).

Hence, merging both important compounds, the gallic acid and indanone could led into a formation of new derivatives which possess a high anti-dengue activity.

2.4 Dengue virus

The increasing risk of being infected with dengue virus are proportional to the increasing of the virus sources for the uninfected mosquitoes as human acted as the main carrier and multipliers of the virus. Environmental management and the pesticide use have been introduced for vector control and dengue prevention to reduce human-vector contact. Some of the methods are eliminating vector larval habitats, installing mosquito screen on windows, doors, and using mosquito nets while sleeping (WHO, 2009; Scritable, 2011; Mahmud *et al.*, 2019).

A minimal change of the total global area at the risk of dengue between 2015 and 2080 was predicted by Messina and co-worker (2019). The climate change resulted in a rising in temperature that intensify the dengue concern in the endemic areas, speed up the viral amplification and increased the vector survival. Prolonged the transmission seasons and increased the number of infected humans that increased the public health burden of the dengue endemic countries need to face. An additional of 2.25 billion people is estimated to be at risk of dengue in 2080 compared to 2015, bringing the total population at risk to over 6.1 billion or 60 % of the world population.

2.4.1 Dengue virus infection in Malaysia

The Ministry of Health (MoHM) surveillance monitoring showed that a particular serotype can be dominated for at least two years before being replaced by other serotypes (Figure 2.9). The serotype shifts led to a reoccurring of dengue outbreak and deaths due to reduction in the herd immunity to the new virus serotypes (Mudin, 2015).

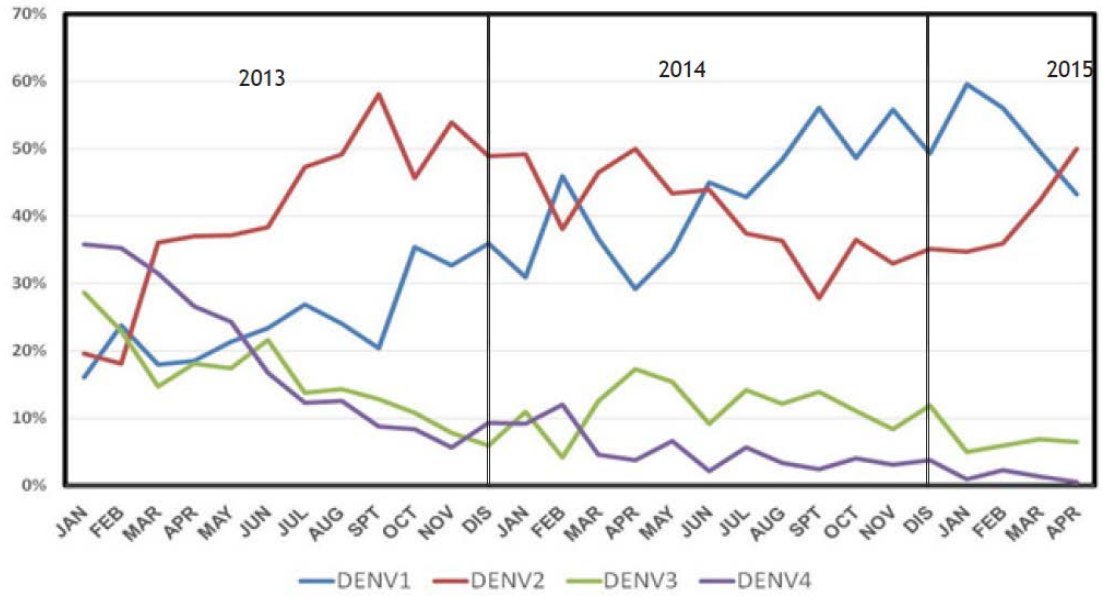

Figure 2.9: The dengue virus serotypes shift in Malaysia (Mudin, 2015).

In a descriptive time series study by Bujang and co-worker (2017) using the dengue surveillance system data developed by Vector Borne Disease Section, MoH, it is forecasted that in 20 years the dengue cases will be increase up to 1561.3 % compared with the dengue cases in 2014 which was 108,698 cases. The increased number of dengue cases in Malaysia were due to the continuous urbanisation process and development, migration or movement from one place to another, and poor environmental management. As most of the factors are hard to be controlled, only manipulation and intervention with the environment cleanliness, vector control and changing in the human behaviour are the key to reduce the dengue cases (Zaki *et al.*, 2019 & Ong, 2016). The integrated management strategy for dengue prevention and control program has been implemented by the Ministry of Health since 2011 to control the factors contributing to the disease transmission (Singh, 2019).

2.4.2 Dengue virus treatment

The critical period of DF is when patients undergo sudden deterioration which is between the first 48–72 hours of infection. The chance of fatal outcome is minimal if the patient managed to go through this phase. Hospitalisation is required when there is a need for fluid replacement under close supervision or if the platelets level is low which need further monitoring for bleeding tendencies. The recovered patients will be temporary immune against the same serotype but not against other dengue virus serotypes (WHO, 2012; Uno & Ross, 2018).

The first licensed dengue vaccine, Dengvaxia by Sanofi Pasteur the first dengue vaccine to market, which is now already licensed in several Asian and Latin American countries (Guy *et al.*, 2011; Guy *et al.*, 2010). Overall, Dengvaxia had satisfactory safety and immunogenicity in both *in vitro* and *in vivo* preclinical models (including nonhuman primates), and potential environmental risks as defined above were also demonstrated to be absent or negligible (Guy *et al.*, 2015). The trials demonstrated vaccine efficacy against all four serotypes, with higher efficacy rates against serotypes 3 and 4 than serotypes 1 and 2, consistent with the earlier phase II trial in Thailand (Sabchareon *et al*., 2012; Guy *et al.*, 2017). Therefore, the quest in searching for most effective anti-dengue drugs or dengue vaccine is still ongoing.

2.4.3 The anti-dengue screening using DENV-2 NS2B/NS3 protease enzyme

The anti-dengue screening using DENV-2 NS2B/NS3 protease enzyme was carried out by observing the cleavage of the 6-amino-4-methyl-coumarin part **[58]** of the peptide substrate by hydrolysis process with the donor/acceptor pair liberates

fluorescence which allowed a qualitative measurement of the enzyme activity using a fluorometer (Schulz *et al.*, 1998 & Carmona *et al.*, 2009).

Such activity resulted in the formation of bonded interaction between enzyme and peptide part of the substrate**.** However no fluorescence been exhibited with the presence of the inhibitor as the inhibitor formed a bonded interaction with the enzyme and ceased the peptide cleavage. The protease assay mechanism without and with the presence of inhibitor were depicted in Scheme 2.5 and 2.6 respectively.

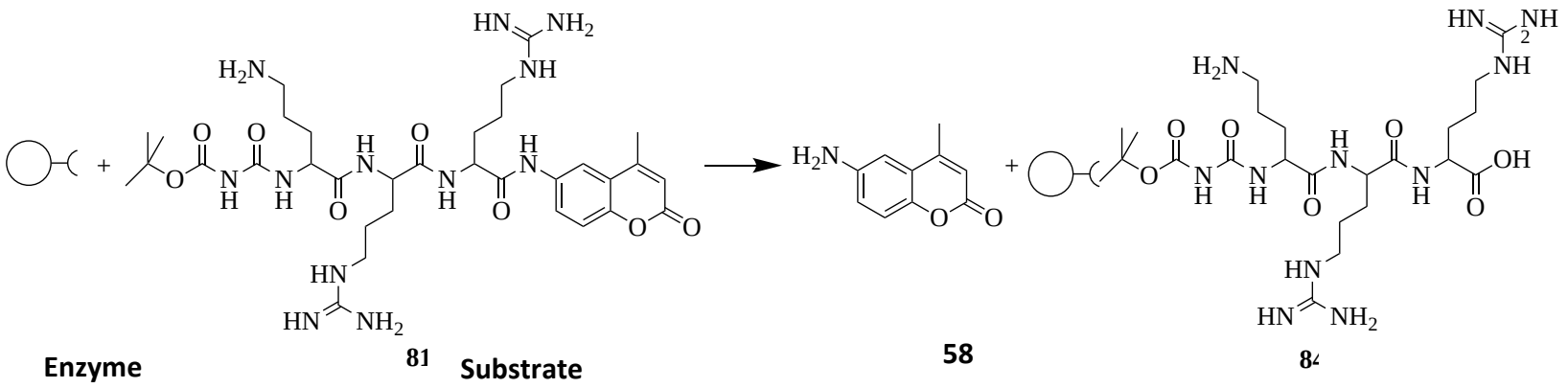

Scheme 2.5: The protease assay mechanism without inhibitor.

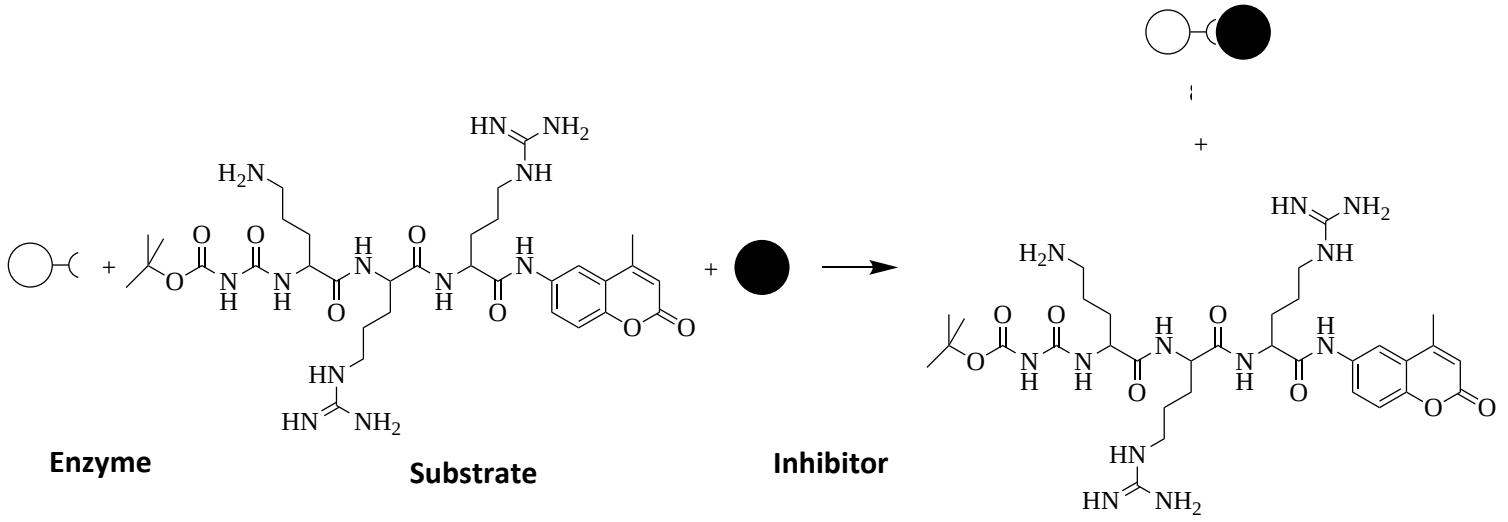

Scheme 2.6: The protease assay mechanism with inhibitor.

Conceptually, the fluorophore parts of the synthetic fluorogenic peptide Boc-Gly-Arg-Arg-AMC (Figure 2.10) undergoes cleavage into 6-amino-4-methyl-coumarin **[58]** (Figure 2.11). The AMC substance possesses the ability to exhibit fluorescence as it contained an electron donor, amino groups that can transfer charge as depicted in Figure 2.11. The subsequent appearance of fluorescence is due to the results in loss of energy transfer by the diffusion of the donor-containing substrate fragment away from the acceptor-containing substrate fragment, which happened substrate is cleaved by the enzyme (Fields, 2001).

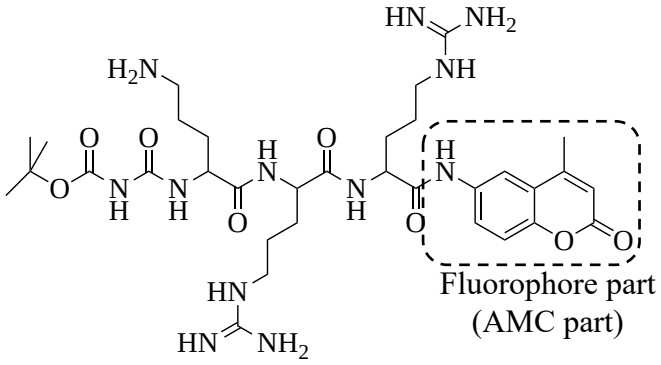

Figure 2.10: The structure of synthetic fluorogenic peptide Boc-Gly-Arg-Arg-AMC.

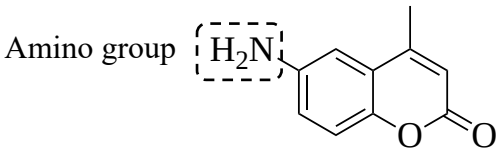

Figure 2.11: The structure of 6-amino-4-methylcoumarin (AMC).

2.4.4 The compounds with anti-dengue properties

Wu and co-worker (2015) synthesized seven novel compounds with a selective and non-competitive inhibition towards the serotype 2 and 3 of dengue virus *in vitro* and *in cells*. The benzothiazole derivatives [74–80] (Figure 2.12) were reported exhibiting 50% inhibitory concentrations in the low-micromolar and sub-micromolar range in cells.

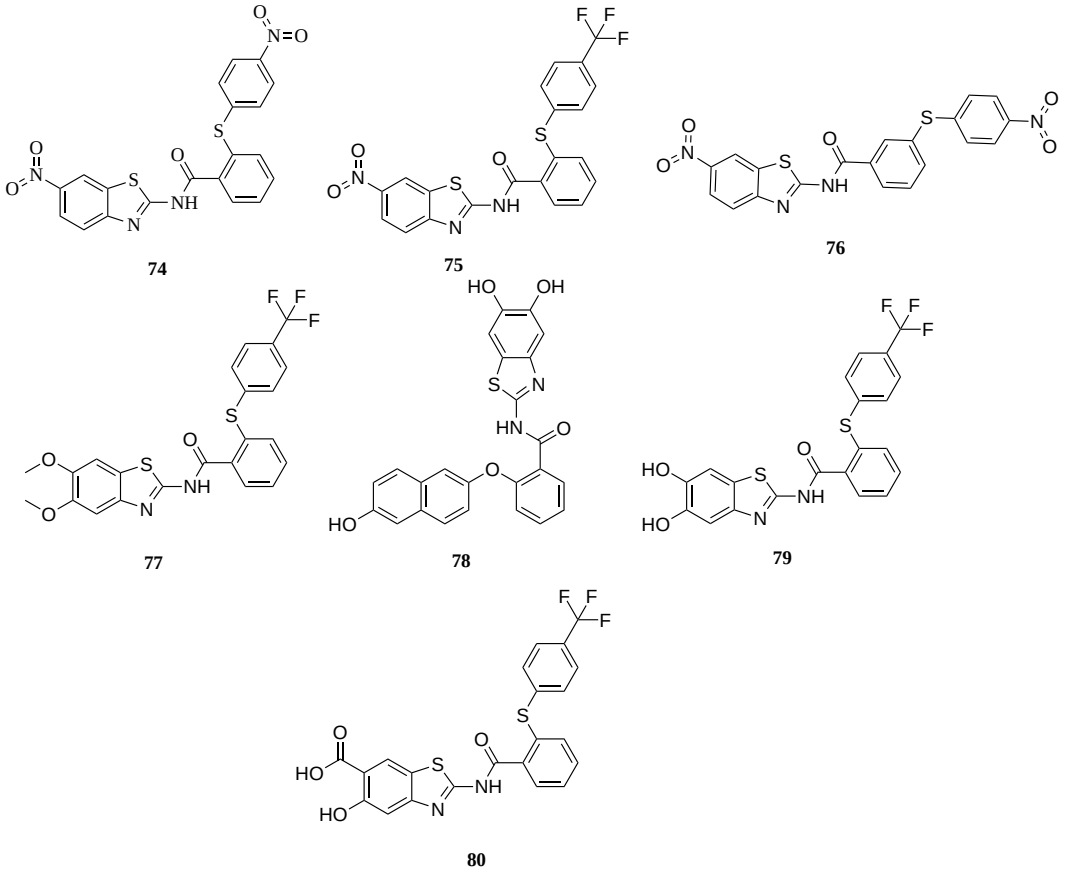

Figure 2.12: The benzothiazole derivatives **[74–80]**.

Apart from that, there are active component of natural product with anti-dengue properties. The time-of-drug-addition assays of *Psiloxylon mauritianum* extract were found interfered with the attachment of the viral particles to the host cells of Dengue virus. The active *P. mauritianum* extract was found to contain

epigallocatechin gallate **[81]**, kaempferol **[82]**, and gallic acid **[15]** as depicted in Figure 2.13 (Clain *et al*., 2019).

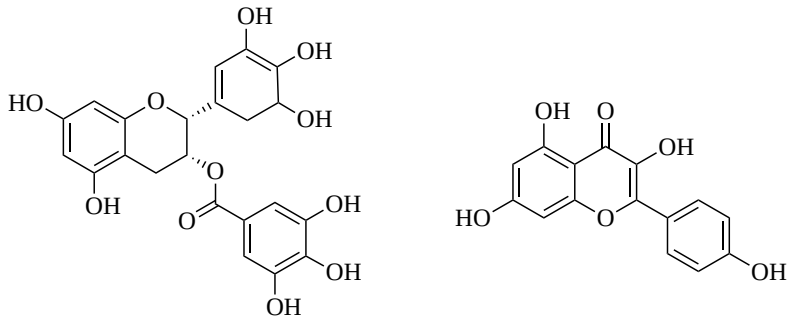

81 **82**

Figure 2.13: The structure of epigallocatechin gallate **[81]** and kaempferol **[82]**

In the study of structure-guided discovery of a novel non peptide inhibitor of dengue virus NS2B-NS3 Protease, Li and co-worker reported on compound 1,2,3,4-tetrahydro-*N*-[2-methyl-4-(4-methyl-1-piperazinyl)phenyl]-2-(phenylmethyl)-benzo[*b*][1,6]naphthyridine-10-carboxamide **[83]** (Figure 2.14) with a good DENV protease inhibitor and fulfilled the pockets of the binding site. The lone pair of compound **83** was able to accept hydrogen in the hydroxyl group of Tyr161 and form a tolerable interaction. Additionally, the benzene ring generated potent π-π stacking with amino acid residue. Besides, the pyrazol-3-one moiety also enhance the binding mode through a hydrogen bond between the carbonyl group amino acid residue (Li *et al.*, 2015).

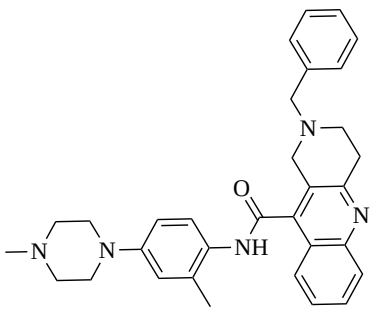

83

Figure 2.14: The structure of compound **83**

In conclusion, the presence of lone pair molecule such as, nitrogen will increase the possibility of hydrogen bond formation. Besides, the benzene ring will generated potent π-π stacking with amino acid residue. Hence, the synthesized compounds could be fit into the binding pocket of the NS2B/NS3 protease and lower the free energy of binding. Therefore, the inhibitory activity of the synthesized compounds will be increased.

CHAPTER 3

RESEARCH METHODOLOGY

3.1 Chemical and materials

The solvent, chemical and materials used were of analytical grades and used without undergoing further purification or distillation. All the apparatus used were washed with distilled water and rinsed with acetone to ensure the apparatus is clean and to avoid any impurities.

3.2 Characterization methods

3.2.1 Melting point

The melting point was determined by using Stuart Scientific SMP1 melting point apparatus with the temperature range of 50–300 °C at School of Chemical Sciences, Universiti Sains Malaysia.

3.2.2 Fourier-transform infrared (FTIR) spectroscopy

The IR spectra of the compounds were obtained using Frontier® FTIR-ATR spectrometer (PerkinElmer, England). The compounds were placed on the crystal top plate and analysed in the wavelength of 4000–650 cm^{-1}.

3.2.3 Nuclear magnetic resonance (NMR) spectroscopy

The 1D (^{1}H, ^{13}C, and DEPT-135) and 2D (COSY, and HMBC) NMR spectra were recorded using Bruker Avance 500 MHz spectrometers at School of Chemical Sciences, Universiti Sains Malaysia. The compounds (± 15 mg) were dissolved in deuterated solvent; deuterated dimethyl sulfoxide (DMSO-d_6), deuterated chloroform ($CDCl_3$) or deuterated methanol (CD_3OH) into NMR glass tube. The calculation of chemical shifts (δ, ppm) was refer to the TMS signal at 0.00 ppm, and the coupling constants were written in hertz (Hz).

3.2.4 Gas chromatography (GC) analysis

The *M. charantia* extract screening was carried out by Agilent 7890A system (Agilent, U.S.A) in School of Chemical Sciences, USM. The samples diluted with 1 mL of *n*-pentane and 1 µL of sample was injected on DB-5 column (30 × 0.25 mm, 0.25 µm film thickness). The injector and detector temperature were fixed at 270 °C and 280 °C, respectively. Pure helium gas was used as carrier gas at the flow rate of 1 mL/min. The oven temperature was programmed at 60 °C, increased to 280 °C with the heating rate of 5 °C/min and held for 10 minutes.

The oil analysis was carried out by using Shimadzu GC-2010 plus instrument (Shimadzu, Japan) equipped with Zebron capillary GC column ZB-Wax, 60 m × 0.25 mm × 0.25 mm at University of Lorraine, France. Pure helium gas was used as carrier gas, pressurized and flowed at 141.2 kPA and 11.7 mL/min respectively. Then, 1 µL of sample was injected into GC and the oil was separated using temperature programming, starting with 120 °C, held for 2 minutes, increased to 180 °C with

heating rate of 40 °C/ minutes, held for another 2 minutes before been heated to 220 °C with heating rate of 3 °C/ minutes, and held for 25 minutes.

3.2.5 Gas chromatography-mass spectrometry (GC-MS)

The GC-MS analysis for *M. charantia* extracts were performed using Perkin Elmer Clarus 600T system (PerkinElmer, England) which operated at 70eV with a mass range of m/z 50-500 at School of Chemical Sciences, USM. The injection was done on HP-5 semi-polar capillary column (30 m × 320 μm) with the same temperature programmed used in GC analysis.

3.2.6 Liquid chromatography - mass spectrometry (LC-MS)

The molecular mass of selected synthesized compounds was determined by Agilent Technologies 6224 TOF LC/MS spectrometer (Agilent, U.S.A) at School of Pharmaceutical Sciences, USM. Samples were prepared as solutions of 0.1 to 1.0 mL in HPLC grade acetonitrile. The measurements were carried out in the positive mode.

3.3 The studies of *M. charantia* fruits flesh and seed

The studies of *M. charantia* fruits flesh and seed are divided into two parts. First part involved the extraction of *M. charantia* seed oil using hydro distillation method and Aqueous Enzyme Extraction (AEE) method as well as the studies of its lignocellulosic biomass. The second part involved the preparation of *M. charantia* fruits pulp extract for anti-dengue screening. Figure 3.1 summarized the study framework.

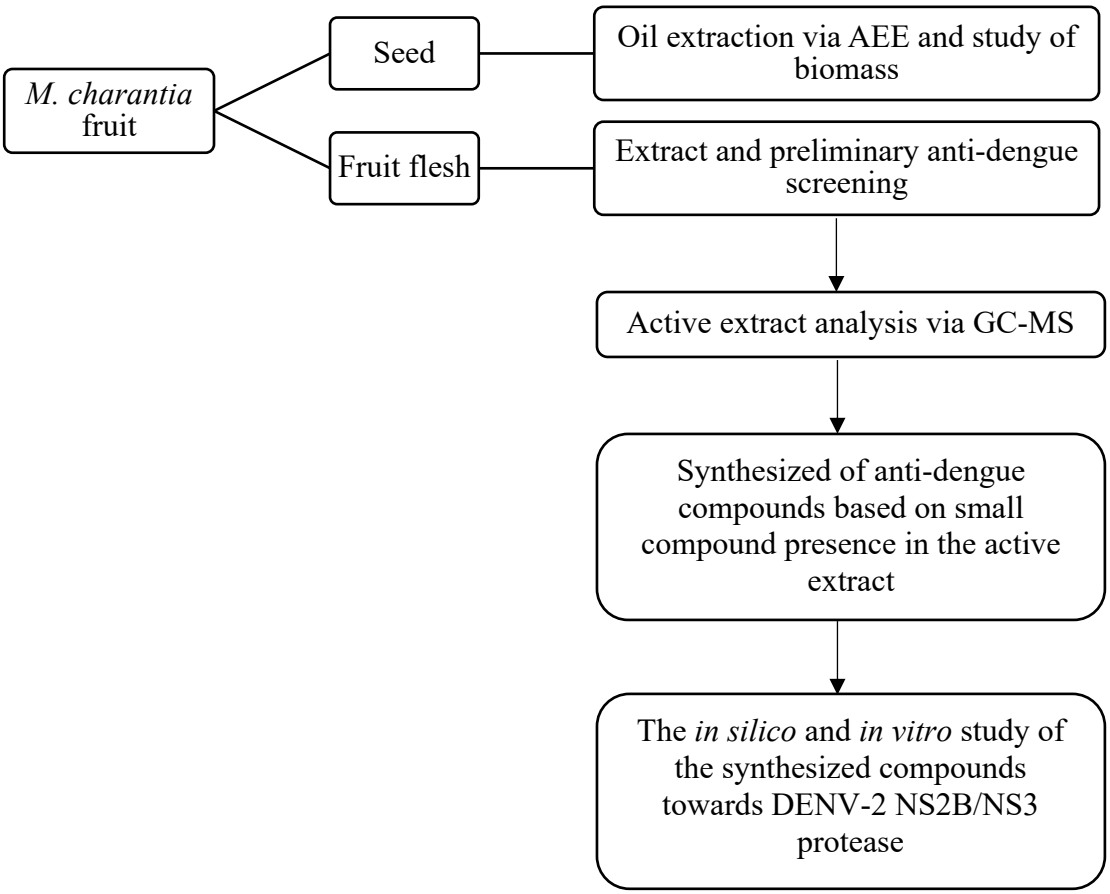

Figure 3.1: The summary of *M. charantia* fruits and seed study

The *M. charantia* fruits flesh underwent extraction via maceration to extract the active compounds in which possess the anti-dengue properties. After that, hemisynthesizes of pyrazolyl substituted benzylidene indanone derivatives will be carried out as a potent DENV-2 NS2B/NS3 protease inhibitor. Meanwhile, the oil of *M. charantia* seeds was extracted using AEE and the extracted free materials (the oil extraction waste) underwent further characterization to study the biochemical properties of the lignocellulosic biomass.

3.3.1 Sample preparation

The unripe *M. charantia* fruits were purchased from a vegetable farm located at Ara Kuda, Seberang Perai Utara, Penang, Malaysia between June to August 2015 (USM Herbarium: 11727, deposited by Syafinaz Bt Zainol on 14/09/2016). Only unripe and fresh fruits were selected for extraction. The fruits were washed thoroughly with tap water to remove any unwanted contamination and cut to separate the flesh with the seed. After that, the fruits (flesh) and seed were sun-dried at room temperature. The fruits and seed were turned over every 24 hours to ensure completely dried. The dried fruits and seed were grounded into small pieces before being kept in a dried polyethylene bags until further used.

3.3.1(a) PART 1: Aqueous enzyme extraction (AEE) of *M. charantia* seed oil

The AEE was performed to extract oil from the *M. charantia* seed according to the method as described by Muniglia *et al*. (2011)**.** The enzyme cocktails, HEL1 and X7 were blended in the Laboratoire D'ingénierie des Biomolécules (Nancy, France), which contained cellulase, betaglucosidase, endocellulase, exocellulase, arabinase, xylanase, galactanase, endopolygalacturonase, hemicellulase, proteinase, pectinase, and pectine methylesterase at different concentrations.

Initially, the freshly ground dried *M. charantia* seed were mixed with distilled water in a ratio of 1:4 into a pre-programmed bioreactor (Celligen Plus, New Brunswick Scientific, U.S.A) with continuous stirring. Then, the enzyme cocktails were added consecutively into the bioreactor once the temperature of the bioreactor reached 50 °C starting with HEL1 followed by X7 at their different ratios as tabulated in Table 3.1.

Table 3.1: Seed samples and their enzyme cocktail ratios.

Seed samples	Enzyme (%)/Seed weight (g)	
	HEL1	X7
M0	-	-
M1	5	-
M2	5	1.25
M3	5	2.5
M4	5	5

The reaction was left to carry on for four hours in the bioreactor followed by centrifugation (0.158 kilohertz, 20 minutes, 20 °C) to separate the products. The final products of this extraction process were: 1) oil, 2) seed residue, and 3) aqueous part. The oil and seed residue obtained was proceed for analysis via GC and identification of the seed lignocellulosic biomass respectively. The aqueous part was discarded.

3.3.1(a)(i) The analysis of *M. charantia* seed oil

The seed oil samples were initially derivatized to fatty acid methyl esters (FAMEs) using esterification process as described by Metcalfe and Schmitz (1961) before further analyses to identify their biochemical compositions using gas chromatography (GC). The polar properties of underivatized fatty acid normally lead to the formation of hydrogen bonding, which results in adsorption issue. Hence, reducing their polarity by derivatisation make them more amenable for analysis. Each derivatized oil (FAME) was analysed to identify its biochemical composition using flame ionisation detector gas chromatography.

3.3.1(a)(ii) The Soxhlet extraction of the seed residue

The dried seed residue was further extracted using Soxhlet extraction method to ensure all extractive components were removed prior the hydrolysis to determine their lignin and acid-soluble sugar contents. The presence of extractive components will hinder the hydrolysis process by cross-reacting with acid and condense to acid-insoluble components resulting in inaccurate analysis.

An amount of 50 g of each dried seed residue sample was loaded into an extraction thimble, which was placed into a Soxhlet extractor (Pyrex, U.S.A) fitted with a condenser (Pyrex, U.S.A) on an isomantle heater (Fisherbrand, U.S.A) to execute the Soxhlet extraction. Then, 250 mL of *n*-hexane was added into a 500 mL round bottom flask fixed to the Soxhlet extractor. The solvent was heated at 150 °C and began to evaporate. The condensate dripped into the reservoir containing the thimble. The solvent from the reservoir was poured into a round bottom flask once the solvent level reached the siphon. The process was continued for five hours. Then, n-hexane was evaporated using a rotary evaporator (Buchi, Switzerland). The final products of Soxhlet extraction process were: 1) extracted-free materials (EFM) and 2) extractive materials. The extractive materials were discarded and the EFM was weighed and kept for further analysis.

3.3.1(a)(iii) Determinations of lignin, soluble sugars, and uronic acid of EFM

An amount of 175 mg of each dried EFM sample was placed in a conical bottom centrifuge tube, and 1.5 mL of 72 % sulfuric acid was added dropwise. The mixture was placed into a water bath and heated at 30 ºC for one hour with periodical stirring using a glass rod. A volume of 42 mL of distilled water was added into the

mixture to achieve a concentration of 4 % sulfuric acid by mass. The mixture was then autoclaved at 121 ºC for one hour. The mixture was allowed to cool down to room temperature before being filtered. The filtrate was then diluted with 56.5 mL of distilled water in a 100 mL volumetric flask. The resulting solution was further analysed by high performance anion exchange chromatography with pulsed amperometry detection (HPAEC-PAD) (PerkinElmer, U.S.A) to determine its soluble sugar and uronic acid contents. The solid residue (lignin) was dried and weighed. The seed sample codes for soluble sugar and uronic acid analysis is tabulated in Table 3.2.

Table 3.2: Seed sample codes for acid soluble sugar analysis and their descriptions.

Sample codes	Enzyme (%)/Sample Weight	
	HEL1	X7
$M0_L$	-	-
$M1_L$	5	-
$M2_L$	5	1.25
$M3_L$	5	2.5
$M4_L$	5	5

Note: M refers to the EFM, which had undergone AEE. While, $_L$ refers to the soluble sugar and uronic acid sample of the EFM.

3.3.1(a)(iv) Determination of soluble sugar and uronic acid contents of EFM

The separation and quantification of soluble sugars and uronic acids of the EFM were carried out using HPAEC-PAD operating on Dionex ICS-3000 system, which consisted of a gradient pump SP, a passer AS, an electrochemical detector ED operating with a gold electrode, a reference electrode Ag/AgCl, and Chromeleon version 6.8 (Dionex Corp, USA). A Carbopac PA20 column (3 × 150 mm, Dionex) with a guard column (3 × 30 mm, Dionex) was used in the stationary phase. The mobile

phase was made of water, 250 mM NaOH in water, and 1 M NaOAc/20 mM NaOH in water. A diluted 46–48 % sodium hydroxide solution and anhydrous sodium acetate in ultrapure water were used as eluents.

The eluents were degassed with helium gas for 20 minutes before being injected. After each analysis, the column was flushed for 10 minutes with 250 mM NaOH solution and restored for 10 minutes to the initial conditions of the analysis. The samples were injected with an entire loop of 25 μm and the separations were carried out at 35 °C at a flow rate of 0.4 mL/min. The pulse sequence for pulsed amperometry detection consisted of potentials of +100 mV (0–200 ms), +100 mV integration (200–400 ms), +100 mV (400–410 ms), -2000 mV (410–420 ms), +600 mV (430 ms), and -100 mV (440–500 ms).

3.3.1(a)(v) Hemicellulose extraction from EFM

Initially, the EFM was subjected to bleaching process to produce holocellulose. Sodium chlorite was used as the bleaching agent due to its moderately strong oxidation properties. The bleaching process was conducted by milling 1.5 g of each dried treated EFM sample into 0.05 mm size before being dispersed slowly into 125 mL deionized water in a 250 mL round bottom flask. Acetic acid glacial, 1 mL was added into the mixture with an additional 1 g of sodium chlorite. The mixture was refluxed at 80 °C for two hours. Then, another 1 mL of acetic acid glacial and 1 g of sodium chlorite were added, consecutively into the reaction mixture with continuous stirring in the same conditions for two hours. The process was repeated until the colour of the residue turned to white to ensure that the bleaching process was completed. The reaction mixture was filtered and washed thoroughly with deionized water. The holocellulose

obtained was collected and dried overnight in a fume hood, which was then further reprecipitated into hemicellulose.

An amount 200 mL of 2 % w/v sodium hydroxide aqueous solution was added into 10 g of each holocellulose sample in a round bottom flask and stirred for two hours at 80 °C. Then, an additional of 200 mL of 2 % w/v sodium hydroxide aqueous solution was added into the reaction mixture and stirred for another two hours. The mixture pH was adjusted to 5–6 by adding 20 % w/v acetic acid solution. The reprecipitation process of the mixture was repeated using 800 mL ethanol. The precipitate formed was recovered by centrifugation. The percentage yield of hemicellulose was calculated and analysed using Fourier-transform infrared (FTIR) spectroscopy as well as size exclusion chromatography (SEC).

3.3.1(a)(vi) The SEC analysis of hemicellulose

The molecular weight distribution of hemicellulose was determined by SEC. The analysis was performed using a Hewlett–Packard 1090 series HPLC system consisting of an autosampler, a UV detector, and three columns of Styragel HR1, HR3, and HR4 (Waters Inc.) linked in series using tetrahydrofuran (THF) as the eluent. The hemicellulose was dissolved in 1 mg/mL of THF, and the solution was filtered through a 0.45 mm filter. Then, 20 mL of the filtered solution was injected into the system and was detected using a UV detector at 280 nm. The data were collected using Agilent ChemStation rev. A.10.01 and analysed using Agilent GPC Addon rev. A.02.02 software (Agilent, U.S.A).

3.3.1(b) PART 2: Preparation of *M. charantia* fruit flesh extract

The crushed dried fruits flesh (0.5 kg) were then exhaustively extracted by maceration sequentially in *n*-hexane, ethyl acetate and methanol twice in triplicate for 7–14 days at room temperature (25–30 °C) in fume hood. The mixtures were shaken and stirred on a daily basis. The extracts were then filtered using Whatman filter paper No. 1 (Whatman, England) and the solvent was removed by rotary evaporator (Büchi, Germany) under reduced pressure. The extract was then kept refrigerated in a sealed sample bottle before proceed with anti-dengue screening and the most active extract will underwent GC-MS analysis.

3.3.2 Anti-dengue testing of *M. charantia* fruits flesh extract

The *in vitro* assays testing for *M. charantia* fruits flesh extracts were performed following the method by Yusof *et al.* (2000). An enzymatic reaction mixture with a total volume of 100 µL with the concentration of 200 ppm was prepared in black 96 well plates as presented in Figure 3.2. Each well in the black 96 well plates consist 94.9 µL of Tris-HCl buffer solution at pH 8.5, 3.1 µL of the enzyme, and 1 µL of extract (200 mg/L in DMSO). The mixtures were incubated and shook at 37 °C for 10 minutes. Then, 1 µL substrate 10 mM in DMSO (Peptide Institute, Japan) was added into the mixture to initiate the reaction. The mixture was then incubated and shook for another 60 minutes at 37 °C using Ambient shaker incubator SI-50 (Protech, Malaysia). The assay was triplicated. The extract with the most anti-dengue activity will be further analysed using GC-MS to identify it compositions.

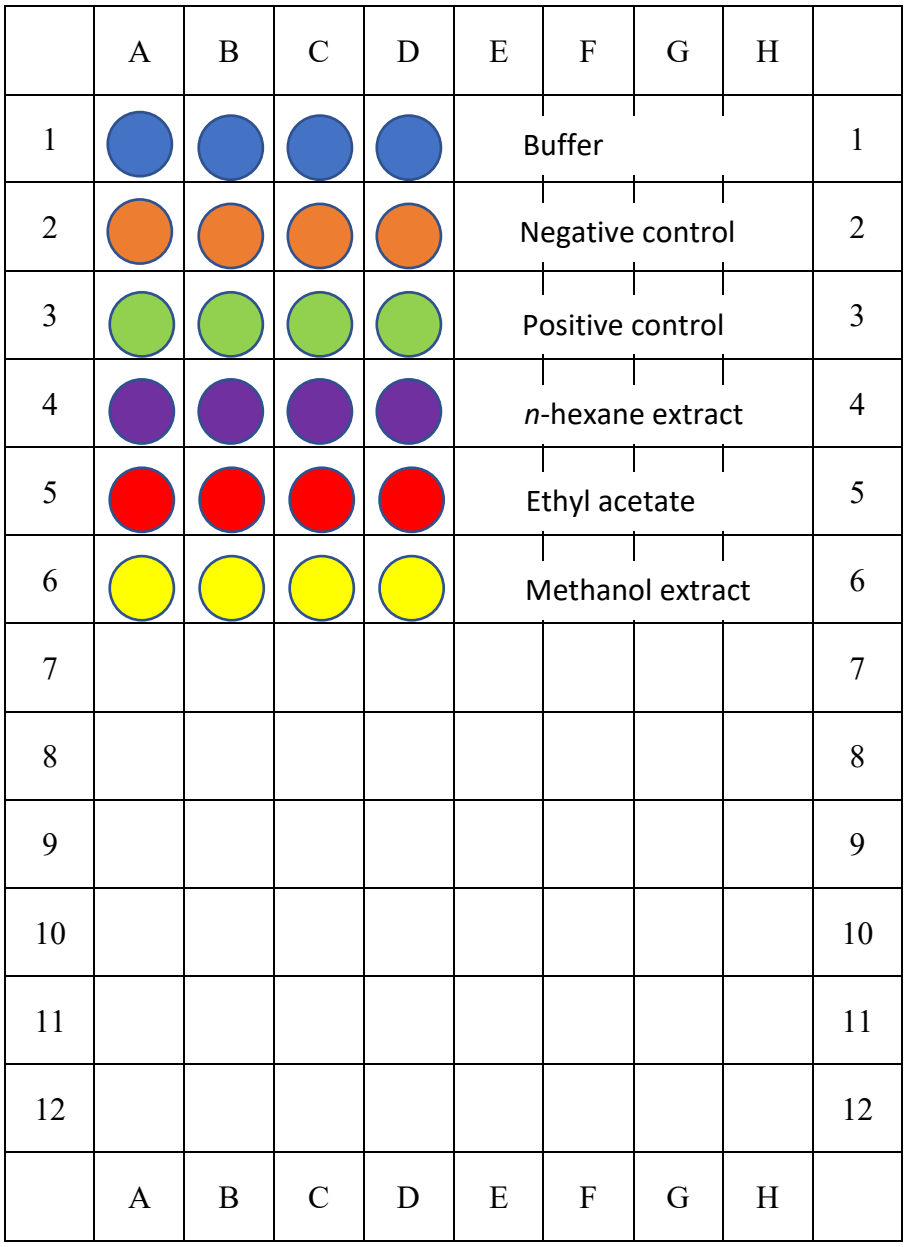

Figure 3.2: The DENV-2 NS2B/NS3 protease assay procedure using *M. charantia* fruit extract.

3.4 The synthesis of pyrazolyl substituted benzylidene indanone derivatives

The reaction summary was depicted as Scheme 3.1 below.

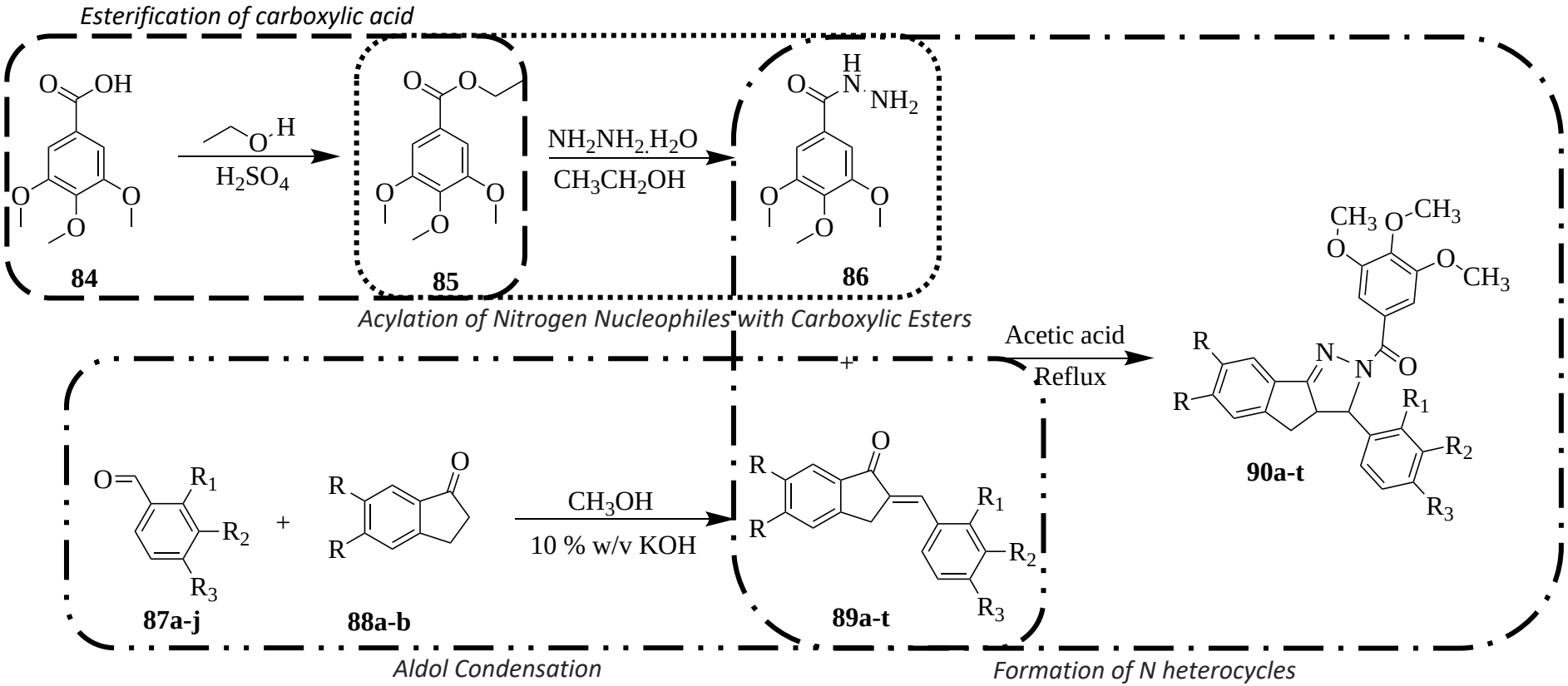

Scheme 3.1: The synthesis of pyrazolyl substituted benzylidene indanone derivatives

3.4.1 The synthesis of ethyl 3,4,5-trimethoxybenzoate, 85 and 4,5-trimethoxybenzohydrazide, 86

The commercially available 3,4,5-trimethoxy benzoic acid **[84]**, undergo esterification using sulfuric acid and ethanol to produce ethyl 3,4,5-trimethoxybenzoate **[85]** (Li *et al.*, 2017 and Schejbal *et al.*, 2014). The reaction scheme was illustrated in Scheme 3.2 below.

Benzoic acid (0.1 mmol) was added in ethanol (1.0 mmol) with presence of sulfuric acid (0.01 mmol). The solution was heated under reflux. After 3 h, the reaction was monitored by TLC using ethyl acetate and hexane (3:7) system. Stirring was continued for about 12 hours or until the TLC indicated the completion of reaction. The excess ethanol was removed by using rotary evaporator. The resulting solution was then mixed with 10 mL ethyl acetate and sodium chloride solution (10 % w/v.). After that, the organic phase was separated by using separating funnel. The excess solvent was removed from the organic phase using rotary evaporator. The precipitated was dried under vacuum to obtained compound **85**. Chemical structures of the compound were confirmed by ^{1}H NMR, ^{13}C NMR, and FTIR.

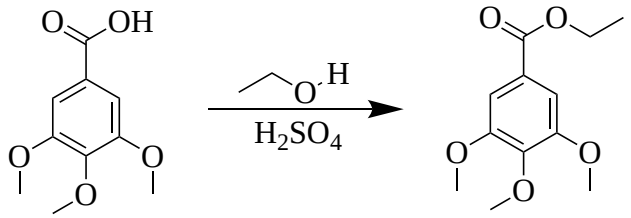

84 **85**

Scheme 3.2: The synthesis of ethyl 3,4,5-trimethoxybenzoate **[85]** intermediate.

The synthesized compound **85** was further reacted with hydrazine monohydrate to obtain 3,4,5-trimethoxybenzohydrazide [**86]**. Compound **85** (1.00 mmol) was dissolved in 10 mL ethanol and stirred for 30 minutes. Then, hydrazine

monohydrate (5.00 mmol) was added into the solution and stirred overnight until a white precipitate was formed (Scheme 3.3). The precipitate **[86]** was filtered and washed using cold ethanol (Kamal *et al.*, 2014). Chemical structures of the compound were confirmed by ^{1}H NMR, and ^{13}C NMR,

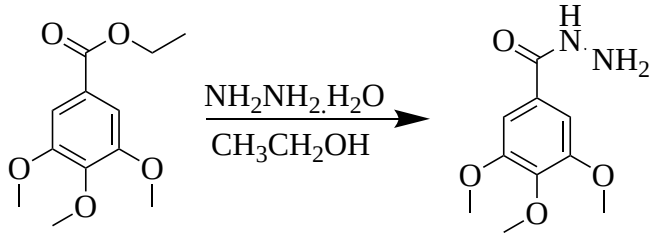

85 **86**

Scheme 3.3: The synthesis of 3,4,5-trimethoxybenzohydrazide **[86]**.

3.4.1(a) Ethyl 3,4,5-trimethoxybenzoate, 85

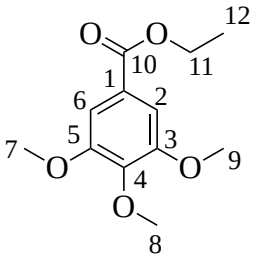

85

Colour: Colourless crystal; Weight: 3.87 g, 85.99 % (yield); mp. 50–53 °C; Molecular weight: 240.0997 $gmol^{-1}$; $C_{12}H_{16}O_5$; FTIR ATR (V_{max}/cm^{-1}): 2940 (C_{sp}^{3}-H), 1715 (C=O ester), 1181 (C-O, ester); ^{1}H NMR (500 MHz, DMSO-d_6): δ_H, ppm, 1.3 (3H, t, J = 7.09, CH_3), 3.7 (3H, s, OCH_3), 3.8 (6H, s, OCH_3), 4.3 (2H, q, J = 7.09, CH_2), 7.2 (2H, s, CH). ^{13}C NMR (125 MHz, DMSO-d_6): δ_C, ppm, 14.6 (C12), 56.5 (C7, C9), 60.6 (C11), 61.3 (C8), 106.9 (C2, C6), 125.5 (C1), 142.2 (C4), 153.2 (C3, C5), 165.9 (C10).

3.4.1(b) 3,4,5-trimethoxybenzohydrazide, 86

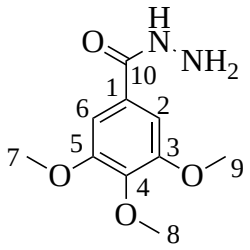

86

Colour: Light brown crystalline solid; Weight: 2.41 g, 85.31 % (yield); mp. 157–160 °C; Molecular weight: 226.0953 $gmol^{-1}$; $C_{10}H_{14}N_2O_4$; FTIR ATR (V_{max}/cm^{-1}): 3364 (N-H), 3319 (N-H), 1659 (C=O), 1385(C-N); ^1H NMR (500 MHz, DMSO-d_6): δ_H, ppm, 3.7 (6H, s, OCH_3), 3.8 (3H, s, OCH_3), 4.5 (2H, s, NH_2), 7.1 (2H, s, CH), 9.7 (1H, s, NH); ^{13}C NMR (125 MHz, DMSO-d_6): δ_C, ppm, 56.1 (C7, C9), 60.5 (C8), 104.9 (C2, C6), 128.8 (C1), 140.2 (C4), 152.1 (C3, C5), 165.9 (C10).

3.4.2 The synthesis of benzylidene indanone derivatives, 89a-t

An indanone (2.0 mmol) **[87a-b]** was dissolved and stirred in 10 % w/v of potassium hydroxide (KOH) in methanol for about 15 minutes. After that, a different type of aromatic aldehyde (2.0 mmol) **[88a-b]** was added into the solution and the reaction mixture was stirred for an hour or until the reaction was completed under reflux (Korotchenko *et al.*, 2014 & Ishimaru *et al.*, 2008). Scheme 3.4 depicted the reaction scheme to synthesis the benzylidene indanone derivatives **[89a-t]**. The reaction was monitored using TLC until it completed. The reaction mixture pH was then adjusted to 5–6 by adding 10 % w/v hydrochloric acid solution. The precipitated was filtered using vacuum filtration, washed using cold methanol and dried under vacuum. The synthesized compounds were further recrystallized using single-solvent

recrystallization technique. The synthesized compounds were then undergone characterization analysis to determine its physicochemical properties.

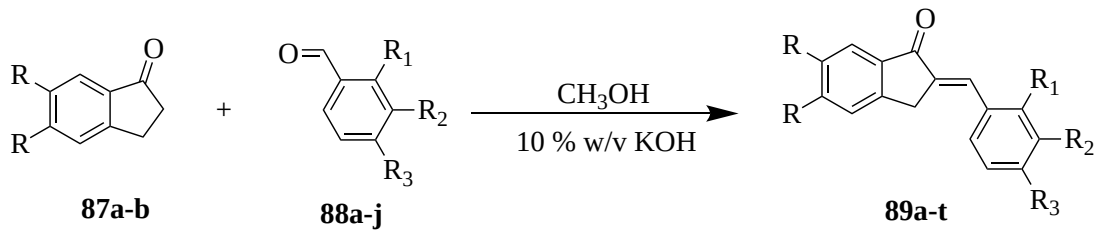

87a-b **88a-j** **89a-t**

Where **87a** = R = H
89a: R_1 = H; R_2 = H; R_3 = H
89b: R_1 = H; R_2 = H; R_3 = OCH_3
89c: R_1 = H; R_2 = H; R_3 = CH_3
89d: R_1 = H; R_2 = H; R_3 = Cl
89e: R_1 = H; R_2 = H; R_3 = $CH(CH_3)_2$
89f: R_1 = H; R_2= H; R_3 = $N(CH_3)_2$
89g: R_1 = H; R_2 = H; R_3 = NC_4H_8O
89h: R_1 = H; R_2 = H; R_3 = NC_4H_{10}
89i: R_1 = OCH_3; R_2 = H; R_3 = OCH_3
89j: R_1 = H; R_2 = NO_2; R_3 = OCH_3

Where **87b** = R = OCH_3
89k: R_1 = H; R_2 = H; R_3 = H
89l: R_1 = H; R_2 = H; R_3 = OCH_3
89m: R_1 = H; R_2 = H; R_3 = CH_3
89n: R_1 = H; R_2 = H; R_3 = Cl
89o: R_1 = H; R_2 = H; R_3 = $CH(CH_3)_2$
89p: R_1 = H; R_2= H; R_3 = $N(CH_3)_2$
89q: R_1 = H; R_2 = H; R_3 = NC_4H_8O
89r: R_1 = H; R_2 = H; R_3 = NC_4H_{10}
89s: R_1 = OCH_3; R_2 = H; R_3 = OCH_3
89t: R_1 = H; R_2 = NO_2; R_3 = OCH_3

Scheme 3.4: The synthesis of benzylidene indanone derivatives.

3.4.2(a) *(E)*-2-benzylidene-1-indanone, 89a

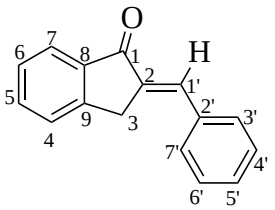

Colour: White solid; Weight: 230.00 mg, 72.21 % (yield); mp. 105–109 °C; Molecular weight: 220.2642 $gmol^{-1}$; FTIR ATR (V_{max}/cm^{-1}): 2910 (C_{sp}^3-H), 1693 (C=O ketone), 1576 (C=C aromatic); ^1H NMR (500 MHz, DMSO-d_6): δ_H, ppm,), 4.14 (s, 2H, ArH_2), 7.45–7.53 (m, 5H, ArH), 7.56 (s, 1H, H-1', =CH-Ar), 7.68–7.74 (m, 3H, ArH), 7.79 (d, 1H, J = 7.5, ArH); ^{13}C NMR (125 MHz, DMSO-d_6): δ_C, ppm, 32.38 (C-3), 124.10 (C-1'), 127.19 (C-7), 128.19 (C-5), 129.49 (C-6, C-4',

C-6'), 130.31 (C-5'), 131.23 (C-4, C-3', C-7'), 133.30 (C-2'), 135.42 (C-2), 135.59 (C-8), 137.65 (C-9), 193.56 (C-1).

3.4.2(b) *(E)*-5'-methoxybenzylidene-1-indanone, 89b

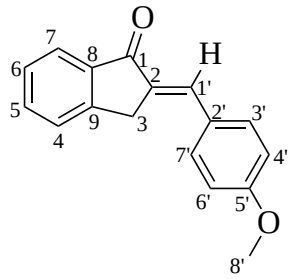

Colour: White solid; Weight: 434.40 mg, 86.78 % (yield); mp. 138–140 °C; Molecular weight: 250.2899 $gmol^{-1}$; FTIR ATR (V_{max}/cm^{-1}): 2914 (C_{sp}^3-H), 1694 (C=O ketone), 1573 (C=C aromatic), 1244 (C-O); ^{1}H NMR (500 MHz, DMSO-d_6): δ_H, ppm,), 3.82 (s, 3H, -OCH_3), 4.05 (s, 2H, ArH_2), 7.07 (d, 2H, J=9.0, ArH), 7.45 (t, 1H, ArH), 7.50 (s, 1H, =CH-Ar), 7.66–7.71 (m, 2H, ArH), 7.76 (s, 1H, ArH), 7.77 (s, 1H, ArH), 7.78 (s, 1H, ArH); ^{13}C NMR (125 MHz, DMSO-d_6): δ_C, ppm, 32.37 (C-3), 55.83 (C-8'), 115.04 (C-4', C-6'), 123.93 (C-1'), 127.08 (C-7), 127.98 (C-5), 128.07 (C-6), 133.02 (C-4), 133.15 (C-3', C-7'), 133.30 (C-2'), 135.06 (C-2), 137.94 (C-8), 150.30 (C-9), 161.11 (C-5'), 193.71 (C-1).

3.4.2(c) (E)-5'-methylbenzylidine-1-indanone, 89c

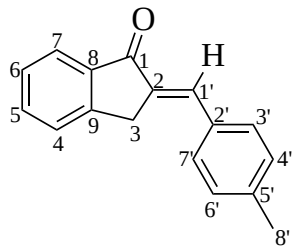

Colour: White solid; Weight: 439.00 mg, 93.68 % (yield); mp. 137–139 °C; Molecular weight: 234.2905 gmol^{-1}; FTIR ATR (V_{max}/cm^{-1}): 2916 (C_{sp}^3-H), 1694 (C=O ketone), 1574 (C=C aromatic); ^{1}H NMR (500 MHz, DMSO-d_6): δ_H, ppm, 2.42 (s, 3H, $ArCH_3$), 3.99 (s, 2H, ArH_2), 7.28 (d, 2H, J=8.0, ArH), 7.31–7.38 (m, 2H, ArH), 7.43 (t, 1H, J=7.4, ArH), 7.51–7.59 (m, 2H, ArH), 7.63 (s, 1H, =CH-Ar) 7.81 (d, 1H, J=7.5); ^{13}C NMR (125 MHz, DMSO-d_6): δ_C, ppm, 2.104 (C-8'), 35.37 (C-3), 123.60 (C-1'), 124.11 (C-7), 124.93 (C-5), 125.09 (C-6), 126.90 (C-4), 128.78 (C-4', C-6'), 131.27 (C-3', C-7'), 132.45 (C-2'), 134.89 (C-2), 139.50 (C-8), 141.85 (C-5'), 147.30 (C-9), 193.35 (C-1).

3.4.2(d) *(E)*-5'-chlorolbenzylidine-1-indanone, 89d

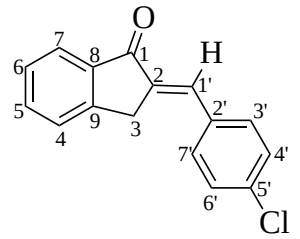

Colour: White solid; Weight: 481.30 mg, 94.48 % (yield); mp. 137–139 °C; Molecular weight: 254.7094 gmol^{-1}; FTIR ATR (V_{max}/cm^{-1}): 2913 (C_{sp}^3-H), 1694 (C=O ketone), 1581 (C=C aromatic), 865 (C-Cl); ^{1}H NMR (500 MHz, DMSO-d_6): δ_H, ppm, 3.85 (s, 2H, ArH_2), 7.40–7.44 (m, 2H, ArH), 7.49 (d, 2H, J=7.5, ArH), 7.49 (d, 2H, J=7.5, ArH), 7.52 (t, 1H, J=7.0, ArH), 7.56 (s, 1H, =CH-Ar), 7.76 (d, 1H,

J=7.5, ArH); ^{13}C NMR (125 MHz, DMSO-d_6): δ_C, ppm, 34.44 (C-3), 123.02 (C-1'), 123.98 (C-7), 124.52 (C-5), 125.35 (C-6), 126.12 (C-4), 129.58 (C-4', C-6'), 130.64 (C-3', C-7'), 132.21 (C-2'), 134.70 (C-2), 137.45 (C-5'), 140.39 (C-8), 147.41 (C-9), 194.44 (C-1).

3.4.2(e) *(E)*-2-(5'-isopropylbenzylidene)-1-indanone, 89e

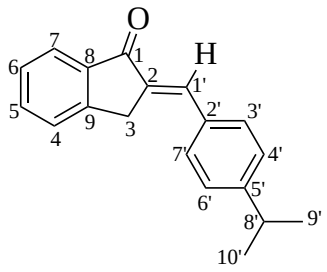

Colour: Cream solid; Weight: 340.40 mg, 64.87 % (yield); mp. 134–137 °C; Molecular weight: 262.3431 gmol^{-1}; FTIR ATR (V_{max}/cm^{-1}): 2914 (C_{sp}^3-H), 1692 (C=O ketone), 1575 (C=C aromatic); ^{1}H NMR (500 MHz, DMSO-d_6): δ_H, ppm, 1.24 (d, 6H, J=6.9, -CH_3), 2.92 (m, 1H, ArCH<), 4.00 (s, 2H, ArH_2), 7.28 (s, 2H, ArH), 7.37 (d, 2H, J=8.3, ArH), 7.52 (s, 1H, =CH-Ar), 7.73 (d, 1H, J=8.0, ArH), 7.77–7.69 (m, 3H, ArH); ^{13}C NMR (125 MHz, DMSO-d_6): δ_C, ppm, 24.11 (C-9', C-10'), 32.10 (C-8'), 33.82 (C-3), 121.93 (C-1'), 124.12 (C-7), 125.31 (C-5), 126.87 (C-4), 127.47 (C-4', C-6'), 130.54 (C-6), 131.16 (C-3', C-7'), 131.55 (C-2'), 134.06 (C-2), 135.49 (C-8), 145.85 (C-5'), 149.85 (C-9), 194.27 (C-1).

3.4.2(f) *(E)*-2-(5'-dimethylaminobenzylidene)-1-indanone, 89f

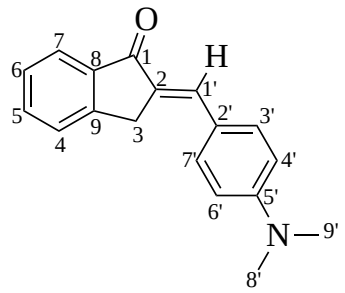

Colour: Yellow solid; Weight: 463.30 mg, 87.95 % (yield); mp. 164–168 °C; Molecular weight: 263.3313 $gmol^{-1}$; FTIR ATR (V_{max}/cm^{-1}): 2911 (C_{sp}^3-H), 1696 (C=O ketone), 1575 (C=C aromatic), 1339 (C-H); ^{1}H NMR (500 MHz, DMSO-d_6): δ_H, ppm, 3.02 (s, 6H, N-CH_3), 4.03 (s, 2H, ArH_2), 6.80 (d, 2H, J=9.0, ArH), 7.51 (s, 1H, =CH-Ar), 7.63 (d, 2H, J=8.5, ArH), 7.67–7.68 (m, 3H, ArH), 7.74 (d, 1H, J=7.6, ArH); ^{13}C NMR (125 MHz, DMSO-d_6): δ_C, ppm, 32.61 (C-3), 112.46 (C-4', C-6'), 122.68 (C-1'), 123.67 (C-7), 126.99 (C-5), 127.95 (C-4), 129.95 (C-6), 133.19 (C-3', C-7'), 134.56 (C-2'), 138.47 (C-2), 145.53 (C-5'), 149.98 (C-8), 151.79 (C-9), 193.39 (C-1).

3.4.2(g) *(E)*-2-[5'-(4"-morpholinobenzylidene)]-1-indanone, 89g

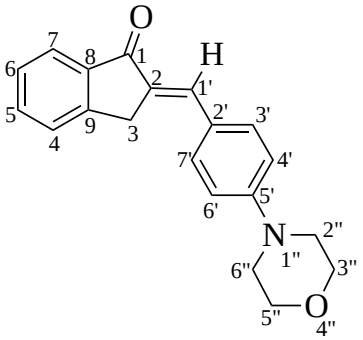

Colour: Yellow solid; Weight: 571.80 mg, 93.62 % (yield); mp. 179–190 °C; Molecular weight: 305.3677 $gmol^{-1}$; FTIR ATR (V_{max}/cm^{-1}): 2915 (C_{sp}^3-H), 1694 (C=O ketone), 1581 (C=C aromatic), 1170 (C-O-C); ^{1}H NMR (500 MHz, DMSO-d_6):

δ_H, ppm, 3.43 (d, 4H, J=5.0, ArH_2), 3.83 (d, 4H, J=5.0, ArH_2), 4.05 (s, 2H, ArH_2), 6.77 (d, 2H, J=7.5, ArH), 7.20 (d, 2H, J=8.0, ArH), 7.54 (s, 1H, =CH-Ar), 7.74 (d, 1H, J=8.0, ArH), 7.81–7.83 (m, 3H, ArH); ^{13}C NMR (125 MHz, DMSO-d_6): δ_C, ppm, 34.24 (C-3), 48.18 (C-2", C-6"), 66.62 (C-3", C-5"), 112.16 (C-1'), 123.86 (C-7), 125.60 (C-5), 127.08 (C-4), 128.01 (C-4', C-6'), 130.54 (C-6), 131.88 (C-3', C-7'), 132.26 (C-2'), 133.60 (C-2), 139.50 (C-8), 148.53 (C-5'), 150.80 (C-9), 194.09 (C-1).

3.4.2(h) *(E)*-2-(5'-piperidinylbenzylidene)-1-indanone, 89h

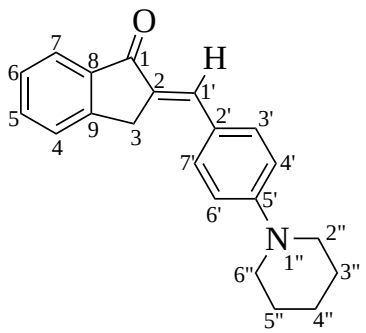

Colour: Cream solid; Weight: 550.33 mg, 90.69 % (yield); mp. 178–181 °C; Molecular weight: 303.3946 gmol^{-1}; FTIR ATR (V_{max}/cm^{-1}): 2917 (C_{sp}^3-H), 1692 (C=O ketone), 1574 (C=C aromatic); ^{1}H NMR (500 MHz, DMSO-d_6): δ_H, ppm, 1.64–1.66 (m, 1H, ArH), 1.71 (d, 4H, J=5.0, ArH_2), 3.39 (d, 4H, J=5.0, ArH_2), 3.83 (s, 2H, ArH_2), 7.51 (s, 1H, =CH-Ar), 7,62 (d, 2H, J=9.0, ArH), 7.67–7.69 (m, 3H, ArH); ^{13}C NMR (125 MHz, DMSO-d_6): δ_C, ppm, 24.44 (C-4"), 25.38 (C-3", C-5"), 32.58 (C-3), 48.50 (C-2", C-6"), 114.85 (C-1'), 123.73 (C-7), 125.99 (C-5), 127.03 (C-4), 127.99 (C-4', C-6'), 130.76 (C-6), 133.15 (C-3', C-7'), 134.12 (C-2'), 134.69 (C-2), 138.32 (C-8), 150.06 (C-5'), 152.30 (C-9), 193.48 (C-1).

3.4.2(i) *(E)*-2-(3',5'-dimethoxybenzylidene)-1-indanone, 89i

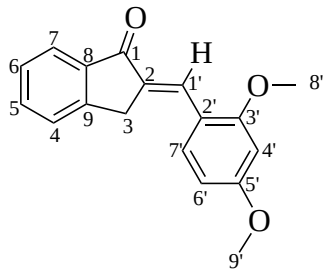

Colour: Yellow solid; Weight: 471.64 mg, 84.12 % (yield); mp. 181–189 °C; Molecular weight: 280.3156 $gmol^{-1}$; FTIR ATR (V_{max}/cm^{-1}): 2915 (C_{sp}^3-H), 1693 (C=O ketone), 1610 (C=C aromatic), 1238 (C-O); ^{1}H NMR (500 MHz, DMSO-d_6): δ_H, ppm, 3.86 (s, 3H, -OCH_3), 3.91 (s, 3H, -OCH_3), 4.05 (s, 2H, ArH_2), 6.68–6.69 (m, 3H, ArH), 7.53 (s, 1H, =CH-Ar), 7.75–7.77 (m, 3H, ArH), 7.88–7.90 (m, 2H, ArH); ^{13}C NMR (125 MHz, DMSO-d_6): δ_C, ppm, 37.01 (C-3), 56.01 (C-9'), 56.38 (C-8'), 96.27 (C-4'), 109.15 (C-6'), 118.17 (C-1'), 123.60 (C-7), 125.90 (C-4), 128.67 (C-5), 130.71 (C-7'), 133.60 (C-6), 139.15 (C-2'), 141.33 (C-2), 145.36 (C-8), 148.33 (C-9), 156.63 (C-3'), 161.01 (C-5'), 193.87 (C-1).

3.4.2(j) *(E)*-2-(4'-nitro-5'methoxybenzylidene)-1-indanone, 89j

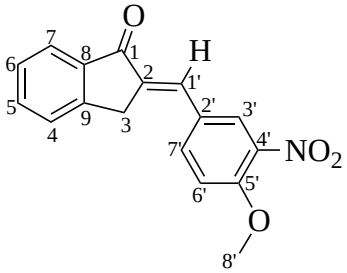

Colour: Cream solid; Weight: 494.70 mg, 83.74 % (yield); mp. 189–191 °C; Molecular weight: 295.2876 $gmol^{-1}$; FTIR ATR (V_{max}/cm^{-1}): 2914 (C_{sp}^3-H), 1694 (C=O ketone), 1578 (C=C aromatic), 1507(N-O), 1240 (C-O); ^{1}H NMR (500 MHz, DMSO-d_6): δ_H, ppm, 3.91 (s, 3H, -OCH_3), 4.08 (s, 2H, ArH_2), 7.34–7.46 (m, 2H, ArH),

7.48 (s, 1H, =CH-Ar), 7.68–7.71 (m, 4H, ArH), 8.28 (s, 1H, ArH); ^{13}C NMR (125 MHz, DMSO-d_6): δ_C, ppm, 36.46 (C-2), 56.76 (C-8'), 115.93 (C-6'), 119.70 (C-1'), 123.60 (C-7), 125.90 (C-4), 127.30 (C-5), 129.33 (C-4'), 130.21 (C-3'), 131.11 (C-7'), 132.33 (C-6), 140.83 (C-2'), 142.65 (C-2), 146.49 (C-8), 148.13 (C-9), 157.36 (C-5'), 194.88 (C-1).

3.4.2(k) *(E)*-2-benzylidine-5,6-dimethoxy-1-indanone, 89k

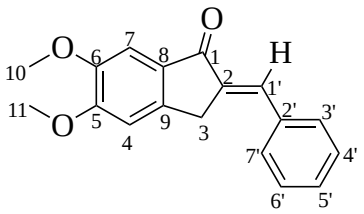

Colour: Light yellow solid; Weight: 238.00 mg, 84.90 % (yield); mp. 178–184 °C; Molecular weight 280.3156 gmol^{-1}; FTIR ATR (V_{max}/cm^{-1}): 2915 (C_{sp}^3-H), 1693 (C=O ketone), 1581 (C=C aromatic), 1189 (C-O); ^{1}H NMR (500 MHz, DMSO-d_6): δ_H, ppm, 3.79 (s, 6H, -OCH_3), 3.91 (s, 2H, ArH_2), 6.71 (s, 1H, ArH), 7.15 (s, 1H, ArH), 7.25–7.45 (m, 4H, ArH), 7.58 (s, 1H, =CH-Ar); ^{13}C NMR (125 MHz, DMSO-d_6): δ_C, ppm, 37.86 (C-3), 57.11 (C-10, C-11), 101.63 (C-7), 108.45 (C-4), 114.81 (C-1'), 126.81 (C-4', C-6'), 127.57 (C-3', C-7'), 129.81 (C-5'), 131.96 (C-2'), 134.88 (C-9), 135.77 (C-8), 136.87 (C-2), 155.30 (C-5), 150.30 (C-6), 191.54 (C-1).

3.4.2(l) *(E)*-(5'-methoxybenzylidene)-5,6-dimethoxy-1-indanone, 89l

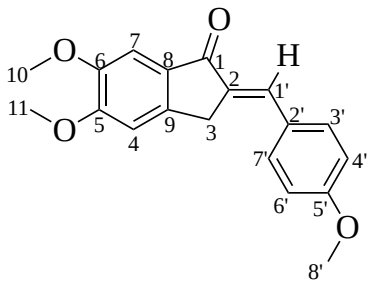

Colour: Light yellow solid; Weight: 292.60 mg, 94.28 % (yield); mp. 210–216 °C; Molecular weight 310.3413 $gmol^{-1}$; FTIR ATR (V_{max}/cm^{-1}): 2914 (C_{sp}^3-H), 1694 (C=O ketone), 1628 (C=C aromatic), 1210 (C-O); ^{1}H NMR (500 MHz, DMSO-d_6): δ_H, ppm, 3.79 (s, 6H, -OCH_3), 3.87 (s, 3H, -CH_3), 3.92 (s, 2H, ArH_2), 7.02 (s, 1H, ArH), 7.04 (s, 1H, ArH), 7.17 (d, 2H, J=7.1), 7.53 (s, 1H, =CH-Ar), 7.68 (d, 2H, J=8.2, ArH); ^{13}C NMR (125 MHz, DMSO-d_6): δ_C, ppm 32.01 (C-3), 55.80 (C-8'), 56.10 (C-10), 56.44 (C-11), 104.94 (C-7), 108.58 (C-4), 115.03 (C-4', C-6'), 128.12 (C-1'), 130.52 (C-2'), 131.66 (C-8), 132.86 (C-3', C-7'), 133.81 (C-9), 145.52 (C-2), 149.72 (C-6), 155.62 (C-5), 160.84 (C-5'), 192.64 (C-1).

3.4.2(m) *(E)*-(5'-methylbenzylidine)-5,6-dimethoxy-1-indanone, 89m

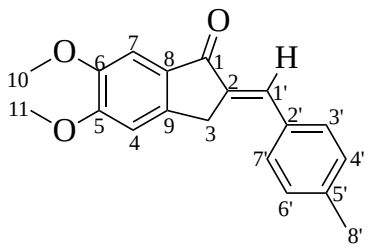

Colour: White solid; Weight: 245.40 mg, 83.37 % (yield); mp. 198–210 °C; Molecular weight 294.3419 $gmol^{-1}$; FTIR ATR (V_{max}/cm^{-1}): 29147(C_{sp}^3-H), 1695 (C=O ketone), 1574 (C=C aromatic), 1223 (C-O); ^{1}H NMR (500 MHz, DMSO-d_6): δ_H, ppm, 2.36 (s, 3H, $ArCH_3$), 3.36 (s, 2H, ArH_2), 3.90 (s, 3H, -OCH_3), 3.97 (s, 3H,

-OCH_3), 7.20 (s, 1H, ArH), 7.21 (s, 1H, ArH), 7.30 (d, 2H, J=6.9, ArH), 7.58 (s, 1H, =CH-Ar), 7.63 (d, 2H, J=8.2, ArH); ^{13}C NMR (125 MHz, DMSO-d_6): δ_C, ppm, 21.49 (C-8'), 32.09 (C-3), 56.10 (C-10), 56.44 (C-11), 104.98 (C-7), 108.50 (C-4), 130.09 (C-4', C-6'), 130.50 (C-2'), 131.01 (C-3', C-7'), 131.56 (C-8), 132.82 (C-9), 135.37 (C-2), 139.92 (C-1'), 145.49 (C-5'), 149.76 (C-6), 155.68 (C-5), 192.35 (C-1).

3.4.2(n) *(E)*-(5'-chlorobenzylidine)-5,6-dimethoxy-1-indanone, 89n

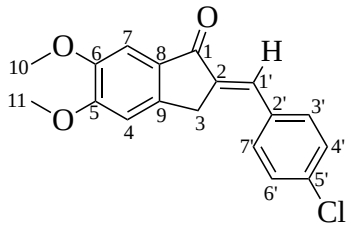

Colour: Cream solid; Weight: 184.50 mg, 78.62 % (yield); mp. 178–181 °C; Molecular weight 314.7608 gmol^{-1}; FTIR ATR (V_{max}/cm^{-1}): 2915 (C_{sp}^3-H), 1693 (C=O ketone), 1574 (C=C aromatic), 865(C-Cl); ^{1}H NMR (500 MHz, DMSO-d_6): δ_H, ppm, 3.73 (s, 6H, -OCH_3), 3.86 (s, 2H, ArH_2), 6.71 (s, 1H, ArH), 7.11 (s, 1H, ArH), 7.41 (d, 2H, J=7.0 ArH), 7.51 (s, 1H, =CH-Ar), 7.83(d, 2H, J=8.8, ArH); ^{13}C NMR (125 MHz, DMSO-d_6): δ_C, ppm, 34.86 (C-3), 56.01 (C-10, C-11), 105.37 (C-7), 112.05 (C-4), 118.63 (C-1'), 129.01 (C-4', C-6'), 131.12 (C-3', C-7'), 132.05 (C-2'), 133.98 (C-8), 134.51 (C-2), 138.45 (C-5'), 137.80 (C-9), 148.80 (C-6), 155.40 (C-5), 193.70 (C-1).

3.4.2(o) *(E)*-2-(5'-isopropylbenzylidene)-5,6-dimethoxy-1-indanone, 89o

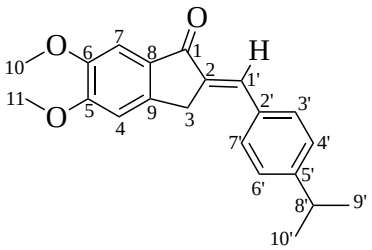

Colour: Light yellow Solid; Weight: 266.83 mg, 82.76 % (yield); mp. 168–175 °C; Molecular weight 322.3945 gmol^{-1}; FTIR ATR (V_{max}/cm^{-1}): 2914 (C_{sp}^3-H), 1694 (C=O ketone), 1575 (C=C aromatic), 1181 (C-O); ^{1}H NMR (500 MHz, DMSO-d_6): δ_H, ppm, 1.27 (d, 6H, J=7.0, -CH_3), 2.92–2.98 (m, 1H, -CH) 3.93 (s, 6H, -OCH_3), 3.99 (s, 2H, ArCH_2), 6.97 (s, 1H, ArH), 7.27 (s, 1H, ArH), 7.30 (s, 1H, =CH-Ar), 7.33 (d, 2H, J=6.9 ,ArH), 7.59 (d, 2H, J=8.3, ArH); ^{13}C NMR (125 MHz, DMSO-d_6): δ_C, ppm, 23.58 (C-9', C-10'), 33.60 (C-8'), 35.33 (C-3), 56.15 (C-10, C-11), 105.37 (C-7), 112.05 (C-4), 126.30 (C-4', C-6'), 127.76 (C-3', C-7'), 130.27 (C-1'), 132.26 (C-2'), 134.05 (C-2), 137.43 (C-9), 138.21 (C-8), 139.03 (C-5'), 140.38 (C-6), 155.34 (C-5), 193.83 (C-1).

3.4.2(p) *(E)*-2-(5'-dimethylaminobenzylidene)-5,6-dimethoxy-1-indanone, 89p

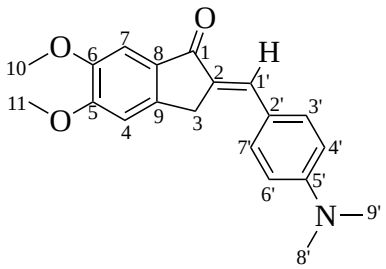

Colour: Orange Solid; Weight: 247.70 mg, 76.59 % (yield); mp. 165–180 °C; Molecular weight 323.3827 gmol^{-1}; FTIR ATR (V_{max}/cm^{-1}): 2913 (C_{sp}^3-H), 1695 (C=O ketone), 1573 (C=C aromatic), 1189 (C-O); ^{1}H NMR (500 MHz, DMSO-d_6): δ_H, ppm, 3.01 (s, 6H, -CH_3), 3.33 (s, 6H, -OCH_3), 3.83 (s, 2H, ArH_2), 6.79 (d, 2H,

J=8.8, ArH), 7.20 (s, 1H, ArH), 7.21 (s, 1H, ArH), 7.36 (s, 1H, =CH-Ar), 7.58 (d, 2H, J=8.8, ArH); ^{13}C NMR (125 MHz, DMSO-d_6): δ_C, ppm, 32.28 (C-3), 56.11 (C-8', C-9'), 56.41 (C-10, C-11), 104.95 (C-7), 108.59 (C-4), 112.49 (C-4', C-6'), 122.92 (C-1'), 130.89 (C-2'), 131.09 (C-8), 132.70 (C-2), 132.78 (C-3', C-7'), 144.80 (C-9), 149.03 (C-5'), 151.17 (C-6), 155.17 (C-5), 192.14 (C-1).

3.4.2(q) *(E)*-2-[5'-(4"-morpholinobenzylidene)]-5,6-dimethoxy-1-indanone, 89q

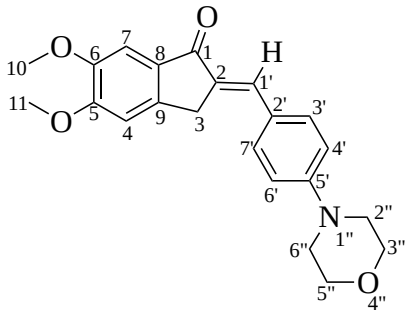

Colour: Light orange solid; Weight: 315.00 mg, 86.20 % (yield); mp. 195–205 °C; Molecular weight 341.3977 gmol^{-1}; FTIR ATR (V_{max}/cm^{-1}): 2915 (C_{sp}^3-H), 1695 (C=O ketone), 1575 (C=C aromatic), 1089 (C-O-C); ^{1}H NMR (500 MHz, DMSO-d_6): δ_H, ppm, 3.26 (t, 4H, J=0.01, -NCH_2), 3.86 (t, 4H, J=4.7, -OCH_2), 3.90 (s, 3H, -OCH_3), 3.94 (s, 3H, -OCH_3), 3.99 (s, 2H, ArH_2), 6.92 (d, 2H, J=8.9, ArH), 6.97 (s, 1H, ArH), 7.33 (s, 1H, ArH), 7.53 (s, 1H, =CH-Ar), 7.57 (d, 2H, J=8.6, ArH); ^{13}C NMR (125 MHz, DMSO-d_6): δ_C, ppm, 32.27 (C-3), 58.30 (C-2", C-6"), 56.17 (C-10), 56.26 (C-11), 66.58 (C-3", C-5"), 105.10 (C-7), 107.22 (C-4), 114.98 (C-4', C-6'), 127.01 (C-1'), 131.14 (C-2'), 132.19 (C-8, C-3', C-7'), 132.46 (C-9), 132.54 (C-2), 144.54 (C-6), 149.58 (C-5'), 155.11 (C-5), 193.25 (C-1).

3.4.2(r) *(E)*-2-(5'-piperidinylbenzylidene)-5,6-dimethoxy-1-indanone, 89r

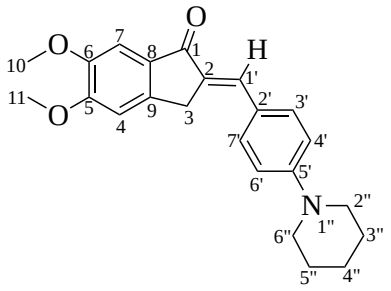

Colour: Brown solid; Weight: 307.20 mg, 84.52 % (yield); mp. 200–210 °C; Molecular weight 323.3827 $gmol^{-1}$; FTIR ATR (V_{max}/cm^{-1}): 2916 (C_{sp}^3-H), 1694 (C=O ketone), 1587 (C=C aromatic), 1223 (C-O); ^{1}H NMR (500 MHz, DMSO-d_6): δ_H, ppm, 1.59 (s, 6H, ArH_2), 2.51 (s, 4H, ArH_2), 3.37 (s, 6H, -OCH_3), 3.93 (s, 2H, ArH_2), 6.80 (s, 1H, ArH_2), 7.01 (dd, 2H, J=2.1, ArH), 7.10 (s, 1H, ArH), 7.22 (d, 2H, J=8.3, ArH), 7.35 (s, 1H, =CH-Ar); ^{13}C NMR (125 MHz, DMSO-d_6): δ_C, ppm, 24.39 (C-4"), 25.53 (C-3", C-5"), 32.25 (C-3), 51.83 (C-2", C-6"), 56.73 (C-10, C-11), 104.97 (C-7), 108.60 (C-3), 113.52 (C-1'), 108.12 (C-4), 114.97 (C-4', C-6'), 131.14 (C-2'), 132.26 (C-3', C-7'), 132.73 (C-9), 133.95 (C-2), 144.92 (C-8), 148.80 (C-6), 152.09 (C-5'), 155.27 (C-5), 192.26 (C-1).

3.4.2(s) *(E)*-2-(3',5'-dimethoxybenzylidene)-5,6-dimethoxy-1-indanone, 89s

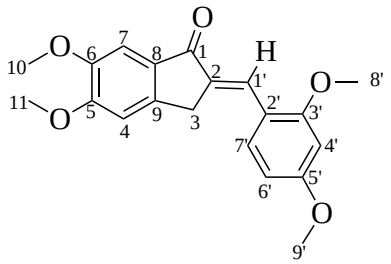

Colour: Yellow solid; Weight: 80.58 % (yield); mp. 200–205 °C; Molecular weight 340.3670 $gmol^{-1}$; FTIR ATR (V_{max}/cm^{-1}): 2917 (C_{sp}^3-H), 1694 (C=O ketone), 1608 (C=C aromatic), 1226 (C-O); ^{1}H NMR (500 MHz, DMSO-d_6):

δ_H, ppm, 3.86 (s, 6H, -OCH_3), 3.88 (s, 3H, -OCH_3), 3.95 (s, 3H, -OCH_3), 3.99 (s, 2H, ArH_2), 6.48 (s, 1H, ArH), 6.54 (dd, 1H, J=2.2, ArH), 6.95 (s, 1H, ArH_2), 7.33 (s, 1H, =CH-Ar), 7.59 (d, 1H, J=8.6, ArH), 8.01 (s, 1H, ArH); ^{13}C NMR (125 MHz, DMSO-d_6): δ_C, ppm, 32.25 (C-3), 55.43 (C-9'), 55.58 (C-8'), 56.13 (C-10), 56.21 (C-11), 98.32 (C-4'), 105.09 (C-6'), 105.17 (C-7), 107.20 (C-4), 117.70 (C-1'), 126.74 (C-2'), 130.62 (C-7'), 131.48 (C-8), 132.94 (C-9), 144.65 (C-2), 149.47 (C-6), 154.99 (C-5), 160.57 (C-3'), 162.24 (C-5'), 193.22 (C-1).

3.4.2(t) *(E)*-2-(4'-nitro-5'methoxybenzylidene)-5,6-dimethoxy-1-indanone, 89t

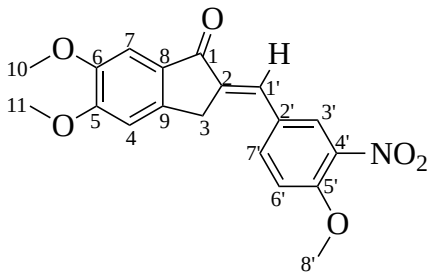

Colour: Cream solid; Weight: 268.70 mg, 75.62 % (yield); mp. 235–240 °C; Molecular weight 355.3390 $gmol^{-1}$; FTIR ATR (V_{max}/cm^{-1}): 2917 (C_{sp}^3-H), 1693 (C=O ketone), 1592 (C=C aromatic), 1502 (N-O), 11870 (C-O); ^{1}H NMR (500 MHz, DMSO-d_6): δ_H, ppm, 3.78 (s, 3H, -OCH_3), 3.78 (s, 3H, -OCH_3), 3.75 (s, 2H, ArH_2), 4.02 (s, 3H, -OCH_3), 6.91 (s, 1H, ArH), 7.28 (s, 1H, =CH-Ar), 7.35 (d, 1H, J=8.8, ArH), 7.68 (d, 1H, J=3.0, ArH), 8.01 (s, 1H, ArH), 8.33 (s, 1H, ArH); ^{13}C NMR (125 MHz, DMSO-d_6): δ_C, ppm, 34.7 (C-3), 56.19 (C-10, C-11), 55.78 (C-8'), 105.37 (C-7), 112.05 (C-4), 115.52 (C-6'), 119.40 (C-1'), 124.52 (C-3'), 129.64 (C-2'), 132.32 (C-7'), 137.52 (C-2), 138.01 (C-9), 138.87 (C-4'), 140.33 (C-8), 148.80 (C-6), 152.33 (C-5'), 155.40 (C-5), 193.61 (C-1).

3.4.3 The synthesis of pyrazolyl substituted benzylidene indanone derivatives

The previously synthesized benzylidene indanone derivatives, **89a-t** (1.0 mmol) were further reacted with compound **86** (1.0 mmol) in the presence of 10 mL acetic acid under reflux for 12 h as depicted in Scheme 3.5.

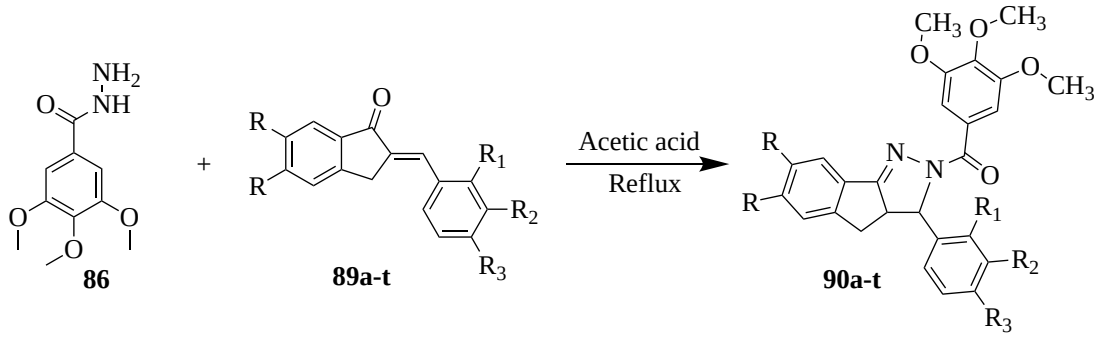

Scheme 3.5: The synthesis of pyrazolyl substituted benzylidene indanone derivatives.

The excess solvent was removed under reduced pressure. The reaction mixture was then poured into the crushed ice. The precipitated was filtered using gravitational filtration, washed using cold methanol and dried in the fume hood. The synthesized compounds were further recrystallized by single-solvent recrystallization technique using ethanol. The compounds were then undergone characterization analysis to determine their physicochemical properties.

3.4.3(a) 3-phenyl-(3,4,5-trimethoxyphenyl)-3*a*,4-dihydroinden-1,2-*c*-2-pyrazolyl methanone, 90a

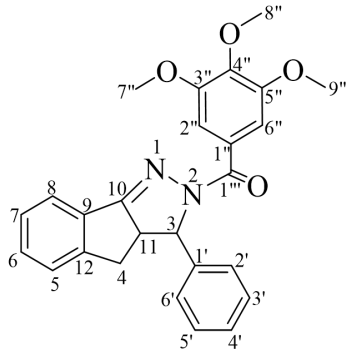

Colour: Light yellow solid; Weight: 164.62 mg, 76.84 % (yield); mp. 200–205 °C; Molecular weight 428.4788 $gmol^{-1}$; EI-MS (m/z): 429.4847 (M^{+1}); FTIR ATR (V_{max}/cm^{-1}): 1678 (C=O), 1588 (C=N), 1320 (C-N); ^{1}H NMR (500 MHz, DMSO-d_6): δ_H, ppm, 2.36–2.39 (m, 2H, ArH_2), 3.72–3.73 (t, 1H, J=3.8, ArH), 3.83 (s, 9H, $-OCH_3$), 5.06 (1H, d, J=7.0, ArH), 6.99 (2H, s, ArH), 7.09–7.24 (m, 9H, ArH); ^{13}C NMR (125 MHz, DMSO-d_6): δ_C, ppm, 31.85, 39.32, 56.25, 60.80, 68.05, 77.45, 105.87, 122.41, 123.01, 124.09, 125.32, 126.83, 127.34, 128.40, 134.55, 139.10, 140.50, 149.60, 149.60, 153.20, 173.10, 192.35.

3.4.3(b) 3-(4'-methoxyphenyl)-(3,4,5-trimethoxyphenyl)-3*a*,4-dihydroindeno -1,2-*c*-2-pyrazolylmethanone, 90b

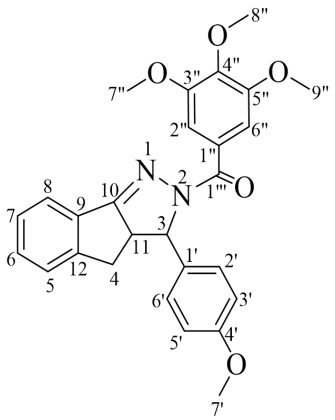

Colour: Cream solid; Weight: 192.70 mg, 84.05 % (yield); mp. 179–185 °C; Molecular weight 458.5057 $gmol^{-1}$; EI-MS (m/z): 459.4460 (M^{+1});

FTIR ATR (V_{max}/cm^{-1}): 1697 (C=O), 1568 (C=N), 1320 (C-N); ^{1}H NMR (500 MHz, $CDCl_3$): δ_H, ppm, 2.78 (s, 1H, ArH_2), 3.09 (s, 1H, ArH_2), 3.78 (s, 6H, -OCH_3), 3.80 (s, 6H, -OCH_3), 3.96 (s, 1H, ArH), 5.45 (s, 1H, ArH), 6.91 (d, 2H, J=8.8, ArH), 6.99 (s, 2H, ArH), 7.19 (s, 2H, ArH), 7.34 (t, 1H, J=7.5, ArH), 7.44–7.59 (m, 4H, ArH); ^{13}C NMR (125 MHz, $CDCl_3$): δ_H, ppm, 32.51, 55.43, 56.24, 60.93, 77.24, 104.53, 113.71, 114.48, 124.35, 126.13, 127.62, 128.17, 132.40, 132.61, 133.91, 134.39, 138.26, 141.55, 149.53, 153.20, 160.87, 164.59, 168.19, 194.90.

3.4.3(c) 3-(4'-methylphenyl)-(3,4,5-trimethoxyphenyl)-3*a*,4-dihydroindeno-1,2-*c*-2-pyrazolylmethanone, 90c

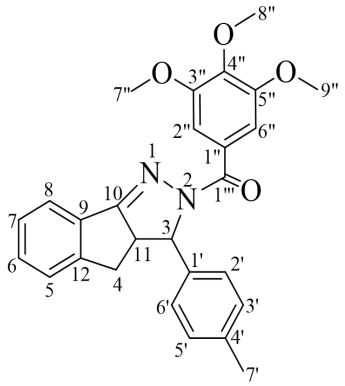

Colour: White solid; Weight: 172.10 mg, 77.78 % (yield); mp. 189–193 °C; Molecular weight 442.5063 $gmol^{-1}$; EI-MS (m/z): 443.1400 (M^{+1}); FTIR ATR (V_{max}/cm^{-1}): 1680 (C=O), 1585 (C=N), 1330 (C-N); ^{1}H NMR (500 MHz, DMSO-d_6): δ_H, ppm, 2.36 (s, 3H, -CH_3), 3.33 (s, 2H, ArH_2), 3.83 (s, 6H, -OCH_3), 3.91 (s, 3H, -OCH_3), 3.98 (s, 1H, ArH), 5.01 (s, 1H, ArH), 7.21 (dd, 2H, J=3.2, ArH), 7.30 (d, 2H, J=8.0, ArH), 7.40 (s, 2H, ArH), 7.63 (s, 4H, ArH); ^{13}C NMR (125 MHz, DMSO-d_6): δ_C, ppm, 32.05, 56.10, 56.13, 63.05, 77.41, 104.11, 118.23, 122.41, 123.06, 126.61, 127.51, 129.40, 133.12, 136.10, 139.02, 148.17, 152.76, 193.43.

3.4.3(d) 3-(4'-chlorophenyl)-(3,4,5-trimethoxyphenyl)-3*a*,4-dihydroindeno-1,2-*c*-2-pyrazolylmethanone, 90d

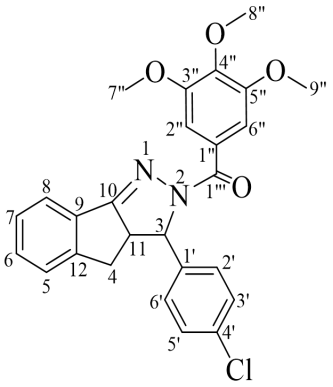

Colour: Cream solid; Weight: 192.70 mg, 84.05 % (yield); mp. 179–185 °C; Molecular weight 462.9248 $gmol^{-1}$; EI-MS (m/z): 463.8210 (M^{+1}); FTIR ATR (V_{max}/cm^{-1}): 1683 (C=O), 1590 (C=N), 1325 (C-N); ^{1}H NMR (500 MHz, DMSO-d_6): δ_H, ppm, 2.33–2.39 (m, 2H, ArH_2), 3.79 (s, 3H, -OCH_3), 3.88 (s, 6H, -OCH_3), 4.05 (s, 1H, ArH), 5.83 (s, 1H, ArH), 6.90 (s, 2H, ArH), 7.32–7.44 (m, 8H, ArH). ^{13}C NMR (125 MHz, DMSO- d_6): δ_C, ppm, 32.23, 56.76, 59.71, 61.95, 77.39, 107.36, 121.17, 125.17, 126.03, 128.54, 129.90, 130.85, 131.93, 134.89, 138.20, 149.80, 151.25, 155.82, 169.96, 193.13.

3.4.3(e) 3-(4'-isopropylphenyl)-(3,4,5-trimethoxyphenyl)-3a,4-dihydroindeno-1,2-c-2-pyrazolylmethanone, 90e

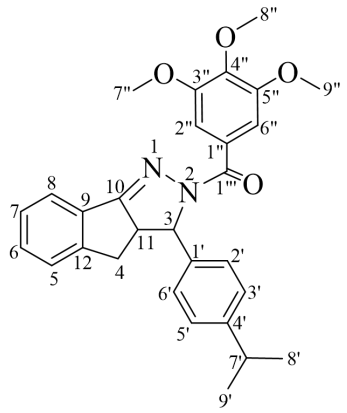

Colour: Cream solid; Weight: 157.70 mg, 67.03 % (yield); mp. 178–183 °C; Molecular weight 470.5595 $gmol^{-1}$; EI-MS (m/z): 471.2600 (M^{+1}); FTIR ATR (V_{max}/cm^{-1}): 1672 (C=O), 1592 (C=N), 1320 (C-N); ^{1}H NMR (500 MHz, DMSO- d_6): δ_H, ppm, 1.26 (s, 6H, $-CH_3$), 2.98 (m, 3H, -CH), 3.71 (s, 3H, $-OCH_3$), 3.93 (s, 6H, $-OCH_3$), 4.98 (s, 1H, ArH), 7.17–7.26 (m, 6H, ArH), 7.33–7.41 (m, 5H, ArH); ^{13}C NMR (125 MHz, DMSO- d_6): δ_C, ppm, 23.61, 30.11, 33.81, 41.89, 58.25, 60.13, 77.91, 107.81, 120.40, 124.31, 125.56, 126.49, 126.87, 127.91, 128.41, 136.73, 138.11, 140.23, 148.98, 149.17, 153.28, 158.11, 172.10, 193.14.

3.4.3(f) 3-(4'-dimethylaminophenyl)-(3,4,5-trimethoxyphenyl)-3*a*,4-dihydroinde no-1,2-*c*-2-pyrazolylmethanone, 90f

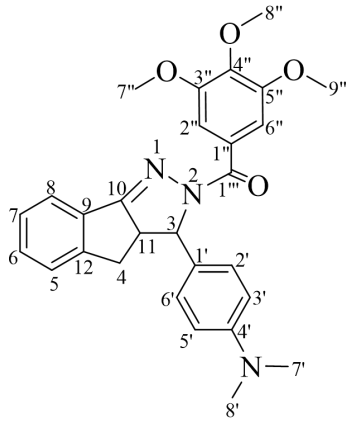

Colour: Dark orange solid; Weight: 171.70 mg, 72.82 % (yield); mp. 178–182 °C; Molecular weight 471.5476 $gmol^{-1}$; EI-MS (m/z): 473.1800 (M^{+1}); FTIR ATR (V_{max}/cm^{-1}): 1675 (C=O), 1590 (C=N), 1321 (C-N); ^{1}H NMR (500 MHz, DMSO- d_6): δ_H, ppm, 2.71 (s, 2H, ArH), 3.10 (s, 6H, $-CH_3$), 3.87 (s, 6H, $-OCH_3$), 3.98 (s, 3H, $-OCH_3$), 5.01 (s, 1H, ArH), 7.28–7.35 (m, 6H, ArH), 7.69–7.73 (m, 5H, ArH); ^{13}C NMR (125 MHz, DMSO- d_6): δ_C, ppm, 28.37, 35.11, 40.18, 58.73, 60.11, 77.24, 105.81, 119.37, 120.89, 123.47, 125.25, 136.37, 137.18, 139.85, 141.11, 142.71, 143. 89, 146.01, 148.01, 153.28, 155.87, 169.73, 192.04.

3.4.3(g) 3-(4'-morpholinophenyl)-(3,4,5-trimethoxyphenyl)-3*a*,4-dihydroindeno-1,2-*c*-2-pyrazolylmethanone, 90g

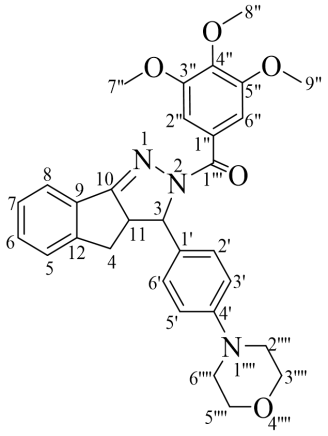

Colour: Light brown solid; Weight: 204.10 mg, 79.48 % (yield); mp. 176–184 °C; Molecular weight 513.5842 $gmol^{-1}$; EI-MS (m/z): 514.1100 (M^{+1}); Anal. for $C_{30}H_{31}N_3O_5$; % calculated (% found): C: 70.16 (68.93), H: 6.08 (5.59), N: 8.18 (7.86). IR (ATR, cm^{-1}) υmax: 1672 (C=O), 1590 (C=N), 1320 (C-N); ^1H NMR (500 MHz, $CDCl_3$): δ_H, ppm, 1.27 (s, 4H, ArH), 2.14 (s, 2H, ArH_2), 3.87–3.90 (m, 9H, $-OCH_3$), 4.04 (s, 1H, ArH), 7.09 (s, 2H, ArH), 7.43–7.46 (m, 3H, ArH), 7.58–7.70 (m, 5H, ArH), 7.92 (d, 2H, J=7.6, ArH); ^{13}C NMR (125 MHz, $CDCl_3$): δ_H, ppm, 20.89, 29.69, 56.28, 60.90, 65.80, 77.55, 104.66, 123.37, 126.13, 126.25, 127.68, 132.41, 133.24, 134.46, 138.20, 141.72, 149.42, 153.24, 164.27, 167.74, 193.92.

3.4.3(h) 3-(4'-piperidinylphenyl)-(3,4,5-trimethoxyphenyl)-3*a*,4-dihydroindeno-1,2-*c*-2-pyrazolylmethanone, 90h

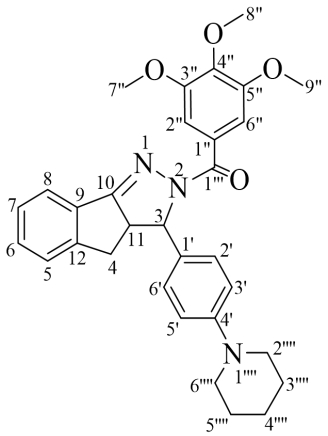

Colour: Light brown solid; Weight: 124.20 mg, 48.55 % (yield); mp. 183–187 °C; Molecular weight 511.6114 $gmol^{-1}$; EI-MS (m/z): 512.6138 (M^{+1}); FTIR ATR (V_{max}/cm^{-1}): 1675 (C=O), 1585 (C=N), 1319 (C-N); ^{1}H NMR (500 MHz, DMSO-d_6): δ_H, ppm, 1.57–1.65 (m, 8H, ArH_2), 2.01–2.08 (m, 2H, ArH_2), 2.89 (s, 2H, ArH_2), 3.33 (s, 6H, $-OCH_3$), 3.48 (s, 6H, $-OCH_3$), 4.03 (s, 1H, ArH), 6.99–7.03 (m, 3H, ArH), 7.38–7.49 (m, 5H, ArH), 7.81–7.89 (m, 3H, ArH); ^{13}C NMR (125 MHz, DMSO-d_6): δ_C, ppm, 24.43, 25.37, 32.57, 48.08, 48.48, 58.93, 60.31, 67.81, 77.63, 104.31, 114.82, 123.72, 124.12, 130.74, 133.13, 134.12, 138.36, 149.03, 156.28, 158.11, 163.01, 169.17, 193.47.

3.4.3(i) 3-(2',4'-dimethoxyphenyl)-(3,4,5-trimethoxyphenyl)-3*a*,4-dihydroindeno -1,2-*c*-2-pyrazolylmethanone, 90i

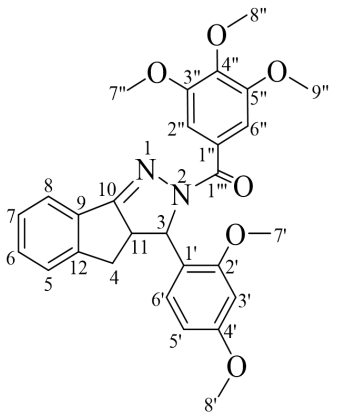

Colour: Yellow solid; Weight: 124.65 mg, 51.03 % (yield); mp. 198–210 °C; Molecular weight $gmol^{-1}$ 488.5317; EI-MS (m/z): 489.1384 (M^{+1}); FTIR ATR (V_{max}/cm^{-1}): 1680 (C=O), 1590 (C=N), 1320 (C-N); ^{1}H NMR (500 MHz, $CDCl_3$): δ_H, ppm, 2.04 (s, 2H, ArH_2), 3.79–3.82 (m, 9H, -OCH_3), 3.91 (s, 6H, -OCH_3), 4.32 (s, 1H, ArH), 5.50 (s, 1H, ArH), 6.43–6.53 (m, 2H, ArH), 6.99 (dd, 1H, J=8.8, ArH), 7.19 (s, 1H, ArH), 7.32 (t, 1H, J=7.3, ArH), 7.45–7.52 (m, 5H, ArH), 7.58 (d, 2H, J=8.7, ArH), 7.82 (d, 1H, J=7.7, ArH); ^{13}C NMR (125 MHz, $CDCl_3$): δ_H, ppm,20.88, 29.69, 32.59, 55.47, 55.63, 56.30, 60.92, 77.41, 98.37, 104.66, 105.25, 117.62, 124.28, 127.46, 130.84, 134.09, 138.52, 149.58, 153.28, 160.79, 162.54, 194.42.

3.4.3(j) 3-(3'-nitro-4'methoxyphenyl)-(3,4,5-trimethoxyphenyl)-3*a*,4-dihydroindeno-1,2-*c*-2-pyrazolylmethanone, 90j

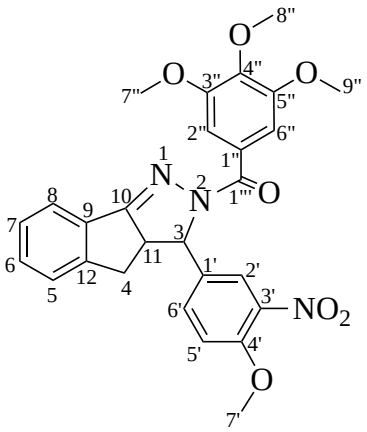

Colour: Light brown solid; Weight: 124.93 mg, 49.62 % (yield); mp. 205–208 °C; Molecular weight 503.5033 $gmol^{-1}$; EI-MS (m/z): 505.1142 (M^{+1}); FTIR ATR (V_{max}/cm^{-1}): 1678 (C=O), 1588 (C=N), 1320 (C-N); ^{1}H NMR (500 MHz, $CDCl_3$): δ_H, ppm, 2.31 (s, 2H, ArH_2), 3.81 (s, 6H, $-OCH_3$), 3.85–3.88 (m, 6H, $-OCH_3$), 4.31 (s, 1H, ArH), 5.56 (s, 1H, ArH), 7.18–7.21 (d, 2H, J=8.8, ArH), 7.59–7.67 (m, 6H, ArH), 7.92 (d, 1H, J=7.6, ArH); ^{13}C NMR (125 MHz, $CDCl_3$): δ_H, ppm, 29.62, 32.10, 56.78, 60.17, 63.71, 77.81, 105.71, 114.01, 124.52, 126.19, 126.59, 127.85, 128.27, 130.71, 134.80, 135.30, 136.41, 137.84, 140.18, 149.81, 153.47, 160.73, 163.59, 193.56.

3.4.3(k) 3-phenyl-(3,4,5-trimethoxyphenyl)-(6,7-dimethoxy)-3*a*,4-dihydroindeno -1,2-*c*-2-pyrazolylmethanone, 90k

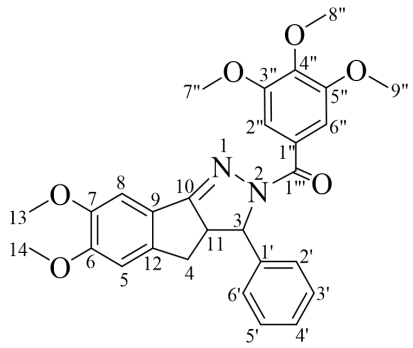

Colour: Cream solid; Weight: 172.70 mg, 70.70 % (yield); mp. 195–200 °C; Molecular weight 488.5317 $gmol^{-1}$; EI-MS (m/z): 489.5395 (M^{+1}); FTIR ATR (V_{max}/cm^{-1}): 1673 (C=O), 1588 (C=N), 1319 (C-N); ^{1}H NMR (500 MHz, DMSO-d_6): δ_H, ppm, 2.39–2.41 (m, 2H, ArH_2), 3.71 (s, 6H, -OCH_3), 3.82–3.84 (m, 9H, -OCH_3), 4.01 (s, 1H, ArH), 5.16 (1H, d, J=7.0, ArH), 7.21–7.23 (m, 2H, ArH), 7.42–7.45 (m, 1H, ArH), 7.49–7.52 (m, 2H, ArH), 7.76–7.78 (m, 4H, ArH); ^{13}C NMR (125 MHz, DMSO-d_6): δ_C, ppm, 21.07, 32.04, 56.12, 56.46, 60.56, 77.32, 105.36, 105.52, 108.52, 127.98, 129.45, 129.96, 130.39, 130.97, 131.50, 135.57, 136.37, 140.76, 145.67, 149.80, 153.09, 155.79, 169.04, 192.35.

3.4.3(l) 3-(4'-methoxyphenyl)-(3,4,5-trimethoxyphenyl)-(6,7-dimethoxy)-3*a*,4-dihydroindeno-1,2-*c*-2-pyrazolylmethanone, 90l

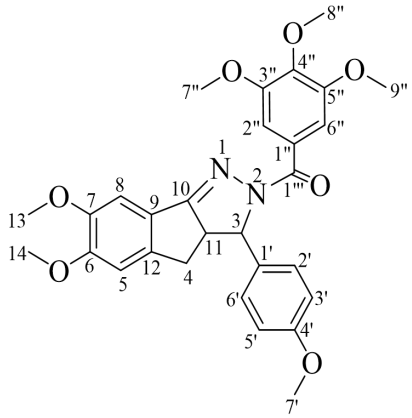

Colour: Light yellow solid; Weight: 179.30 mg, 69.15 % (yield); mp. 198–210 °C; Molecular weight 518.5577 $gmol^{-1}$; EI-MS (m/z): 490.1500 (M^{+1}); FTIR ATR (V_{max}/cm^{-1}): 1672 (C=O), 1592 (C=N), 1320 (C-N); ^{1}H NMR (500 MHz, $CDCl_3$): δ_H, ppm, 1.76 (s, 2H, ArH_2), 3.88–4.01 (m, 15H, $-OCH_3$), 4.55 (s, 1H, ArH), 5.52 (s, 1H, ArH), 6.99 (d, 2H, J=8.2, ArH), 7.28 (s, 1H, ArH), 7.58–7.64 (m, 7H, ArH); ^{13}C NMR (125 MHz, $CDCl_3$): δ_H, ppm, 28.11, 32.18, 55.38, 56.17, 56.26, 77.33, 105.17, 107.23, 113.70, 114.43, 128.39, 130.33, 131.31, 132.29, 133.18, 144.66, 149.65, 155.27, 160.65, 193.25.

3.4.3(m) 3-(4'-methylphenyl)-(3,4,5-trimethoxyphenyl)-(6,7-dimethoxy)-3*a*,4-dihydroindeno-1,2-*c*-2-pyrazolylmethanone, 90m

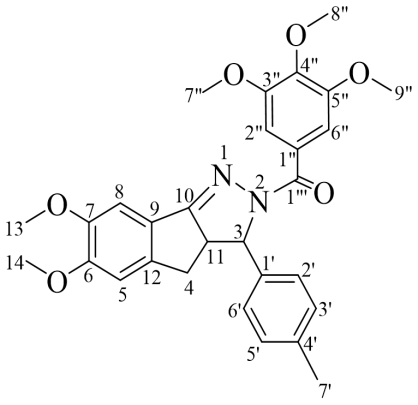

Colour: White solid; Weight: 129.70 mg, 51.62 % (yield); mp. 180–187 °C; Molecular weight 502.5583 $gmol^{-1}$; EI-MS (m/z): 503.4131 (M^{+1}); FTIR ATR (V_{max}/cm^{-1}): 1678 (C=O), 1588 (C=N), 1320 (C-N); ^{1}H NMR (500 MHz, DMSO-d_6): δ_H, ppm, 2.35 (s, 3H, -CH_3), 3.23 (s, 2H, ArH_2), 3.74 (s, 1H, ArH), 3.82 (s, 6H, -OCH_3), 3.98 (s, 9H, -OCH_3), 5.07 (s, 1H, ArH), 6.93 (s, 1H, ArH), 7.11–7.21 (m, 7H, ArH); ^{13}C NMR (125 MHz, DMSO-d_6): δ_C, ppm, 21.70, 30.14, 56.31, 56.99, 64.05, 77.24, 105.15, 108.11, 109.73, 124.84, 126.68, 127.55, 129.16, 131.69, 136.89, 137.10, 140.51, 149.17, 153.25, 155.33, 170.44, 193.81.

3.4.3(n) 3-(4'-chlorophenyl)-(3,4,5-trimethoxyphenyl)-(6,7-dimethoxy)-3*a*,4-dihydroindeno-1,2-*c*-2-pyrazolylmethanone, 90n

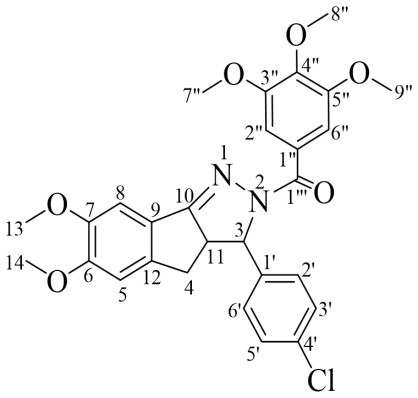

Colour: Cream solid; Weight: 57.90 mg, 44.28 % (yield); mp. 175–183 °C; Molecular weight 522.9768 $gmol^{-1}$; EI-MS (m/z): 523.1600 (M^{+1}); FTIR ATR (V_{max}/cm^{-1}): 1678 (C=O), 1585 (C=N), 1318 (C-N); ^{1}H NMR (500 MHz, DMSO-d_6): δ_H, ppm, 2.31–2.36 (m, 2H, ArH_2), 3.73 (s, 6H, -OCH_3), 3.89 (s, 9H, -OCH_3), 4.11 (s, 1H, ArH), 5.06 (s, 1H, ArH), 7.11–7.15 (m, 2H, ArH), 7.39–7.43 (m, 7H, ArH); ^{13}C NMR (125 MHz, DMSO-d_6): δ_C, ppm, 21.76, 39.11, 56.25, 56.89, 60.57, 77.51, 104.81, 105.99, 107.17, 127.35, 129.11, 130.40, 131.01, 131.97, 135.67, 150.01, 151.56, 155.88, 170.90, 192.81.

3.4.3(o) 3-(4'-isopropylphenyl)-(3,4,5-trimethoxyphenyl)-(6,7-dimethoxy)-3*a*,4-dihydroindeno-1,2-*c*-2-pyrazolylmethanone, 90o

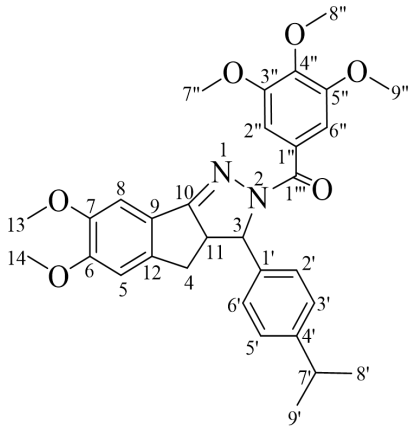

Colour: Cream solid; Weight: 190.10 mg, 71.65 % (yield); mp. 180–183 °C; Molecular weight 498.6127 $gmol^{-1}$; EI-MS (m/z): 499.0600 (M^{+1}); FTIR ATR (V_{max}/cm^{-1}): 1676 (C=O), 1560 (C=N), 1321 (C-N); ^{1}H NMR (500 MHz, DMSO-d_6): δ_H, ppm, 1.29 (s, 6H, -CH_3), 2.89–2.94 (m, 3H, -CH), 3.72 (s, 6H, -OCH_3), 3.99 (s, 9H, -OCH_3), 5.01 (s, 1H, ArH), 7.49–7.55 (m, 5H, ArH), 7.76–7.78 (m, 4H, ArH); ^{13}C NMR (125 MHz, DMSO-d_6): δ_C, ppm, 21.07, 32.04, 33.18, 40.97, 58.25, 59.31, 60.13, 77.43, 106.11, 120.40, 123.33, 124.11, 126.95, 130.39, 138.91, 143.21, 154.31, 155.11, 158.80, 169.71, 193.35.

3.4.3(p) 3-(4'-dimethylaminophenyl)-(3,4,5-trimethoxyphenyl)-(6,7-dimethoxy) -3*a*,4-dihydroindeno-1,2-*c*-2-pyrazolylmethanone, 90p

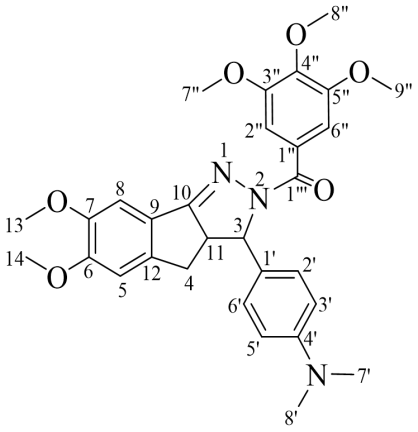

Colour: Light orange solid; Weight: 167.90 mg, 63.17 % (yield); mp. 183–187 °C; Molecular weight 531.5995 $gmol^{-1}$; EI-MS (m/z): 532.4800 (M^{+1}); FTIR ATR (V_{max}/cm^{-1}): 1680 (C=O), 1585 (C=N), 1318 (C-N); ^{1}H NMR (500 MHz, DMSO-d_6): δ_H, ppm, 2.87 (s, 2H, ArH), 3.05 (s, 6H, -NH_3), 3.87 (s, 6H, -OCH_3), 3.98 (s, 9H, -OCH_3), 5.09 (s, 1H, ArH), 7.37–7.39 (m, 4H, ArH), 7.70–7.73 (m, 5H, ArH). ^{13}C NMR (125 MHz, DMSO-d_6): δ_C, ppm, 22.67, 40.87, 57.13, 59.55, 60.31, 77.63, 106.11, 113.05, 121.41, 122.89, 126.05, 127.11, 128.92, 130.17, 138.75, 140.93, 145.35, 153.11, 155.08, 155.61, 171.94, 193.17.

3.4.3(q) 3-(4'-morpholinophenyl)-(3,4,5-trimethoxyphenyl)-(6,7-dimethoxy)-3*a*,4-dihydroindeno-1,2-*c*-2-pyrazolylmethanone, 90q

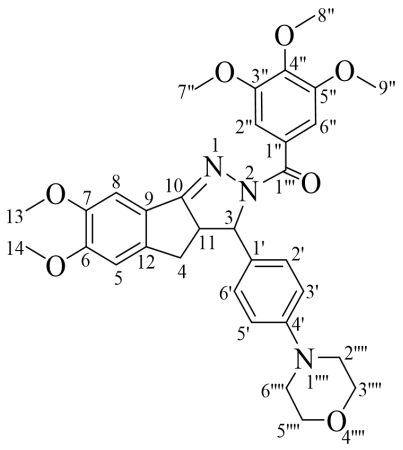

Colour: Cream solid; Weight: 176.70 mg, 61.61 % (yield); mp. 175–185 °C; Molecular weight 572.6283 $gmol^{-1}$; EI-MS (m/z): 571.3100 (M^{+1}); Anal. for $C_{32}H_{35}N_3O_7$; % calculated (% found): C: 67.00 (67.28), H: 6.15 (5.29), N: 7.33 (6.40); IR (ATR, cm^{-1}) υmax: 1675 (C=O), 1590 (C=N), 1320 (C-N); ^{1}H NMR (500 MHz, DMSO-d_6): δ_H, ppm, 1.24 (s, 1H, ArH), 2.76 (s, 2H, ArH_2), 3.74 (s, 6H, -OCH_3), 3.90 (s, 9H, -OCH_3), 4.05 (s, 1H, ArH), 7.10 (s, 2H, ArH), 7.39–7.45 (m, 3H, ArH), 7.50–7.53 (m, 5H, ArH), 7.87–7.91 (m, 3H, ArH); ^{13}C NMR (125 MHz, DMSO-d_6): δ_C, ppm, 20.79, 29.78, 32.49, 56.73, 58.93, 60.31, 61.07, 66.81, 77.59, 105.73, 125.43, 127.68, 132.41, 133.74, 135.16, 138.97, 141.72, 153.24, 155.67, 163.01, 168.97, 192.89.

3.4.3(r) 3-(4'-piperidinylphenyl)-(3,4,5-trimethoxyphenyl)-(6,7-dimethoxy)-3*a*,4-dihydroindeno-1,2-*c*-2-pyrazolylmethanone, 90r

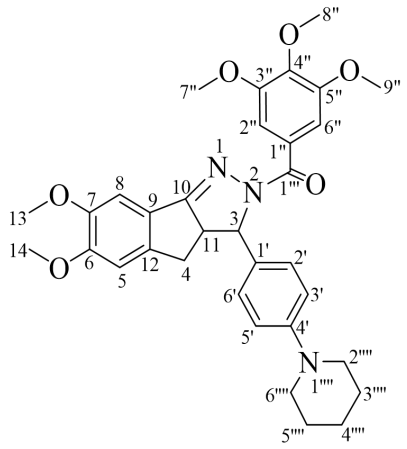

Colour: Cream solid; Weight: 85.30 mg, 59.68 % (yield); mp. 179–185 °C; Molecular weight 571.6634 $gmol^{-1}$; EI-MS (m/z): 574.2900 (M^{+1}); FTIR ATR (V_{max}/cm^{-1}): 1678 (C=O), 1588 (C=N), 1320 (C-N); ^{1}H NMR (500 MHz, DMSO-d_6): δ_H, ppm, 1.57–1.63 (m, 8H, ArH_2), 2.09–2.17 (m, 2H, ArH_2), 2.97 (s, 2H, ArH_2), 3.70 (s, 6H, $-OCH_3$), 3.83 (s, 3H, $-OCH_3$), 3.98 (s, 6H, $-OCH_3$), 4.10 (s, 1H, ArH), 7.01–7.13 (m, 5H, ArH), 7.47–7.53 (m, 1H, ArH); ^{13}C NMR (125 MHz, DMSO-d_6): δ_C, ppm, 25.41, 26.71, 32.57, 40.82, 48.17, 56.93, 58.11, 60.69, 77.25, 105.13, 108.17, 109.23, 115.97, 123.77, 125.72, 128.18, 131.95, 137.02, 140.55, 148.46, 151.43, 153.60, 158.25, 169.77, 193.81.

3.4.3(s) 3-(2',4'-dimethoxyphenyl)-(3,4,5-trimethoxyphenyl)-(6,7-dimethoxy)-3*a*,4-dihydroindeno-1,2-*c*-2-pyrazolylmethanone, 90s

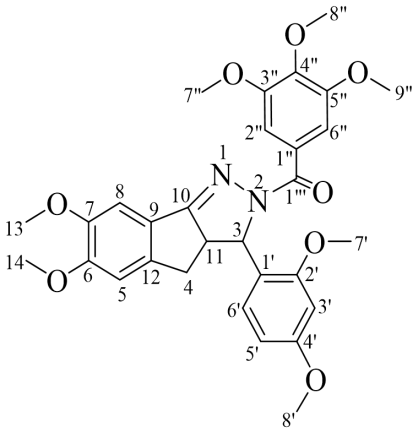

Colour: Yellow solid; Weight: 130.10 mg, 47.43 % (yield); mp. 179–185 °C; Molecular weight 548.5837 $gmol^{-1}$; EI-MS (m/z): 549.1167 (M^{+1}); FTIR ATR (V_{max}/cm^{-1}): 1672 (C=O), 1589 (C=N), 1317 (C-N); ^{1}H NMR (500 MHz, $CDCl_3$): δ_H, ppm, 2.11 (s, 2H, ArH_2), 3.94 (s, 2H, $-OCH_3$), 6.50–6.58 (m, 3H, ArH), 6.97 (s, 1H, ArH), 7.26 (s, 1H, ArH), 7.37 (s, 1H, ArH), 7.62 (d, 1H, J=8.7, ArH), 8.03 (s, 1H, ArH); ^{13}C NMR (125 MHz, $CDCl_3$): δ_H, ppm, 20.37, 32.27, 55.45, 55.60, 56.16, 56.22, 60.11, 77.34, 98.35, 105.18, 105.20, 107.19, 117.74, 126.91, 130.65, 131.48, 132.94, 144.71, 149.50, 155.06, 160.60, 162.28, 193.28.

3.4.3(t) 3-(3'-nitro-4'methoxyphenyl)-(3,4,5-trimethoxyphenyl)-(6,7-dimethoxy) -3*a*,4-dihydroindeno-1,2-*c*-2-pyrazolylmethanone, 90t

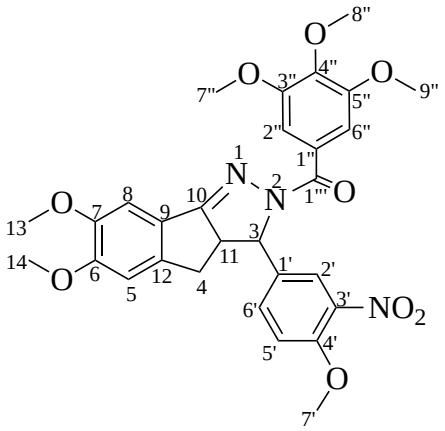

Colour: Light brown solid; Weight: 61.81 mg, 41.45 % (yield); mp. 208–213 °C; Molecular weight 563.553 $gmol^{-1}$; EI-MS (m/z): 562.8913 (M^{+1}); FTIR ATR (V_{max}/cm^{-1}): 1672 (C=O), 1585 (C=N), 1320 (C-N); ^{1}H NMR (500 MHz, $CDCl_3$): δ_H, ppm, 2.89 (s, 2H, ArH_2), 3.77 (s, 6H, $-OCH_3$), 3.82 (s, 6H, $-OCH_3$), .94 (s, 6H, $-OCH_3$), 4.51 (s, 1H, ArH), 5.41 (s, 1H, ArH), 6.93–7.00 (m, 2H, ArH), 7.49–7.58 (m, 5H, ArH); ^{13}C NMR (125 MHz, $CDCl_3$): δ_H, ppm, 28.85, 37.87, 56.08, 56.79, 57.02, 60.71, 60.96, 77.55, 105.15, 108.11, 109.73, 114.93, 122.37, 123.68, 124.71, 127.51, 133.23, 136.27, 138.51, 140.55, 148.46, 154.17, 155.98, 156.30, 160.81, 164.29, 193.01.

3.5 The *in silico* studies towards DENV-2 NS2B/NS3 protease

The synthesized compound structure was sketched using Marvin Sketch 19.4.0 (ChemAxon, 2019) and converted into a 3D structure using HyperChem pro 8.0 software (www.hyper.com). The molecular docking was performed using AutoDock4.2 to identify the binding mode and conformation of the synthesized compound with the protease (Morris *et al.*, 2009). The homology protein crystal structure generated by Wichapong and co-worker was used (2010). AutoDock Tools

(ADT) version 1.5.6 was used in the preparation of docking stimulation. The dimension of 74 × 43 × 64 in x,y,z coordination were employed as the grid box size to cover the protease active site.

3.6 The *in vitro* assays studies towards DENV-2 NS2B/NS3 protease

The *in vitro* assay preliminary screening studies for five top docked synthesized compounds were performed following method by Yusof *et al*. (2000). An enzymatic reaction mixture with a total volume of 100 µL was prepared in black 96 well plates. Each well in the black 96 well plates were consisting of 94.9 µL Tris-HCl buffer solution at pH 8.5, 3.1 µL of the enzyme, and 1 µL of synthesized compound (200 mg/L in DMSO). The mixtures were incubated and shook at 37 °C for 10 minutes. After that, 1 µL substrate 10 mM in DMSO (Peptide Institute, Japan) was added into the mixture to initiate the reaction. The mixture was then incubated and shook for another 60 minutes at 37 °C using Ambient shaker incubatorSI-50 (Protech, Malaysia). The assay was triplicated or more.

A selected compound was chosen for IC_{50} studies as presented in Figure 3.3. The concentration series of a synthesized compound in DMSO (6.25 ppm, 12.5 ppm, 25 ppm, 50 ppm, 100 ppm, 200 ppm) were prepared and the *in vitro* assay was performed using the procedure as mention above.

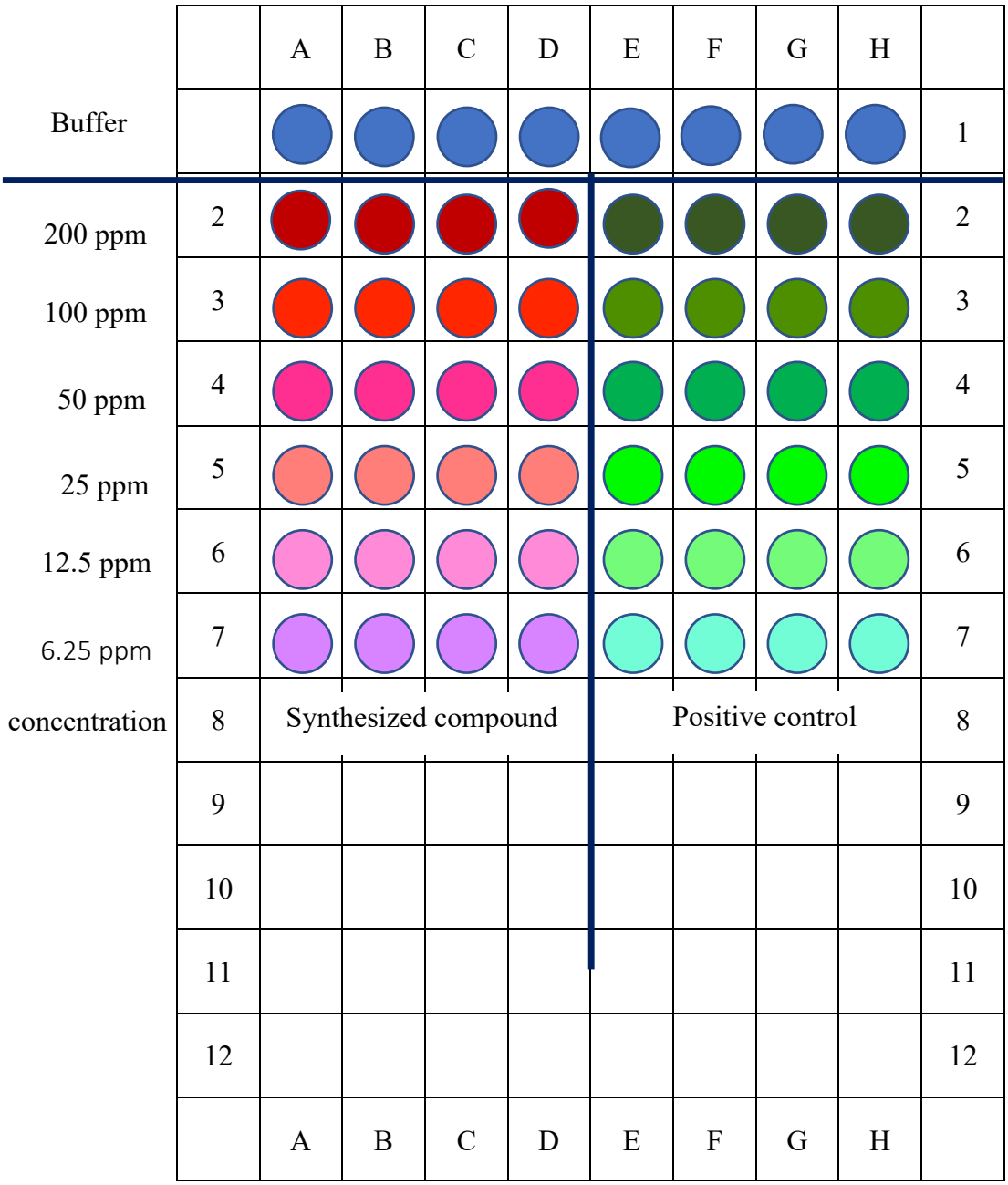

Figure 3.3: The IC_{50} DENV-2 NS2B/NS3 protease assay procedure using the synthesized compound.

CHAPTER 4

RESULT AND DISCUSSION

4.1 The studies of *M. charantia* seeds oil and lignocellulosic biomass

The *M. charantia* seeds oil were extracted using aqueous enzyme extraction (AEE) method. The seed oil composition was determined using GC-MS. The seeds lignocellulosic biomass composition were identified in terms of lignin, soluble sugars, uronic acid, and hemicelullose content.

4.1.1 Aqueous enzyme extraction (AEE) of *M. charantia* seed oil

The idea of using enzyme in aqueous extraction process was to facilitate the breakdown of cellular and subcellular structures of the seed and increased the dissolution of the soluble compound presence in the seed into the water matrix as well as promote oil released (Ricochon & Muniglia, 2010). Theoretically, this method based on the insolubility of oil rather than on dissolution of oil (Johnson & Lusas, 1983; Rosenthal *et al.*, 1996; Kalia *et al.*, 2001). Table 4.1 shows the amount of enzyme cocktail introduced in the reaction process and the percentages of seed oil recovered by aqueous enzymatic extraction method using combination of different enzyme cocktail ratios.

Table 4.1: Percentages of seed oil recovered by aqueous enzymatic extraction method using combination of different enzyme cocktail ratios

Seed samples	Enzyme (%)/Seed weight (g)		Oil extracted (%)
	HEL1	X7	
M0	-	-	3.32 ± 0.38
M1	5	-	4.67 ± 0.11
M2	5	1.25	6.26 ± 0.53
M3	5	2.5	4.10 ± 0.44
M4	5	5	5.03 ± 0.28

Note: The extraction process was triplicated.

The percentage of seed oil extracted = $\frac{\text{Weight of oil obtained (mg)}}{\text{Weight of dry seed used (mg)}} \times 100\%$

In the control experiment, without the addition of enzyme cocktail (M0), only 3.32 ± 0.38 % of seed oil was extracted. The highest percentage seed oil (6.26 ± 0.53 %) was extracted from M2 using a combination of 5 % HEL1 to 1.25 % X7 enzyme cocktails, followed by M4 (5.03 ± 0.28) using a combination of an equal ratio of HEL1 and X7 enzyme cocktails. Based on the results obtained, the amount of the extracted oil showed that the increment of enzyme cocktail X7 to HEL1 ratio used in the extraction was not proportional to the percentage of oil being extracted. This can be seen from the percentage oil being extracted do not show any significant increase by the increment of enzyme ratio after M2.

The results indicated that cellulase, proteinase, and pectinase present in the enzyme cocktails HEL1 and X7 could facilitate the breakdown of cellular and subcellular structures of the seed to promote oil release. The enzymes could have weakened the vegetal cells in the seed to help released the oil (Baby & Ranganathan, 2016). In a previous study, Latif and Anwar (2011) reported that the active mechanism of a selected enzyme cocktail during enzymatic aqueous extraction was the degradation of cellulose, pectin, and protein, thus, destructing the structural cell wall

integrity of the seed cells (Jiao *et al.*, 2014). The cross-sections of immature seeds of *M. charantia* and the shape of cotyledon was presented in Figure 4.1.

As depicted in Figure 4.1(a) above, the *M. charantia* seed were built up off one outer layer called aril and five distinct layers made up a cotyledon. The first layer was epidermis which consists of a single layer of prismatic palisade cells. The second layer was hypodermis, a tissue made up of four layers of small, isodiametric, tightly closed sclerenchymatized cells, without intercellular spaces. The third layer was sclerenchyma that consists of exceedingly thick-walled cells. The fourth layer was made up of layers of spongy parenchyma called aerenchyma. The last layer was a parenchyma cells, containing chlorophyll, forms the inner tissue, called chlorenchyma **(**Giuliani *et al.,* 2016**)**.

All the layer made up a leaf-like shaped cotyledon cell, which contained abundant lipophilic cellular droplets, and oil and protein granules as depicted in Figure 4.1(b). The plant cell walls are a complex structure which mainly made of cellulose, hemicellulose, lignin and protein in addition to pectin (Carpita *et al.*, 1993; Buckeridge *et al.*, 2000; Waldron *et al.*, 2003; Park & Cosgrove, 2012; Soto & Saldívar, 2020).

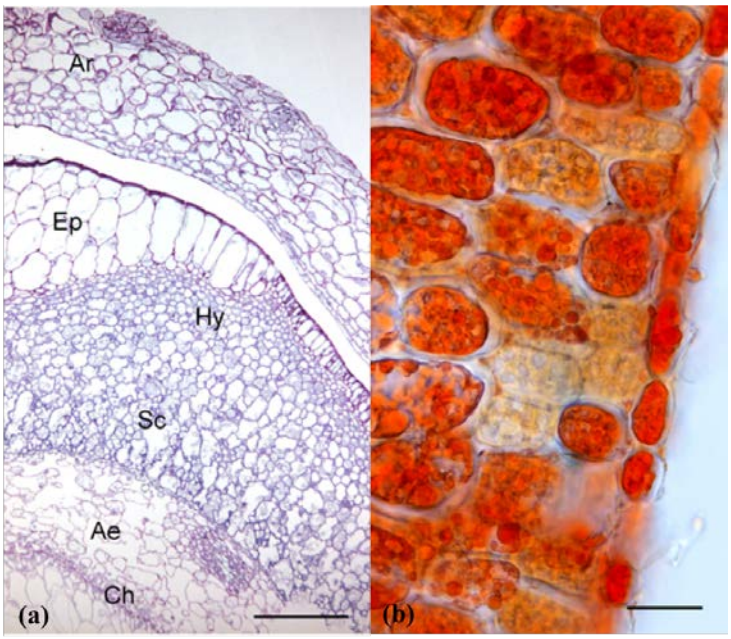

Figure 4.1: (a) Light micrographs of cross-sections of immature seed of *M. charantia* (b) cotyledon with abundant lipophilic cellular droplets. Scale bars = (a) 10 µm, (b) 25µm. Ae–aerenchyma; Ar–aril; Ch–chlorenchyma; Ep–epidermis; Hy–hypodermis; Sc–sclerenchyma (Giuliani *et al.,* 2016).

The hydrolytic enzyme such as cellulases, hemicellulases, and pectinases in the AEE is to break the structure of cotyledon cell walls (Adler-Nissen, 1976; Giovane *et al.*, 2004; Ghosh *et al.*, 2017). The enzyme made the cell walls structure more permeable (Rosenthal *et al.*, 1996). In addition, the incorporation of enzymes may cleave the protein networks of the cotyledon cells and oleosin-based membranes that surround the lipid bodies of the seed cell wall resulting in oil released (Kamatou & Viljoen, 2017; Baharum *et al.,* 2010; Kalia *et al.*, 2001).

4.1.2 The analysis of *M. Charantia* seed oil

The extracted seed oil samples (M0, M1, M2, M3, and M4) were subjected to derivatisation into FAMEs before identification of their biochemical compositions by GC-FID since the FAMEs are more volatile and more easily analysed. GC-FID has been widely used in the separation and detection of FAMEs. The GC chromatogram

revealed the presence of some common and non-essential FAMEs, as shown in Table 4.2. Seven known fatty acids were identified. Three unknown fatty acids were also detected. However, three unknown peaks of free fatty acid were observed from the chromatogram that is co-eluting almost at the same time. It is suggested that some compounds may co-elute more significant in size and elute together at the end during separation (Kamatou & Viljeon, 2017; Baharum *et al.*, 2010).

Table 4.2: The FAMEs compositions (%) of *M. charantia* seed oils

Fatty Acid	Compositions (%)				
	M0	M1	M2	M3	M4
Palmitic Acid (C16)	8.84 ± 0.12	7.21 ± 0.09	17.97 ± 0.11	17.26 ± 0.10	11.23 ± 0.09
Stearic Acid (C18)	-	-	3.28 ± 0.13	-	-
Elaidic acid (C18:1n9t)	0.47 ± 0.11	8.06 ± 0.08	20.42 ± 0.09	28.06 ± 0.11	29.63 ± 0.08
Oleic acid (C18:1n9c)	35.80 ± 0.08	17.31 ± 0.11	-	-	-
Vaccenic acid (C18:1n7)	2.84 ±0.10	5.02 ± 0.09	2.52 ± 0.09	5.02 ± 0.11	7.58 ± 0.10
Stearidonic acid (C18:4n3)	13.55 ± 0.11	13.42 ± 0.11	19.43 ± 0.08	16.42 ± 0.08	12.83 ± 0.09
Paullinic acid (C20.1)	6.50 ± 0.12	6.19 ± 0.12	13.51 ± 0.11	5.19 ± 0.09	2.41 ± 0.10
Unknown 1	10.66 ± 0.09	10.14 ± 0.09	7.81 ± 0.10	15.14 ± 0.09	15.31 ± 0.10
Unknown 2	9.55 ± 0.11	9.96 ± 0.10	6.00 ± 0.10	4.96 ± 0.10	8.69 ± 0.11
Unknown 3	11.79 ± 0.12	8.83 ± 0.11	9.07 ± 0.09	7.98 ± 0.11	12.32 ± 0.11

Note: Values are % of total fatty acid expressed as mean ± SD of three separate determinations

Based on the composition of *M. charantia* seed oil (Table 4.2), the percentage of elaidic and palmitic acids increased with the introduction of the enzyme cocktails. In the control experiment (M0), only 0.47 % of elaidic acid was present in the extracted oil. With the introduction of the enzyme cocktails, the percentage of elaidic acid increased to 8.06%, 20.42%, 28.06%, and 29.63% for M1, M2, M3, and M4, respectively. The presence of the enzyme cocktails showed a similar trend for palmitic acid, albeit lesser increment.

The oil release could be due to the presence of cellulase in the enzyme cocktail, which disrupted other polysaccharide constituents in the seed cell wall. The cellulase presence in HEL1 and X7 promoted an efficient cellulose degradation. The cellulase mechanism, described as the cleavage of internal glucosidic bonds within an unbroken glucan chain by endoglucanase enzyme, could result in the creation of a non-reducing chain of cellobiohydrolase substrate, cleaving the cellobiose dimers from the glucan chain that was released in the solution (White, 2013). Furthermore, β-glucosidase split the cellobiose dimer into glucose monomer, concluding the cellulose hydrolysis process (White & Brown, 1981). The combination of enzymes played a dominant effect in disrupting the seed cell walls, which was also reported in other findings (Wu *et al.*, 2017).

These results also showed that the oil composition differed with different X7 enzyme ratios. In M4, the percentage distribution of elaidic acid, vaccenic acid, palmitic acid, stearidonic acid, and paullinic acid increased with increasing ratio of X7. The results suggested that the enzyme cocktail X7 supported the reaction of enzyme cocktail HEL1 to hydrolyse the seed cellular structures as each enzyme cocktail consisted of different types of an enzyme mixture.

Besides, the biochemical composition of extracted oil also differ from the previous studies. Ali and co-worker extracted the seed oil with the compositions of palmatic acid (4.84 ± 0.13 %), stearic acid (20.21 ± 0.40 %), linoleic acid (6.37 ± 0.46 %) ,and eleostearic acid (53.22 ± 0.36 %) (Ali *et al.*, 2008). Whilst, the seed oil being extracted using AEE have a higher amount of palmitic acid. In addition, the saturated fatty acid, stearic acid was only detected in M2. In addition, the omega-3 fatty acid detected by Ali and co-worker was eleostearic acid whilst the oil extracted using AEE was the highly unsaturated stearidonic acid.

This finding was in agreement with the findings of earlier researchers who showed that enzyme assisted extraction can lead to an increase in oil yield as well as slightly modification in the biochemical properties of the extracted oil (Zuorro *et al.*, 2018). It can be concluded that the *M. charantia* seed oil obtained from the AEE exhibited slight changes in the integrity and percentage distribution of the active constituents.

4.1.3 Determinations of lignin, soluble sugars, and uronic acid of EFM

The lignin, soluble sugar, and uronic acid contents of the EFM were determined. Lignin consists of a very complex structure which is difficult to cleave (Liu *et al.*, 2016). The lignin content of the EFM; M0, M1 (15.91 %) > M2 (15.06 %) > M4 (14.71 %) > M3 (14.54 %) did not show any significant changes with the presence of enzymes in the AEE. Different types of soluble sugars and uronic acid were released and further analysed with HPAEC-PAD.

The main soluble sugar composition of EFM was glucose and rhamnose, respectively. No definite trend was observed between the percentage of enzyme ratios

used with the percentage distribution of soluble sugars and uronic acid obtained. The results are presented in Table 4.3.

$M0_L$ showed the lowest amount of acid galacturonic (8.42 %). The percentage of acid galacturonic increased with the presence of enzyme cocktails in $M3_L$ (16.12 %) < $M4_L$ (16.37 %) < $M1_L$ (22.00 %) < $M2_L$ (22.25 %). These results suggested that the presence of pectinase in the enzyme cocktails facilitated the breakdown of cell wall pectic polysaccharides into simpler molecules like acid galacturonic (Abdulkarim *et al.*, 2005; Welker *et al.*, 2015; Biz *et al.*, 2014).

The concentration of glucose in M0 was only 57 %. The percentage of glucose increased with the introduction of enzyme cocktails; M3 (65.42 %) < M4 (66.77 %) < M1 (71.34 %) < M2 (76.20 %). These results indicated that more cellulose from the cell wall was cleaved into different types of sugars (glucose, xylose, galactose, arabinose, rhamnose, mannose, and fucose) with the help of the enzyme cocktails (Pedrolli *et al.*, 2009; Segato *et al.*, 2014; Zhong *et al.*, 2008).

Table 4.3: Sugar analysis of EFM by HPAEC-PAD

Samples	HEL1	X7	Percentage of Yield (%)								
			Glucose	Xylose	Galactose	Arabinose	Rhamnose	Mannose	Fucose	Acid galacturonic	Acid glucuronic
M0	-	-	57.00	19.02	4.21	3.95	1.70	1.09	0.42	11.77	0.83
$M0_L$			0.61	1.84	7.60	6.98	62.98	6.41	2.40	8.42	2.77
M1	5	-	71.34	13.85	2.57	2.28	1.07	0.91	0.25	7.31	0.42
$M1_L$			1.29	2.67	9.17	10.37	35.36	12.64	5.24	22.00	1.26
M2	5	1.25	76.20	10.36	2.60	1.98	1.06	0.79	0.17	6.54	0.30
$M2_L$			1.10	2.32	9.16	9.40	37.26	12.62	4.54	22.25	1.34
M3	5	2.5	65.42	22.34	2.72	3.37	1.41	0.78	0.18	2.94	0.83
$M3_L$			0.57	1.19	8.92	7.13	48.00	13.16	3.94	16.12	0.96
M4	5	5	66.77	22.06	2.48	2.77	1.21	1.00	0.17	2.69	0.85
$M4_L$			0.61	1.66	7.96	5.95	48.34	14.40	2.93	16.37	1.79

Note: M refers to the EFM, which had undergone AEE. While, $_L$ refers to the soluble sugars and uronic acid samples of the EFM.

4.1.4 The FTIR and SEC analysis of hemicellulose

The amount of hemicellulose extracted from the lignocellulose biomass of *M. charantia* seeds vary with the presence of enzyme during AEE; $M3_L$ (0.29 %) < $M4_L$ (0.38 %) < $M1_L$ (0.41 %) < $M2_L$ (0.58 %). Only 0.22 % of hemicelullose was recovered in $M0_L$.

Despite significant knowledge in the synergism among cellulase and enzyme cocktail components, a full mechanistic understanding of lignocellulose hydrolysis by cellulolytic enzymes is still limited and needs further refinement (Nill *et al.*, 2018). The variation in the hemicellulose composition showed that as polysaccharides of simpler structure than cellulose, hemicellulose was also prone to breakdown with the presence of hemicellulase (Zhao *et al.*, 2018).

The hemicellulase obtained were further analysed using FTIR spectroscopy as shown in Figure 4.2. The FTIR spectrum showed that there were differences in the peak intensity and between the absorption bands obtained. The absorption of 3272, 2927, 1628, 1416, 1239, and 1038 cm^{-1} peaks represented the characteristic absorption of hemicellulose (Popescu *et al.*, 2010).

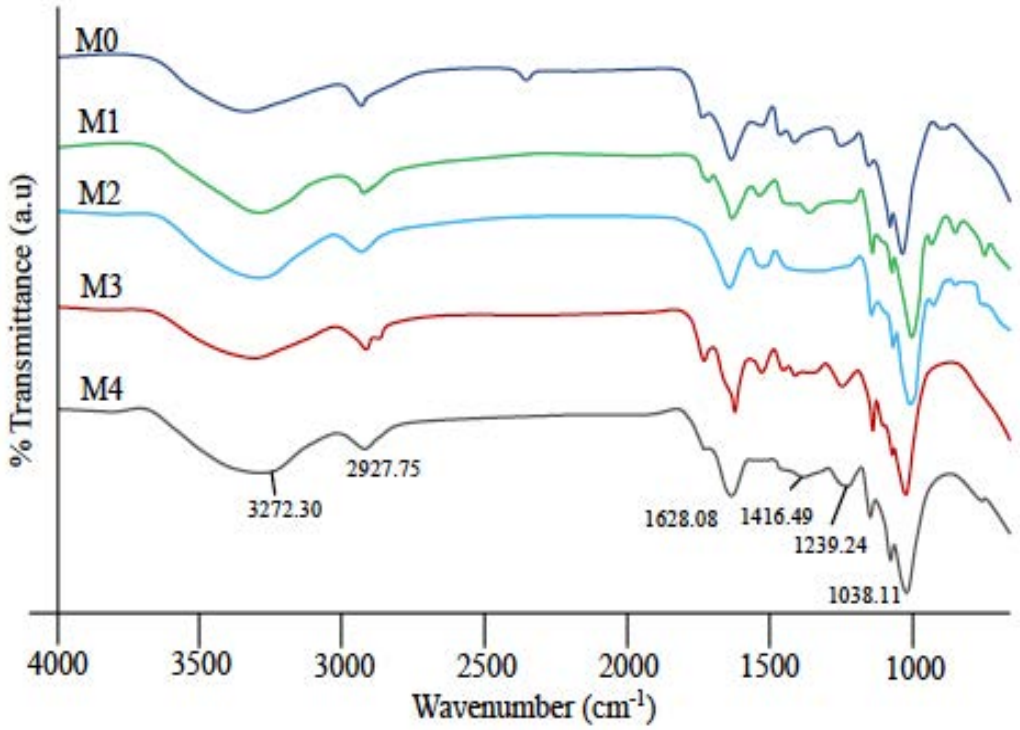

Figure 4.2: The FTIR spectrum of hemicellulose

The broad absorption band at ~3272 cm^{-1} usually represents the O-H or the absorption of a large number of individual molecules, that hydrogen is bonded to a slightly different compound. Meanwhile, the absorption band ~2927 cm^{-1} indicated the presence of C_{sp}^3-H bond stretching vibration. The band ~1737 cm^{-1} referred to the conjugated C=O stretching band of a carbonyl group, be attributed to the presence of the acetyl moiety in the hemicellulose. The absorption that appeared in ~1628 cm^{-1} is usually associated with the absorbed water (Peng *et al.*, 2013). A strong band that appeared at ~1038 cm^{-1} was assigned to C-O bending in sugar (Naidu *et al.*, 2018).

The extracted hemicelluloses were then subjected to size exclusion chromatography analysis to evaluate the effects of the enzymes on their molecular mass distribution. Each extracted sample was observed to have slightly different molecular mass distribution trend. The difference in the molecular mass distribution trend could be due to the effects of different enzymes towards the enzymatic cleavage

of cellulose chain that transformed the hemicelullose into a hemicellulose chains with different unit of sugar depends on the type of enzyme presence in the enzyme cocktails used.

The M0 had the highest weight average (M_w) of 447148–457148 followed by M4 (M_w: 36186–378116), M3 (M_w: 120339), M1 (M_w: 87865), and lastly M2 (M_w: 55915). These results indicated that the treatment degraded the macromolecular structure of hemicellulose to a noticeable extent with the incorporation of enzyme (Izydorczyk & Biliaderis, 1995).

In addition, the high hemicellulose polydispersity (M_w/M_n) from M0 M_w/M_n of 1.15–7.17, to M2 M_w/M_n of 6.06, to M4 M_w/M_n of 1.9- 21.72, to M1 M_w/M_n of 107.71, and lastly to M3 M_w/M_n of 284.30 indicated a wide molecular weight distribution which showed that the hemicellulose obtained was in a big polymer form that might be caused by hemicellulose chain aggregation (Eremeeva, 2003). Figure 4.3 shows the size exclusion chromatogram of the extracted samples.

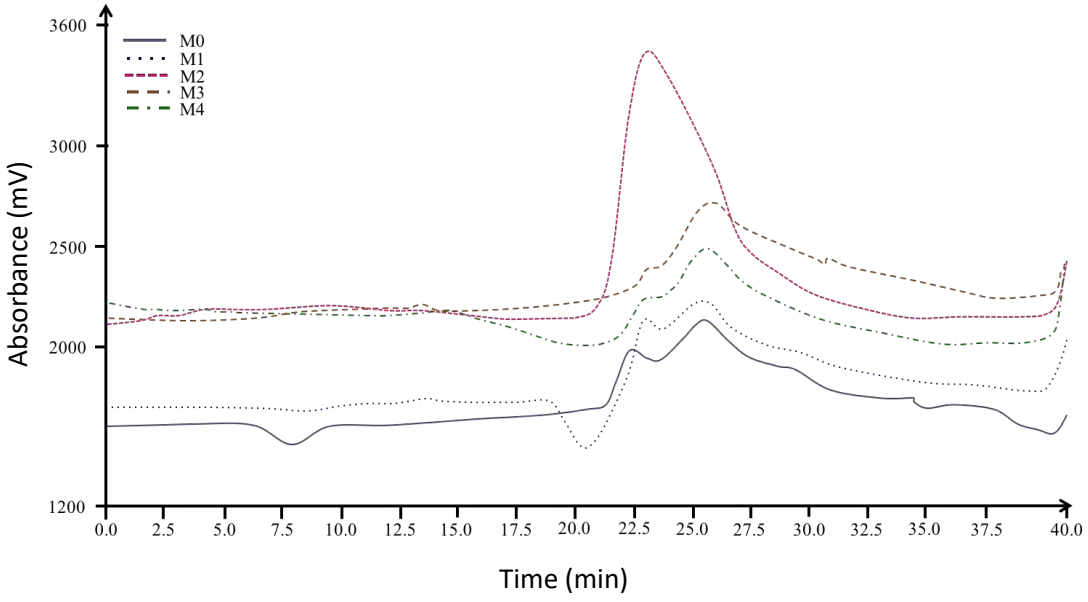

Figure 4.3: The size exclusion chromatogram of hemicelluloses from different *M. charantia* seed extracted free materials.

Based on the FTIR spectrum the introduction of enzyme does not affect the hemicellulose backbone structure despite difference molecular mass distribution was observed in SEC analysis. In addition, it can be concluded that the optimum seed samples and their enzyme cocktail ratios for the HEL1: X7 were found to be 5:1.25 as in M2.

4.2 The studies of *M. charantia* fruits flesh

In this study, the *n*-hexane, ethyl acetate, and methanol extract of *M. charantia* fruit underwent preliminary *in vitro* screening of the anti-dengue activity. The composition of the active extract was screen by using GC-MS.

4.2.1 Preparation of *M. charantia* fruit flesh extract

The *M. charantia* fruits were sun-dried prior to extraction as the drying process removed the water and halt any enzymatic activity present in the plant cell (Mozhaev, 1998). This step was to minimize the hydrogen bonding interaction of water in the fruits with its metabolites that disrupted the solvent extraction process and affected the amount of solute been extracted. (Brini *et al.*, 2017).

The drying temperature also played an essential role as Anwar and co-workers concluded that the drying temperature of below 60 °C did not adversely affect the total phenolic content of cauliflower extract (Anwar *et al.*, 2013). However, the total phenolic content of cauliflower extract decreased significantly when the drying temperature was set above 70 °C. Hence, the sun-dried temperature (31– 39 °C) of *M. charantia* fruits preserved its chemicals composition.

The dried fruits were grounded into a course size before the extraction process to create more space for the solvent to penetrate the cells and extract the secondary metabolites. The grounded condition would increase the particle surface area and increased the solvent and fruit contact point (Al-Sumri *et al.*, 2016). However, if the dried fruits being grounded too fine, it will cause the excessive absorption of solute in solid and difficulty in subsequent filtration (Zhang *et al.*, 2018).

The solvent-to-solid ratio of 10:1 was used. The solvent-to-solid ratio also played an essential role in the extraction process. The higher solvent-to-solid ratio will increase the concentration gradient and diffusion rate. Hence, the equilibrium constant will be affected with the increments of the extractive yield. However, a high solvent-to-solid ratio will cause excessive extraction solvent, and a longer time is required for concentration using a rotary evaporator (Predescu *et al.*, 2016).

The mixtures were then shaken and stirred to facilitate the extraction process and enhanced its diffusivity (Mohdaly & Smetanska, 2010). The extraction process was carried out at room temperature. Even though high temperature increased the solubility and diffusivity, too high temperature may cause the loss of solvents, the extraction of the undesirable impurities, and the decomposition of thermolabile compounds, such as anthocyanins (Seidel, 2006; Selvamuthukumaran & Shi, 2017).

The quantity of the extract is corresponding to the type of solvents being used base on the law of similarity and intermiscibility. Solvents with a polarity value near to the polarity of the solute are likely to perform better and vice versa (Burke, 1984). The quantity of extractive material extracted from the *M. charantia* fruits with the use of non-polar to polar solvent implies the variation of phytochemical compounds (Muhamad *et al.*, 2014).

As plants contained a variety of bioactive compounds with difference solubility properties in a different solvent, the optimal solvent used for extraction depends on the particular plant materials, and the compounds that are to be isolated (Truong *et al.*, 2019; Mahdi-Pour *et al.*, 2012; Masoko, 2007). The use of a non-polar solvent showed the lowest amount of extractive being extract with the percentage of yield of 0.49 ± 0.03 % followed by extractive extract by ethyl acetate, 1.48 ± 0.11 %, and methanol, 3.4 7±0 .04 %, as presented in Table 4.4.

Table 4.4: The percentage of yield for *M. charantia* fruits extraction

Extract	Percentage of yield (%)
n-hexane	0.49 ± 0.03
Ethyl acetate	1.48 ± 0.11
Methanol	3.47 ± 0.04

Note: The extraction process was triplicated.

$$\text{The percentage of fruits flesh extracted} = \frac{\text{Weight of extract obtained (mg)}}{\text{Weight of dry fruits flesh used (mg)}} \times 100\%$$

4.2.1(a) Anti-dengue screening of *M. charantia* fruits flesh extract

In the *M. charantia* fruit flesh extracts anti-dengue screening study, the extracts were incorporated into the protease reaction to a final concentration of 200 ppm. Each extract was tested in triplicate and each set was repeated twice.

In this study, the ethyl acetate extract showed an highest inhibition activity. The methanol extract showed the least inhibitory activity towards DENV-2 NS2B/NS3 protease with only 10.37 ± 1.13 %. The semi-polar *M. charantia* extract from ethyl acetate showed the highest DENV-2 NS2B/NS3 protease inhibitory activity of 38.11 ± 1.06 %. The difference in the inhibitory activity obtained was suggested due to the type of bioactive compounds being extracted in a different type of solvent (Altemimi

et al., 2017; Farahmandfar *et al.*, 2019). The result of this preliminary anti-dengue screening is shown in Table 4.5.

Table 4.5: The inhibition activity of *M. charantia* fruits extract towards DENV-2 NS2B/NS3 protease.

Extract	% Inhibition
n-hexane	21.73 ± 1.01
Ethyl acetate	38.11 ± 1.06
Methanol	10.37 ± 1.13

Note: The assay was triplicated with the final concentration of 200 ppm.

The ethyl acetate extract with the most DENV-2 NS2B/NS3 protease inhibitory activity underwent screening using GC-MS to identify its bioactive components.

4.2.1(b) The GC-MS screening of *M. charantia* fruit flesh extract

In choosing ethyl acetate as one of the solvents utilized during the extraction process, the factor such as its polarity index of 4.4 P′ was taken into consideration. As a semi-polar solvent was used, it was anticipated that ethyl acetate extract might contain many bioactive compounds such as alkaloids, phenols, steroids, flavonoids, saponins, and terpenoids (Pham *et al.*, 2019; Harlita *et al.*, 2018; Arega, 2018; Jia *et al.*, 2017).

The ethyl acetate extract could be analysed using either LC-MS or GC-MS. In this study, the most widely used techniques GC-MS was used to identify the bioactive compounds presence in the ethyl acetate extract of *M. charantia* fruits flesh. GC-MS is exclusively used for the analysis of esters, fatty acids, alcohols, aldehydes, terpenes.

Intrinsically, with the use of the flame ionization detector and the electron capture detector (which have very high sensitivities) gas chromatography can quantitatively determine materials present at very low concentrations (Al-Rubaye *et al.*, 2017).

Figure 4.4 showed various peaks indicating the presents of different compounds in the *M. charantia* fruit ethyl acetate extract. The GC-MS chromatogram profile revealed the presence of 32 different peaks and was characterized and identified by comparison of their mass fraction patterns with similar National Institute of Standards and Technology (NIST) library or published data. These compounds represented different phytochemical classes, including sterol, fatty acid, triterpene, and phenol. Whilst, the major compounds were tabulated in Table 4.6.

Some of the remaining compounds with the peak area of 1–2 % were 1,4-bis(trimethylsilyl)benzene (rt. 44.395 min, 1.953 %), hexamethyl-cyclotrisiloxane (rt. 44.288 min, 1.9 %), 25-desacetoxy cucurbitacin b (rt. 44.670 min, 1.574 %), butyl ester acetic acid (rt. 2.485 min, 1.539 %), 3,5-bis-trimethylsilyl-2,4,6-cycloheptatrien-1-one (rt. 33.29, 1.434 %), 1,2-bis(trimethylsily)benzene (rt. 44.923 min, 1.433 %), bis(2-ethylhexyl) ester decanedioic acid (rt. 40.552 min, 1.346 %), diisooctyl phthalate (rt. 36.806 min, 1.297 %), *N*-trifluoroacetyl-1-aminononadecane (rt. 47.265 min, 1.297 %), retinal (rt. 33.660 min, 1.23 %), and 2,6-dihydroxyacetophenone (rt. 47.825, 1.035 %) . Whereas, the remaining compounds were present in a trace amount with the peak area less than 1 % including gallic acid (rt. 5.017 min, 0.54 %).

As been observed from the chromatogram (Figure 4.4), the baseline are not straight and there is high bleed, suggested due to leak in the system or oxidation of the stationary phase of the column despite the sample being injected for more than three times. However, this bleed does not visible as peaks and not affecting the qualitative analysis (Rood, 1995 & Stein, 1999). Some peaks seem to be broad suggested due to

the incomplete vaporisation of the analyte despite using 5 °C per minutes temperature gradient as the extract usually containing a complex mixtures of volatile compounds (Vial *et al.*, 2009 & Hites, 1997).

It shall be noted that the compounds present, their identities, and the number of identified compounds were not absolute and limited as per material only utilized in this study only. Although the peak of gallic acid was observed in less 1 %. Jia and co-worker (2017), reported that gallic acid to be the main phenolic acids presence in *M. charantia* fruit flesh.

In addition, the dengue fever treatment with a pentaherbal medicine; Denguenil Vati, significantly recovered the virus by increasing the total platelet numbers and total red blood cell count. The high performance liquid chromatography (HPLC) analysis detected gallic acid as one of the Denguenil formulation (Balkrishna *et al.*, 2020).

Besides, the gallic acid and its derivatives appeared to be the most readily available chemical that is easily found in the laboratory (Ow & Stupans, 2005; Choubey *et al.*, 2015; Belin *et al.*, 2003). However, among all the compounds, gallic acid is the ideal compound be a structure analogue for hemisynthesis. Hence, this study focused on the synthesis of therapeutically promising gallic acid derivatives as the scaffolder to produce a hit-to-led compounds with anti-dengue properties.

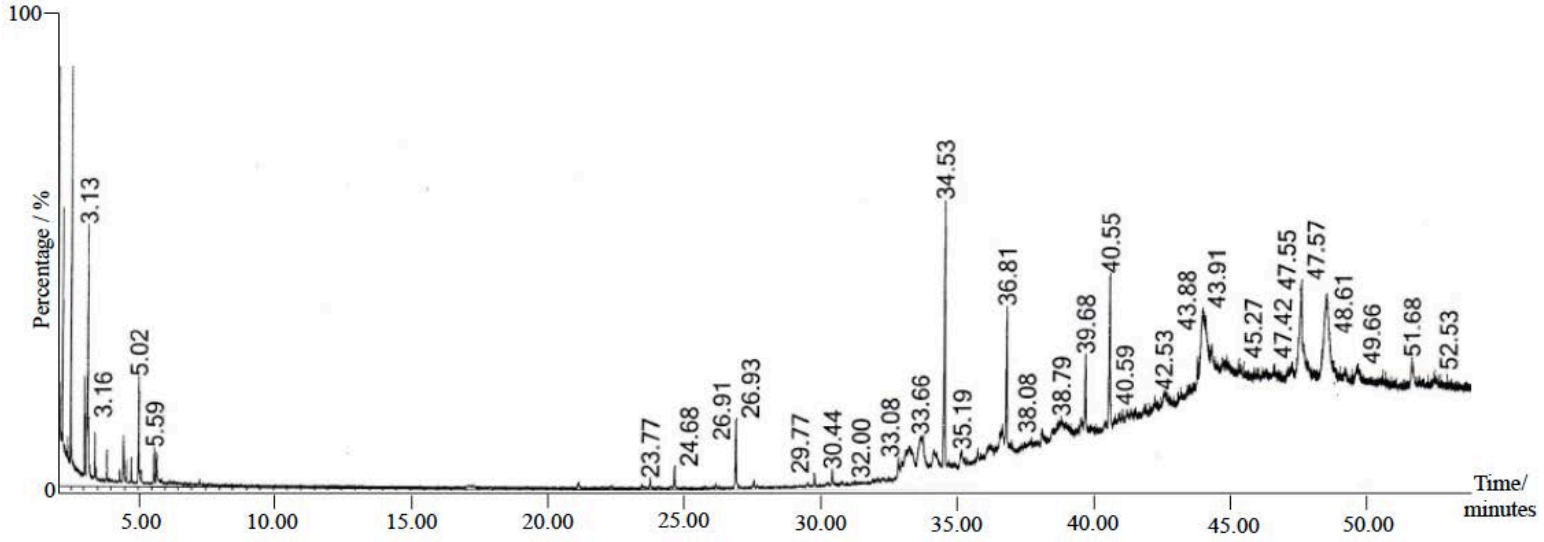

Figure 4.4: The GC-MS chromatogram of *M. charantia* fruit ethyl acetate extract.

Table 4.6: The major phytochemicals identified in the *M. charantia* fruit ethyl acetate extract by GC-MS.

No.	Retention time (min)	Peak total area (%)	Compound name	CAS No.	Library match (%)
1	48.521	5.707	10,12,14-nonacosatriynoic acid	126115-85-3	53.0
2	43.915	5.439	(5α)-3-Ethyl-3-hydroxyandrostan-17-one	57344-99-7	49.1
3	47.573	4.891	(3β,5*S*,22*E*)-3,5-cyclostigmasta-6,22-diene	107304-12-1	56.1
4	34.533	2.111	bis(2-ethylhexyl) ester hexanedioic acid	103-23-1	63.7

4.3 The synthesis of pyrazolyl substituted benzylidene indanone derivatives

4.3.1 The synthesis of ethyl 3,4,5-trimethoxybenzoate, 85

The reaction involved in the formation of compound **85** start with the esterification of compound **84**.The mechanism associated with the esterification of carboxylic acid using alcohol and sulfuric acid catalyst were described by Zimmermann & Rudolph (1965) as the following; The compound **84** extract a hydrogen ion from the concentrated sulphuric acid catalyst. The hydrogen ion attached to the oxygen with the lone pairs located at the carbonyl group.

Next, the electron charge present in compound **84** cation was delocalised to form the resonance structures making the carbonyl carbon a much better electrophile. Later, the compound **84** the carbonyl carbon is attacked by the lone pairs of the ethanol molecule to form a an unstable tetrahedral intermediate. The unstable tetrahedral intermediate carbocation underwent a transfer of an electron from the ethanol to one of the oxygen atom of the hydroxy groups.

The unstable tetrahedral intermediate reforms a carbonyl compound by eliminating the weakest base. The tetrahedral intermediate formed by the nucleophilic attack of the alcohol can then isomerise by means of proton migration, to allow water to behave as a leaving group. Hence, the water being eliminated and a carbocation was formed. The carbocation was stabilised by resonance. Lastly, the ester is deprotonated by the hydrogen sulphate ion, resulted in the formation of compound **85** and the regeneration of sulphuric acid catalyst. The formation of compound 85 was shown in Figure 4.5.

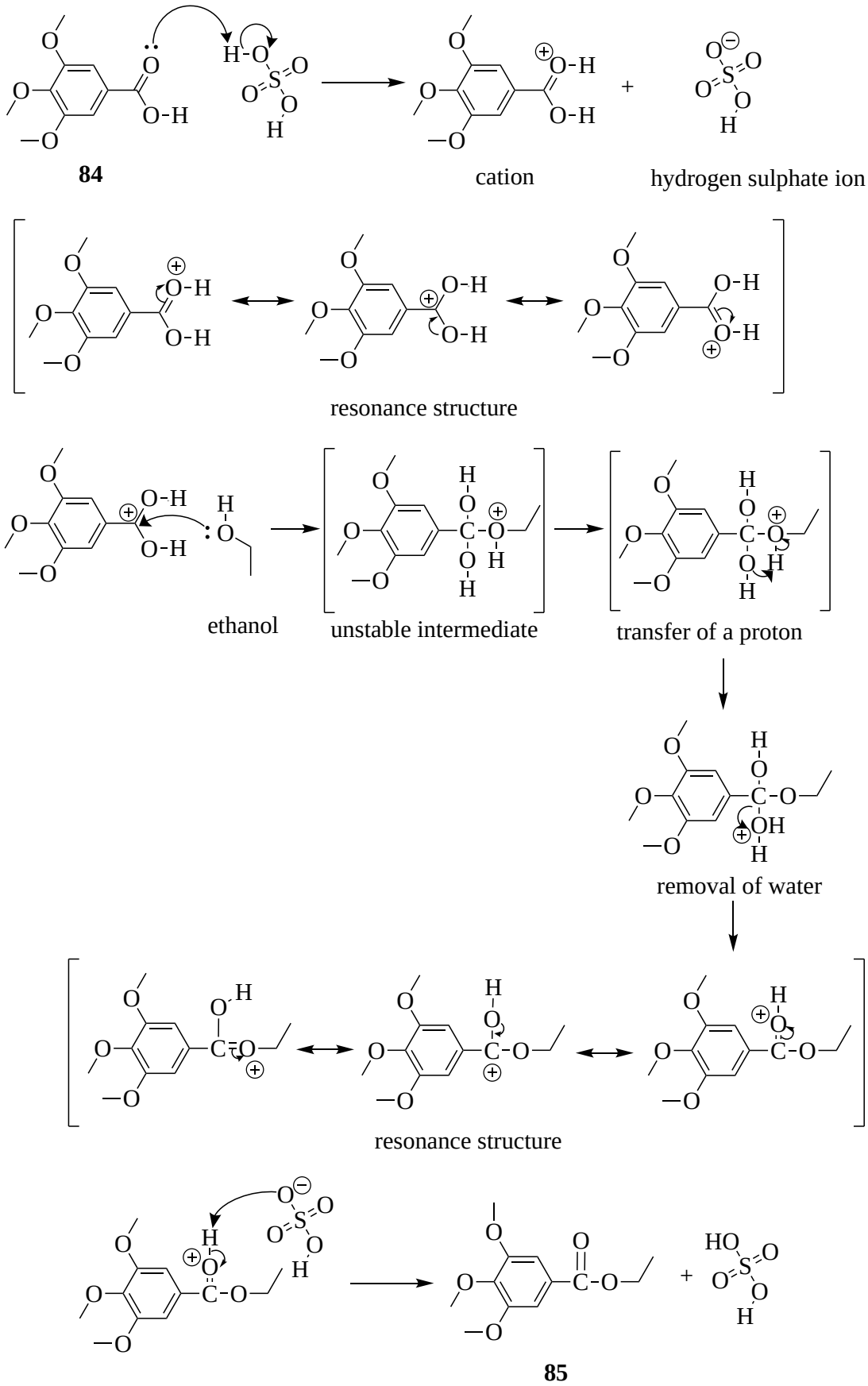

Figure 4.5: The formation of compound **85**

Sulfuric acid is chosen as the catalyst to facilitate the nucleophilic attack of the alcohol at the carbonyl carbon of the carboxylic acid (Ahmad *et al.*, 2007). Besides, the reaction was carried out in the excess solvent to drive the equilibrium shifted to the product to obtained more ester by the Le Chatelier's Principle (Sandler *et al.*, 1992).

The synthesized compound **85** afforded in a good yield of 85.99 % as a colourless crystal with a melting point of 50–53 °C. Schejbal and co-worker (2014) reported a colourless crystal been synthesized with the melting point of 54–55 °C. The compound was characterized using, FTIR, ^{1}H-NMR, and ^{13}C-NMR.

4.3.1(a) The characterization of ethyl 3,4,5-trimethoxybenzoate, 85

The FTIR was used to characterize the structure of chemical compound as it has the ability to identify the functional group of the chemical compound. The comparison between the FTIR spectrum of starting material, compound **84** and synthesized compound **85** were depicted in Figure 4.6.

The important absorption bands in IR spectrum of compound **85** were observed at 2940 (C_{sp}^{3}-H), 1715 (C=O ester), 1181 (C-O, ester). The different in absorption band characteristic were observed at 2940–3020 cm^{-1} for both compounds. The FTIR spectrum of compound **84** absorption band was broader indicating at 2940–3020 cm^{-1} indicated the presence of O-H stretching frequencies with the overlapped signal of C_{sp^3}-H stretching.

In the preparation of compound **85**, the starting material **84** underwent esterification process, which led to the removal of hydrogen and the formation of ester group resulting in the appearance of a sharp α,β-unsaturated ester C=O band at

1715 cm^{-1}, which replace the C=O acid band at 1698 cm^{-1} of compound **84**. Besides, the broad -OH absorption at ~3020 cm^{-1} disappeared indicating that the esterification step is completed. In addition, the O-C band can be observed at the 1181 cm^{-1} and 1227 cm^{-1} (Pavia *et al.*, 2015).

In compound **84**, the resonance between the carbonyl group with it neighbouring oxygen atom of -OH acid group resulted in weakening of the C=O vibration. Hence the wavenumber/frequency of C=O acid decreased compared with the wavenumber/frequency of C=O ester.

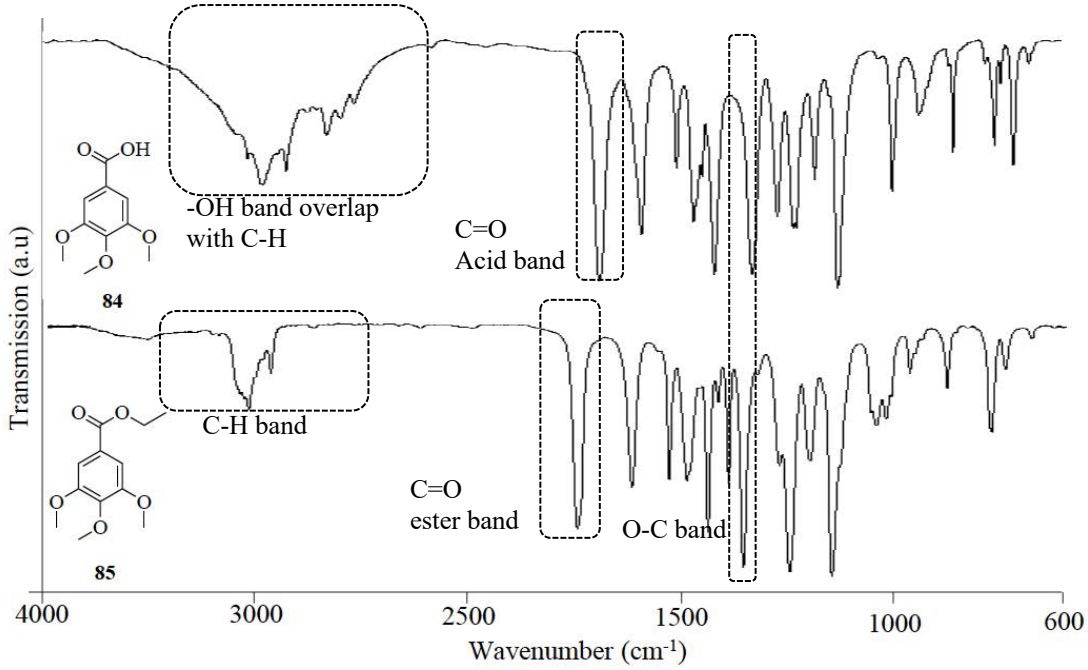

Figure 4.6: The comparison between FTIR spectrum of compound **84** (starting material) and synthesized compound **85**

The synthesized compound was further characterized by ^{1}H-NMR, and ^{13}C-NMR using DMSO-d_6 as a solvent. In the ^{1}H NMR spectrum (Figure 4.7), the appearance of a triplet signal at δ_H 1.33 (J=7.09, 8.00 Hz) was assigned to the methyl group with three protons located at H-12. The two prominent singlet signals at δ_H 3.73,

and 3.83 were assigned to the methoxy group with three protons located at H-8 and six protons located at H-7 and H-9 respectively. A small quartet signal appeared at δ_H 4.32 (J=7.09, 8.00 Hz) was assigned to two methylene protons located at H-11. Whilst, the two protons signal for the aromatic hydrocarbon, -CH, of C-2, and H-6, appeared at δ_H 7.23. The signal appeared at the most downfield area compared to other proton signals due to the deshielding effect of both aromatic and double bond near it (Lampman *et al.*, 2010).

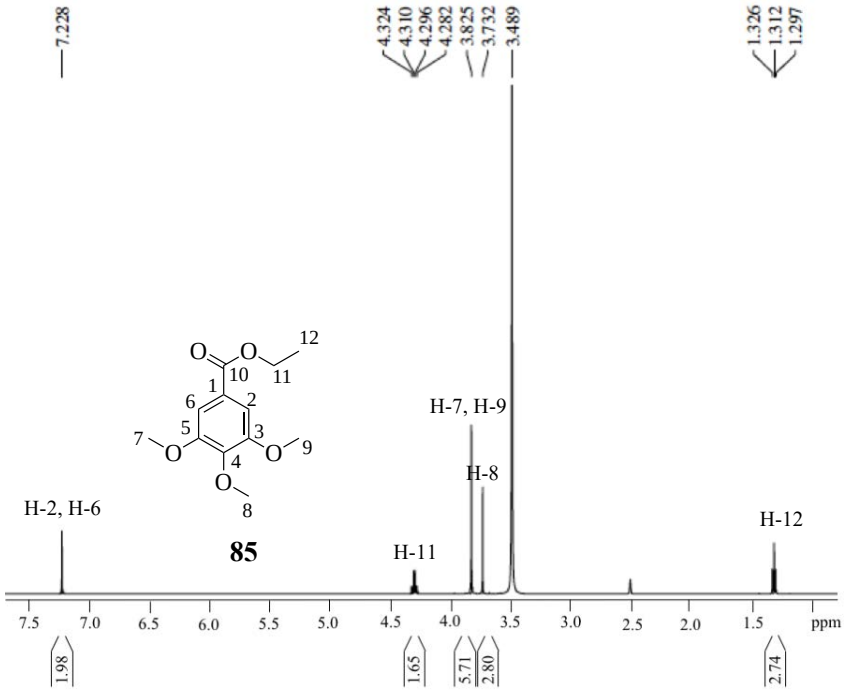

Figure 4.7: The ^{1}H NMR spectrum of compound **85**

The type of carbon present in compound **85** was determined by the ^{13}C NMR spectroscopy. The ^{13}C NMR spectrum (Figure 4.8) showed the appearance of a signal at δ_c 14.64 which indicated the presence of methyl group. The aromatic hydrocarbon, -CH, signal appeared at δ_c 106.87. One methoxy and one methylene carbon signal appeared at the range of δ_c = 56.00–62.00 ppm. Hence, the characterization results

obtained were in agreement with the previous studies (Schejbal *et al.*, 2014; Verma *et al.*, 2012; Li *et al.*, 2017).

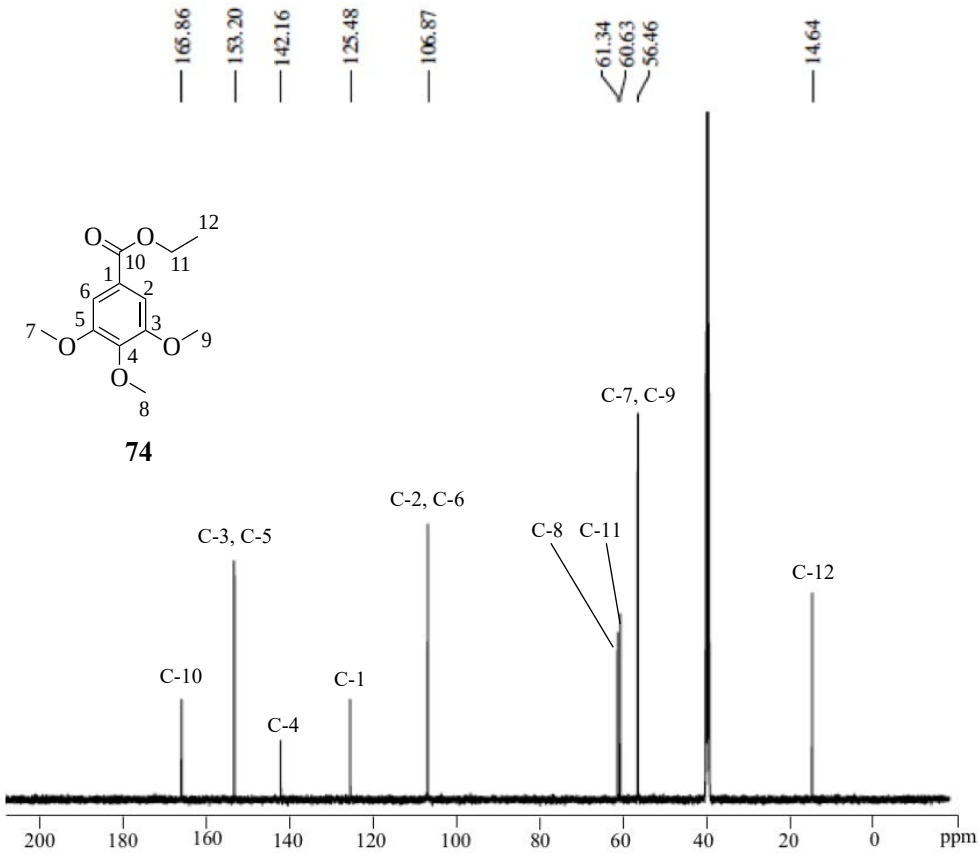

Figure 4.8: The ^{13}C NMR spectrum of compound **85**

4.3.2 The synthesis of 3,4,5-trimethoxybenzohydrazide, 86

The compound **85** underwent further nucleophilic acyl substitution reaction with hydrazine monohydrate to obtain the desired compound **86**. In the first step, the prior synthesized compound **85** carbonyl carbon is attacked by the lone pairs from the nitrogen atom of the hydrazine molecule to form a tetrahedral intermediate. The ethoxy group attached to the new tetrahedral carbon atom leaved with the negative charge as it is a weaker base than the amino group. The extra hydrogen atom at the hydrazine leaved with a positive charge (Smith & March, 2006 & Bruice, 2004), led to the

formation of the compound **86** and ethanol as the side product. The reaction mechanism were illustrated in the Figure 4.9.

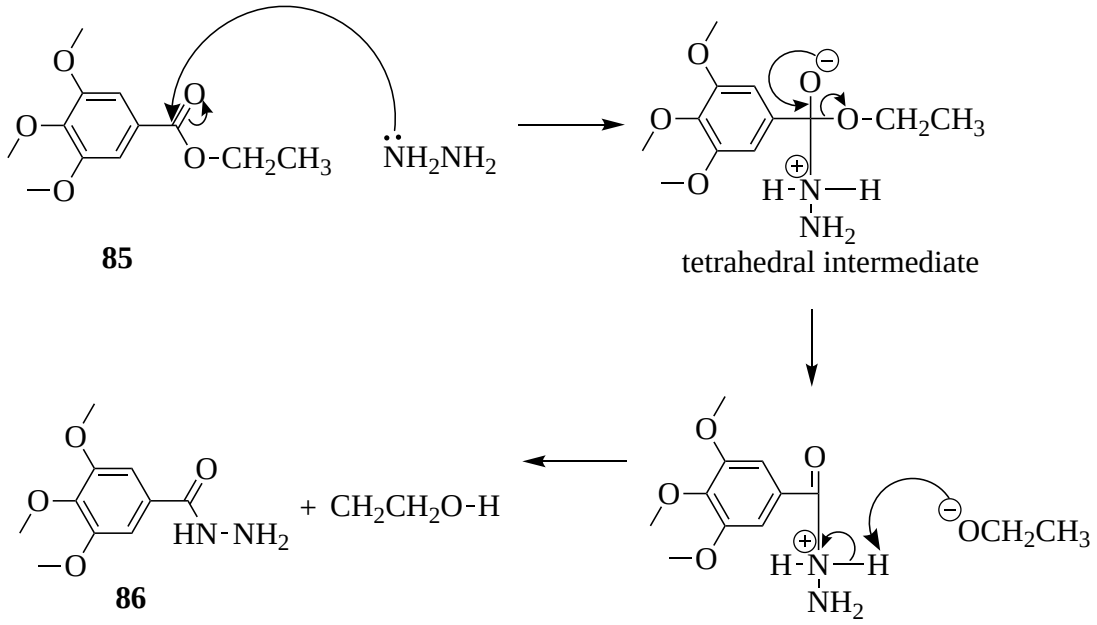

Figure 4.9: The reaction mechanism for the formation of compound **86**

The synthesized compound **86**, yielding a good result of 85.31 % as a light brown crystalline solid with a melting point of 157–160 °C. Kamal and co-worker (2014) reported that compound **86** was obtained as a crystalline solid with a melting point of 158–160 °C. The compound was characterized using, FTIR, ^{1}H-NMR, and ^{13}C-NMR.

4.3.2(a) The characterization 3,4,5-trimethoxybenzohydrazide, 86

The important absorption bands in IR spectrum of compound **86** were observed at 3364 (N-H), 3319 (N-H), 1659 (amide C=O), 1385(C-N). The major difference between the two FTIR spectrum are the appearance of primary and secondary amine peak in compound **86** at 3364 cm^{-1} and 3319 cm^{-1}. Besides, the disappearance of a

sharp C=O ester band of compound **85** at 1715 cm^{-1} and the appearance by the sharp C=O amide band at 1659 cm^{-1} showed that amide was formed.

The conjugation of carbonyl group in compound **86** with the neighbouring nitrogen atom of amide, -NH-NH_2 weakening the C=O vibration. Hence, the wavenumber/frequency of C=O amide was lower compared with the wavenumber/frequency of C=O ester in compound **85**. The comparison between the FTIR spectrum of compound **85** and synthesized compound **86** were depict in Figure 4.10.

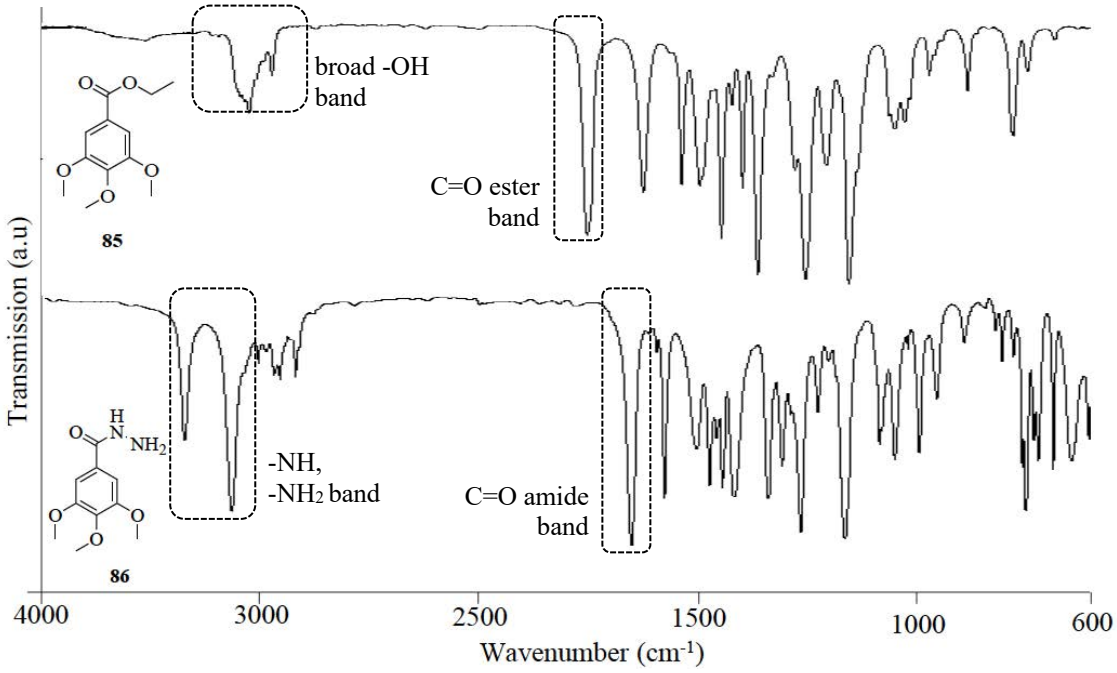

Figure 4.10: The comparison of compound **85** and compound **86** FTIR spectra.

The synthesized compound was further characterized by ^{1}H-NMR, and ^{13}C-NMR using DMSO-d_6 as a solvent. The ^{1}H NMR and ^{13}C-NMR spectrum of compound **86** are shown in Figure 4.11 and Figure 4.12 respectively. The important

chemical shift, which are the appearance of primary and secondary amine signals at of δ_H 4.47 and δ_H 9.74, respectively in the ^{1}H-NMR spectrum.

In addition, only two signals are observed at the range δ_c 56.00–62.00, which represent the carbon attached to a methoxy group signal in the ^{13}C-NMR spectrum of compound **86**. Besides, the methyl group signal at δ_c 14.64 disappeared. This indicate the success of acylation of amine process. The characterization results of compound **86** were in agreement with the previous studies (Kamal *et al.*, 2014; Ahmed *et al.*, 2018; Murty *et al.*, 2016).

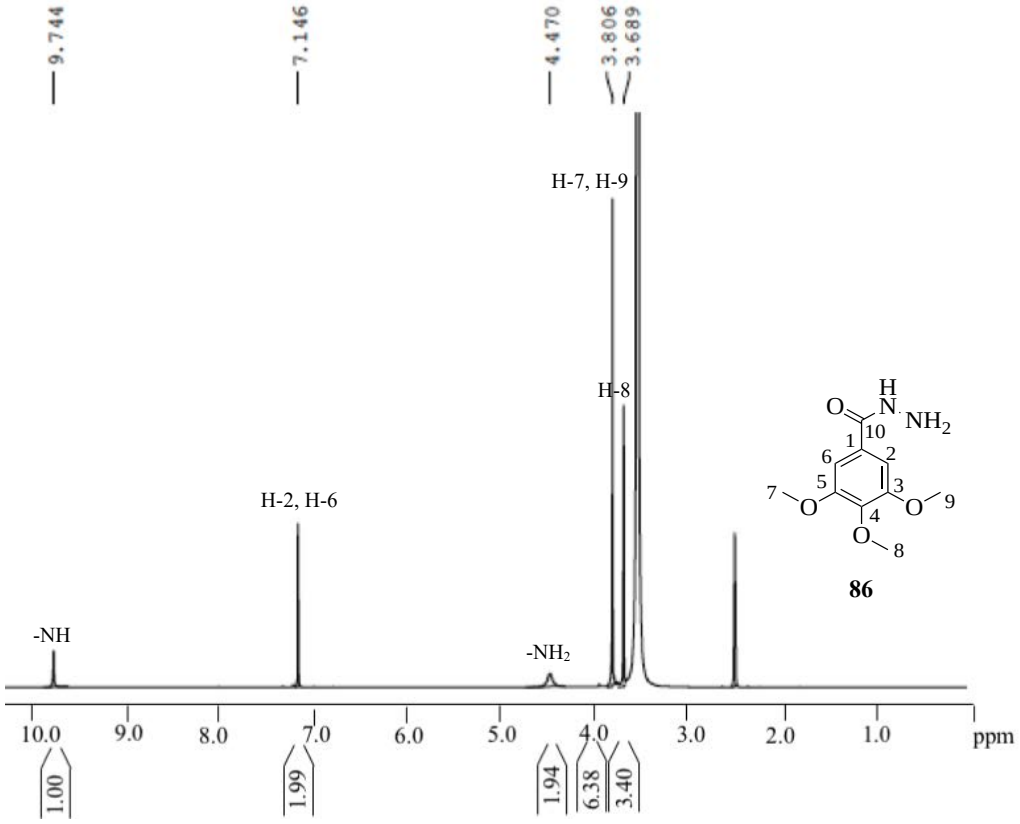

Figure 4.11: The ^{1}H NMR spectrum of compound **86**

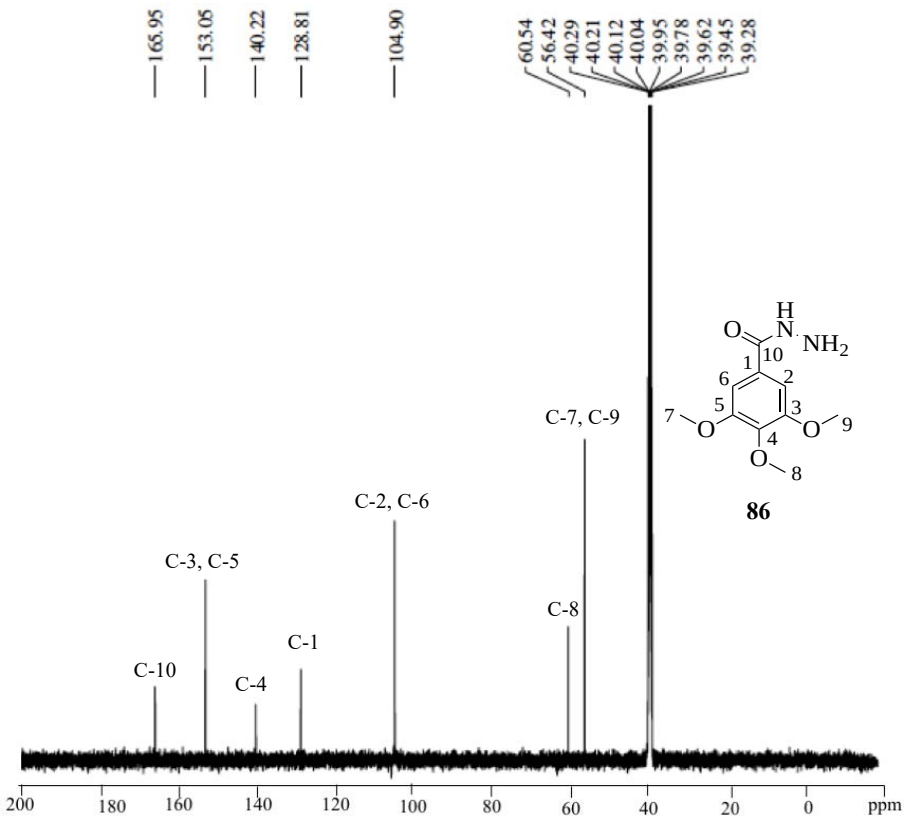

Figure 4.12: The ^{13}C-NMR spectrum of compound **86**

4.3.3 The synthesis of benzylidene indanone derivatives, 89a-t

In step 3, the benzylidene indanone derivatives [**89a-t**] were synthesized using aldol condensation method. The aromatic aldehyde were reacted with aromatic ketone in the presence of potassium hydroxide as a basic catalyst. Its required an aldehyde or ketone that contains at least one α-hydrogen. The α-carbon became nucleophilic when it is deprotonated by a base. The carbonyl carbon is electrophilic. The two oppositely charged species were bring together by Coulomb Law to form a C-C bond (Bruice, 2004).

The reaction start with the deprotonation of aromatic ketone **[88a-b]** by the hydroxide ion to generate an enolate ion. The enolate was formed at the indanone as the α-hydrogen exhibited acidity properties in the presence of a carbonyl group. Hence, strong base was chosen as the catalyst in the reaction to produce the hydroxide ion that

attacked the acidic α-hydrogen in the ketone, which led to the formation of reactive enolate ion (Clayden *et al.*, 2012). The enolate ion was able to undergo an electron rearrangement to obtain a more stable enolate ion. After that, the enolate ion underwent a nucleophilic addition of the enolate ion to the carbonyl group of the aromatic aldehyde **[87a-j]**. The electron rich carbanion acted as a nucleophile and attacked the electron-deficient carbon located at the carbonyl group of the aldehyde by nucleophilic addition reaction. The alkoxide ion was formed. The alkoxide ion underwent protonation by extracting the proton from the methanol, resulting in the aldol product formation. Since, this reaction was carried out under reflux, the heated reaction mixture of ß-hydroxyl carbonyl underwent an E_2 reaction to form a double bond between the α and ß position (Matt, 2011; Vollhardt *et al.*, 2007). The reactions mechanism as depicted in Figure 4.13. Table 4.7 summarized the percentage of yield and the physical properties of compounds **89a-t**.

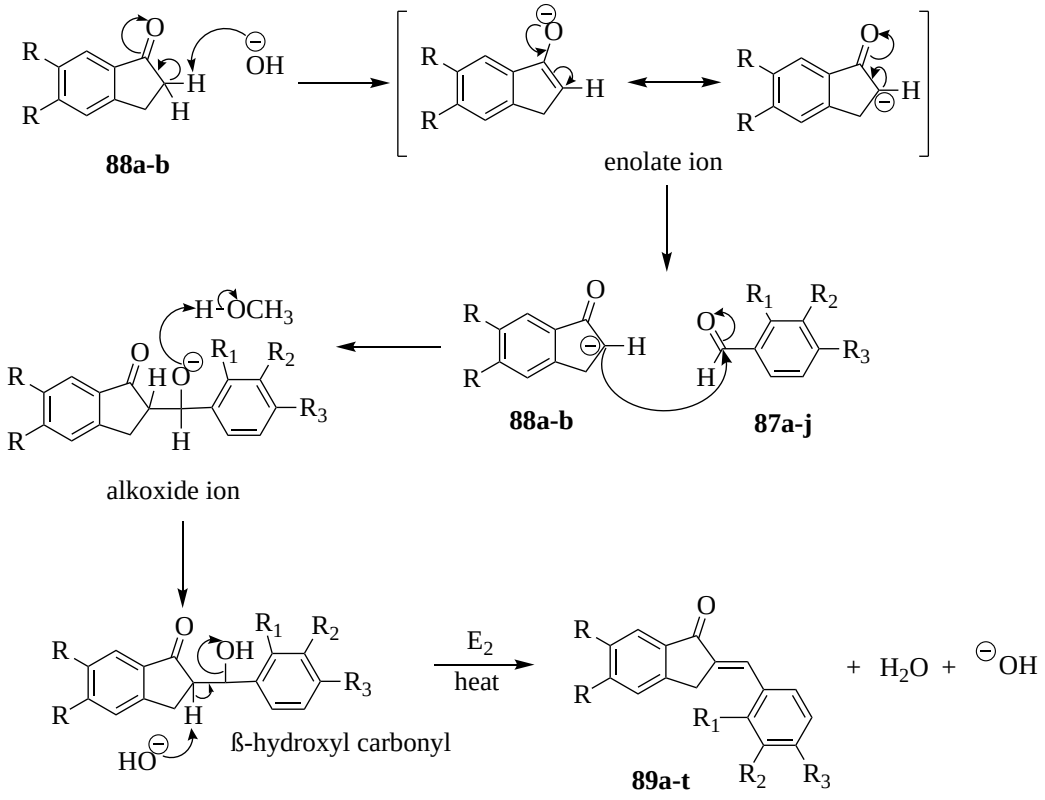

Figure 4.13: The formation of compounds **89a-t**

Table 4.7: The physical properties of synthesized compounds **89a-t**

Compounds	Formula	Yield (%)	Colour	Melting point (ºC)
89a	$C_{16}H_{12}O$	72.21	White	105–109
89b	$C_{17}H_{14}O_2$	86.78	White	138–140
89c	$C_{17}H_{14}O$	93.68	White	137–139
89d	$C_{16}H_{11}ClO$	94.48	White	137–139
89e	$C_{19}H_{18}O$	64.87	Cream	134–137
89f	$C_{18}H_{17}NO$	87.95	Yellow	164–168
89g	$C_{20}H_{19}NO_2$	93.62	Yellow	177–181
89h	$C_{21}H_{21}NO$	90.69	Cream	178–181
89i	$C_{18}H_{16}O_3$	84.12	Yellow	181–185
89j	$C_{17}H_{13}NO_4$	83.74	Cream	189–191
89k	$C_{18}H_{16}O_3$	84.90	Light yellow	178–181
89l	$C_{19}H_{18}O_4$	94.28	Light yellow	210–216
89m	$C_{19}H_{18}O_3$	83.37	White	198–210
89n	$C_{18}H_{15}O_3Cl$	78.62	Cream	178–181
89o	$C_{21}H_{22}O_3$	82.76	Light yellow	168–175
89p	$C_{20}H_{21}NO_3$	76.59	Orange	165–180
89q	$C_{20}H_{23}NO_4$	86.20	Light orange	195–199
89r	$C_{20}H_{21}NO_3$	84.52	Brown	200–203
89s	$C_{20}H_{20}O_5$	80.58	Yellow	200–205
89t	$C_{19}H_{17}NO_6$	75.62	Cream	233–237

This reaction was a water sensitive reaction, where water was eliminated as one of the end product. The used of ethanolic potassium hydroxide avoid the presence of water that facilitate the reaction to shift towards the left (the starting material) due to the decrease in dehydration reaction rate with the presence of water (Sandler *et al.*, 1992).

The reactions took up to 24 hours to be completed. It is suggested that aldehyde is used as the electron-donating substituent, which has a less electrophilic character. Hence, it slowed down the rate of reaction (Ali *et al*., 2013). Despite the prolonged reaction time, the synthesized benzylidene indanone derivatives, **89a-t** afforded in a good yield in the range of 60–95 %.

The compounds were characterized using, FTIR, ^{1}H-NMR, and ^{13}C-NMR. The compounds with a suitable crystal size and form were submitted for X-ray crystallography analysis.

4.3.3(a) The characterization of benzylidene indanone derivatives, 89a-t

There are four key FTIR absorption bands in compounds **89a-t**; the C_{sp}^{3}-H bonds vibration at the range of 2910–2920 cm^{-1}, the strong C=O stretching at 1690–1695 cm^{-1}, the -CH aromatic stretching at 1580–1620 cm^{-1} and the C-H out-of-plane bending vibration of aromatic ring substituents at 600–900 cm^{-1} (Table 4.8).

Compound **89b** is the representative compound from the benzylidene indanone derivatives. The FTIR spectrum of compound **89b** (Figure 4.15) displayed an absorption band at 2914 cm^{-1}, which assigned to the C_{sp}^{3}-H bonds vibration. The strong peak of conjugated C=O stretching indicated the carbonyl moiety of ketone was observed at 1694 cm^{-1}. In addition, the absorption of -CH aromatic stretching can be

seen at 1575–1629 cm^{-1}. Apart from that, the absorption at 692–836 cm^{-1} located at the fingerprint region can be attributed to the C-H out-of-plane bending vibration of aromatic ring (Wang & Sanders, 1959).

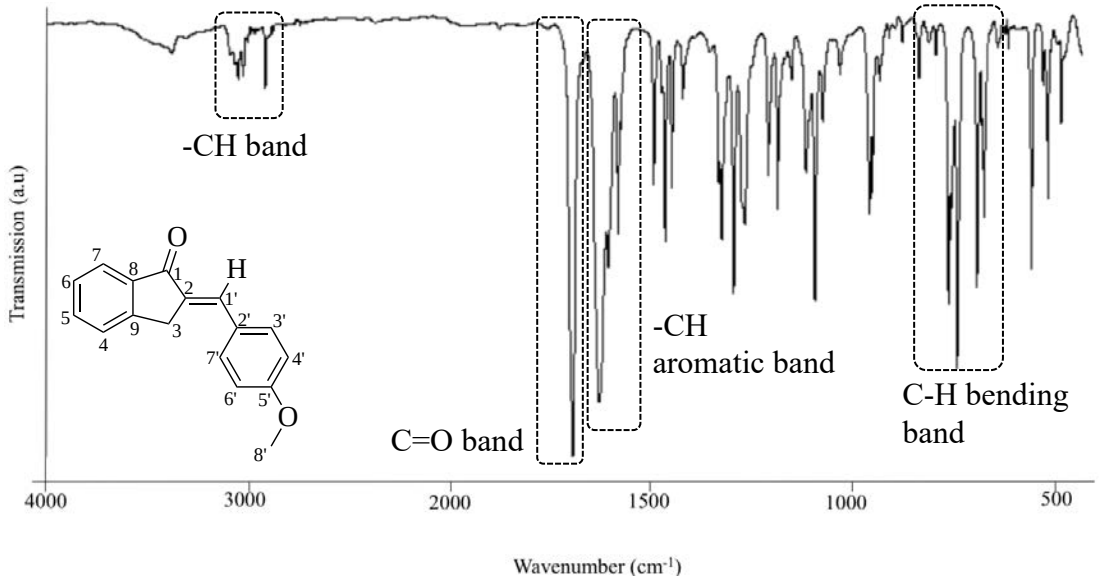

Figure 4.14: The FTIR spectrum of compound **89b**

In aldol condensation, the reaction involved the formation of carbon-carbon bond when the aromatic aldehyde **[87a-j]** reacted with the enolate ion of ketone **[88a-b]**. The carbon-carbon (-C=CH) peak usually appear δ_H 7.50–7.60. In addition, compounds **89a-t** showed similar trend of signals and the number of carbon atoms were in accordance to the structures. The chemical shift of ^1H and ^{13}C for compounds **89a-t** were tabulated in Table 4.8.

In compound **89b**, a singlet peak appear at the downfield region, δ_H 7.51 attributed to the -C=CH proton of H-1' that formed during the condensation of indanone with anisaldehyde. A broad methylene peak of H-3 appeared at δ_H 4.05 and the sharp singlet peak of H-8' was observed at δ_H 3.82 attributed to $-OCH_3$ in the ^1H NMR spectrum of compound **89b** as depicted in Figure 4.15 (Sabri *et al.*, 2018). In

addition, the doublet peaks at δ_H 7.055–7.073 with J = 9.0 attributed to the proton-proton coupling in aromatic ring located at the benzene moiety of H-3' and H-7'. The triplet peaks were observed at δ_H 7.455–7.484 with J = 9.0 attributed to H-4. While multiplet peaks at δ_H 7.657–7.709 and 7.736–7.780 that attributed H-4', H-6', H-5, H-6, and H-7. The triplet and multiplet peaks formed were suggested due to the proton of indanone group of is influenced by the spinning arrangement of the protons in the adjacent aromatic aldehyde group (Lampman *et al.*, 2010).

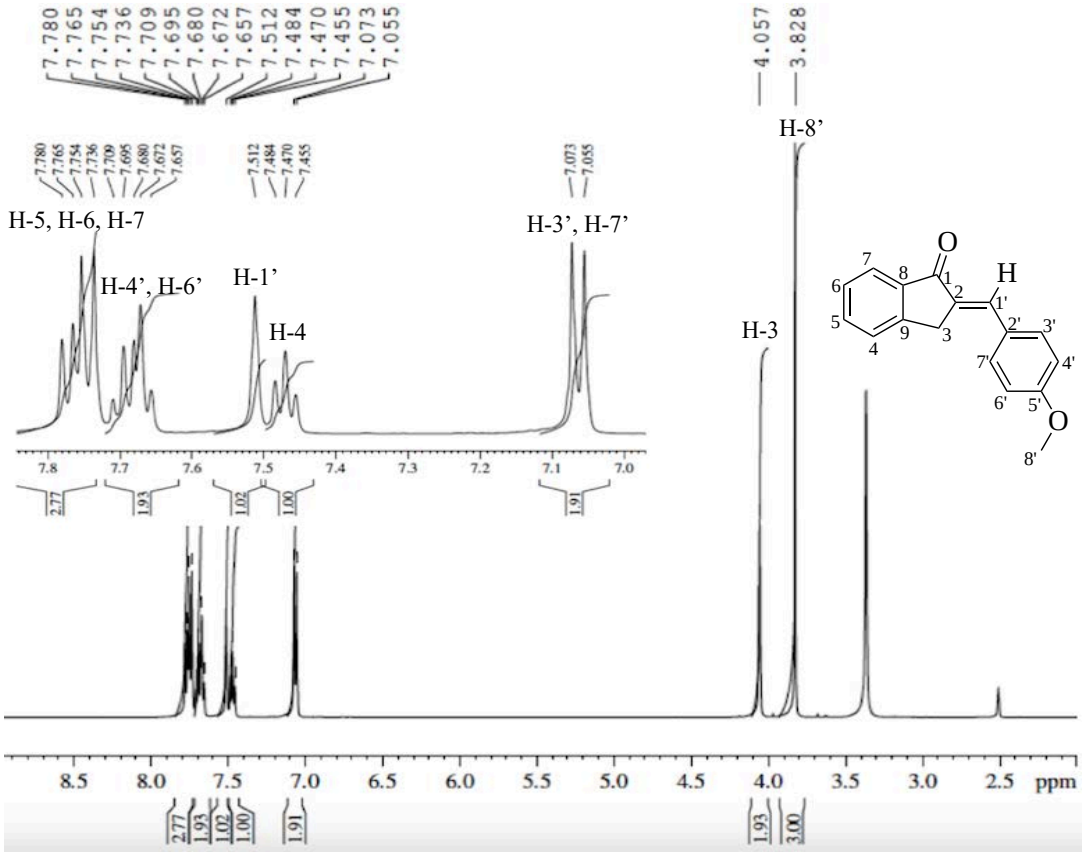

Figure 4.15: The ^{1}H NMR spectrum of compound **89b**

Meanwhile, the carbonyl carbon peak for C=O appeared at δ_C 193.71 in the ^{13}C NMR spectrum. The secondary carbon, -CH_2 aromatic of appeared at δ_C 32.37 as proven by the ^{135}DEPT NMR analysis (Figure 4.16). At δ_C 123.93 the alkene carbon

of C-1' can be observed. The ^{13}C NMR spectrum of compound **89b** was presented in Figure 4.17.

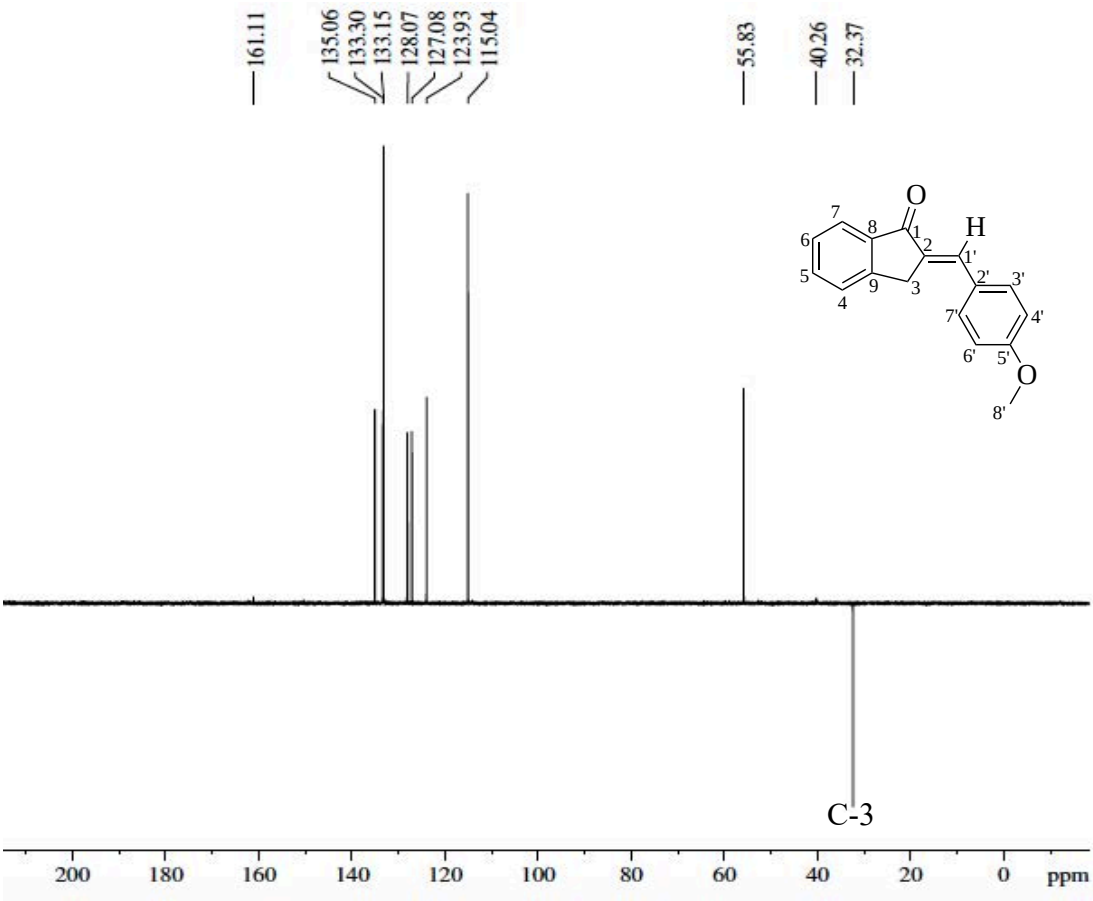

Figure 4.16: The ^{135}DEPT NMR spectrum of compound **89b**

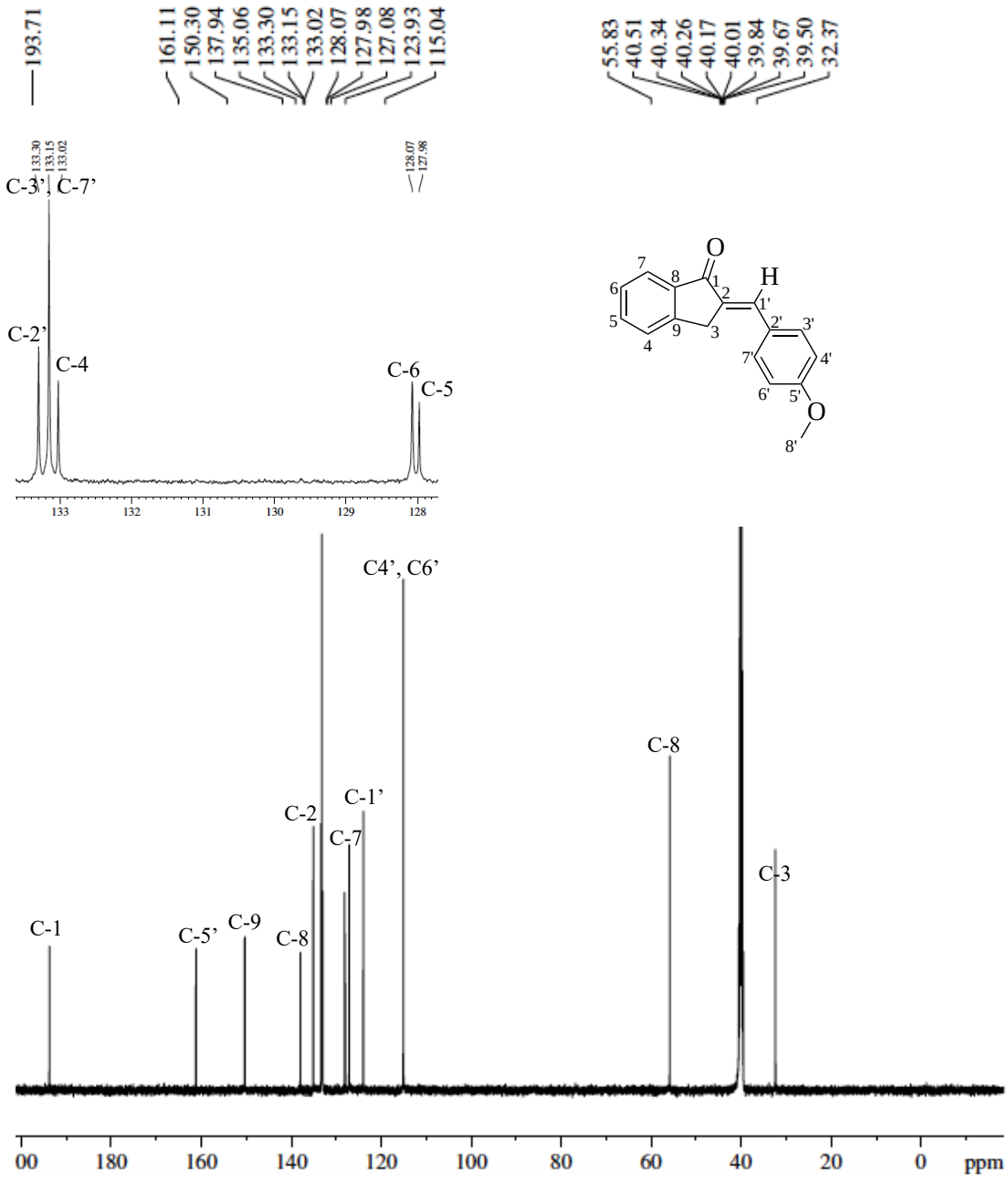

Figure 4.17: The ^{1}C NMR spectrum of compound **89b**

Table 4.8: The important FTIR and ^{1}H, ^{13}C NMR data of compounds **89a-t**

Compound	FTIR (cm^{-1})					^{1}H, ^{13}C NMR (ppm)						
	$-C_{sp^3}-H$ band	C=O	-O-C band	-CH aromatic	C-H bending	H-1'	C-1	C-2	C-5	C-6	C-1'	C-2'
89a	2910	1693	-	1576–1629	690–840	7.56	193.56	135.42	128.19	129.49	124.10	133.30
89b	2914	1694	-	1575–1629	692–836	7.51	193.71	135.06	127.98	128.07	123.93	133.30
89c	2916	1694	-	1574–1630	695–837	7.63	193.35	134.89	124.93	125.09	123.60	132.45
89d	2913	1691	-	1575–1628	693–837	7.56	194.44	134.70	124.52	125.35	123.02	132.21
89e	2914	1692	-	1573–1627	692–837	7.52	194.27	134.06	125.31	130.54	121.93	131.55
89f	2911	1696	-	1575–1629	690–835	7.51	193.39	138.47	126.99	129.95	122.68	134.56
89g	2915	1694	-	1574–1628	691–836	7.54	194.09	133.60	125.60	130.54	112.16	132.26
89h	2917	1692	-	1574–1629	692–839	7.51	193.48	134.69	125.99	130.76	114.85	134.12
89i	2915	1693	-	1576–1630	692–835	7.53	193.87	141.33	128.67	133.60	118.17	139.15
89j	2914	1694	-	1575–1627	691–837	7.48	194.88	142.65	127.30	132.33	119.70	140.83

Table 4.8: The important FTIR and ^{1}H, ^{13}C NMR data of compounds **89a-t** (continue)

Compound	Wavenumber (cm^{-1})					^{1}H, ^{13}C NMR (ppm)						
	$-C_{sp}^{3}-H$ band	C=O	-O-C band	-CH aromatic	C-H bending	H-1'	C-1	C-2	C-5	C-6	C-1'	C-2'
89k	2915	1693	1180–1225	1574–1629	691–837	7.58	191.54	136.87	155.30	150.30	114.81	131.96
89l	2913	1694	1183–1228	1575–1628	693–838	7.53	192.64	145.52	155.62	149.72	128.12	130.52
89m	2917	1695	1179–1223	1574–1630	694–836	7.58	192.35	149.76	155.68	149.76	139.92	130.50
89n	2915	1693	1180–1225	1574–1628	692–838	7.51	193.70	134.51	155.40	148.80	118.63	134.51
89o	2914	1694	1181–1224	1575–1629	691–838	7.30	193.83	134.05	155.34	140.38	130.27	132.26
89p	2913	1695	1180–1225	1573–1627	694–836	7.36	192.14	132.70	155.17	151.17	122.92	130.89
89q	2915	1695	1180–1226	1575–1628	692–837	7.53	193.25	132.54	155.11	144.54	127.01	131.14
89r	2916	1694	1180–1223	1574–1629	691–839	7.35	192.26	133.95	155.27	148.80	113.52	131.14
89s	2917	1694	1182–1226	1577–1630	692–835	7.33	193.22	144.65	154.99	149.47	117.70	126.74
89t	2913	1693	1180–1225	1574–1629	691–834	7.28	163.61	137.52	155.40	148.80	119.40	129.64

The spectroscopy data showed that the compounds **89a-t** have been formed. The compounds were recrystallized to obtain crystal. Compounds **89k**, and **89p** with a sturdy and big crystal size were submitted for x-ray crystallography study. The x-ray crystallography study showed that the crystal structures obtained proven the formation of compounds **89k**, and **89p** with the atom were located in accordance with the proposed structure. Besides, the crystal structures showed that the compound obtained were in the trans configuration. Figure 4.18 depicted the X-ray crystallography structure of compound **89k**, and **89p**.

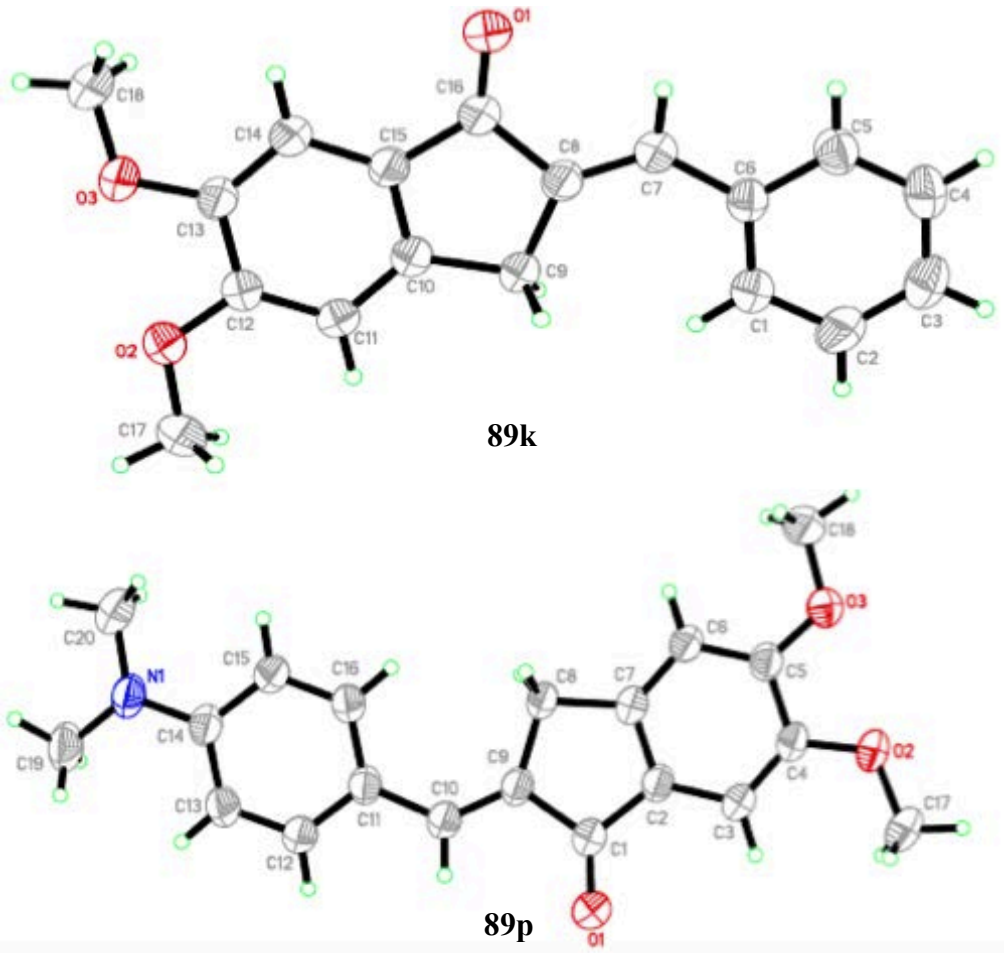

Figure 4.18: The X-ray crystallography structure of compound **89k**, and **89p**.

4.3.4 The synthesis of pyrazolyl substituted benzylidene indanone derivatives, 90a-t

The formation of pyrazolyl substituted indanone derivatives, **90a-t** involved a formation of N heterocycles of compound **86** and benzylidene indanone derivatives, **89a-t**. The reaction associated with the formation of N heterocycles using acetic acid as a catalyst (Ali *et al.*, 2011).

The reaction mechanism started with the protonation of benzylidene indanone derivatives, **89a-t** with the acetic acid. The hydrogen ion attached to the oxygen with the lone pairs located at the carbonyl group to form a carbocation. The carbocation was than underwent rearrangement to form a more stable state through structural reorganisation shifts within the molecule to form its structural isomer (Vogel, 1985).

The carbocation was then attacked by the electronegative nucleophile located in the compound **86** moiety to form an intermediate cation. Next, the acidic hydrogen attached to the nitrogen was removed and the intermediate underwent subsequent water elimination to form an intermediate carbocation. The intermediate carbocation underwent further rearrangement to form a more stable state called carbocation isomer.

The carbocation isomer was captured by the nucleophilic electron from the amine moiety to form a pyrazolyl scaffolding consist of an aromatic five member ring called pyrazolyl cation intermediate. It is due to the subsequently molecular dipole moment can be high as C-N bond is strongly polarised towards nitrogen (McMurray, 2010). The hydride shift occurred at the pyrazolyl cation intermediate with the hydrogen ion shifted to C-11 (Dinnocenzo & Banach, 1989). Consequently, the double bond formed between C-10 and N-1. Thus, the compound was rearranged to a more stable form by delocalization of π-bond. Next, acidic hydrogen from the amine moiety was eliminated as the nitrogen need to form three covalent bonds to achieve its stable

configuration. Hence, the acetic acid catalyst was regenerated (Clayden *et al.*, 2001). The mechanism was presented in Figure 4.19.

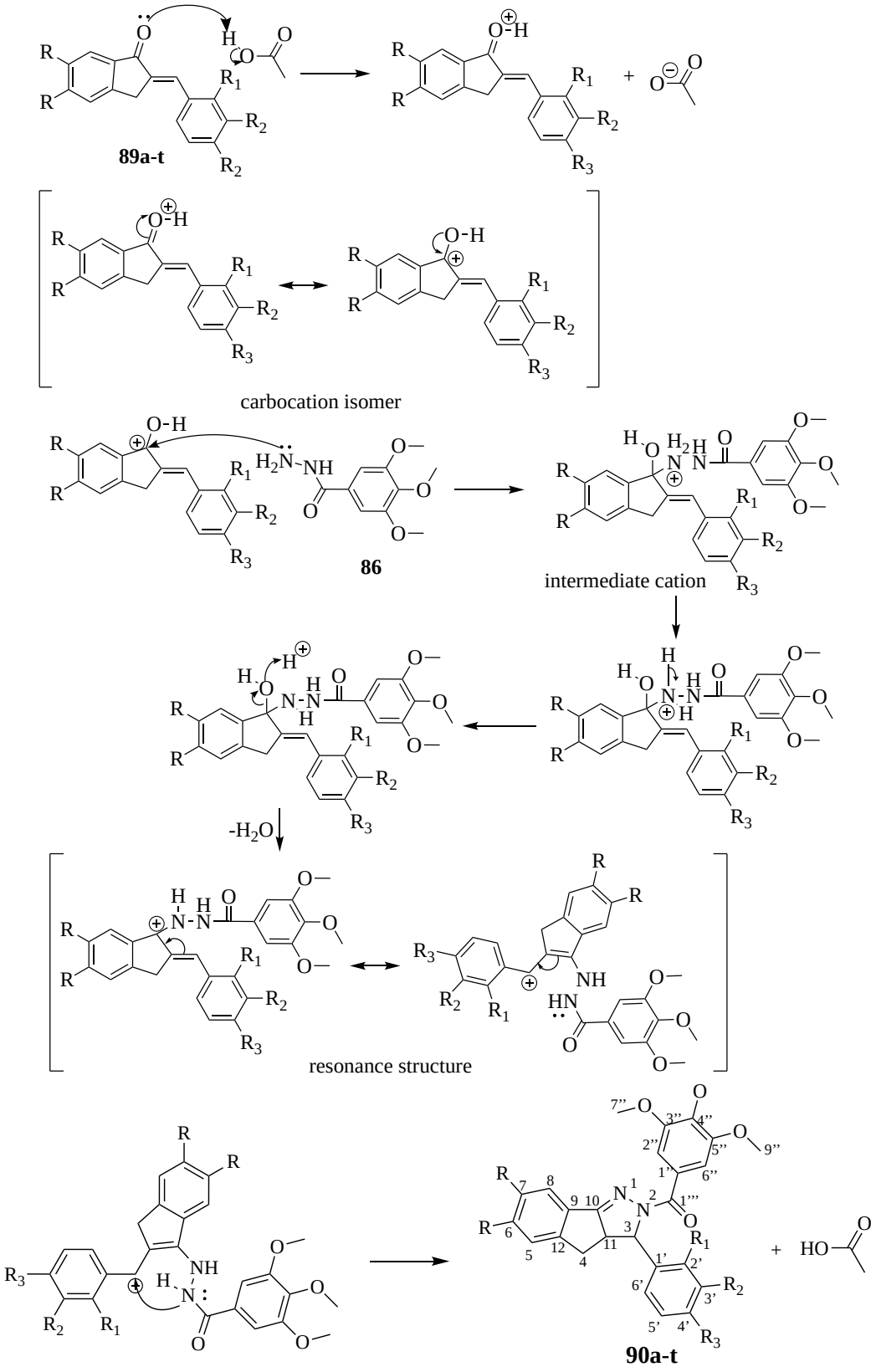

Figure 4.19: The formation of compounds **90a-t**

The compounds **90a-t** afforded an appropriated amount of product being synthesized with the percentage of yield in the range of 40–85 % and the melting point in the range of 175–215 ºC. Table 4.9 summarised the percentage of yield and the physical properties of compounds **90a-t**.

The percentage yields of the obtained products were in the range of 40–85 %. It is suggested that some of the product might be loss during the sample recovery, such as during pouring, filtering or column chromatography, resulted in the low yield. In addition, the low products percentage of yield could be due to an incomplete reactions, in which some of the reactants do not react to form the product.

It were observed that the percentage yield of compounds **90h**, **90j**, **90n**, **90s**, and **90t** were bellow 50 %. Based on observation, the compounds with lower yield tend to have a substituents other than hydrogen at R_1, R_2, and R_3 in the benzylidene moiety, making it a bulk compounds. Bulkier substituents significantly slows the reaction because larger groups effectively increased the steric repulsion with the incoming nucleophile. Thus, the reaction took longer time (Liu *et al.*, 2010a). Figure 4.20 depicted the structure of compounds with the percentage yield lower than 50 %.

Table 4.9: The physical properties of synthesized compounds **90a-t**

Compounds	Formula	Yield (%)	Colour	Melting point (°C)	Molecular Weight (M^{+1})
90a	$C_{26}H_{24}N_2O_4$	76.84	Light yellow	200–205	429.4847
90b	$C_{27}H_{26}N_2O_5$	84.05	Cream	179–185	460.6440
90c	$C_{27}H_{26}N_2O_4$	77.78	White	189–193	443.1400
90d	$C_{26}H_{23}ClN_2O_4$	83.45	Cream	179–185	463.8210
90e	$C_{29}H_{30}N_2O_4$	67.03	Cream	178–183	471.2600
90f	$C_{28}H_{29}N_3O_4$	72.82	Dark orange	178–182	473.1800
90g	$C_{30}H_{31}N_3O_5$	79.48	Light brown	176–184	514.1100
90h	$C_{31}H_{33}N_3O_4$	48.55	Light brown	183–187	512.6138
90i	$C_{28}H_{28}N_2O_6$	51.03	Yellow	198–210	489.1384
90j	$C_{27}H_{25}N_3O_7$	49.62	Light brown	205–208	505.1142
90k	$C_{28}H_{28}N_2O_6$	70.70	Cream	195–200	489.5395
90l	$C_{29}H_{30}N_2O_7$	69.15	Light yellow	201–204	490.1500
90m	$C_{29}H_{30}N_2O_6$	51.62	White	180–187	503.4131
90n	$C_{28}H_{27}ClN_2O_6$	44.28	Cream	175–183	523.1600
90o	$C_{31}H_{34}N_2O_4$	71.65	Cream	180–183	499.0600
90p	$C_{30}H_{33}N_3O_6$	63.17	Light orange	183–187	532.4800
90q	$C_{32}H_{35}N_3O_7$	61.61	Cream	183–186	571.3100
90r	$C_{33}H_{37}N_3O_6$	59.68	Cream	179–185	574.2900
90s	$C_{30}H_{32}N_2O_8$	47.43	Yellow	179–185	549.1167
90t	$C_{29}H_{29}N_3O_9$	41.45	Light brown	208–213	562.8913

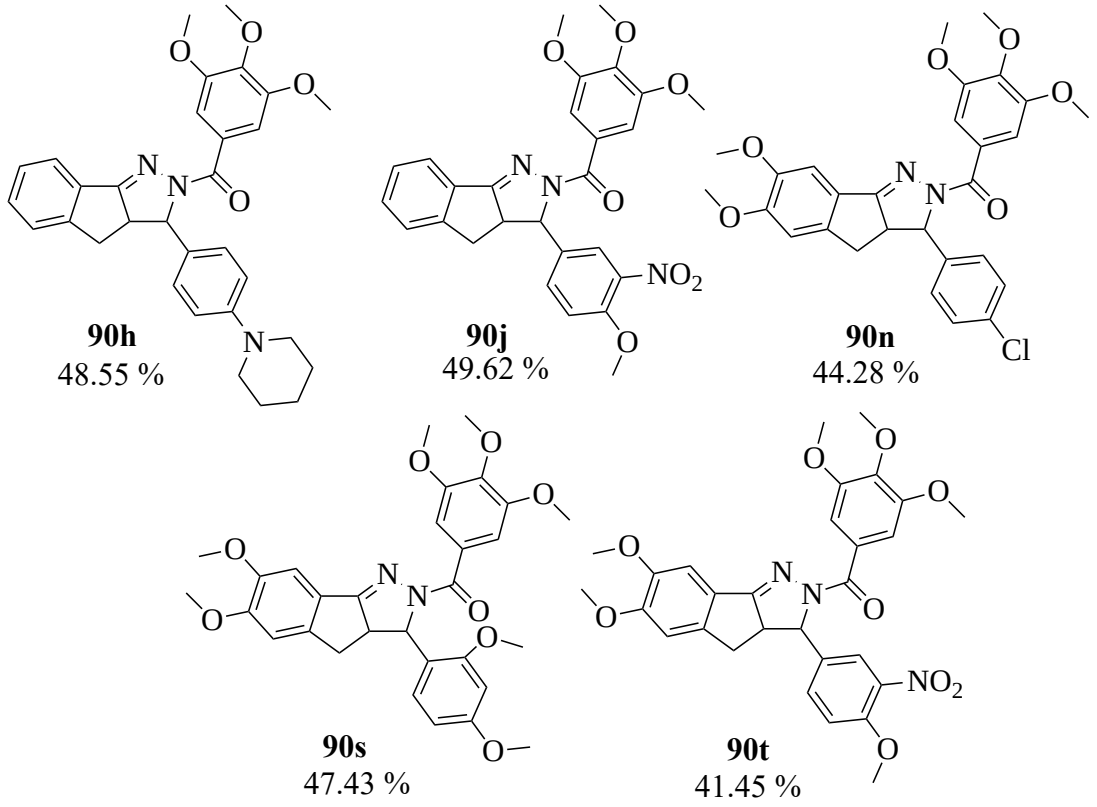

Figure 4.20: The compounds with lowest percentage yield

4.3.4(a) The characterization of pyrazolyl substituted benzylidene indanone derivatives, 90a-t

One of the method in monitoring the formation of pyrazolyl substituted indanone derivatives **[90a-t]** are by the FTIR spectra comparisons of compound **86** and **89a-t**. This reaction involved a ring formation which transformed the primary and secondary amine in compound **86** to tertiary amine in compound **90a-t**. Hence, two -NH and $-NH_2$ absorption band at 3364 cm^{-1} and 3319 cm^{-1} will be absence in compound **90a-t** FTIR spectra.

The FTIR spectrum of compound **90b** manifest an absorption band at 2938 cm^{-1} attributed to the C_{sp}^3-H bonds vibration. In compound **90b**, the C=O absorption strength at 1697 cm^{-1} decreased compared to the C=O absorption strength of compound **78b**. It is suggested due to the loss of conjugation from one side at the

C=O moiety in compound **90b** is located next to amine moiety (Hassaneen *et al.*, 2017 & Sheat *et al.*, 2018). While, the strong out of plane C-H bending appeared at 820 cm^{-1} indicated that the present of para disubstituted ring in compound **90b** (Lampman *et al.*, 2010).

The comparison between the FTIR spectrum of compound **86, 89b** and synthesized compound **90b** were presented in Figure 4.21 and the other absorption band for compounds **90a-t** were tabulated in Table 4.10.

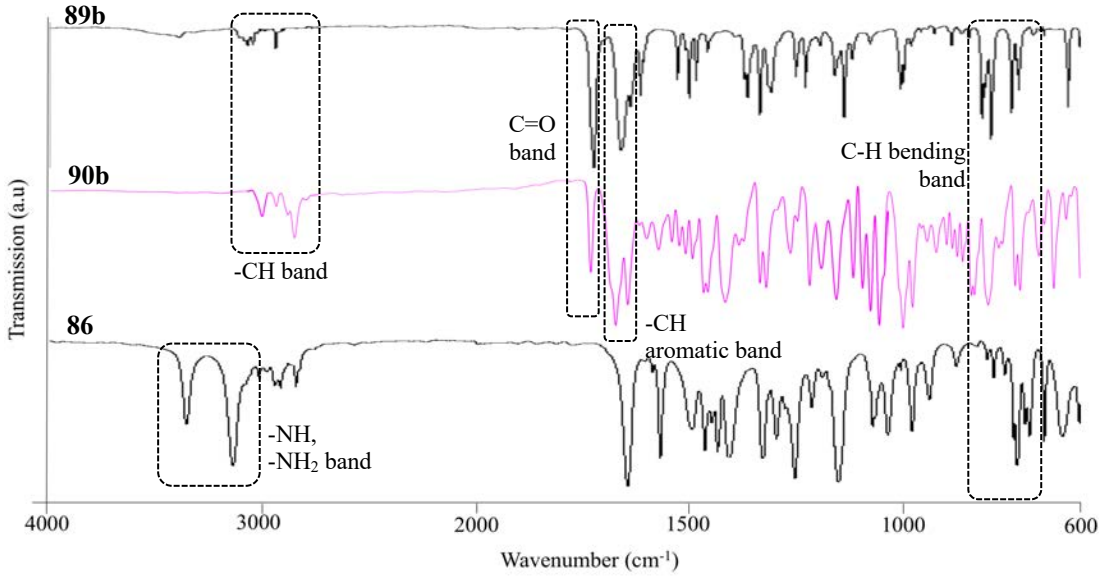

Figure 4.21: The comparison between FTIR spectrum of compound **86, 89b** and synthesized compound **90a-t**

Table 4.10: The FTIR absorption band of compounds **90a-t**

Compound	Wavenumber (cm^{-1})				
	$-C_{sp}^3-H$ band	C=O	C-N band	C=N band	-CH aromatic
90a	2910	1678	1320	1588	1452–1512
90b	2938	1697	1320	1568	1454–1512
90c	2921	1680	1330	1585	1450–1518
90d	2911	1683	1325	1590	1452–1512
90e	2925	1672	1320	1592	1451–1513
90f	2920	1675	1321	1590	1451–1512
90g	2910	1672	1320	1590	1452–1512
90h	2913	1675	1319	1585	1453–1515
90i	2918	1680	1320	1590	1450–1511
90j	2915	1678	1320	1588	1452–1515

Table 4.10: The FTIR absorption band of compounds **90a-t** (continue)

Compound	Wavenumber (cm^{-1})				
	$-C_{sp^3}-H$ band	C=O	C-N band	C=N band	-CH aromatic
90k	2911	1673	1319	1588	1453–1510
90l	2918	1672	1320	1592	1451–1515
90m	2920	1678	1320	1588	1452–1512
90n	2918	1678	1318	1585	1453–1511
90o	2923	1676	1321	1560	1452–1512
90p	2921	1680	1320	1586	1450–1511
90q	2916	1680	1318	1585	1453–1515
90r	2913	1675	1320	1590	1452–1512
90s	2910	1678	1320	1588	1450–1512
90t	2915	1672	1317	1589	1451–1516

The LC-MS spectrum (Figure 4.22) indicated the molecular ion peak $[MH]^+$, (+ESI) at m/z 459.4460 which further confirmed the molecular mass of the structure.

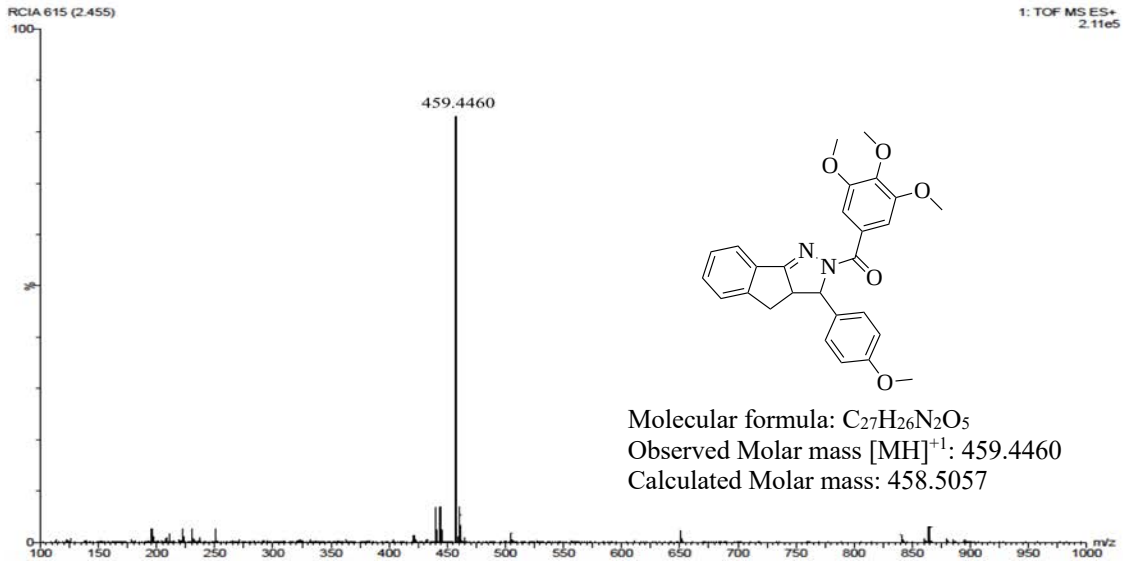

Figure 4.22: The LC-MS spectrum of compound **90b**

The structural elucidation of compounds **90a-t** were accomplished by using one and two dimensional NMR spectroscopic study. In the main difference between the ^1H NMR spectrum of compounds **90a-t** and the reactant compound **86** was the disappearance of N-H and N-H_2 shift. There is no chemical shifts observed at δ_H 9.744 and δ_H 4.470 indicating the success in the cyclization of amines from primary and secondary amine into tertiary amine. The ^1H and ^{13}C chemical shift of the compounds were reported in Table 4.11.

Table 4.11: The chemical shifts of ^{1}H NMR and ^{13}C NMR spectrum of compounds **90a-t**.

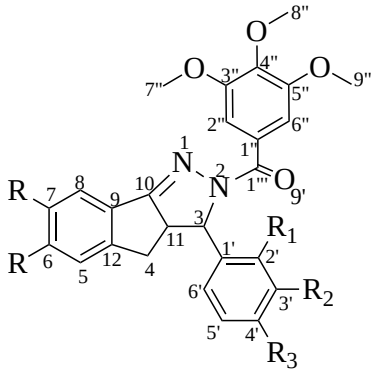

Compound	Chemical shift NMR (δ, ppm)						
	H-3	C-3	C-11	C-4	C-1’	C-1’’	C-1’’’
90a	5.06	77.45	105.87	31.85	139.10	128.50	192.35
90b	5.45	77.24	104.53	32.51	138.26	133.91	194.90
90c	5.01	77.41	104.11	32.05	139.02	133.12	193.43
90d	5.83	77.39	107.36	32.23	138.20	134.89	193.13
90e	4.98	77.91	107.81	32.81	138.11	136.73	193.14

Table 4.11: The chemical shifts of ^{1}H NMR and ^{13}C NMR spectra of compounds **90a-t** (continue).

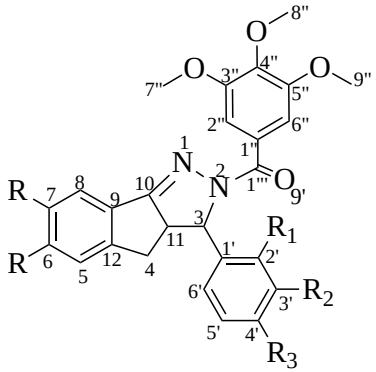

Compound	Chemical shift NMR (δ, ppm)						
	H-3	C-3	C-11	C-4	C-1’	C-1’’	C-1’’’
90f	5.01	77.24	105.81	35.11	139.85	136.37	192.04
90g	4.04	77.55	104.66	32.49	138.20	133.24	193.92
90h	4.03	77.63	104.31	32.57	138.36	133.13	193.47
90i	5.50	77.41	104.66	32.59	138.52	134.09	194.42
90j	5.56	77.81	105.71	32.10	137.84	134.80	193.56

Table 4.11: The chemical shifts of ^{1}H NMR and ^{13}C NMR spectra of compounds **90a-t** (continue).

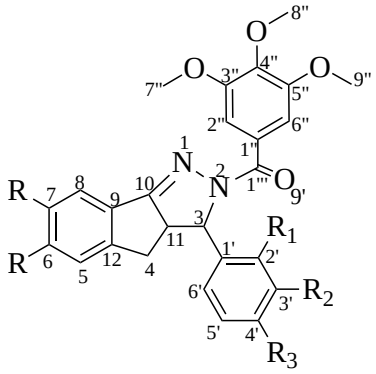

Compound	Chemical shift NMR (δ, ppm)						
	H-3	C-3	C-11	C-4	C-1’	C-1’’	C-1’’’
90k	5.16	77.32	105.36	32.04	140.76	135.57	192.35
90l	5.52	77.33	105.17	32.18	144.66	133.18	193.25
90m	5.07	77.24	105.15	30.14	137.10	131.69	193.81
90n	5.06	77.51	104.81	39.11	135.67	130.40	192.81
90o	5.01	77.43	106.11	33.18	138.91	130.39	193.35.

Table 4.11: The chemical shifts of ^{1}H NMR and ^{13}C NMR spectra of compounds **90a-t**(continue).

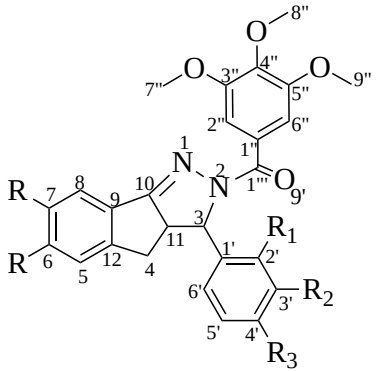

Compound	Chemical shift NMR (δ, ppm)						
	H-3	C-3	C-11	C-4	C-1’	C-1’’	C-1’’’
90p	5.09	77.63	106.11	40.87	138.75	130.17	193.17
90q	4.05	77.59	105.73	32.49	138.97	133.74	192.89
90r	4.10	77.25	105.13	32.57	137.02	131.95	193.81
90s	6.97	77.34	105.18	32.27	144.71	132.94	193.28
90t	5.41	77.55	105.15	37.87	138.51	133.23	193.01

In the ^{1}H NMR spectrum (Figure 4.23) of compound **90b**, the -CH signal of H-3 was observed at δ_H 5.45 indicating the formation of ring as there are no signal observed at δ_H 5.45–5.00 in compound **86** and **89b** (Ali *et al.*, 2011). Besides, two high intensity singlet signals were observed at δ_H 3.82 and 3.85 corresponding to the four methoxy -OCH_3 moieties of H-7', H-7'', H-8'' and H-9''. However, only two chemical shifts were observed indicating that the signal were overlapped as the nuclei are magnetically equivalent to each other (Pavia *et al.*, 2015). The signal integrals showed a proximate number of proton, 7 and 5 which similar the number of proton presence in the H-7', H-7'', H-8'' and H-9''.

The multiplet can be observed at the downfield region of δ_H 7.48–7.64 was assigned as the H-aromatic of benzene ring. The two doublet located at δ_H 6.96 (*J*=8.5 Hz) and δ_H 7.88 (*J*=10.0 Hz) with a triplet located at δ_H 7.39 (*J*= 5.0 Hz) were assigned to aromatic proton as the signal appeared in the aromatic region (Lampman *et al.*, 2010). It is hard to assign the proton presence in a benzene or multiple aromatic in this case compound **90b**. Three benzene rings in compound **90b** increased the deshielded effect by creating its own ring current when placed in the magnetic field. In addition, the carbons with sp^2 bond in the benzene ring holds charge closer to the nucleus, thus easier to be deshielded (Balci, 2005a).

The two low intensity signal were observed at δ_H 2.78 and 3.09 of H-4. The ^{1}H-^{1}H COSY NMR spectrum (Figure 4.24) showed a cross peak between the neighbouring proton H-11 at δ_H 3.96. The signal appears as two singlet signals instead of doublet suggested due to the identification of each hydrogen as it is equivalent to each other (Balci, 2005b). The spectrum revealed a cross peak of H-3 and H-11 at δ_H 5.45 and 3.96 respectively, indicating that both signal are correlated with each other.

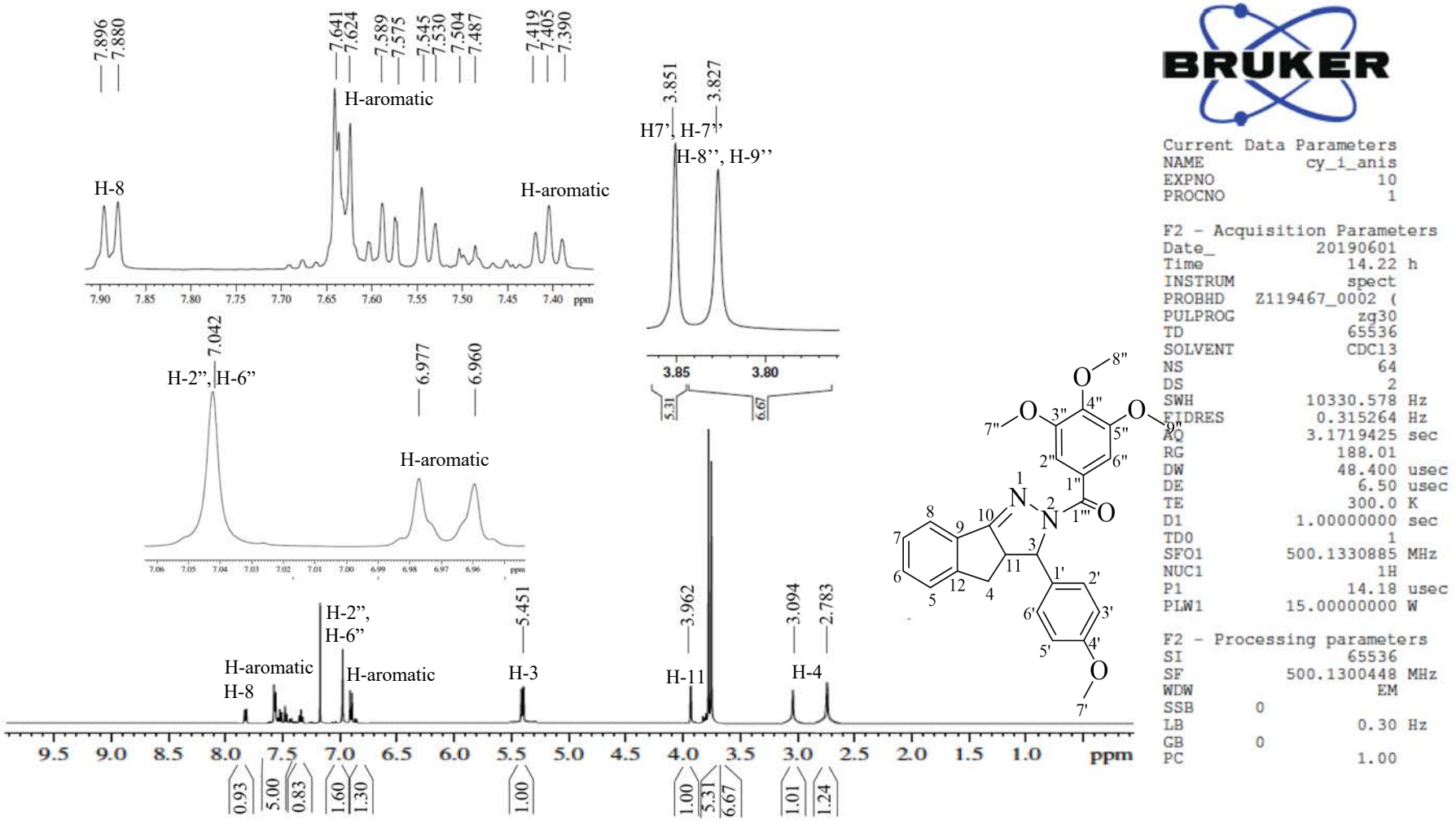

Figure 4.23: The ^{1}H NMR spectrum for compound **90b**

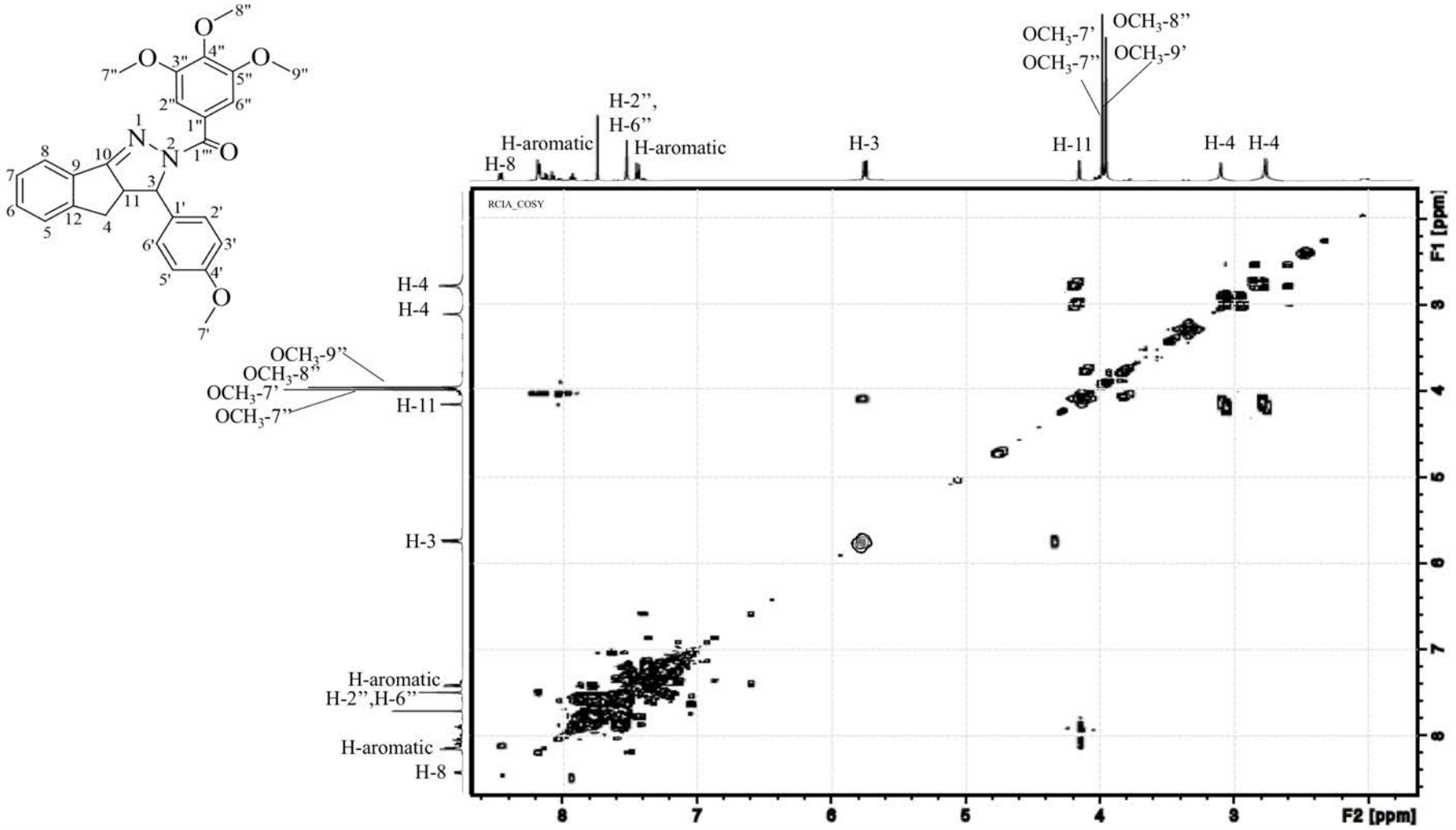

Figure 4.24: The ^{1}H-^{1}H-COSY NMR spectrum for compound **90b**

In compound **90b** ^{13}C NMR spectrum (Figure 4.25) showed a signal at δ_C 168.20 indicating the sp^2 carbon bonded to the amine group of C-10. Three signals in the range of δ_C 55.44–60.94 showed the presence of -OCH_3 of C-4', C-7", C-8", and C-9". The C-1"' of carbonyl moiety was assigned to δ_C 194.50. While the C-10 of C=N was assigned to δ_C 168.20 (Pavia *et al.*, 2015).

However, important signal of C-3 in the range of δ_C 70–80 which indicated the attachment of compound **86** and compound **89b** to form compound **90b** was not observed in the ^{13}C NMR spectrum suggested that the signal was overlapped with the $CDCl_3$ signal that appeared at δ_C = 77 ppm.

In ^{135}DEPT NMR spectrum (Figure 4.26), the C-3 signal of compound **90b** appeared at δ_C 77.24. In addition, the spectrum showed the signal at δ_C 32.51 which belonged to the aromatic carbon (C-4).

All prominent signal that indicated the formation of compound **90b** have been assigned and in accordance with the proposed structure. However, due to the presence of more than one aromatic ring in compound **90b**, the signals of carbons and protons for aromatic region were not assigned in details.

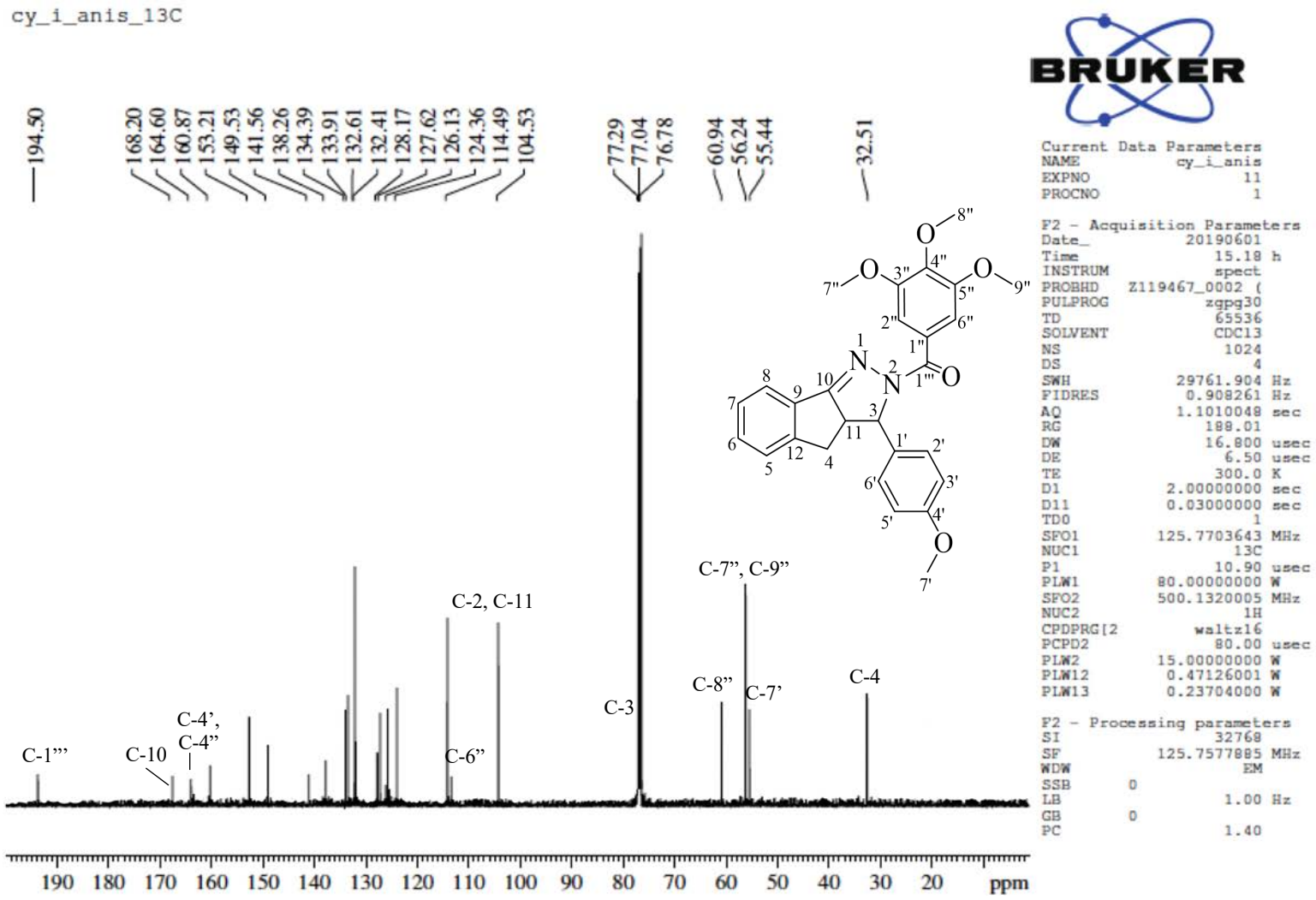

Figure 4.25: The ^{13}C NMR spectrum for compound **90b**

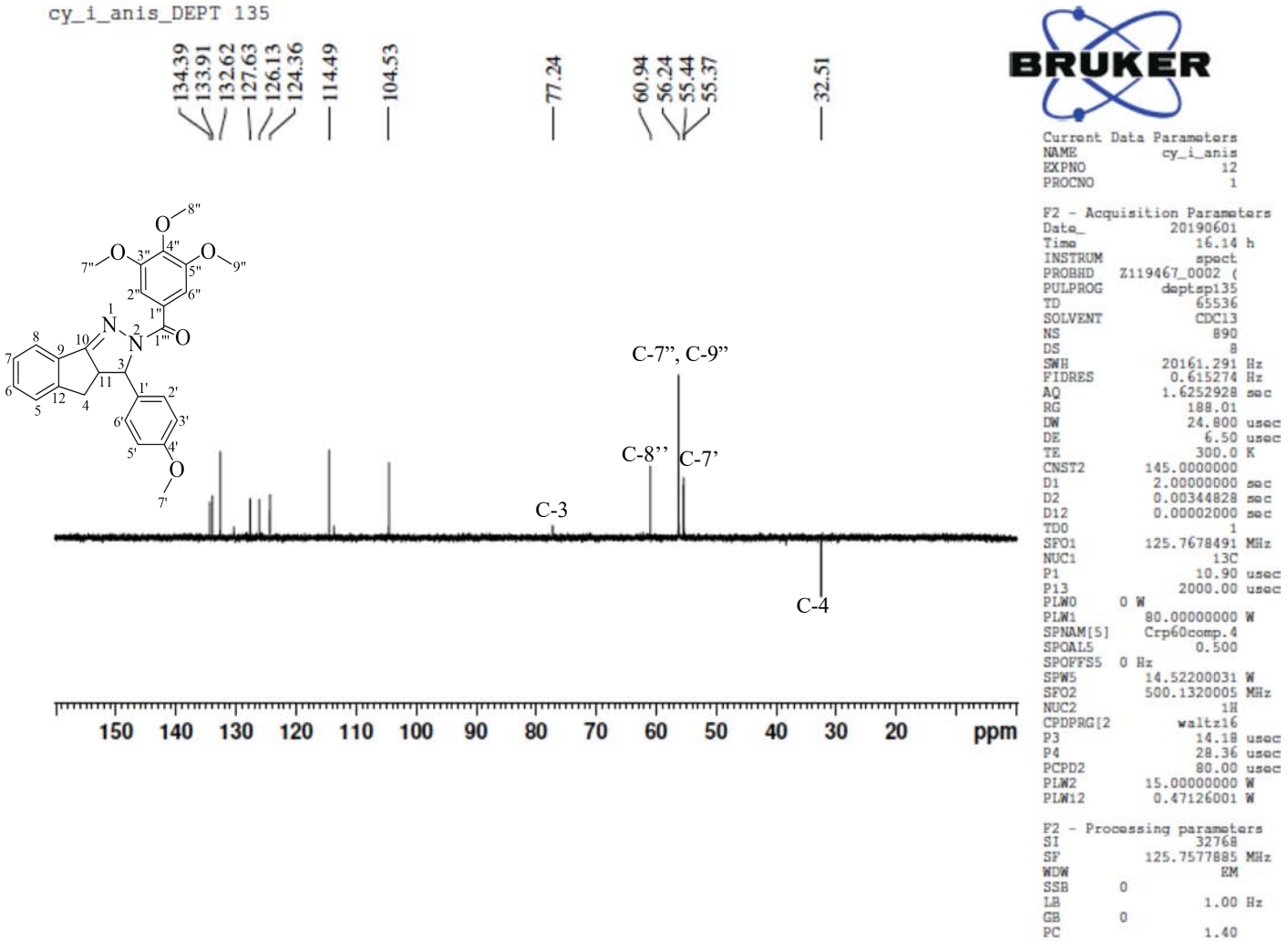

Figure 4.26: The ^{135}DEPT NMR spectrum of compound **90b**

4.4 The *in silico* studies towards DENV-2 NS2B/NS3 protease

The *in silico* studies was conducted for all the synthesized compounds with DENV-2 NS2B/NS3 protease, and its binding mode and conformation were determined. AutoDock4.2 procedure was used extensively in predicting the interaction of ligands with the bio-macromolecular target.

4.4.1 The ligand preparation

In this study, a total of 20 compounds **[90a-t]** were prepared for docking. The 3D structure of the synthesized compounds was built initially starting with the construction of 2D structures (.mol) using MarvinSketch 19.4.0 (ChemAxon, 2019). The 2D structures were then underwent geometry optimisation and energy minimisation using a molecular mechanic method with MM+ force field embedded in HyperChem pro 8.0 software (www.hyper.com) to obtain the 3D structure in .pdb format. Lastly, the AutoDock suited, raccoon.py was utilized to convert the .pdb file into a .pdbqt formatted ligand which required by the AutoDock4.2 (Forli *et al.*, 2016).

The energy minimisation steps are necessary to reduce the gradient of the ligand potential energy to zero. Besides, this refined the ligand conformations in the crystal structures to best fit the electron density map (Wang & Pang, 2007). All molecules were in equilibrium bond distance of 1.242 Å after geometry optimisation resulting in an ideal structure behaviour. Besides, the equilibrium bond distance increased structure stability (Brown, 2019).

4.4.2 The DENV-2 NS2B/NS3 protease preparation

In this study, the homology protein crystal structure generated by Wichapong and co-worker were used. Some crystal structures were reported to have some missing amino acid residue or cofactor that hinder a precise interaction analysis of a complete NS2B/NS3 protein and potential inhibitors (Erbel *et al.*, 2006 & Wichapong *et al.*, 2010). In addition, the available crystal structure 2FOM does not show a direct C-terminal domain of DENV-2 NS2B interaction with the substrate-binding site of the NS3 protease, which made it a non-suitable target structure for analysing the binding interaction with a potential inhibitor (Aleshin *et al.*, 2007). Hence, the use of homology model, a reliable 3D model generated by from its amino acid sequence is acceptable (Vyas *et al.*, 2012).

In the preparation for docking simulation, only protease was retained as a part of the macromolecule file, while the Bz-Nle-Lys-Arg-Arg-H was extracted and saved as a positive control ligand. The crystal water molecules were removed from the macromolecule file to ease the simulation process and to clear the binding site from possible water molecules that can distort the search (Wong & Lightstone, 2011). After that, the ADT was utilized in adding the hydrogen atoms into the macromolecule system, calculated the charge and merged the non-polar hydrogens with the carbon atoms as some hydrogen atom might be missing in the crystal structure. In addition, the added hydrogen atom allowed the establishment of hydrogen bonds that may be present between the macromolecule and the potential inhibitor or ligand tested in accordance with the docking algorithm (Ferreira *et al.*, 2015). The macromolecule was saved in .pdbqt format prior to docking simulation.

4.4.3 The positive control docking

In positive control docking, the Bz-Nle-Lys-Arg-Arg-H was extracted and re-docked into the binding site in order to evaluate the success of the docking method in reproducing the experimentally-known complex. In this study, the centre of the grid box was determined using the centre of Bz-Nle-Lys-Arg-Arg-H ligand at 22.781, 43.373, -0.358 in x,y,z coordinates, a grid box size of 74 × 43 × 64 and spacing of 0.375 Å to cover the protease active site. The Lamarckian genetic algorithm was employed in Autodock 4.2 with a covalent map parameter was used during positive control docking simulation to constrain the molecular geometry of the peptide inhibitor (Morris *et al.*, 2009 & Bianco *et al.*, 2016).

The re-docked was carried out successfully with the root mean square deviation (RMSD) value of 1.23 Å. Hevener and co-worker (2009) stated that the programs that able to poses the RMSD value in the range of 1.5–2 Å, depending on ligand size, are considered to have performed successfully. The overlay docked conformation between the Wichapong homology model and Bz-Nle-Lys-Arg-Arg-H referenced ligand is shown in Figure 4.27.

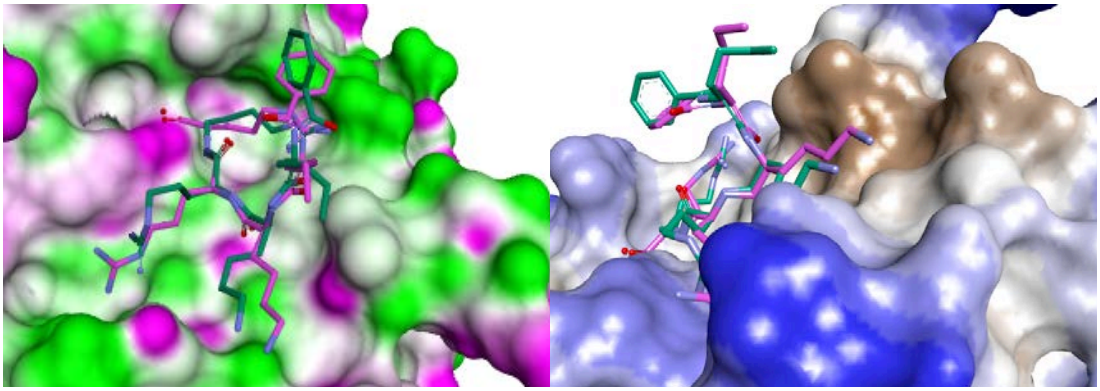

Figure 4.27: The overlay docked conformation between the Wichapong homology model and Bz-Nle-Lys-Arg-Arg-H referenced ligand (- original ligand conformation; - docked ligand conformation)

This figure highlighted the binding interaction of the original ligand and positive docked ligand confirmation with the protease active site, which were in an almost identical conformation with each other. The similar conformation indicated that programs used were able to reproduce the experimentally-known complex. The docking parameters obtained was utilized in the ligand-DENV-2 NS2B/NS3 protease docking studies using the synthesized compounds.

4.4.4 The ligand-DENV-2 NS2B/NS3 protease docking studies

The DENV-2 NS2B/NS3 protease was built up by a single-stranded RNA of positive polarity with 3391 amino acids residue comprising three structural and seven non-structural proteins, arranged in the order of C-prM-E-NS1-NS2A-NS2B-NS3-NS4A-NS4B-NS5 (Irie *et al.*, 1989). The NS2B/NS3 protease played an essential role in virus replication (Othman *et al.*, 2008 & Phong *et al.*, 2011). Thus, it been selected as the anti-dengue target.

The targeted amino acid residue possesses in the NS2B/NS3 protease were identified as three catalytic triad amino acid residues that located in NS3 serine protease, namely His51, Asp75 and Ser135. Whilst, the NS2B protease acted as a NS3 serine protease co-factor for an optimal catalytic activity and reported to be responsible for cleaving the NS2A/NS2B, NS2B/NS3, NS3/NS4A and NS4B/NS5 junctions, preferentially with adjacent basic residues (Arias *et al.*, 1993; Preugschat *et al.*, 1990; Cahour *et al.*, 1992; Falgout *et al.*, 1991).

Altogether, 20 final synthesized compounds **[90a–t]**, and gallic acid were docked excluding, the positive control peptide inhibitor. The ligand-protein docking results based on the free energy of binding (FEB) scores are tabulated in Table 4.12.

The scores were ranked by the most active down to the least. The activity was based on the binding interaction, in which, the more negative the score, the stronger the binding.

Table 4.12: The FEB of ligand-protein docking.

Ligand	FEB (kcal/mol)
Positive Control (Peptide Inhibitor)	-6.58
Gallic Acid	-5.73
90p	-8.12
90c	-7.75
90e	-7.71
90g	-7.63
90r	-7.61
90h	-7.53
90o	-7.51
90q	-7.54
90d	-7.36
90j	-7.21
90a	-7.14
90i	-7.13
90t	-7.09
90s	-7.01
90b	-6.99
90k	-6.95
90n	-6.90
90l	-6.87
90m	-6.82
90f	-6.71

All the docked ligand showed positive interaction with the DENV-2 NS2B/NS3 protease with the binding energy less than -5.0 kcal/mol. The synthesized compounds displayed good binding interaction with the FEB less than the gallic acid and the peptide inhibitor. Five synthesized compounds displayed the FEB less than -7.55 kcal/mol with the synthesized compound **90p** showed the lowest FEB of -8.12 kcal/mol and the binding interaction of synthesized compound **90p** was selected to be discussed further. Figure 4.28 represents the illustration of synthesized compound **90p** binding interaction with the DENV-2 NS2B/NS3 protease.

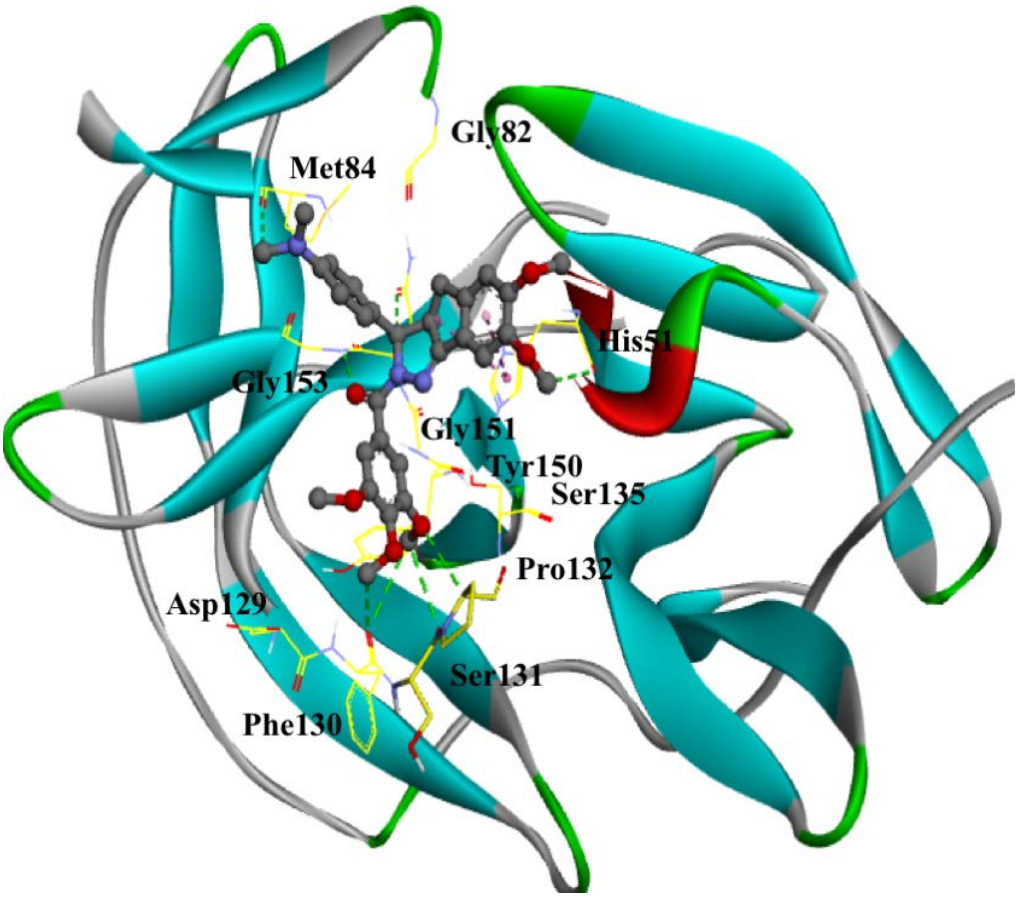

Figure 4.28: The binding interaction of **90p** with the DENV-2 NS2B/NS3 protease.
(-- hydrogen bond; -- π- π stacking; -- π-alkyl)

The intermolecular interaction between the inhibitor (synthesized compound) and the surrounding amino acid residue at the binding pocket of DENV-2 NS2B/NS3 protease played an important role in determining the NS2B/NS3pro-mediated cleavage of the capsid, intNS3, 2A/2B, 4B/5, 3/4A and 2B/3 substrates. Two criteria probed the strength of the binding interaction specifically; (i) a proton donor-acceptor distance of ≤3.5 Å, and (ii) a donor-H acceptor bond angle of ≥120 º (Yotmanee *et al.*, 2015 & Li *et al.*, 2011).

The hydrogen bonding was the most stable and strongest intermolecular forces. Hence, the stability of the hydrogen bond network between the synthesized compounds and the amino acid residues dominates the binding strength and therefore affecting the rate of inhibitors (Lin *et al.*, 2016). It is suggested that the shorter the hydrogen bond distance, the stronger the hydrogen bonding interaction. Whilst, the donor-H acceptor bond angle of ≥120º is required for the bond to receive favourable energy and avoids including the non-physical H-bonds with angles near 90 º (Thorpe *et al.*, 2005).

The synthesized compound **90p** showed eight hydrogen bond interactions, one π-π stacking interaction, and one π-alkyl interaction with the amino acid residue in the DENV-2 NS2B/NS3 protease. It was noted that the interactions formed at this site were mostly contributed from the NS3 residues with different interaction type and strengths. The residue NS3 protein is essential for viral replication and maturation of virions. Hence, more interaction with the residue suggested giving more promising result in inhibitory activity (Yin *et al.*, 2006).

The presence of the aromatic group located at the benzylidene moiety in the synthesized compound **90p** enhances the possibilities of van der Waals interaction. The π-π stacking interaction and π-alkyl interaction between the His51 and the

benzylidene moiety in compound **90p** suggested affecting DENV-2 NS2B/NS3 replication as His51 is one of the catalytic triads of NS3 residue, which required to cleavage the NS2B residue for virus replication activities (Noble *et al.*, 2012 & Niyomrattanakit *et al.*, 2004). The geometry of this stacking interaction suggests that the electrostatics cloud localization play a role in the attraction between both aromatic systems (Zhao & Zhang, 2016).

The synthesized compound **90p** formed hydrogen bonds with one of the catalytic triad amino acid residues were located in NS3 serine protease, His51, as well as other amino acid residues namely, Gly153, Asn152, Phe130, Pro132, Ser131, and Phe130. Only one hydrogen bonding interaction occurred between synthesized compound **90p** with the amino acid in NS2B residue, which is Met84. The details on the hydrogen bonding interaction were tabulated in Table 4.13 below.

Table 4.13: The hydrogen bonding details of compound **90p.**

Name	H-bond distance (Å)	H-bond angle (º)
NS3:Gly153:HN-**90p**:O	2.56	139.93
90p:C-NS3:Asn152:OD1	3.10	149.89
90p:C-NS3:Phe130:O	3.38	149.78
NS3:Pro132:CA-**90p**:O	3.47	110.96
90p:C-NS3:His51:O	3.51	138.78
90p:C-NS3:Ser131:O	3.54	116.99
90p:C-NS2B:Met84:O	3.61	170.88
90p:C-NS3:Phe130:O	3.74	131.52

There are four hydrogen bond interactions with the distance lower than 3.5 Å between the compound **90p** with the amino acid residue in the DENV-2 NS2B/NS3

protease. The shortest hydrogen bond distance of 2.56 Å with a bond angle of 139.93º was formed between the synthesized compound **90p** and amino moiety in $_{NS3}$Gly153. The oxygen atom in the carbonyl group moiety of the synthesized compound **90p** suggested acting as the H-acceptor, while the hydrogen attached to the nitrogen atom present in the simple amino acid of glycine suggested acting as the H-donor (Itoh *et al.*, 2019).

The top five compounds with the lowest FEB namely, **90c**, **90e**, **90g**, **90p**, and **90r** from the *in silico* studies were chosen to examine it's *in vitro* activity towards DENV-2 NS2B/NS3 protease. Generally, the difference between compounds **90c**, **90e**, **90g**, **90p**, and **90r** are the substitute at the para position in the benzene ring. The ability of the substituent form the intermolecular bonding with the amino acid in NS2B/NS3 protease determined the binding energy. Synthesized compound **90p** have a dimethylamino-group, the nitrogen could act as the hydrogen bond donor to enhance the intermolecular bonding with the amino acid in NS2B/NS3 protease. While, the bulk structure of synthesized compounds **90g** and **90r** with morpholine and piperidine substituents respectively, increased the steric hindrance that affected the binding energy.

Overall, the synthesized compound **90p** displayed a promising *in silico* activity towards DENV-2 NS2B/NS3 protease with lots of intermolecular bonding formed between the synthesized compound and macromolecule. Figure 4.29 depicted the structure of the top five compounds with the lowest FEB.

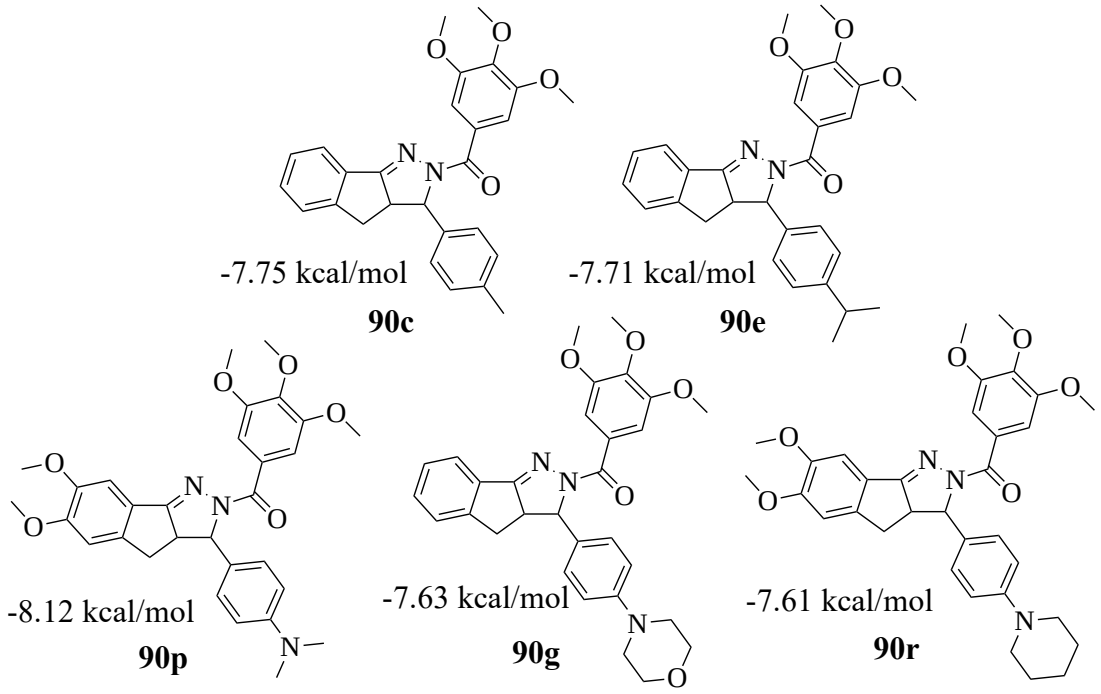

Figure 4.29: The top five compounds with the lowest FEB

4.5 The *in vitro* studies towards DENV-2 NS2B/NS3 protease

The screening of top five docked synthesized compound activity towards DENV-2 NS2B/NS3 protease by using fluorogenic peptide substrate Boc-Gly-Arg-7-amino-4-methylcoumarin was conducted, and the most active compound proceeded for fifty per cent inhibitory concentration (IC_{50}) values analysis. Panduratin A was used as a positive control in this study.

The compound **90p** showed quite high DENV-2 NS2B/NS3 protease inhibitor activity (65.61 ± 0.98 %), followed by compound **90r** with 53.62 ± 1.05 %, compound **90g** with 48.03 ± 1.01 %, panduratin A with 47.59 ± 1.03 %, gallic acid with 25.11 ± 1.11 %, compound **90e** with 20.06±0.99 %, and lastly compound **90c** with only 16.11 ± 0.95 %. Figure 4.30 charted the anti-dengue screening of the selected synthesized compounds and their structure.

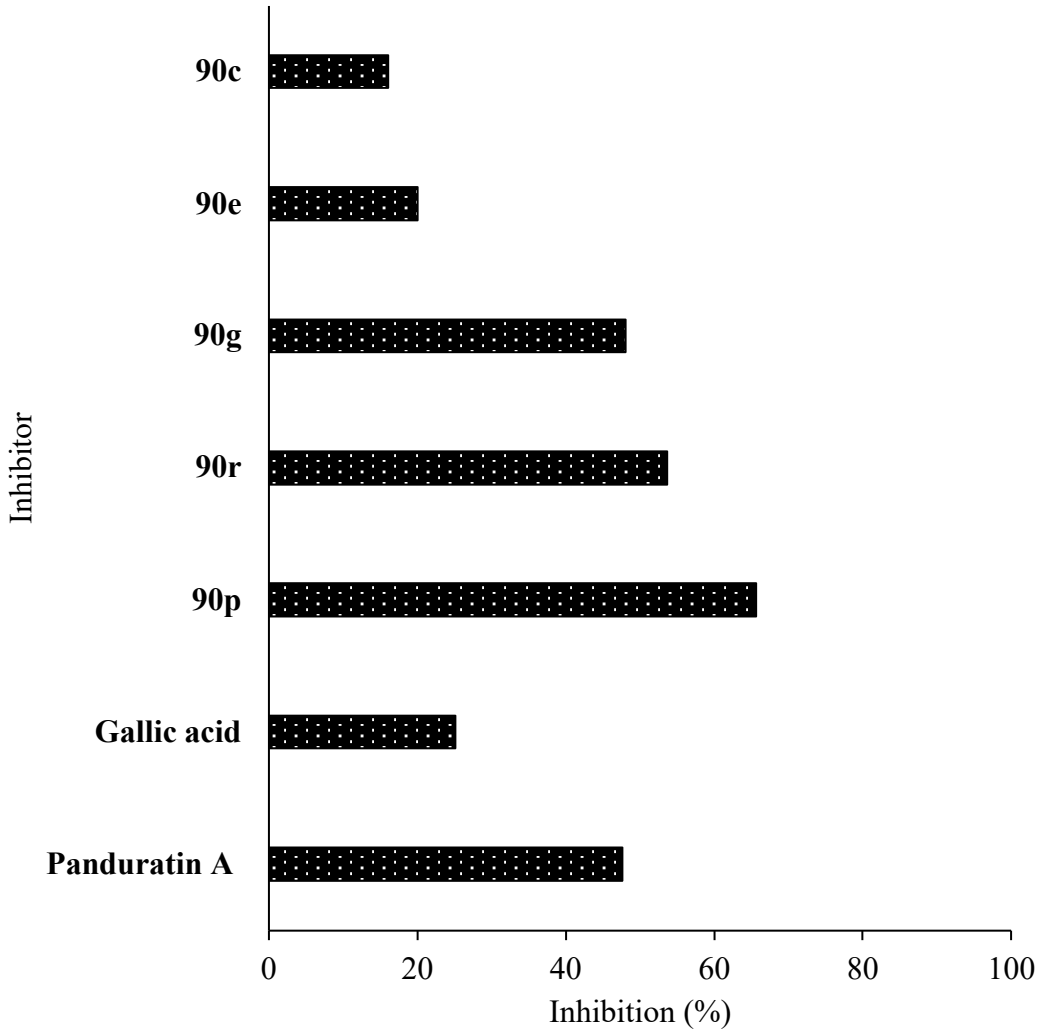

Figure 4.30: The anti-dengue screening of the selected synthesized compounds
Note: The final concentration of synthesized compounds was 200 ppm.

The selected synthesized compounds showed a promising DENV-2 NS2B/NS3 protease inhibitor activity with three synthesized compounds, namely compound **90p**, **90r**, and **90g** obtained the percentage inhibition higher than panduratin A and gallic acid. The structure of the synthesized compounds **90p**, **90r**, and **90g** ,were compared with the structure of gallic acid and panduratin A. The synthesized compound possesses more methoxy group and electron withdrawing group, which suggested to be the factor of the increment of its inhibitory activity.

In addition, the dimethoxy group in the indanone moiety of synthesized compounds **90r** and **90p** played a role in increasing the electron donating potential of the compound. It increased the percentage of intermolecular bonding formation with the catalytic triad, which will halt the dengue virus replication (Yin *et al.*, 2006). Thus, the synthesized compounds **90r** and **90p** obtained the top two highest inhibitory activity, surpassing panduratin A.

The presence of alkyl group with a hydrophobic property in the synthesized compounds **90c** and **90e** are not tolerated and lowered the inhibitory activity. This finding is in agreement with the finding of Steuer and co-worker (2011) in evaluating the inhibitory activity of α-ketoamides as DENV-2 protease inhibitors.

The active functional group present in the synthesized compound suggested playing a role in the formation of bonded interaction between enzyme and peptide part of the substrate**.** No fluorescence has been exhibited with the presence of the inhibitor as the inhibitor formed a bonded interaction with the enzyme and ceased the peptide cleavage (refer to the Chapter 2, page 30, Scheme 2.6).

The most potent synthesized compound, **90p**, underwent further analysis to determined it IC_{50} value and the dose-response curved were plotted in Figure 4.31.

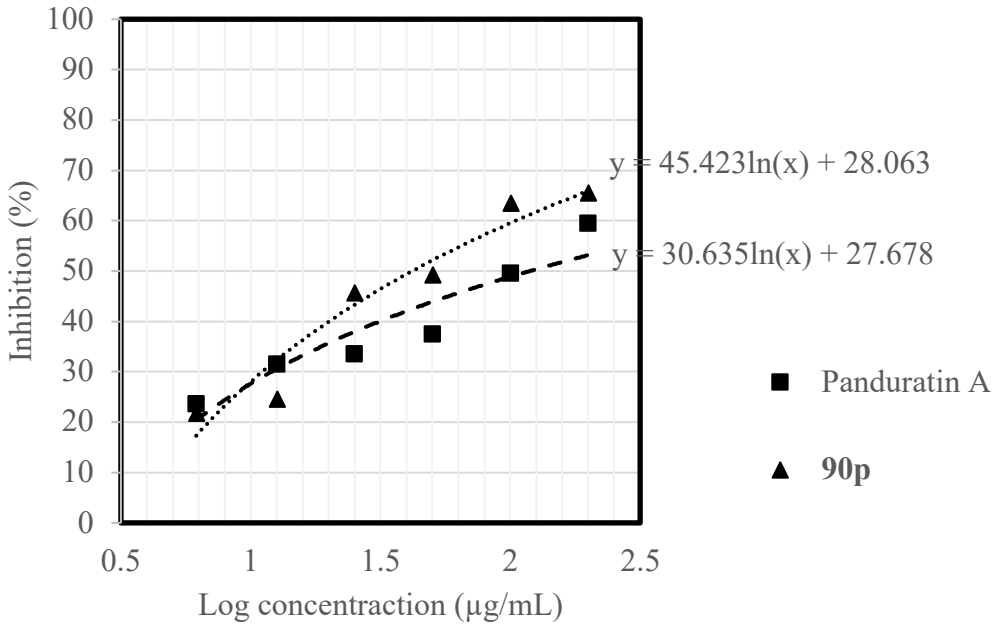

Figure 4.31: Dose-response curves of synthesized compound **90p** and panduratin A on DENV-2 NS2B/NS3 proteases.

The IC_{50} values were determined graphically from inhibition curves (log inhibitor concentration vs. percentage of inhibition) using Microsoft excel. From the curved, the IC_{50} value for compound **90p** was observed to be 42 ppm which is lower compared to the panduratin A, 118 ppm. The concentrations obtained were converted to µM using this equation

$$\mu M = \frac{ppm \times 1000}{Molecular\ weight}$$

$$\text{Compound } \mathbf{90p} = \frac{42 \times 1000}{532.48} = 78.87\ \mu M$$

$$\text{panduratin A} = \frac{118 \times 1000}{406.52} = 290.27\ \mu M$$

Compound **90p** showed a good IC_{50} value suggested to the presence of the more methoxy moieties than the panduratin A. Lai and co-worker (2013) elucidated

the binding mode of the 8-hydroxyquinoline derivatives with DENV-2 NS2B/NS3 protease using molecular docking showed that the *p*-methoxy group of the phenyl moiety may possess an excellent steric fit for the catalytic triad, which resulted in good inhibitory activity.

Another factor affecting the inhibitory activity was the number of electron withdrawing group possess in the compound. Compound **90p** have several electron withdrawing groups in its moiety. The number of electron withdrawing group, such as sulfonyl, aldehyde, nitro, methoxy, halogen and other increased the inhibitory activity of the quinoline derivatives towards the DENV-2 NS2B/NS3 protease (Deng *et al.*, 2012).

In summary, the finding of this study showed the results is in agreement with the previous works. The synthesized compound **90p** displayed a good DENV-2 NS2B/NS3 protease inhibitory activity performed following method by Yusof *et al*. (2000) by using synthetic fluorogenic peptide Boc-Gly-Arg-Arg-AMC. It can be concluded that synthesized compound **90p** could be a potent inhibitor of DENV-2 NS2B/NS3 protease.

CHAPTER 5

CONCLUSION AND RECOMMENDATION

5.1 Conclusion

This study highlighted the potential of *M. charantia* fruits. The fruits flesh and seeds part were both utilized.

The *M. charantia* seeds oil can be extracted. It can be concluded that the enzyme assisted extraction can lead to an increase in oil yield and hemicelullose. Besides, slightly modification in the biochemical properties of the extracted oil were detected. Apart from that, the lignocellulosic biomass seed composition of seeds underwent aqueous enzymatic extraction seems to be have different amount of soluble sugars, and uronic acids.

The *M. charantia* fruits flesh ethyl acetate extract displayed a promising anti-dengue activity towards DENV-2 NS2B/NS3 protease. The GC-MS chromatogram profile of the ethyl acetate extract revealed the presence of gallic acid, a highly anti-viral compound. The gallic acid was chosen for hemisynthesis of DENV-2 NS2B/NS3 protease inhibitor.

The pyrazolyl substituted benzylidene indanone derivatives, **90a-t** were successfully synthesized by the formation of *N* heterocycles using acetic acid. The synthesized compounds showed a promising DENV-2 NS2B/NS3 protease inhibitory in both *in silico* and *in vitro* analysis. The compound **90p** showed lower IC_{50} value of 78.87 μM compared with the panduratin A, 290.27 μM. It can be concluded that the

compound **90p** could be a potent hit-to-led compound in the search of DENV-2 NS2B/NS3 protease inhibitor.

In summary, the *M. charantia* showed a versatile characteristic. The seed oil that contained omega-3 fatty acid and seed's lignocellulosic biomass could be a useful in developing a sustainable product as it possess hemicellulose, soluble sugar and uronic acid. Meanwhile, the fruits flesh could be a good source of chemical constituents with the anti-dengue properties.

5.2 Recommendations for Future Studies

Broadening the scope of this study will produce multidisciplinary knowledge contributions. Several additional works are recommended, such as:

1. In objective 1: To test the activity of *M. charantia* fruits ethyl acetate extract towards DENV-2 NS2B/NS3 protease.

    a. The *M. charantia* fruits could undergo isolation to identify the compound that acts as DENV-2 NS2B/NS3 protease inhibitor.

2. In objective 2: To extract the seed oil of *M. charantia* and study the composition of the seed lignocellulosic biomass.

    a. The aqueous enzymatic extraction in this study used the enzyme cocktail HEL1 and X7. In future studies, a single enzyme such as cellulase, endocellulase, arabinase, xylanase, galactanase, hemicellulase, proteinase, or pectinase can be used in the aqueous enzymatic extraction to obtain an appropriate amount of hemicellulose.

b. The use of hemicellulose in producing a sustainable product such as biodegradables plastic or thin film.

3. In objective 3: To synthesize and characterize the indanone derivatives derived from small molecule present in the *M. charantia* fruit extract.

a. Compound **90p** having the highest DENV-2 NS2B/NS3 protease inhibitory activity. In synthesizing compound **90p**, only 63.17 % yield was obtained. The further method optimization to increase the yield of **90p** can be initiated.

4. In objective 4: To conduct *in silico* molecular docking screening of the synthesized compounds.

a. The compound could undergo a qualitative structure-activity relationship study to get details insight into each functional group per its function.

b. Other crystal structures or protease from dengue virus type-1 can be used to analyse it's in binding interaction.

5. In objective 5: To perform in vitro studies towards DENV-2 NS2B/NS3 protease of synthesized compounds.

a. Further analysis such as toxicity study, MIC, and *in vivo* analysis can be done to investigate compound **90p** potential as DENV-2 NS2B/NS3 protease inhibitor.

REFERENCES

Abdulkarim, S. M., Long, K., Lai, O. M., Muhammad, S. K. S., & Ghazali, H. M. (2005). Some physico-chemical properties of *Moringa oleifera* seed oil extracted using solvent and aqueous enzymatic methods. *Food Chemistry*, **93**, 253–263.

Adler-Nissen, J. (1976). Enzymatic Hydrolysis of Proteins for Increased Solubility. *Journal of Agricultural and Food Chemistry*, **24(6)**, 1090–1093.

Ahmad, N. M., Balasubramanian, M., Brewer, A. R. E., Clay, Ju. M., Curran, T. T., Fuchter, M. J., Glatsis, P., Gribble, G. W., Hagen, T. J., Holsworth, D. D., Lula, D. M., Janey, J. M., Lall, M. S., Li, J. J., Li, J., Mergott, D. J., Mullins, R. J., Shea, K. M., & Wolfe, J. P. (2007). *Name Reactions of Functional Group Transformations*. (J. J. Li & E. J. Corey, Eds.), *Wiley-Interscience*, 457-545.

Ahmad, N., Fazal, H., Ayaz, M., Abbasi, B. H., Mohammad, I., & Fazal, L. (2011). Dengue fever treatment with *Carica papaya* leaves extracts. *Asian Pacific Journal of Tropical Disease*, **1**, 330–333.

Ahmad, N., Hasan, N., Ahmad, Z., Zishan, M., & Zohrameena, S. (2016). *Momordica charantia*: for Traditional Uses and Pharmacological Actions. *Journal of Drug Delivery and Therapeutics*, **6(2)**, 40–44.

Ahmed, F. F., Abd El-Hafeez, A. A., Abbas, S. H., Abdelhamid, D., & Abdel-Aziz, M. (2018). New 1,2,4-triazole-Chalcone hybrids induce Caspase-3 dependent apoptosis in A549 human lung adenocarcinoma cells. *European Journal of Medicinal Chemistry*, **151**, 705–722.

Akihisa, T., Higo, N., Tokuda, H., Ukiya, M., Akazawa, H., Tochigi, Y., Kimura, Y., Suzuki, T., & Nishino, H. (2007). Cucurbitane-type triterpenoids from the fruits of *Momordica charantia* and their cancer chemopreventive effects. *Journal of Natural Products*, **70(8)**, 1233–1239.

Al-Rubaye, A. F., Hameed, I. H., & Kadhim, M. J. (2017). A review: Uses of gas chromatography-mass spectrometry (GC-MS) technique for analysis of bioactive natural compounds of some plants. *International Journal of Toxicological and Pharmacological Research*, **9(01)**, 81–85.

Al-Sumri, A., Al-Siyabi, N., Al-Saadi, R., Al-Rasbi, S., & Al-Dallal, A. (2016). Extraction of Date Palm Seed Oil by Soxhlet Apparatus. *International Journal of Scientific & Engineering Research*, **7(12)**, 1266–1270.

Aleshin, A. E., Shiryaev, S. A., Strongin, A. Y., & Liddington, R. C. (2007). Structural evidence for regulation and specificity of flaviviral proteases and evolution of the Flaviviridae fold. *Protein Science*, **16(5)**, 795–806.

Ali, A., Naznin, S., Ahed, A.-K., & Mohammed, R. A. K. (2014). Review on some Malaysian traditional medicinal plants with therapeutic properties. *Journal of Basic & Applied Sciences*, **10**, 149–159.

Ali, A., Naznin, S., Mohammed, R. A. K., & Aburjai, T. (2012). Enthnopharmacological survey of medicinal plants in Malaysia, the Kangkar Pulai region. *International Journal of Pharmacology*, **8(8**), 697–686.

Ali, M. A., Bastian, S., Ismail, R., Choon, T. S., Ali, S., Aubry, A., Pandian, S., Saraswat, P., Singh, A., & Gaur, R. (2011). Discovery of novel methanone derivatives acting as antimycobacterial agents. *Journal of Enzyme Inhibition and Medicinal Chemistry*, **26(6**), 890–894.

Ali, M. A., Lakshmipathi V. S., Beevi, F., Kumar, R. S., Ismail, R., Choon, T. S., Wei, A. C., Yoon, Y. K., & Basiri, A. (2013). Antimycobacterial Activity: Synthesis and Biological Evaluation of Novel Substituted (3E,5E)-3,5-diarylidene-1-phenethylpiperidine-4-one Derivatives. *Letters in Drug Design & Discovery*. **10**, 471–476.

Ali, M. A., Sayeed, M. A., Reza, M. S., Yeasmin, M. S., & Khan, A. M. (2008). Characteristics of seed oils and nutritional compositions of seeds from different varieties of *Momordica charantia Linn*. cultivated in Bangladesh. *Czech Journal of Food Science*, **26(4)**, 275–283.

Alippilakkotte, S., Kumar, S., & Sreejith, L. (2017). Fabrication of PLA/Ag nanofibers by green synthesis method using *Momordica charantia* fruit extract for wound dressing applications. *Colloids and Surfaces, A: Physicochemical and Engineering Aspects*, **529**, 771–782.

Altemimi, A., Lakhssassi, N., Baharlouei, A., Watson, D. G., & Lightfoot, D. A. (2017). Phytochemicals: Extraction, Isolation, and Identification of Bioactive Compounds from Plant Extracts. *Plants (Basel, Switzerland)*, **6(4)**, 42.

Anwar, F., Kalsoom, U., Sultana, B., Mushtaq, M., Mehmood, T., & Arshad, H. A. (2013). Effect of drying method and extraction solvent on the total phenolics and antioxidant activity of cauliflower (*Brassica oleracea L.)* Extracts. *International Food Research Journal*, **20(2)**, 653–659.

Arega, E. D. (2018). Phytochemical Studies of the Ethyl Acetate Extract of the Fruit of *Piper capense*. *Journal of Pharmacognosy & Natural Products*, **4(1)**, 1–5.

Arias, C. F., Preugschat, F., & Strass, J. H. (1993). Dengue 2 virus ns2b and ns3 form a stable complex that can cleave ns3 within the helicase domain. *Virology*, **193(2)**, 888–899.

Atanasov, A. G., Waltenberger, B., Pferschy-Wenzig, E. M., Linder, T., Wawrosch, C., Uhrin, P., Temml, V., Wang, L., Schwaiger, S., Heiss, E. H., Rollinger, J. M., Schuster, D., Breuss, J. M., Bochkov, V., Mihovilovic, M. D., Kopp, B., Bauer, R., Dirsch, V. M., & Stuppner, H. (2015). Discovery and resupply of pharmacologically active plant-derived natural products: A review. *Biotechnology advances*, **33(8)**, 1582–1614.

Aydin, G., & Kaya, E. (2020). A Review : *Momordica charantia L* .' s Biological Active Components and Its Potential Use in Traditional Therapies. *International Journal of Traditional Complementary Medicine Research*, **1(2)**, 79–95.

Baby, K. C., & Ranganathan, T. V. (2016). Effect of enzyme pre-treatment on extraction yield and quality of fennel (*Foeniculum vulgare*) volatile oil. *Biocatalysis and Agricultural Biotechnology*, **8**, 248–256.

Badhani, B., Sharma, N., & Kakkar, R. (2015). Gallic acid: A versatile antioxidant with promising therapeutic and industrial applications. *RSC Advances*, **5(35)**, 27540–27557.

Bahagian Kawalan Penyakit (BKP). (2019). iDengue. *Kementerian Kesihatan Malaysia*. [online] Accessed on 16 September 2019. Available from: http://idengue.arsm.gov.my

Baharum, S. N., Bunawan, H., Ghani, M. A., Wan Aida Wan Mustapha, & Noor, N. M. (2010). Analysis of the chemical composition of the essential oil of *Polygonum minus Huds*. Using two-dimensional gas chromatography-time-of-flight mass spectrometry (GC-TOF MS). *Molecules*, **15(10)**, 7006–7015.

Balci, M. (2005a). Chapter 3: Chemical Shift. In *Basic 1H- and 13C-NMR Spectroscopy*. 41–75.

Balci, M. (2005b). Chapter 12: Chemical Shift. In *Basic 1H- and 13C-NMR Spectroscopy*, 283–292.

Balkrishna, A., Solleti, S. K., Verma, S., & Varshney, A. (2020). Validation of a novel zebrafish model of dengue virus (DENV-3) pathology using the Penta herbal medicine Denguenil Vati. *Biomolecules*, **10(7)**, 971.

Belin, F., Barthélémy, P., Ruiz, K., Lacombe, J. M., & Pucci, B. (2003). Synthetic gallic acid derivatives as models for a comprehensive study of antioxidant activity. *Helvetica Chimica Acta*, **86(2)**, 247–265.

Beloin, N., Gbeassor, M., Akpagana, K., Hudson, J., De Soussa, K., Koumaglo, K., & Arnason, J. T. (2005). Ethnomedicinal uses of *Momordica charantia* (*Cucurbitaceae*) in Togo and relation to its phytochemistry and biological activity. *Journal of Ethnopharmacology*, **96(1–2)**, 49–55.

Bernama. (2019). Dengue cases up by 89.5% from January to July 2019, says Health Minister. *The Star.* [online] Accessed on 16 September 2019. Available from: https://www.thestar.com.my/news/nation/2019/07/28/dengue-cases-up-by-89pt5pc-from-january-to-july-2019-says-health-minister

Bianco, G., Forli, S., Goodsell, D. S., & Olson, A. J. (2016). Covalent docking using autodock: Two-point attractor and flexible side chain methods. *Protein Science*, **25(1)**, 295–301.

Biz, A., Farias, F. C., Motter, F. A., De Paula, D. H., Richard, P., Krieger, N., & Mitchell, D. A. (2014). Pectinase activity determination: An early deceleration in the release of reducing sugars throws a spanner in the works! *PLoS ONE*, **9(10)**, 1–8.

Braca, A., Siciliano, T., D'Arrigo, M., & Germanò, M. P. (2008). Chemical composition and antimicrobial activity of *Momordica charantia* seed essential oil. *Fitoterapia*, **79(2)**, 123–125.

Brewer, M. S. (2011). Natural Antioxidants: Sources, Compounds, Mechanisms of Action, and Potential Applications. *Comprehensive Reviews in Food Science and Food Safety*, **10(4)**, 221–247.

Brini, E., Fennell, C. J., Fernandez-Serra, M., Hribar-Lee, B., Lukšič, M., & Dill, K. A. (2017). How Water's Properties Are Encoded in Its Molecular Structure and Energies. *Chemical Reviews*, **117(19)**, 12385–12414.

Brown, S. D. (2019). Using HyperChem. *Princeton University: Chemical and Biological Engineering Group*. [online]. Accessed on 09 December 2019. Available from: http://paros.princeton.edu/ench468/hyperchem.htm

Bruice, P. Y. (2004). Part 6: Carbonyl Compounds and Amines. Organic Chemistry. *Pearson Education, Inc, NJ.*, **4th edn.**, 669–912.

Buckeridge, M. S., Pessoa dos Santos, H., & Tiné, M. A. S. (2000). Mobilisation of storage cell wall polysaccharides in seeds. *Plant Physiology and Biochemistry*, **38(1–2)**, 141–156.

Bujang, M. A., Mudin, R. N., Haniff, J., Ikhwan, T. M., Sidik, T. A. B., Md Nordin, N. A., Sulaiman, N., Sani, S. S. M., Kadir, S. S. A., Mohammed, S., & Pin, G. P. (2017). Trend of dengue infection in Malaysia and the forecast up until year 2040. *International Medical Journal*, **24(6)**, 438–441.

Burke, J. (1984). Solubility Parameters : Theory and Application. *The Book and Paper Group*, **3**, 1–35.

Cahour, A., Falgout, B., & Lai, C. J. (1992). Cleavage of the dengue virus polyprotein at the NS3/NS4A and NS4B/NS5 junctions is mediated by viral protease NS2B-NS3, whereas NS4A/NS4B may be processed by a cellular protease. *Journal of Virology*, **66(3)**, 1535–1542.

Cao, J., Zhang, B., & Zhao, Y. (2013). A New Cucurbitane Triterpene in Acid-treated Ethanol Extract from *Momordica charantia*. *Chinese Herbal Medicines*, **5(3)**, 234–236.

Carmona, A. K., Juliano, M. A., & Juliano, L. (2009). The use of fluorescence resonance energy transfer (FRET) peptides for measurement of clinically important proteolytic enzymes. *Anais Da Academia Brasileira de Ciencias*, **81(3)**, 381–392.

Carpita, N. C. & Gibeaut, D. M. (1993). Structural models of primary cell walls in flowering plants: Consistency of molecular structure with the physical properties of the walls during growth. *Plant Journal*, **3(1)**, 1–30.

Chanda, D., Bhushan, S., Guru, S. K., Shanker, K., Wani, Z. A., Rah, B. A., Luqman, S., Mondhe, D. M., Pal, A. & Negi, A. S. (2012). Anticancer activity, toxicity and pharmacokinetic profile of an indanone derivative. *European Journal of Pharmaceutical Sciences*, **47(5)**, 988–995.

Chang, C. I., Chen, C. R., Liao, Y. W., Cheng, H. L., Chen, Y. C., & Chou, C. H. (2006). Cucurbitane-Type Triterpenoids from *Momordica charantia*. *Journal of Natural Products*, **69(8)**, 1168–1171.

Chen, G. C., Su, H. M., Lin, Y. S., Tsou, P. Y., Chyuan, J. H., & Chao, P. M. (2016). A conjugated fatty acid present at high levels in bitter melon seed favorably affects lipid metabolism in hepatocytes by increasing NAD+/NADH ratio and activating PPARα, AMPK and SIRT1 signalling pathway. *Journal of Nutritional Biochemistry*, **33**, 28–35.

Ching, S. M., Zakaria, Z. A., Paimin, F., & Jalalian, M. (2013). Complementary alternative medicine use among patients with type 2 diabetes mellitus in the primary care setting: a cross-sectional study in Malaysia. *BMC Complementary and Alternative Medicine*, **13**, 148.

Cho, Y. S., Kim, S. K., Ahn, C. B., & Je, J. Y. (2011). Inhibition of acetylcholinesterase by gallic acid-grafted-chitosans. *Carbohydrate Polymers*, **84(1)**, 690–693.

Choubey, S., Varughese, L. R. ache., Kumar, V., & Beniwal, V. (2015). Medicinal importance of gallic acid and its ester derivatives: a patent review. *Pharmaceutical Patent Analyst*, **4(4)**, 305–315.

Clain, E., Haddad, J. G., Koishi, A. C., Sinigaglia, L., Rachidi, W., Despres, P., Santos, C. N. D., Guiraud, P., Jouvenet, N., & El Kalamouni, C. (2019). The polyphenol-rich extract from *Psiloxylon mauritianum*, an endemic medicinal plant from reunion island, inhibits the early stages of dengue and Zika virus infection. *International Journal of Molecular Sciences*, **20(8)**, 1860.

Clayden, J., Greeves, N., & Warren, S. G. (2012). Organic chemistry. *Oxford: Oxford University Press. Chicago.* **15th edn.**

Costanzo, P., Cariati, L., Desiderio, D., Sgammato, R., Lamberti, A., Arcone, R., Salerno, R., Nardi, M., Masullo, M., & Oliverio, M. (2016). Design, Synthesis, and Evaluation of Donepezil-Like Compounds as AChE and BACE-1 Inhibitors. *ACS Medicinal Chemistry Letters*, **7(5)**, 470–475.

Dandawate, P. R., Subramaniam, D., Padhye, S. B., & Anant, S. (2016). Bitter melon: A panacea for inflammation and cancer. *Chinese Journal of Natural Medicines*, **14(2)**, 81–100.

de Guzman, G. Q., Dacanay, A. T. L., Andaya, B. A., & Alejandro, G. J. D. (2016). Ethnopharmacological studies on the uses of *Euphorbia hirta* in the treatment of dengue in selected indigenous communities in pangasinan (Philippines). *Journal of Intercultural Ethnopharmacology*, **5(3)**, 239–243.

Deng, J., Li, N., Liu, H., Zuo, Z., Liew, O. W., Xu, W., Chen, G., Tong, X., Zhu, J., Zuo, J., Jiang, H., Yang, C., Li, J., & Zhu, W. (2012). Discovery of novel small molecule inhibitors of dengue viral NS2B-NS3 protease using virtual screening and scaffold hopping. *Journal of Medicinal Chemistry*, **55(14)**, 6278–6293.

Department of Agriculture (DoA), Putrajaya, Malaysia, (2014). Vegetables and Cash Crops Statistic. Accessed on 2nd September 2018. Available from: https://www.google.com/url?sa=t&rct=j&q=&esrc=s&source=web&cd=&cad=rja&uact=8&ved=2ahUKEwijormtgvLrAhUFWCsKHfcDC5QQFjABegQICBAB&url=http%3A%2F%2Fwww.doa.gov.my%2Findex%2Fresources%2Faktiviti_sumber%2Fsumber_awam%2Fmaklumat_pertanian%2Fperangkaan_tanaman%2Fperangkaan_sayur_tnmn_ladang_2015.pdf&usg=AOvVaw3P4mC7bNUq_pVPCVfHYnyC

Dharmarathna, S. L. C. A., Wickramasinghe, S., Waduge, R. N., Rajapakse, R. P. V. J., & Kularatne, S. A. M. (2013). Does *Carica papaya* leaf-extract increase the platelet count? An experimental study in a murine model. *Asian Pacific Journal of Tropical Biomedicine*, **3(9)**, 720–724.

Dinnocenzo, J. P., & Banach, T. E. (1989). Deprotonation of Tertiary Amine Cation Radicals. A Direct Experimental Approach. *Journal of the American Chemical Society*, **111(23)**, 8646–8653.

Dwivedi, G. R., Tiwari, N., Singh, A., Kumar, A., Roy, S., Negi, A. S., Pal, A., Chanda, D., Sharma, A., & Darokar, M. P. (2016). Gallic acid-based indanone derivative interacts synergistically with tetracycline by inhibiting efflux pump in multidrug resistant *E. coli*. *Applied Microbiology and Biotechnology*, **100(5)**, 2311–2325.

Erbel, P., Schiering, N., D'Arcy, A., Renatus, M., Kroemer, M., Lim, S. P., Yin, Z., Keller, T. H., Vasudevan, S. G., & Hommel, U. (2006). Structural basis for the activation of flaviviral NS3 proteases from dengue and West Nile virus. *Nature Structural and Molecular Biology*, **13(4)**, 372–373.

Eremeeva, T. (2003). Size-exclusion chromatography of enzymatically treated cellulose and related polysaccharides: A review. *Journal of Biochemical and Biophysical Methods*, **56(1–3)**, 253–264.

Falgout, B., Pethel, M., Zhang, Y. M., & Lai, C. J. (1991). Both nonstructural proteins NS2B and NS3 are required for the proteolytic processing of dengue virus nonstructural proteins. *Journal of Virology*, **65(5)**, 2467–2475.

Farahmandfar, R., Esmaeilzadeh Kenari, R., Asnaashari, M., Shahrampour, D., & Bakhshandeh, T. (2019). Bioactive compounds, antioxidant and antimicrobial activities of Arum maculatum leaves extracts as affected by various solvents and extraction methods. *Food Science and Nutrition*, **7(2)**, 465–475.

Fatma Yelda, Ö. (2009). The Syntheses of Indanones and Indenones Via Rhodium Catalyzed. İzmir Institute of Technology, 36–56.

Fatope, M. O., Takeda, Y., Yamashita, H., Okabe, H., & Yamauchi, T. (1990). New cucurbitane triterpenoids from *Momordica charantia*. *Journal of Natural Products*, **53(6)**, 1491.

Ferreira, L. G., Dos Santos, R. N., Oliva, G., & Andricopulo, A. D. (2015). Molecular docking and structure-based drug design strategies. *Molecules*, **20**, 13384–13421.

Fields, G. B. (2001). Using Fluorogenic Peptide Substrates to Assay Matrix Metalloproteinases Gregg. *Methods in Molecular Biology*, **151**, 495–518.

Forli, S., Huey, R., Pique, M. E., Sanner, M. F., Goodsell, D. S., & Olson, A. J. (2016). Computational protein–ligand docking and virtual drug screening with the AutoDock suite. *Nature Protocol*, **11(5)**, 905–919.

Foster, S. (2009). Balancing Nature and Wellness -Malaysian Traditions of "Ramuan" The History, Culture, Biodiversity and Scientific Assimilation of Medicinal Plants in Malaysia. *HerbaGram*, **84**, 30–43.

Garcia-Rivera, D., Delgado, R., Bougarne, N., Haegeman, G., & Vanden Berghe, W. (2011). Gallic acid indanone and mangiferin xanthone are strong determinants of immunosuppressive anti-tumour effects of *Mangifera indica L.* bark in MDA-MB231 breast cancer cells. *Cancer Letters (New York, NY, United States)*, **305(1)**, 21–31.

Ghosh, B. C., Prasad, L. N., & Saha, N. P. (2017). Enzymatic hydrolysis of whey and its analysis. *Journal of Food Science and Technology*, **54(6)**, 1476–1483.

Giovane, A., Servillo, L., Balestrieri, C., Raiola, A., D'Avino, R., Tamburrini, M., Ciardiello, M. A., & Camardella, L. (2004). Pectin methylesterase inhibitor. *Biochimica et Biophysica Acta - Proteins and Proteomics*, **1696(2)**, 245–252.

Giuliani, C., Tani, C., & Bini, L. M. (2016). Micromorphology and anatomy of fruits and seeds of bitter melon (*Momordica charantia L.*, *Cucurbitaceae*). *Acta Societatis Botanicorum Poloniae*, **85(1)**, 1–7.

Grover, J. K., & Yadav, S. P. (2004). Pharmacological actions and potential uses of *Momordica charantia*: A review. *Journal of Ethnopharmacology*, **93(1)**, 123–132.

Guy, B., Barrere, B., Malinowski, C., Saville, M., Teyssou, R., & Lang, J. (2011). From research to phase III : Preclinical , industrial and clinical development of the Sanofi Pasteur tetravalent dengue vaccine. *Vaccine*, **29(42)**, 7229–7241.

Guy, B., Briand, O., Lang, J., Saville, M., & Jackson, N. (2015). Development of the Sanofi Pasteur tetravalent dengue vaccine: one more step forward. *Vaccine*, **33**, 7100–7111.

Guy, B., Guirakhoo, F., Barban, V., & Higgs, S. (2010). Preclinical and clinical development of YFV 17D-based chimeric vaccines against dengue, West Nile and Japanese encephalitis viruses. *Vaccine*, **28**, 632–649.

Guy, B., Noriega, F., Ochiai, R. L., L'azou, M., Delore, V., Skipetrova, A., Verdier, F., Coudeville, L., Savarino, S., & Jackson, N. (2017). A recombinant live attenuated tetravalent vaccine for the prevention of dengue. *Expert Review of Vaccines*, **16(7)**, 671–683.

Guzman, M. G., & Kouri, G. (2003). Dengue and dengue hemorrhagic fever in the Americas: Lessons and challenges. *Journal of Clinical Virology*, **27(1)**, 1–13.

Harinantenaina, L., Tanaka, M., Takaoka, S., Oda, M., Mogami, O., Uchida, M., & Asakawa, Y. (2006). *Momordica charantia* constituents and antidiabetic screening of the isolated major compounds. *Chemical & Pharmaceutical Bulletin*, **54(7)**, 1017–1021.

Harlita, T. D., Oedjijono, & Asnani, A. (2018). The Antibacterial Activity of Dayak Onion (Eleutherine palmifolia (L.) Merr) toward Pathogenic Bacteria. *Tropical Life Sciences Research*, **29(2)**, 39–52.

Hassaneen, H. M. E., Eid, E. M., Eid, H. A., Farghaly, T. A., & Mabkhot, Y. N. (2017). Facial regioselective synthesis of novel bioactive spiropyrrolidine/pyrrolizine-oxindole derivatives via a three components reaction as potential antimicrobial agents. *Molecules*, **22(3)**, 1–15.

Hevener, K. E., Zhao, W., Ball, D. M., Babaoglu, K., Qi, J., White, S. W., & Lee, R. E. (2009). Validation of Molecular Docking Programs for Virtual Screening against Dihydropteroate Synthase. *Journal of Chemical Information and Modeling*, **49(2)**, 44–460.

Hites, R. A. (1997). Gas Chromatography Mass Spectroscopy. In: *Handbook of Instrumental Techniques for Analytical Chemistry*. F. A. Settle, (ed). Prentice Hall, NJ., 609–624.

Horax, R., Hettiarachchy, N., & Chen, P. (2010). Extraction, quantification, and antioxidant activities of phenolics from pericarp and seeds of bitter melons (*Momordica charantia*) harvested at three maturity stages (Immature, Mature, and Ripe). *Journal of Agricultural and Food Chemistry*, **58(7)**, 4428–4433.

Huang, L., Lu, C., Sun, Y., Mao, F., Luo, Z., Su, T., Jiang, H., Shan, W., & Li, X. (2012). Multitarget-directed benzylideneindanone derivatives: Anti-β-amyloid (Aβ) aggregation, antioxidant, metal chelation, and monoamine oxidase B (MAO-B) inhibition properties against Alzheimer's disease. *Journal of Medicinal Chemistry*, **55(19)**, 8483–8492.

Ibrahim, T. A., El-Hefnawy, H. M., & El-Hela, A. A. (2010). Antioxidant potential and phenolic acid content of certain cucurbitaceous plants cultivated in Egypt. *Natural Product Research*, **24(16)**, 1537–1545.

Irie, K., Mohan, P. M., Sasaguri, Y., Putnak, R., & Padmanabhan, R. (1989). Sequence analysis of cloned dengue virus type 2 genome (New Guinea-C strain). *Gene*, **75(2)**, 197–211.

Ishimaru, T., Shibata, N., Horikawa, T., Yasuda, N., Nakamura, S., Toru, T., & Shiro, M. (2008). Cinchona alkaloid catalyzed enantioselective fluorination of allyl silanes, silyl enol ethers, and oxindoles. *Angewandte Chemie, International Edition*, **47(22)**, 4157–4161.

Itoh, Y., Nakashima, Y., Tsukamoto, S., Kurohara, T., Suzuki, M., Sakae, Y., Oda, M., Okamoto, Y., & Suzuki, T. (2019). N+-C-H···O Hydrogen bonds in protein-ligand complexes. *Scientific Reports*, **9(1)**, 1–5.

Izydorczyk, M. S., & Biliaderis, C. G. (1995). Cereal arabinoxylans: advances in structure and physicochemical properties. *Carbohydrate Polymers*, **28(1)**, 33–48.

Jia, S., Shen, M., Zhang, F., & Xie, J. (2017). Recent Advances in *Momordica charantia* : Functional Components and Biological Activities. *International Journal of Molecular Sciences*, **18(2555)**, 1–25.

Jiao, J., Li, Z. G., Gai, Q. Y., Li, X. J., Wei, F. Y., Fu, Y. J., & Ma, W. (2014). Microwave-assisted aqueous enzymatic extraction of oil from pumpkin seeds and evaluation of its physicochemical properties, fatty acid compositions and antioxidant activities. *Food Chemistry*, **147**, 17–24.

Johnson, L. A., & Lusas, E. W. (1983). Comparison of alternative solvents for oils extraction. *Journal of the American Oil Chemists' Society*, **60(2)**, 229–242.

Joseph, B., & Jini, D. (2013). Antidiabetic effects of *Momordica charantia* (bitter melon) and its medicinal potency. *Asian Pacific Journal of Tropical Disease*, ***3*(2),** 93–102.

Kalia, V. C., Rashmi, Lal, S., & Gupta, M. N. (2001). Using Enzymes for Oil Recovery from Edible Seeds. *Journal of Scientific and Industrial Research*, **60(4)**, 298–310.

Kamal, A., Shaik, A. B., Reddy, G. N., Kumar, C. G., Joseph, J., Kumar, G. B., & Sastry, G. N. (2014). Synthesis, biological evaluation, and molecular modeling of (E)-2-aryl-5-styryl-1,3,4-oxadiazole derivatives as acetylcholine esterase inhibitors. *Medicinal Chemistry Research*, **23(4),** 2080–2092.

Kamatou, G. P. P., & Viljoen, A. M. (2017). Comparison of fatty acid methyl esters of palm and palmist oils determined by GCxGC–ToF–MS and GC–MS/FID. *South African Journal of Botany*, **112**, 483–488.

Kaneria, M. J., Rakholiya, K. D., Marsonia, L. R., Dave, R. A., & Golakiya, B. A. (2018). Nontargeted metabolomics approach to determine metabolites profile and antioxidant study of Tropical Almond (*Terminalia catappa L.*) fruit peels using GC-QTOF-MS and LC-QTOF-MS. *Journal of Pharmaceutical and Biomedical Analysis*, **160**, 415–427.

Kenny, O., Smyth, T. J., Hewage, C. M., & Brunton, N. P. (2013). Antioxidant properties and quantitative UPLC-MS analysis of phenolic compounds from extracts of fenugreek (*Trigonella foenum-graecum*) seeds and bitter melon (*Momordica charantia*) fruit. *Food Chemistry*, **141(4)**, 4295–4302.

Kimura, Y., Akihisa, T., Yuasa, N., Ukiya, M., Suzuki, T., Toriyama, M., Motohashi, S., & Tokuda, H. (2005). Cucurbitane-type triterpenoids from the fruit of *Momordica charantia*. *Journal of Natural Products*, **68(5)**, 807–809.

Komakech, R. (2018), Herbs & People. *Momordica charantia:* A unique anti-diabetic plant. *Southworld: Culture,* August 2018. Accessed on 19 September 2020. Available from: https://www.southworld.net/herbs-people-momordica-charantia-a-unique-anti-diabetic-plant/

Korotchenko, V. N., Saydmohammed, M., Vollmer, L. L., Bakan, A., Sheetz, K., Debiec, K. T., & Tsang, M. (2014). In Vivo Structure-Activity Relationship Studies Support Allosteric Targeting of a Dual Specificity Phosphatase. *ChemBioChem*, **15(10)**, 1436–1445.

Kumar, K. P. S., & Bhowmik, D. (2010). Traditional medicinal uses and therapeutic benefits of *Momordica charantia Linn*. *International Journal of Pharmaceutical Sciences Review and Research*, ***4*(3)**, 23–28.

Kumar, R. C., Benal, M. M., Prasad, B. D., Krupashankara, M. S., Kulkarni, R. S., & Siddaligaswamy, N. H. (2018). Microwave Assisted Extraction of Oil from *Pongamia pinnata* Seeds. *Mater. Today: Proceedings*, **5**, 2960–2964.

Lai, H., Prasad, G. S., & Padmanabhan, R. (2013). Characterization of 8-hydroxyquinoline derivatives containing aminobenzothiazole as inhibitors of dengue virus type 2 protease in vitro. *Antiviral Research*, **97(1)**, 74–80.

Lampman, G., Pavia, D. L., Kriz, G. S., & Vyvyan, J. (2010). Spectroscopy. *Brooks/Cole Cengage Learning***, International edn.**, 15–198.

Lanciotti R S, Calisher C H, Gubler D J, Chang G J, & Vorndam A V. (1992). Rapid detection and typing of dengue viruses from clinical samples by using reverse transcriptase-polymerase chain reaction. *Journal of Clinical Microbiology*, **30(3)**, 545–551.

Latif, S., & Anwar, F. (2011). Aqueous enzymatic sesame oil and protein extraction. *Food Chemistry*, **125(2)**, 679–684.

Li, D., Ji, B., Hwang, K. C., & Huang, Y. (2011). Strength of hydrogen bond network takes crucial roles in the dissociation process of inhibitors from the hiv-1 protease binding pocket. *PLoS ONE*, **6(4)**, 1–13.

Li, L., Basavannacharya, C., Chan, K. W. K., Shang, L., Vasudevan, S. G., & Yin, Z. (2015). Structure-guided discovery of a novel non-peptide inhibitor of dengue virus NS2B-NS3 protease. *Chemical Biology and Drug Design*, **86(3)**, 255–264.

Li, Y. H., Zhang, B., Yang, H. K., Li, Q., Diao, P. C., You, W. W., & Zhao, P.-L. (2017). Design, synthesis, and biological evaluation of novel alkylsulfanyl-1,2,4-triazoles as cis-restricted combretastatin A-4 analogues. *European Journal of Medicinal Chemistry*, **123**, 1098–1106.

Lin, K. H., Nalivaika, E. A., Prachanronarong, K. L., Yilmaz, N. K., & Schiffer, C. A. (2016). Dengue Protease Substrate Recognition: Binding of the Prime Side. *ACS Infectious Diseases*, **2(10)**, 734–743.

Lindenbach, B. D., Thiel, H. J., & Rice, C. M. (2007). Flaviviridae: The Viruses and Their Replication. In D. M. Knipe & P. M. Howley (Eds.), *Fields Virology,* Lippincott-Raven Publishers, Philadelphia, ***5th Edition***,1101-1152.

Liu, L., Hammond, E. G., & Nikolau, B. J. (1998). In vivo studies of the biosynthesis of vernolic acid in the seed of *Vernonia galamensis*. *Lipids*, **33(12)**, 1217–1221.

Liu, S., Hu, H., & Pedersen, L. G. (2010a). Steric, Quantum, and Electrostatic Effects on SN2 Reaction Barriers in Gas Phase. *Journal of Physical Chemistry A*, **114(18)**, 5913–5918.

Liu, X., Deng, Z., Fan, Y., Li, J., & Liu, Z. (2010b). Mineral elements analysis of *Momordica charantia* seeds by ICP-AES and fatty acid profile identification of seed oil by GC-MS. *Guangpuxue Yu Guangpu Fenxi*, **30(8)**, 2265–2268.

Maarten, J. M. C., & James, W. B. (2016). The number of known plants species in the world and its annual increase. *Phytotaxa*, **261(3)**, 201–217.

Mahdi-Pour, B., Jothy, S. L., Latha, L. Y., Chen, Y., & Sasidharan, S. (2012). Antioxidant activity of methanol extracts of different parts of *Lantana camara*. *Asian Pacific Journal of Tropical Biomedicine*, **2(12)**, 960–965.

Mahmud, M. A. F., Abdul Mutalip, M. H., Lodz, N. A., Muhammad, E. N., Yoep, N., Hashim, M. H., Paiwai, F., Rajarethinam, J., Aik, J., & Muhammad, N. A. (2019). Environmental management for dengue control: A systematic review protocol. *BMJ Open*, **9(5)**, 1–4.

Malik, R. A., Saad, M. M., & Tiwari, S. (2019). Effect of extraction time and solvent power on phytochemical screening and antioxidant activity of *Momordica charantia L.* fruit extracts. *Asian Journal of Chemistry*, **31(3)**, 647–650.

MarvinSketch (version 19.4.0), was used for drawing, displaying and characterizing chemical structures, substructures and reactions, ChemAxon (http://www.chemaxon.com).

Masoko, P. (2007). Chapter 2: Extraction of plant material. *University of Pretoria.* 40–57.

Matt (2011). Organic Chemistry Practice Problems and Problem Sets: Aldehyde and ketone. Accessed on 15 September 2020. Available from:http://www.mendelset.com/articles/695/aldehydes_and_ketones

McMurray, J. (2010). Organic Chemistry with biological application. *Brooks/Cole, Cengage Learning*. **2nd**

Messina, J. P., Brady, O. J., Golding, N., Kraemer, M. U. G., Wint, G. R. W., Ray, S. E., Pigott, D. M., Shearer, F. M., Johnson, K., Earl, L., Marczak, L. B., Shirude, S., Weaver, N. D., Gilbert, M., Velayudhan, R., Jones, P., Jaenisch, T., Scott, T. W., Reiner Jr, R. C., & Hay, S. I. (2019). The current and future global distribution and population at risk of dengue. *Nature Microbiology*, **4(September 2019)**. 1508–1515.

Metcalfe, L. D., & Schmitz, A. A. (1961). The rapid preparation of fatty acid esters for gas chromatographic analysis. *Amour Industrial Chemical Co*. **33(3)**, 363–364.

Ministry of Health Malaysia (MoHM). (2015). CPG Management of Dengue Infection In Adults (Third Edition) *2015*. **3rd ed.** *Malaysia Health Technology Assessment Section (MaHTAS)*.

Mohdaly, A., & Smetanska, I. (2010). Methods for the extraction of metabolites from plant tissues. *Handbook of Nutritional Biochemistry: Genomics, Metabolomics and Food Supply*, **(December)**, 123–164.

Morris, G. M., Huey, R., Lindstrom, W., Sanner, M. F., Belew, R. K., Goodsell, D. S., & Olson, A. J. (2009), AutoDock4 and AutoDockTools4: Automated docking with selective receptor flexibility. *Journal of Computational Science,* **30(16)**, 2785–2791.

Mozhaev V.V. (1998). Enzyme stability in systems with organic solvents. In A. Ballesteros, F. J. Plou, J. . Iborra, & P. . Halling (Eds.), *Stability and Stabilization of Biocatalysis* (pp. 345–356). Elsevier Sciences B. V.

Mudin, R. N. (2015). Dengue incidence and the prevention and control program in Malaysia. *International Medical Journal Malaysia*, **14(1)**, 5–10.

Muhamad, N., Muhmed, S. A., Yusoff, M. M., & Gimbun, J. (2014). Influence of solvent polarity and conditions on extraction of antioxidant, flavonoids and phenolic content from *Averrhoa bilimbi*. *Journal of Food Science and Engineering*, **4(January)**, 255–260.

Muniglia, L., Girardin, M., Piffaut, B., & Ricochon, G. (2011). Enzyme method of extracting oils and proteins from vegetable matter in an aqueous medium. *Institut National De La Propriété Industrielle*, 1–18.

Murty, M. S. R., Penthala, R., Polepalli, S., & Jain, N. (2016). Synthesis and biological evaluation of novel resver atroloxadiazole hybrid heterocycles as potential antiproliferative agent. *Medicinal Chemistry Research*, **25(4)**,627–643.

Naidu, D. S., Hlangothi, S. P., & John, M. J. (2018). Bio-based products from xylan: A review. *Carbohydrate Polymers*, **179(September 2017)**, 28–41.

Nel, M. S., Petzer, A., Petzer, J. P., & Legoabe, L. J. (2016). 2-Heteroarylidene-1-indanone derivatives as inhibitors of monoamine oxidase. *Bioorganic Chemistry*, **69**, 20–28.

Nill, J., Karuna, N., & Jeoh, T. (2018). The impact of kinetic parameters on cellulose hydrolysis rates. *Process Biochemistry*, **74**, 108–117.

Niyomrattanakit, P., Winoyanuwattikun, P., Chanprapaph, S., Angsuthanasombat, C., Panyim, S., & Katzenmeier, G. (2004). Identification of Residues in the Dengue Virus Type 2 NS2B Cofactor That Are Critical for NS3 Protease Activation. *Journal of Virology*, **78(24)**, 13708–13716.

Noble, C. G., Seh, C. C., Chao, A. T., & Shi, P. Y. (2012). Ligand-Bound Structures of the Dengue Virus Protease Reveal the Active Conformation. *Journal of Virology*, **86(1)**, 438–446.

Okabe, H., Miyahara, Y., Yamauchi, T., Miyahara, K., & Kawasaki, T. (1980). Studies on the constituents of *Momordica charantia L. I.* Isolation and characterization of momordicosides A and B, glycosides of a pentahydroxy-cucurbitane triterpene. *Chemical & Pharmaceutical Bulletin*, **28(9)**, 2753.

Omokhua-Uyi, A. G., & Van Staden, J. (2020). Phytomedicinal relevance of South African *Cucurbitaceae* species and their safety assessment: A review. *Journal of Ethnopharmacology*, **259**, 112967.

Ong, H. C., & Azliza, M. A. (2015). Medicinal Plants for Diabetes by the Orang Asli in Selangor, Malaysia. *Ethano Medicine*, **9(1)**, 77–84.

Ong, S. Q. (2016). Dengue vector control in Malaysia: A review for current and alternative strategies. *Sains Malaysiana*, **45(5)**, 777–785.

Othman, R., Kiat, T. S., Khalid, N., Yusof, R., Irene Newhouse, E., Newhouse, J. S., Alam, M., & Rahman, N. A. (2008). Docking of Noncompetitive Inhibitors into Dengue Virus Type 2 Protease: Understanding the Interactions with Allosteric Binding Sites. *Journal of Chemical Information and Modeling*, **48(8)**, 1582–1591.

Ow, Y.-Y., & Stupans, I. (2005). Gallic Acid and Gallic Acid Derivatives: Effects on Drug Metabolizing Enzymes. *Current Drug Metabolism*, **4(3)**, 241–248.

Park, Y. B., & Cosgrove, D. J. (2012). A revised architecture of primary cell walls based on biomechanical changes induced by substrate-specific endoglucanases. *Plant Physiology*, **158(4)**, 1933–1943.

Patil, S. A., Patil, R., & Patil, S. A. (2017). Recent developments in biological activities of indanones. *European Journal of Medicinal Chemistry*, **138**, 182–198.

Pavia, D., Lampman, G., Kriz, G., & Vyvyan, J. (2015). Introduction to spectroscopy. *SERBIULA (sistema Librum 2.0)*, **5th edn.**

Pedrolli, D. B., Monteiro, A. C., Gomes, E., & Carmona, E. C. (2009). Pectin and Pectinases: Production, Characterization and Industrial Application of Microbial Pectinolytic Enzymes. *The Open Biotechnology Journal*, **3(1)**, 9–18.

Peng, X., Bian, J., Li, M., Xiao, X., Xia, X., Yin, W., & Sun, R. (2013). Graded Ethanol Fractionation and Structural Characterization of Alkali-Extractable Hemicelluloses from *Olea europaea L*. *BioResources*, **8(1)**, 1110–1123.

Perera, S. D., Jayawardena, U. A., & Jayasinghe, C. D. (2018). Potential Use of *Euphorbia hirta* for Dengue: A Systematic Review of Scientific Evidence. *Journal of Tropical Medicine*, **2018**, 1–7.

Perez, J. L., Jayaprakasha, G. K., & Patil, B. S. (2014). Chapter 3: Separation and Identification of Cucurbitane-Type Triterpenoids from Bitter Melon. In *Instrumental Methods for the Analysis and Identification of Bioactive Molecules* (pp. 51–78).

Pham, T. M. H., Ngo, D.-H., Ngo, D.-N., & Vo, T. S. (2019). Investigation of Biological Activities of Wild Bitter (*Momordica charantia Linn*. Var. Abbreviata Ser.). *Biomolecules*, **9(211)**, 1–10.

Phong, W. Y., Moreland, N. J., Lim, S. P., Wen, D., Paradkar, P. N., & Vasudevan, S. G. (2011). Dengue protease activity: The structural integrity and interaction of NS2B with NS3 protease and its potential as a drug target. *Bioscience Reports*, **31(5)**, 399–409.

Popescu, C. M., Popescu, M. C., & Vasile, C. (2010). Characterization of fungal degraded lime wood by FT-IR and 2D IR correlation spectroscopy. *Microchemical Journal*, **95(2)**, 377–387.

Predescu, N. C., Papuc, C., Nicorescu, V., Gajaila, I., Goran, G. V., Petcu, C. D., & Stefan, G. (2016). The influence of solid-to-solvent ratio and extraction method on total phenolic content, flavonoid content and antioxidant properties of some ethanolic plant extracts. *Revista de Chimie*, **67(10)**, 1922–1927.

Preugschat, F., Yao, C. W., & Strauss, J. H. (1990). *In vitro* processing of dengue virus type 2 nonstructural proteins NS2A, NS2B, and NS3. *Journal of Virology*, **64(9)**, 4364–4374.

Purnima, J., Dilmani, W., & Harshani, D. (1999). Karawila (*Momordica charantia*). In *Medicinal and Aromatic Plant Series* (pp. 3–36). Information Services Center, Industrial Technology Institute.

Purnima, J., Dilmani, W., & Harshani, D. (1999). Karawila (*Momordica charantia*). In *Medicinal and Aromatic Plant Series* (pp. 3–36). Information Services Center, Industrial Technology Institute.

Rahman, M., Jelip, J., Hassan, M. R., & Isahak, I. (2012). All Serotypes of Dengue Viruses Circulating in Kuala Lumpur, Malaysia. *Current Research Journal of Biological Sciences*, **4(2)**, 229–234.

Rajapakse, S., Rodrigo, C., & Rajapakse, A. (2012). Treatment of dengue fever. *Infection and Drug Resistance*, **5(1)**, 103–112.

Ricochon, G., & Muniglia, L. (2010). Influence of enzymes on the oil extraction processes in aqueous media. *OCL - Oleagineux Corps Gras Lipides*, **17(6)**, 356–359.

Rood, D. (1995). Gas chromatography problem solving and troubleshooting. *Journal of Chromatographic Science*, **33(347)**, 136–137.

Rosenthal, A., Pyle, D. L., & Niranjan, K. (1996). Aqueous and enzymatic processes for edible oil extraction. *Enzyme and Microbial Technology*, **19(6)**, 402–420.

Sabchareon, A., Wallace, D., Sirivichayakul, C., Limkittikul, K., Chanthavanich, P., Suvannadabba, S., Jiwariyavej, V., Dulyachai, W., Pengsaa, K., Wartel, T. A., Moureau, A., Saville, M., Bouckenooghe, A., Viviani, S., Tornieporth, N. G., & Lang, J. (2012). Protective efficacy of the recombinant, live-attenuated, CYD tetravalent dengue vaccine in Thai schoolchildren: a randomised, controlled phase 2b trial. *Lancet (London, England)*, **380(9853)**, 1559–1567.

Sabri, M. S. M., Wei, O. C., & Fei, Y. M. (2018). Synthesis, characterisation and vasolidation properties of indanone-based chalcones. *Journal of Physical Science*, **29**, 99–106.

Saeed, F., Afzaal, M., Niaz, B., Arshad, U., Tufail, T., Hussain, B., & Javed, A. (2018). Bitter melon (*Momordica charantia*): A natural healthy vegetable. *International Journal of Food Properties*, **21(1)**, 1270–1290.

Sandler, S. R., Karo, W., Sandler, S. R., & Karo, W. (1992). 10 – Esters. *Sourcebook of Advanced Organic Laboratory Preparations*, **I**, 83–91.

Saxena, H. O., Faridi, U., Srivastava, S., Kumar, J. K., Darokar, M. P., Luqman, S., Chanotiya, C. S., Krishna, V., Negi, A. S., & Khanuja, S. P. S. (2008). Gallic acid-based indanone derivatives as anticancer agents. *Bioorganic and Medicinal Chemistry Letters*, **18(14)**, 3914–3918.

Schejbal, J., Honzíček, J., Vinklárek, J., Erben, M., & Růžičková, Z. (2014). Acyl-functionalized molybdenum compounds [(η3-C3H5)(η5-Cp')Mo(CO)2]: An experimental study including the X-ray structure of a rare endo conformer. *European Journal of Inorganic Chemistry*, **2014(34)**, 5895–5907.

Schulz, O., Sewell, H. F., & Shakib, F. (1998). A sensitive fluorescent assay for measuring the cysteine protease activity of Der p 1, a major allergen from the dust mite Dermatophagoides pteronyssinus. *Journal of Clinical Pathology - Molecular Pathology*, **51(4)**, 222–224.

Scritable by Nature Education. (2011). Controlling Dengue Outbreaks. [online]. Accessed on 16 September 2019. Available from: http://www.nature.com/scitable/topicpage/controlling-dengue-outbreaks-22403714

Segato, F., Damásio, A. R. L., de Lucas, R. C., Squina, F. M., & Prade, R. A. (2014). Genomics Review of Holocellulose Deconstruction by Aspergilli. *Microbiology and Molecular Biology Reviews*, **78(4)**, 588–613.

Seidel, V. (2006). Initial and Bulk Extraction. In S. D. Sarker, Z. Latif, & A. I. Gray (Eds.), *Natural Products Isolation* (Vol. 2, pp. 27–46). Humana Press Inc.

Selvamuthukumaran, M., & Shi, J. (2017). Recent advances in extraction of antioxidants from plant by-products processing industries. *Food Quality and Safety*, **1(1)**, 61–81.

Sharma, Y. (2019). A chemical and medicinal potency of *Momordica charantia*. *The Pharma Innovation Journal*, **8(6)**, 531-536

Sheat, A. M., Hussein, M. S., & Abood, S. A. (2018). Synthesis and Characterization of Some Spiro Pyrrolidine Compounds. *International Journal of Recent Research and Review*, **10(3)**, 41–47.

Sheldon, R. A. & Pelt. S. (2013). Enzyme immobilisation in biocatalysis: Why, what and how. *Chemistry Society Revision,* **42(15)**, 6223–6235.

Shivanagoudra, S. R., Perera, W. H., Perez, J. L., Athrey, G., Sun, Y., Wu, C. S., Jayaprakasha, G. K., & Patil, B. S. (2019). In vitro and in silico elucidation of antidiabetic and anti-inflammatory activities of bioactive compounds from *Momordica charantia L. Bioorganic & Medicinal Chemistry*, ***27*(14),** 3097–3109.

Singh, A., Fatima, K., Srivastava, A., Khwaja, S., Priya, D., Singh, A., Mahajan, G., Alam, S., Saxena, A. K., Mondhe, D. M., Luqman, S., Chanda, D., Khan, F., & Negi, A. S. (2016). Anticancer activity of gallic acid template-based benzylidene indanone derivative as microtubule destabilizer. *Chemical Biology and Drug Design*, 625–634.

Singh, J. K. R. P. (2019). The many ways to control Aedes and reduce dengue. *The Star*. [online] Accessed on 16 September 2019. Available from: https://www.star2.com/health/2019/06/27/control-aedes-reduce-dengue/

Škorňa, P., Michalík, M., & Klein, E. (2016). Gallic acid: thermodynamics of the homolytic and heterolytic phenolic O—H bonds splitting-off. *Acta Chimica Slovaca*, **9(2)**, 114–123.

Škrbić, B., Cvejanov, J., & Durišić-Mladenović, N. (2015). Chemometric characterization of vegetable oils based on the fatty acid profiles for selection of potential feedstocks for biodiesel production. *Journal of Biobased Materials and Bioenergy*, **9(3)**, 358–371.

Smith, M. B. & March J., (2006). March's Advanced Organic Chemistry: Reactions, Mechanisms, and Structure, *Wiley-VCH, Weinheim*, **5th edn.**, 1559–1567.

Sodeifian, G., Ardestani, N. S., Sajadian, S. A., & Moghadamian., K. (2018). Properties of *Portulaca oleracea* seed oil via supercritical fluid extraction: Experimental and optimization. *Journal of Supercritical. Fluid*, **135**.

Soto, F. E. A., & Saldívar, S. O. S. (2020). Architecture, structure and chemistry of plant cell walls and their constituents. In *Science and Technology of Fibers in Food Systems*, Springer, Cham, 3-14.

Stein, S. E. (1999). An integrated method for spectrum extraction and compound identification from gas chromatography/mass spectrometry data. *Journal of the American Society for Mass Spectrometry*, **10(8)**, 770–781.

Steuer, C., Gege, C., Fischl, W., Heinonen, K. H., Bartenschlager, R., & Klein, C. D. (2011). Synthesis and biological evaluation of α-ketoamides as inhibitors of the Dengue virus protease with antiviral activity in cell-culture. *Bioorganic and Medicinal Chemistry*, **19(13)**, 4067–4074.

Sugimoto, H., Yamanishi, Y., Iimura, Y., & Kawakami, Y. (2000). Donepezil Hydrochloride (E2020) and Other Acetylcholinesterase Inhibitors. *Current Medicinal Chemistry*, **7**, 303–339.

Suppiah, J., Ching, S. M., Amin-Nordin, S., Mat-Nor, L. A., Ahmad-Najimudin, N. A., Low, G. K. K., Abdul-Wahid, M. Z., Thayan, R., & Chee, H. Y. (2018). Clinical manifestations of dengue in relation to dengue serotype and genotype in Malaysia: A retrospective observational study. *PLoS Neglected Tropical Diseases*, **12(9)**.

Tan, S. C. (2014). Alternative treatments for dengue fever. *The Star* [Online]. Accessed on 17 September 2019. Available from: https://www.thestar.com.my/lifestyle/health/2014/04/13/alternative-treatments-for-dengue-fever

The (2018). The dengue vaccine dilemma. *The Lancet Infectious diseases*, **18(2)**, 123.

Thorpe, M. F., Chubynsky, M., Hespenheide, B., Menor, S., Kuhn, L. A., & Zavodszky, M. I. (2005). Flexibility in Biomolecules. *Physical Biology*, **2**, 84–98.

Truong, D. H., Nguyen, D. H., Ta, N. T. A., Bui, A. V., Do, T. H., & Nguyen, H. C. (2019). Evaluation of the use of different solvents for phytochemical constituents, antioxidants, and in vitro anti-inflammatory activities of *severinia buxifolia*. *Journal of Food Quality*, **2019**, 1–9.

Uno, N., & Ross, T. M. (2018). Dengue virus and the host innate immune response. *Emerging Microbes and Infections*, **7(1).**

Verma, A. K., Singh, H., Satyanarayana, M., Srivastava, S. P., Tiwari, P., Singh, A. B., Dwivedi, A. K., Singh, S. K., Srivastava, M., Nath, C., Raghubir, R., Srivastava, A. K., & Pratap, R. (2012). Flavone-based novel antidiabetic and antidyslipidemic agents. *Journal of Medicinal Chemistry*, **55(10)**, 4551–4567.

Verma, J. P., & Aggarwal, J. S. (1956). The component fatty acids of the oil from the seed of *Momordica charantia*. *Journal of the Indian Chemical Society*, **33**, 357.

Verpoorte, R. (1998). Exploration of nature's chemodiversity: the role of secondary metabolites as leads in drug development. *Drug Discovery Today*, **3(5)**, 232–238.

Vial, J., Noçairi, H., Sassiat, P., Mallipatu, S., Cognon, G., Thiébaut, D., Teillet, B., & Rutledge, D. N. (2009). Combination of dynamic time warping and multivariate analysis for the comparison of comprehensive two-dimensional gas chromatograms: application to plant extracts. *Journal of Chromatography. A*, **1216(14)**, 2866–2872.

Vogel, P. (1985). Carbocation Chemistry. *Amsterdam: Elsevier Science Publishers B.V.*, 282.

Vollhardt, K., Peter, C., & Neil, E. S. (2007). Organic chemistry structure and function. 6th edition, *New York: W.H. Freeman*.

Vyas, V. K., Ukawala, R. D., Ghate, M., & Chintha, C. (2012). Homology modeling a fast tool for drug discovery: Current perspectives. *Indian Journal of Pharmaceutical Sciences*, **74(1)**, 1–17.

Waldron, K. W., Parker, M. L., & Smith, A. C. (2003). Plant cell walls and food quality. *Comprehensive Review on Food Sciences and Food Safety*, **2,** 101–119.

Wang, Q., & Pang, Y. P. (2007). Preference of small molecules for local minimum conformations when binding to proteins. *PLoS ONE*, **2(9)**, 1–10.

Wang, T. S., & Sanders, J. M. (1959). An infrared study of the out-of-plane C-H bending vibrations of monosubstituted naphthalenes. *Spectrochimica Acta*, ***15*(C)**, 1118–1124.

Welker, C. M., Balasubramanian, V. K., Petti, C., Rai, K. M., De Bolt, S., & Mendu, V. (2015). Engineering plant biomass lignin content and composition for biofuels and bioproducts. *Energies*, **8**, 7654–7676.

White, A. R. (2013). Chapter 23: Visualisation of Cellulase and Cellulose Dedegradation., Cellulose and Other Natural Polymer Systems: Biogenesis, Structure, and Degradation. *Plenum Press*, **Brown. R. M. edn**, 489–506.

White, A. R., & Brown, R. M. (1981). Enzymatic hydrolysis of cellulose: Visual characterization of the process. *Proceedings of the National Academy of Sciences of the United States of America*, **78(2)**, 1047–1051.

Wichapong, K., Pianwanit, S., Sippl, W., & Kokpol, S. (2010). Homology modeling and molecular dynamics simulations of Dengue virus NS2B/NS3 protease: Insight into molecular interaction. *Journal of Molecular Recognition*, **23(3)**, 283–300.

Wikimedia commons (2005). *Aedes aegypti* blood feeding CDC Gathany.jpg. Accessed on 2nd September 2020. Available from: https://commons.wikimedia.org/wiki/File:Aedes_aegypti_bloodfeeding_CDC_Gathany.jpg

Wikimedia commons (2010). CDC-Gathany *Aedes albopictus* picture. Accessed on 2nd September 2020. Available from: https://commons.wikimedia.org/wiki/File:CDC-Gathany-Aedes-albopictus-1.jpg

Wong, S. E., & Lightstone, F. C. (2011). Accounting for water molecules in drug design. *Expert Opinion on Drug Discovery*, **6(1)**, 65–74.

World Health Organization (WHO). (2009). Dengue: guidelines for diagnosis, treatment, prevention and control - New edition. *WHO Press*. Geneva.

World Health Organization (WHO). (2012). Global Strategy for Dengue Prevention and Control 2012–2020. *World Health Organiszation*. [online] Accessed on 16 September 2019. Available from: https://doi.org//entity/denguecontrol/9789241504034/ en/index.html

World Health Organization (WHO). (2017). Updated Questions and Answers related to information presented in the Sanofi Pasteur press release on 30 November 2017 with regards to the dengue vaccine Dengvaxia® Immunization, Vaccines and Biologicals. Accessed on 2nd September 2020. Available from: https://www.who.int/immunization/diseases/dengue/q_and_a_dengue_vaccine_dengvaxia/en/

World Health Organization (WHO). (2018). News: Dengue and severe dengue [online]. Accessed on 07 April 2019. Available from: https://www.who.int/en/news-room/fact-sheets/detail/dengue-and-severe-dengue.

World Health Organization (WHO). (2019). Dengue and severe dengue [online]. Accessed on 15 September 2019. Available from: https://www.who.int/news-room/fact-sheets/detail/dengue-and-severe-dengue.

Wu, C., Xiao, Y., Lin, W., Li, J., Zhang, S., Zhu, J., & Rong, J. (2017). Aqueous enzymatic process for cell wall degradation and lipid extraction from *Nannochloropsis sp*. *Bioresource Technology*, **223**, 312–316.

Wu, H., Bock, S., Snitko, M., Berger, T., Weidner, T., Holloway, S., Kanitz, M., Diederich, W. E., Steuber, H., Walter, C., Hofmann, D., Weißbrich, B., Spannaus, R., Acosta, E. G., Bartenschlager, R., Engels, B., Schirmeister, T., & Bodem, J. (2015). Novel dengue virus NS2B/NS3 protease inhibitors. *Antimicrobial Agents and Chemotherapy*, **59(2)**, 1100–1109.

WWF-Malaysia. (2019). Forests [online]. Accessed on 6 September 2019. Available from: http://www.wwf.org.my/about_wwf/what_we_do/forests_main/

Xiao, S., Zhang, W., Chen, H., Fang, B., Qiu, Y., Chen, X., Chen, L., Shu, S., Zhang, Y., Zhao, Y., Liu, Z., & Liang, G. (2018). Design, synthesis, and structure-activity relationships of 2-benzylidene-1-indanone derivatives as anti-inflammatory agents for treatment of acute lung injury. *Drug Design, Development and Therapy*, **12**, 887–899.

Yan, Q., Liang, H., Biao, H., Wang, B., & Ying, Y. (2007). A new cucurbitane triterpenoid from *Momordica charantia*. *Chinese Chemical Letters*, **18**, 843–845.

Yasui, Y., Hosokawa, M., Sahara, T., Suzuki, R., Ohgiya, S., Kohno, H., Tanaka, T., & Miyashita, K. (2005). Bitter gourd seed fatty acid rich in 9c,11t,13t-conjugated linolenic acid induces apoptosis and up-regulates the GADD45, p53 and PPARgamma in human colon cancer Caco-2 cells. *Prostaglandins, Leukotrienes, and Essential Fatty Acids*, **73(2)**, 113–119.

Yeo, Y. L., Chia, Y. Y., Lee, C. H., Sheng Sow, H., & Sum Yap, W. (2014). Effectiveness of maceration periods with different extraction solvents on *in vitro* antimicrobial activity from fruit of *Momordica charantia L*. *Journal of Applied Pharmaceutical Science*, **4(10)**, 16–23.

Yin, Z., Patel, S. J., Wang, W. L., Chan, W. L., Ranga Rao, K. R., Wang, G., Ngew, X., Patel, V., Beer, D., Knox, J. E., Ma, N. L., Ehrhardt, C., Lim, S. P., Vasudevan, S. G., & Keller, T. H. (2006). Peptide inhibitors of dengue virus NS3 protease. Part 2: SAR study of tetrapeptide aldehyde inhibitors. *Bioorganic and Medicinal Chemistry Letters*, **16(1)**, 40–43.

Yoshime, L. T., de Melo, I. L. P., Sattler, J. A. G., de Carvalho, E. B. T., & Mancini-Filho, J. (2016). Bitter gourd (*Momordica charantia L.*) seed oil as a naturally rich source of bioactive compounds for nutraceutical purposes. *Nutrire*, **41(1)**, 1–7.

Yotmanee, P., Rungrotmongkol, T., Wichapong, K., Choi, S. B., Wahab, H. A., Kungwan, N., & Hannongbua, S. (2015). Binding specificity of polypeptide substrates in NS2B/NS3pro serine protease of dengue virus type 2: A molecular dynamics Study. *Journal of Molecular Graphics and Modelling*, **60**, 24–33.

Yun, S., Fenghui, S., Jianlong, L., Wu, M., Fan, X., & Meng, Y. (2016). Mono-PEGylation of Alpha-MMC and MAP30 from *Momordica charantia L.*: Production, Identification and Anti-Tumor Activity. *Molecules*, ***21*(1457)**, 1–9.

Yusof, R., Clum, S., Wetzel, M., & Murthy, H. (2000). Purified NS2B/NS3 Serine Protease of Dengue Virus Type 2 Exhibits Cofactor NS2B Dependence for Cleavage of Substrates with Dibasic Amino Acids in Vitro. *Journal of Biological Chemistry*, **275(14)**, 9963–9969.

Yusoff, M. M., Gordon, M. H., Ezeh, O., & Niranjan, K. (2016). Aqueous enzymatic extraction of *Moringa oleifera* oil. *Food Chemistry*, **211**, 400–408.

Zaki, R., Roffeei, S. N., Hii, Y. L., Yahya, A., Appannan, M., Said, M. A., Wan, N. C., Aghamohammadi, N., Hairi, N. N., Bulgiba, A., Quam, M., & Rocklov, J. (2019). Public perception and attitude towards dengue prevention activity and response to dengue early warning in Malaysia. *PLoS ONE*, **14(2)**, 1–22.

Zhan, C., & Yao, J. (2016). More than conformational “twisting” or “coplanarity”: molecular strategies for designing high efficiency nonfullerene organic solar cells. *Chemistry of Materials*, **28(7)**, 1948–1964.

Zhang, Q. W., Lin, L. G., & Ye, W. C. (2018). Techniques for extraction and isolation of natural products: A comprehensive review. *Chinese Medicine (United Kingdom)*, **13(1)**, 1–26.

Zhao, J., Dong, Z., Li, J., Chen, L., Bai, Y., Jia, Y, & Shao, T. (2018). Ensiling as pretreatment of rice straw: The effect of hemicellulase and *Lactobacillus plantarum* on hemicellulose degradation and cellulose conversion. *Bioresource Tech*nology, **266**, 158–165.

Zhao, R., & Zhang, R. Q. (2016). A new insight into π-π Stacking involving remarkable orbital interactions. *Physical Chemistry Chemical Physics*, **18(36)**, 25452–25457.

Zhong, L., Matthews, J. F., Crowley, M. F., Rignall, T., Talón, C., Cleary, J. M., Walker, R. C., Chukkapalli, G., McCabe, C., Nimlos, M. R., Brooks, C. L., Himmel, M. E., & Brady, J. W. (2008). Interactions of the complete cellobiohydrolase I from *Trichodera reesei* with microcrystalline cellulose Iβ. *Cellulose*, **15(2)**, 261–273.

Zimmermann, H., & Rudolph, J. (1965). Protonic States and the Mechanism of Acid-Catalysed Esterification. *Angewandte Chemie International Edition in English*, **4(1)**, 40–49.

Zuorro, A., Malavasi, V., Cao, G., & Lavecchia, R. (2018). Use of cell wall degrading enzymes to improve the recovery of lipids from *Chlorella sorokiniana*. *Chemical Engineering Journal*, **377(November 2018)**, 1–7.

LIST OF CONFERENCE AND PUBLICATION

- Osman, H., **Nesfu, N.**, Mohamad, S., Muniglia, lionel, Brosse, N., Laurrain-mattar, D., Spina, R., & Kamarulzaman, E. E. (2020). The Effect of Aqueous Enzymatic Extraction Method towards Momordica charantia Seed Oil and its Lignocellulosic Biomass. *Walailak Journal of Science and Technology (WJST)*, *18*(1). Retrieved from http://wjst.wu.ac.th/index.php/wjst/article/view/9098
- **Mohd Nesfu, N.Z**., Laurain-Mattar, D., Kamarulzaman, E. E., A. Wahab, H., Zakaria, I. I., Hassan, M. Z., Brosse, N., & Osman, H. (2019). The In-silico Studies of Benzylidene Indanone Derivatives Towards Dengue Virus Type-2 NS2B/NS3 Protease. *Journal of Physical Science*, 30(Supp.2), 191–198. https://doi.org/10.21315/jps2019.30.s2.16
- **Nadirah Zawani Mohd Nesfu**, Lionel Muniglia, Ezatul E. Kamarulzaman, Rosella Spina, Dominique Laurain-Mattar, Hasnah Osman, Nicolas Brosse. Phytochemical Studies of *Momordica charantia* Fruit: Seed Extraction via Aqueous Enzymatic Extraction and Pulp Maceration. Poster Presentation in Journée PhytoDay, University of Lorraine. 21 June 2016.
- **Nadirah Zawani Mohd Nesfu**, Ezatul E. Kamarulzaman, Dominique Laurain-Mattar, Hasnah Osman, Nicolas Brosse. *Momordica charantia* Fruits and Seeds Oil: A Preliminary Study. Poster Presentation in International Conference of Young Chemist (ICYC2015). City Bayview Hotel, Georgetown, Penang, Malaysia. 5–7 August 2015.

1. Introduction

La dengue (DF), une infection virale transmise par les moustiques, est passée de 2.2 millions en 2010 à plus de 3.34 millions en 2016 dans le monde entier (WHO, 2019). Les moustiques femelles infectées d'Aedes aegypti et d'Aedes albopictus (Figure 1.1) ont transmis le virus de la dengue aux humains par leurs piqûres. Les virus de la dengue peuvent être classés en quatre sérotypes en fonction des antigènes présents à la surface du virus, qui sont les virus de la dengue de type 1, 2, 3 et 4 (Guzman & Kouri, 2003).

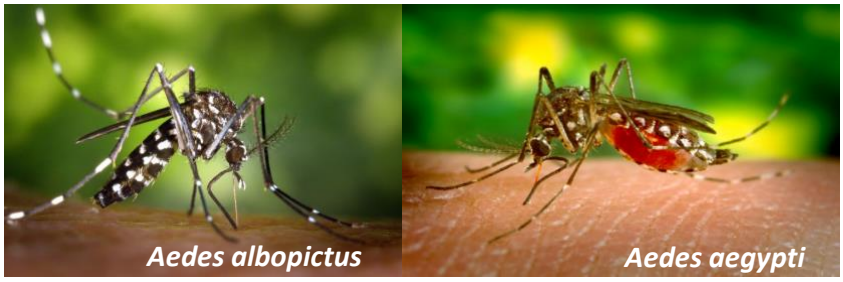

Figure 1.1: Images des deux principaux arthropodes vecteurs du virus de la dengue, *Aedes albopictus* et *Aedes aegypti* (Wikimedia commons, 2010 & 2005).

Aucun symptôme exact de FD n'a été identifié. Cependant, la forte fièvre allant de 39.5 à 41 ºC qui persiste habituellement pendant 2 à 7 jours accompagnée de douleurs musculaires et articulaires pourrait en être le signe. La FD peut survenir dans les 3 à 14 jours suivant une piqûre de moustique infecté. L'homme infecté a ressenti une perte d'appétit et des vomissements. Certains humains infectés ont eu des glandes enflées ou des éruptions cutanées (MoHM, 2015).

Environ 72,356 cas de dengue ont été signalés en Malaisie entre janvier et juillet 2019, soit une augmentation de 89.5 % par rapport à la même période en 2018, dont 138 cas mortels (Bernama, 2019). En Malaisie, les quatre sérotypes de dengue peuvent être isolés en même temps. Cependant, les principaux sérotypes de dengue trouvés en Malaisie étaient le virus de la dengue de type 1 (DENV-1) et le virus de la dengue de type 2 (DENV-2) (Suppiah *et al.*, 2018). Le traitement de la dengue disponible aujourd'hui se limite à des soins médicaux complémentaires et au remplacement des liquides, car il n'existe pas de traitement spécifique.

Comme il n'existe ni traitement curatif ni traitement préventif de la dengue et qu'il n'existe qu'un seul vaccin contre la dengue autorisé, le vaccin Dengvaxia de Sanofi Pasteur a été approuvé par les autorités réglementaires pour une utilisation à titre d'essai dans une zone de forte endémie (WHO, 2017). En dehors de cela, seules des mesures de soutien et une thérapie fluide judicieuse sont disponibles pour le DF (Rajapakse *et al.*, 2012).

Certains patients optent pour un remède traditionnel pour guérir la FD en améliorant leur numération plaquettaire. Au Pakistan, un patient atteint de dengue a été traité avec 25 ml d'extrait aqueux de feuilles de *Carica papaya* (*C. papaya*), deux fois par jour, et a constaté qu'en peu de temps, il avait augmenté le nombre de plaquettes (Ahmad *et al.*, 2011). Les études ont montré que les feuilles de *C. papaya* contenaient certains composés actifs qui peuvent augmenter l'hémopoïèse et la thrombopoïèse (Dharmarathna *et al.*, 2013).

Aux Philippines, les gens utilisaient l'*Euphorbia hirta* (*E. hirta*) pour traiter la dengue car on pense qu'il possède des propriétés antivirales qui accéléreront le processus de guérison et empêcheront le DF de passer en phase critique (Perera *et al.*, 2018). L'*E. hirta* contient des phénoliques et des flavonoïdes qui sont des composés bien connus capables d'augmenter la plaquette.

Le praticien traditionnel chinois, le Dr Yong Kian Fui, a déclaré qu'il n'existe pas de remède contre la dengue dans la médecine traditionnelle chinoise (MTC). Cependant, une concoction à base de plantes appelée *"qin wen bai tu san"*, une soupe faite par la cuisson lente

de *Momordica charantia L.* (*M. charantia*) et de viande de grenouille ou de tout autre type de viande pendant deux heures, peut être consommée en une seule dose par jour pendant trois jours consécutifs. Le *M. charantia* est utilisé pour désintoxiquer le corps en éliminant la chaleur, tandis que la viande neutralise le *M. charantia*, afin qu'il ne se refroidisse pas trop (Tan, 2014).

En l'absence de médicaments anti-dengue ou de vaccins prometteurs, il est nécessaire de rechercher d'autres mesures de prévention et de traitement. Comme de nombreux chercheurs se concentrent sur l'utilisation des feuilles de *C. papaya* et d'*E. hirta*, cette étude s'est intéressée à l'activité anti-dengue des fruits de *M. charantia* ou aussi connus sous le nom de melon amer, de poire baumier, de courge amère ou de gourde amère. Le nom malais local de cette plante est "peria katak" (Ong & Azliza, 2015). M. charantia, plante de la famille des *Cucurbitacées*, possède une vigne grimpante mince avec une feuille à long pétiole et un fruit oblong fusiforme-cylindrique, de forme irrégulière et verruqueuse (Figure 1.2).

Figure 1.2: (a) Plante et fruit de *M. charantia* (b) Coupe transversale du fruit de *M. charantia* (Komakech, 2018).

Le *M. charantia* est mondialement connu pour son efficacité dans le traitement du diabète. En effet, il contient un composé chimique très similaire à l'insuline (Omokhua-Uyi & Van Staden, 2020). Les chercheurs ont montré que lorsqu'il est pris de façon continue pendant une certaine période, il a la capacité de remplacer l'insuline dans l'organisme. Il contient également des saponines stéroïdiennes appelées charantines, des peptides similaires à ceux des peptides et certains alcaloïdes qui contrôlent efficacement le niveau de sucre dans le sang (Kumar & Bhowmik, 2010). Comme les plantes fournissent une multitude de petites molécules aux propriétés semblables à celles des médicaments, elles peuvent servir de modèle éprouvé pour le développement de nouveaux échafaudages de médicaments qui pourraient être utiles à l'optimisation du processus de découverte de médicaments (Atanasov, 2015).

2. Matériaux et méthode

2.1 Matériaux

Le solvant, le produit chimique et les matériaux utilisés étaient de qualité analytique et ont été utilisés sans subir de purification ou de distillation supplémentaire. Tous les appareils utilisés ont été lavés à l'eau distillée et rincés à l'acétone pour garantir la propreté de l'appareil et éviter toute impureté

2.2 Méthodes

Les études de la chair et de la graine des fruits de M. charantia sont divisées en deux parties. La première partie concerne l'extraction de l'huile de graines de M. charantia par hydrodistillation et par extraction enzymatique aqueuse (AEE) ainsi que l'étude de sa biomasse lignocellulosique. La seconde partie a consisté à préparer un extrait de pulpe de fruits de M. charantia pour le criblage anti-dengue. La Figure 2.1 résume le cadre de l'étude.

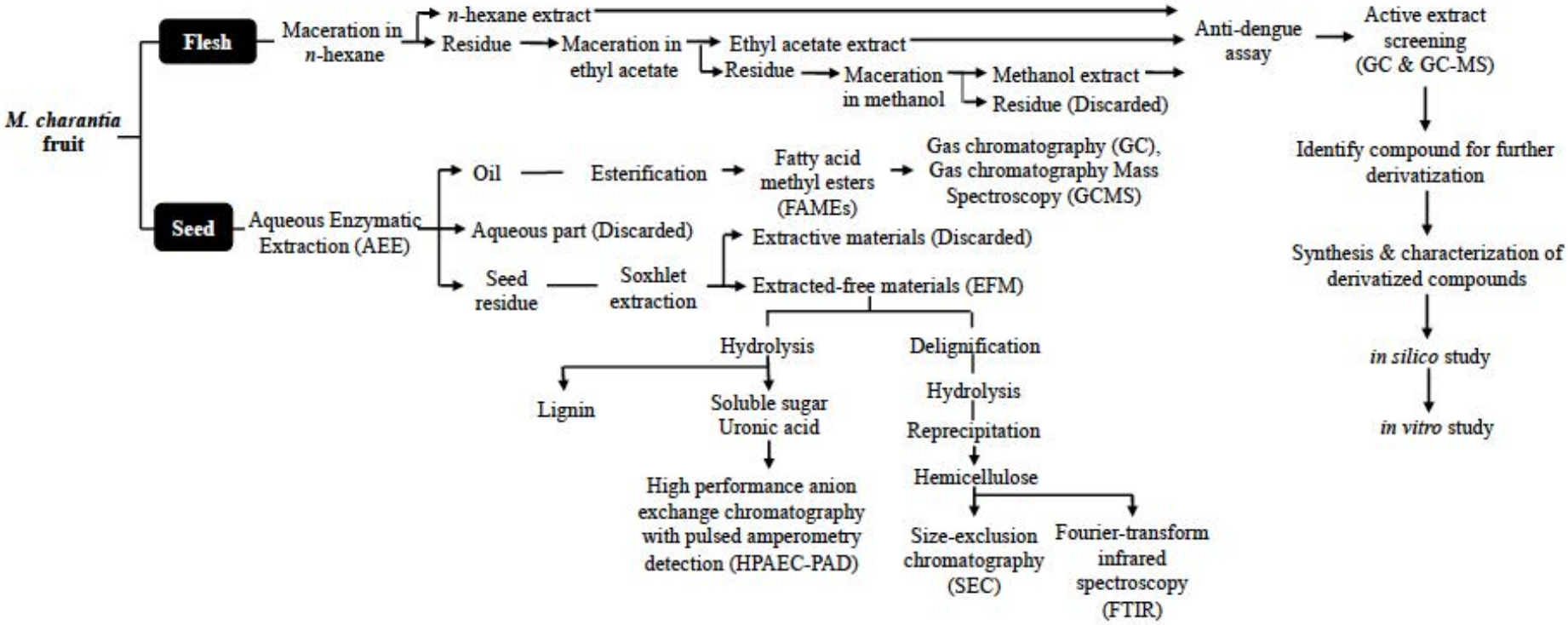

Figure 2.1: Le graphique de présentation des fruits et des graines de *M. charantia*

2.2.1 Préparation de l'échantillon

Les fruits non mûrs de M. charantia ont été achetés dans une ferme maraîchère située à Ara Kuda, Seberang Perai Utara, Penang, Malaisie, entre juin et août 2015. Les fruits ont été lavés à fond à l'eau du robinet pour éliminer toute contamination indésirable et coupés pour séparer la chair avec le pépin. Ensuite, les fruits (chair) et les pépins ont été séchés au soleil à température ambiante. Les fruits et les pépins ont été retournés toutes les 24 heures afin d'assurer un séchage complet. Les fruits et les graines séchés ont été broyés en petits morceaux avant d'être conservés dans des sacs en polyéthylène séchés jusqu'à leur utilisation ultérieure.

2.2.1(a) PARTIE 1: Extraction enzymatique aqueuse (AEE) de l'huile de graines de *M. charantia*

L'AEE a été réalisée pour extraire l'huile de la graine de M. charantia selon la méthode décrite par Muniglia *et al.* (2011). Les cocktails d'enzymes, HEL1 et X7, ont été mélangés au Laboratoire d'ingénierie des Biomolécules (Nancy, France), qui contenait de la cellulase, de la bétaglucosidase, de l'endocellulase, de l'exocellulase, de l'arabinase, de la xylanase, de la galactanase, de l'endopolygalacturonase, de l'hémicellulase, de la protéinase, de la pectinase et de la pectine méthylestérase à différentes concentrations.

Au départ, les graines séchées de M. charantia fraîchement moulues ont été mélangées à de l'eau distillée dans un rapport de 1:4 dans un bioréacteur préprogrammé (Celligen Plus, New Brunswick Scientific, États-Unis) avec agitation continue. Ensuite, les cocktails d'enzymes ont été ajoutés consécutivement dans le bioréacteur une fois que la température a atteint 50 °C selon différents rapports comme indiqué dans le tableau 2.1.

Table 2.1: Échantillons de semences et leurs rapports de cocktail d'enzymes.

Seed samples	Enzyme (%)/Seed weight (g)	
	HEL1	X7
M0	-	-
M1	5	-
M2	5	1.25
M3	5	2.5
M4	5	5

On a laissé la réaction se poursuivre pendant quatre heures dans le bioréacteur, puis on a procédé à une centrifugation (0.158 kilohertz, 20 minutes, 20 °C) pour séparer les produits. Les produits finaux de ce processus d'extraction ont été: 1) huile, 2) résidu de graines et 3) partie aqueuse. L'huile et les résidus de graines obtenus ont été soumis à une analyse par GC et à l'identification de la biomasse lignocellulosique des graines, respectivement. La partie aqueuse a été rejetée.

2.2.1(a)(i) L'analyse de l'huile de graines de *M. charantia*

Les échantillons d'huile de graines ont d'abord été dérivés en esters méthyliques d'acides gras (EMAG) par le procédé d'estérification décrit par Metcalfe et Schmitz (1961), avant de faire l'objet d'analyses complémentaires pour identifier leur composition biochimique par chromatographie en phase gazeuse (CG). Chaque huile dérivée (FAME) a été analysée pour identifier sa composition biochimique par chromatographie en phase gazeuse avec détecteur à ionisation de flamme.

2.2.1(a)(ii) L'analyse de la biomasse lignocellulosique des graines de *M. charantia*

Les résidus de graines séchées ont ensuite été extraits selon la méthode Soxhlet pour s'assurer que tous les composants extractifs ont été éliminés avant l'hydrolyse afin de

déterminer leur teneur en lignine, hémicellulose, acide uronique et sucre soluble dans l'acide. La présence de composants extractifs entravera le processus d'hydrolyse en réagissant avec l'acide et en se condensant en composants insolubles dans l'acide, ce qui entraînera une analyse inexacte.

2.2.1(b) PARTIE 2: Préparation de l'extrait de chair du fruit de *M. charantia*

La chair des fruits secs broyés (0.5 kg) a ensuite été extraite de manière exhaustive par macération séquentielle dans du n-hexane, de l'acétate d'éthyle et du méthanol deux fois en triple exemplaire pendant 7-14 jours à température ambiante (25-30 °C) sous hotte. Les mélanges ont été secoués et agités quotidiennement. Les extraits étaient ensuite filtrés et le solvant était éliminé par un évaporateur rotatif sous pression réduite. L'extrait a ensuite été conservé au réfrigérateur dans une bouteille d'échantillon scellée avant de procéder au criblage anti-dengue et l'extrait le plus actif sera soumis à une analyse par GC-MS.

2.2.2 Test anti-dengue de l'extrait de chair de fruits de *M. charantia*

Les essais in vitro pour les extraits de chair de fruits de M. charantia ont été réalisés selon la méthode de Yusof *et al.* (2000). Un mélange réactionnel enzymatique d'un volume total de 100 L à la concentration de 200 ppm a été préparé dans des plaques noires à 96 puits. Chaque puits des plaques noires à 96 puits est constitué de 94.9 L de solution tampon de Tris-HCl à pH 8.5, de 3.1 L de l'enzyme et de 1 L d'extrait (200 mg/L en DMSO). Les mélanges ont été incubés et agités à 37 C pendant 10 minutes. Ensuite, 1 L de substrat 10 mM dans du DMSO (Peptide Institute, Japon) a été ajouté dans le mélange pour amorcer la réaction. Le mélange a ensuite été incubé et secoué pendant 60 minutes supplémentaires à 37 C en utilisant l'incubateur à agitation SI-50 (Protech, Malaisie). L'essai a été triplé. L'extrait ayant la plus grande activité anti-dengue sera analysé plus avant en utilisant la GC-MS pour identifier ses compositions.

2.2.3 La synthèse de dérivés de benzylidène indanone pyrazolyl substitués

2.2.3(a) La synthèse du 3,4,5-triméthoxybenzoate d'éthyle, 85 et du 4,5-triméthoxybenzohydrazide, 86

L'acide 3,4,5-triméthoxybenzoïque disponible dans le commerce **[84]** est estérifié à l'aide d'acide sulfurique et d'éthanol pour produire du 3,4,5-triméthoxybenzoate d'éthyle **[85]** (Li *et al.*, 2017). Le schéma de réaction a été illustré dans le schéma 2.1 ci-dessous. De l'acide benzoïque (0.1 mmol) a été ajouté dans l'éthanol (1.0 mmol) en présence d'acide sulfurique (0.01 mmol). La solution a été chauffée au reflux. Après 3 h, la réaction a été contrôlée par CCM à l'aide d'un système d'acétate d'éthyle et d'hexane (3:7). L'agitation a été poursuivie pendant environ 12 heures ou jusqu'à ce que la CCM indique la fin de la réaction. L'excès d'éthanol a été éliminé à l'aide d'un évaporateur rotatif. La solution obtenue a ensuite été mélangée à 10 ml de solution d'acétate d'éthyle et de chlorure de sodium (10 % p/v.). Ensuite, la phase organique a été séparée à l'aide d'un entonnoir de séparation. L'excès de solvant a été éliminé de la phase organique à l'aide d'un évaporateur rotatif. Le précipité a été séché sous vide pour obtenir le composé **85**. Les structures chimiques du composé ont été confirmées par RMN ^{1}H, RMN ^{13}C et FTIR.

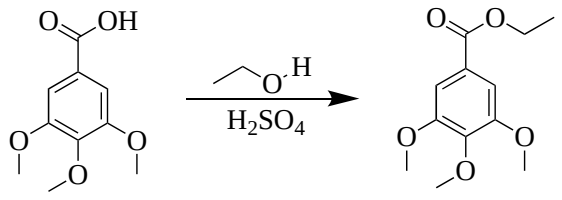

84 **85**

Scheme 2.1: La synthèse de l'intermédiaire 3,4,5-triméthoxybenzoate d'éthyle **[85]**.

Le compose **85** a ensuite réagi avec du monohydrate d'hydrazine pour obtenir du 3,4,5-triméthoxybenzohydrazide **[86]**. Le composé **85** (1.00 mmol) a été dissous dans 10 ml d'éthanol et agité pendant 30 minutes. Ensuite, du monohydrate d'hydrazine (5.00 mmol) a été ajouté à la solution et agité pendant la nuit jusqu'à la formation d'un précipité blanc (Schéma 2.2). Le précipité **[86]** a été filtré et lavé à l'éthanol froid (Kamal *et al.*, 2014). Les structures chimiques du composé ont été confirmées par RMN ^{1}H, et RMN ^{13}C.

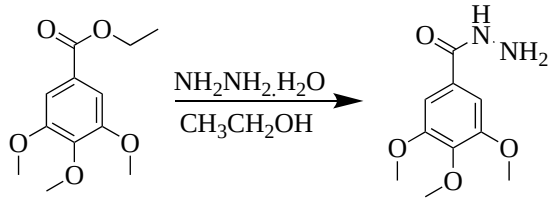

85 **86**

Scheme 2.2: La synthèse du 3,4,5-triméthoxybenzohydrazide **[86].**

2.2.3(b) La synthèse des dérivés de la benzylidène indanone, 89a-t

Une indanone (2.0 mmol) **[87a-b]** a été dissoute et agitée dans 10 % p/v d'hydroxyde de potassium (KOH) dans du méthanol pendant environ 15 minutes. Ensuite, un autre type d'aldéhyde aromatique (2.0 mmol) **[88a-b]** a été ajouté à la solution et le mélange réactionnel a été agité pendant une heure ou jusqu'à la fin de la réaction sous reflux (Korotchenko *et al.*, 2014). Le schéma 2.3 décrit le schéma de réaction pour la synthèse des dérivés de la benzylidène indanone **[89a-t]**. La réaction a été surveillée à l'aide de la CCM jusqu'à son achèvement. Le pH du mélange réactionnel a ensuite été ajusté à 5-6 en ajoutant une solution d'acide chlorhydrique à 10 % p/v. Le précipité a été filtré par filtration sous vide, lavé avec du méthanol froid et séché sous vide. Les composés synthétisés ont ensuite été soumis à une analyse de caractérisation afin de déterminer leurs propriétés physico-chimiques.

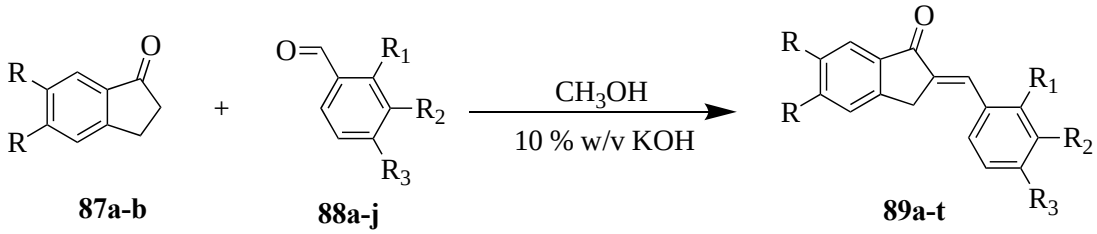

87a-b **88a-j** **89a-t**

Where **87a** = R = H
89a: R_1 = H; R_2 = H; R_3 = H
89b: R_1 = H; R_2 = H; R_3 = OCH_3
89c: R_1 = H; R_2 = H; R_3 = CH_3
89d: R_1 = H; R_2 = H; R_3 = Cl
89e: R_1 = H; R_2 = H; R_3 = $CH(CH_3)_2$
89f: R_1 = H; R_2= H; R_3 = $N(CH_3)_2$
89g: R_1 = H; R_2 = H; R_3 = NC_4H_8O
89h: R_1 = H; R_2 = H; R_3 = NC_4H_{10}
89i: R_1 = OCH_3; R_2 = H; R_3 = OCH_3
89j: R_1 = H; R_2 = NO_2; R_3 = OCH_3

Where **87b** = R = OCH_3
89k: R_1 = H; R_2 = H; R_3 = H
89l: R_1 = H; R_2 = H; R_3 = OCH_3
89m: R_1 = H; R_2 = H; R_3 = CH_3
89n: R_1 = H; R_2 = H; R_3 = Cl
89o: R_1 = H; R_2 = H; R_3 = $CH(CH_3)_2$
89p: R_1 = H; R_2= H; R_3 = $N(CH_3)_2$
89q: R_1 = H; R_2 = H; R_3 = NC_4H_8O
89r: R_1 = H; R_2 = H; R_3 = NC_4H_{10}
89s: R_1 = OCH_3; R_2 = H; R_3 = OCH_3
89t: R_1 = H; R_2 = NO_2; R_3 = OCH_3

Scheme 2.3: La synthèse des dérivés de la benzylidène indanone

2.2.3(c) La synthèse de dérivés de benzylidène indanone substitués par un groupe pyrazolyle

Les dérivés de benzylidène indanone précédemment synthétisés, **89a-t** (1.0 mmol) ont ensuite été mis à réagir avec le composé **86** (1.0 mmol) en présence de 10 ml d'acide acétique sous reflux pendant 12 h, comme indiqué dans le schéma 2.4. L'excès de solvant a été éliminé sous pression réduite. Le mélange réactionnel a ensuite été versé dans la glace concassée. Le précipité a été filtré par filtration gravitationnelle, lavé au méthanol froid et séché sous la hotte. Les composés synthétisés ont ensuite été recristallisés par une technique de recristallisation à solvant unique utilisant de l'éthanol. Les composés ont ensuite été soumis à une analyse de caractérisation afin de déterminer leurs propriétés physico-chimiques.

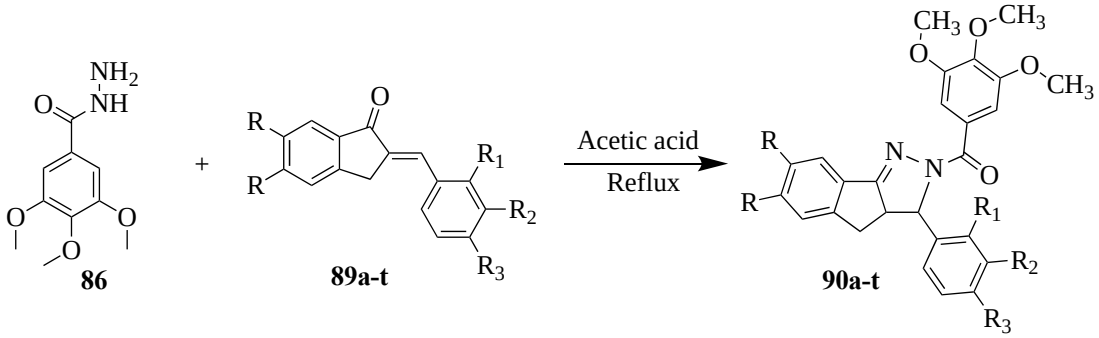

Scheme 2.4: La synthèse de dérivés de benzylidène indanone substitués par un groupe pyrazolyle.

2.2.3(d) Les études in silico vers la protéase DENV-2 NS2B/NS3

La structure composée a été esquissée à l'aide de Marvin Sketch 19.4.0 (ChemAxon, 2019) et convertie en une structure 3D à l'aide du logiciel HyperChem pro 8.0 (www.hyper.com). L'arrimage moléculaire a été réalisé à l'aide d'AutoDock4.2. La structure cristalline de la protéine d'homologie générée par Wichapong et son collègue a été utilisée (2010). La version 1.5.6 d'AutoDock Tools (ADT) a été utilisée pour la préparation de la stimulation de l'amarrage. La dimension de 74 x 43 x 64 en coordination x,y,z a été utilisée comme taille de la grille.

2.2.3(e) Les études d'essais in vitro sur la protéase DENV-2 NS2B/NS3

Un composé sélectionné a été choisi pour les études IC_{50}. Les séries de concentrations d'un composé de DMSO (6.25 ppm, 12.5 ppm, 25 ppm, 50 ppm, 100 ppm, 200 ppm) ont été préparées et le dosage a été effectué selon la procédure mentionnée à la section 2.2.2.

3. Résultats et discussion

3.1 Les études sur l'huile de graines de *M. charantia* et la biomasse lignocellulosique

L'huile de graines de M. charantia a été extraite par la méthode d'extraction enzymatique aqueuse (AEE). La composition de l'huile de graines a été déterminée à l'aide de la GC-MS. La composition de la biomasse lignocellulosique des graines a été identifiée en termes de lignine, de sucres solubles, d'acide uronique et de teneur en hémicélulose.

3.1.1 Extraction enzymatique aqueuse (AEE) de l'huile de graines de *M. charantia*

L'idée d'utiliser l'enzyme dans le processus d'extraction aqueuse était de faciliter la dégradation des structures cellulaires et sous-cellulaires de la graine et d'augmenter la dissolution du composé soluble présent dans la graine dans la matrice d'eau ainsi que de favoriser la libération de l'huile (Ricochon & Muniglia, 2010). Dans l'expérience témoin, sans ajout de cocktail d'enzymes (M0), seulement 3.32 ± 0.38 % de l'huile de graines a été extraite.

Le pourcentage le plus élevé d'huile de graines (6.26 ± 0.53 %) a été extrait de M2 en utilisant une combinaison de 5 % de HEL1 à 1.25 % de cocktails enzymatiques X7, suivi de M4 (5.03 ± 0.28) en utilisant une combinaison d'un rapport égal de HEL1 et de cocktails enzymatiques X7. Sur la base des résultats obtenus, la quantité d'huile extraite a montré que l'augmentation du rapport entre les cocktails d'enzymes X7 et HEL1 utilisés dans l'extraction n'était pas proportionnelle au pourcentage d'huile extraite. Cela peut être observé à partir du pourcentage d'huile extraite ne montrent pas d'augmentation significative par l'augmentation du rapport d'enzymes après M2. Le tableau 3.1 indique la quantité de cocktail d'enzymes introduite dans le processus de réaction et les pourcentages d'huile de graines récupérés par la méthode d'extraction enzymatique aqueuse utilisant la combinaison de différents rapports de cocktail d'enzymes.

Tableau 3.1: Pourcentages d'huile de graines récupérés par la méthode d'extraction enzymatique aqueuse utilisant la combinaison de différents rapports de cocktail d'enzymes

Seed samples	Enzyme (%)/Seed weight (g)		Oil extracted (%)
	HEL1	X7	
M0	-	-	3.32 ± 0.38
M1	5	-	4.67 ± 0.11
M2	5	1.25	6.26 ± 0.53
M3	5	2.5	4.10 ± 0.44
M4	5	5	5.03 ± 0.28

Note: The extraction process was triplicated.

$$\text{The percentage of seed oil extracted} = \frac{\text{Weight of oil obtained (mg)}}{\text{Weight of dry seed used (mg)}} \times 100\%$$

Les résultats ont indiqué que la cellulase, la protéinase et la pectinase présentes dans les cocktails enzymatiques HEL1 et X7 pourraient faciliter la dégradation des structures cellulaires et sous-cellulaires de la graine pour favoriser la libération d'huile. Les enzymes pourraient avoir affaibli les cellules végétales de la graine pour favoriser la libération de l'huile (Baby & Ranganathan, 2016). Dans une étude précédente, Latif et Anwar (2011) ont rapporté que le mécanisme actif d'un cocktail d'enzymes sélectionnées pendant l'extraction aqueuse enzymatique était la dégradation de la cellulose, de la pectine et des protéines, détruisant ainsi l'intégrité de la paroi cellulaire structurelle des cellules de la graine.

3.1.1 L'analyse de l'huile de graines de *M. charantia*

Les échantillons d'huile de graines extraits (M0, M1, M2, M3, et M4) ont été soumis à une dérivatisation en FAME avant l'identification de leurs compositions biochimiques par GC-FID car les FAME sont plus volatiles et plus faciles à analyser. Le GC-FID a été largement utilisé pour la séparation et la détection des FAME. Sept acides gras connus ont été identifiés. Trois acides gras inconnus ont également été détectés. Cependant, trois pics inconnus d'acide gras libre ont été observés sur le chromatogramme qui est en coélution presque en même temps. Il est suggéré que certains composés peuvent coélutions plus importantes en taille et éluer ensemble à la fin pendant la séparation (Kamatou & Viljeon, 2017).

D'après la composition de l'huile de graines de *M. charantia* (Tableau 3.2), le pourcentage d'acides élaïdique et palmitique a augmenté avec l'introduction des cocktails enzymatiques. Dans l'expérience témoin (M0), seulement 0,47 % d'acide élaïdique était présent dans l'huile extraite. Avec l'introduction des cocktails enzymatiques, le pourcentage d'acide élaïdique est passé à 8.06%, 20.42%, 28.06% et 29.63% pour M1, M2, M3 et M4, respectivement. La

présence des cocktails d'enzymes a montré une tendance similaire pour l'acide palmitique, bien que l'augmentation soit moindre.

Tableau 3.2: Les compositions des FAME (%) des huiles de graines de *M. charantia*

Fatty Acid	Compositions (%)				
	M0	M1	M2	M3	M4
Palmitic Acid (C16)	8.84 ± 0.12	7.21 ± 0.09	17.97 ± 0.11	17.26 ± 0.10	11.23 ± 0.09
Stearic Acid (C18)	-	-	3.28 ± 0.13	-	-
Elaidic acid(C18:1n9t)	0.47 ± 0.11	8.06 ± 0.08	20.42 ± 0.09	28.06 ± 0.11	29.63 ± 0.08
Oleic acid (C18:1n9c)	35.80 ± 0.08	17.31 ± 0.11	-	-	-
Vaccenic acid (C18:1n7)	2.84 ±0.10	5.02 ± 0.09	2.52 ± 0.09	5.02 ± 0.11	7.58 ± 0.10
Stearidonic acid (C18:4n3)	13.55 ± 0.11	13.42 ± 0.11	19.43 ± 0.08	16.42 ± 0.08	12.83 ± 0.09
Paullinic acid (C20.1)	6.50 ± 0.12	6.19 ± 0.12	13.51 ± 0.11	5.19 ± 0.09	2.41 ± 0.10
Unknown 1	10.66 ± 0.09	10.14 ± 0.09	7.81 ± 0.10	15.14 ± 0.09	15.31 ± 0.10
Unknown 2	9.55 ± 0.11	9.96 ± 0.10	6.00 ± 0.10	4.96 ± 0.10	8.69 ± 0.11
Unknown 3	11.79 ± 0.12	8.83 ± 0.11	9.07 ± 0.09	7.98 ± 0.11	12.32 ± 0.11

Note: Values are % of total fatty acid expressed as mean ± SD of three separate determinations

La libération d'huile pourrait être due à la présence de cellulase dans le cocktail enzymatique, qui a perturbé d'autres constituants polysaccharidiques dans la paroi cellulaire des graines. La présence de cellulase dans HEL1 et X7 a favorisé une dégradation efficace de la cellulose. Le mécanisme de la cellulase, décrit comme le clivage des liaisons glucosidiques internes au sein d'une chaîne de glucane ininterrompue par l'enzyme endoglucanase, pourrait entraîner la création d'une chaîne non réductrice de substrat de la cellobiohydrolase, clivant les dimères de cellobiose de la chaîne de glucane qui était libérée dans la solution. En outre, β-glucosidase a scindé le dimère de cellobiose en monomère de glucose, concluant ainsi le processus d'hydrolyse de la cellulose. La combinaison d'enzymes a joué un rôle dominant dans la perturbation des parois cellulaires des graines, ce qui a également été signalé dans d'autres conclusions (Wu *et al.*, 2017).

Ces résultats ont également montré que la composition de l'huile différait en fonction des différents rapports d'enzymes X7. Dans M4, la distribution en pourcentage de l'acide élaïdique, de l'acide vaccinique, de l'acide palmitique, de l'acide stéaridonique et de l'acide paullinique augmentait avec l'augmentation du rapport X7. Les résultats suggèrent que le cocktail d'enzymes X7 favorise la réaction du cocktail d'enzymes HEL1 pour hydrolyser les structures cellulaires des graines, car chaque cocktail d'enzymes est constitué de différents types de mélange d'enzymes.

En outre, la composition biochimique du pétrole extrait diffère également des études précédentes. Ali et son collègue ont extrait l'huile de graines avec les compositions suivantes : acide palmatique (4.84 ± 0.13 %), acide stéarique (20.21 ± 0.40 %), acide linoléique (6.37 ± 0.46 %) et acide éléostéarique (53.22 ± 0.36 %) (Ali *et al.*, 2008). Tandis que les huiles de graines extraites à l'aide de l'AEE contiennent une quantité plus importante d'acide palmitique. En outre, l'acide gras saturé, l'acide stéarique, n'a été détecté que dans le M2. En outre, l'acide gras oméga-3 détecté par Ali et son collègue était l'acide éléostéarique, tandis que l'huile extraite à l'aide de l'AEE était l'acide stéaridonique hautement insaturé.

Cette découverte était en accord avec les conclusions de chercheurs antérieurs qui avaient montré que l'extraction assistée par des enzymes peut entraîner une augmentation du rendement en huile ainsi qu'une légère modification des propriétés biochimiques de l'huile extraite (Zuorro

et al., 2018). On peut conclure que l'huile de graines de M. charantia obtenue à partir de l'AEE présentait de légères modifications de l'intégrité et de la répartition en pourcentage des composants actifs.

3.1.2 Détermination de la lignine, des sucres solubles et de l'acide uronique de l'EFM

La teneur en lignine de l'EFM; M0, M1 (15.91 %) > M2 (15.06 %) > M4 (14.71 %) > M3 (14.54 %) n'a pas montré de changements significatifs avec la présence d'enzymes dans l'AEE. Différents types de sucres solubles et d'acide uronique ont été libérés et ont fait l'objet d'une analyse plus poussée avec le HPAEC-PAD. La principale composition en sucres solubles de l'EFM était le glucose et le rhamnose, respectivement. Aucune tendance précise n'a été observée entre le pourcentage des ratios d'enzymes utilisés et le pourcentage de distribution des sucres solubles et de l'acide uronique obtenu. $M0_L$ a montré la plus faible quantité d'acide galacturonique (8.42 %). Le pourcentage de galacturonique acide augmentait avec la présence de cocktails enzymatiques dans $M3_L$ (16.12 %) < $M4_L$ (16.37 %) < $M1_L$ (22.00 %) < $M2_L$ (22.25 %). Ces résultats suggèrent que la présence de pectinase dans les cocktails enzymatiques a facilité la dégradation des polysaccharides pectiques de la paroi cellulaire en molécules plus simples comme l'acide galacturonique (Welker *et al.*, 2015). La concentration de glucose dans le M0 n'était que de 57 %. Le pourcentage de glucose a augmenté avec l'introduction des cocktails d'enzymes; M3 (65.42 %) < M4 (66.77 %) < M1 (71.34 %) < M2 (76.20 %). Ces résultats indiquent qu'une plus grande partie de la cellulose de la paroi cellulaire a été clivée en différents types de sucres (glucose, xylose, galactose, arabinose, rhamnose, mannose et fucose) à l'aide des cocktails enzymatiques (Segato *et al.*, 2014).

3.1.2 L'analyse FTIR de l'hémicellulose

La quantité d'hémicellulose extraite de la biomasse de lignocellulose des graines de M. charantia varie en fonction de la présence de l'enzyme pendant l'AEE; $M3_L$ (0.29 %) < $M4_L$ (0.38 %) < $M1_L$ (0.41 %) < $M2_L$ (0.58 %). Seulement 0.22 % de l'hémicelullose a été récupéré dans $M0_L$. Malgré des connaissances importantes sur la synergie entre les composants de la cellulase et du cocktail enzymatique, une compréhension mécanique complète de l'hydrolyse de la lignocellulose par les enzymes cellulolytiques est encore limitée et doit être affinée (Nill *et al.*, 2018). La variation de la composition de l'hémicellulose a montré qu'en tant que polysaccharides de structure plus simple que la cellulose, l'hémicellulose était également sujette à la dégradation en présence d'hémicellulase (Zhao *et al.*, 2018). L'hémicellulase obtenue a été analysée plus en détail par spectroscopie FTIR, comme le montre la figure 3.1. Le spectre FTIR a montré qu'il y avait des différences dans le pic d'intensité et entre les bandes d'absorption obtenues. L'absorption des pics de 3272, 2927, 1628, 1416, 1239 et 1038 cm^{-1} représentait l'absorption caractéristique de l'hémicellulose (Popescu *et al.*, 2010).

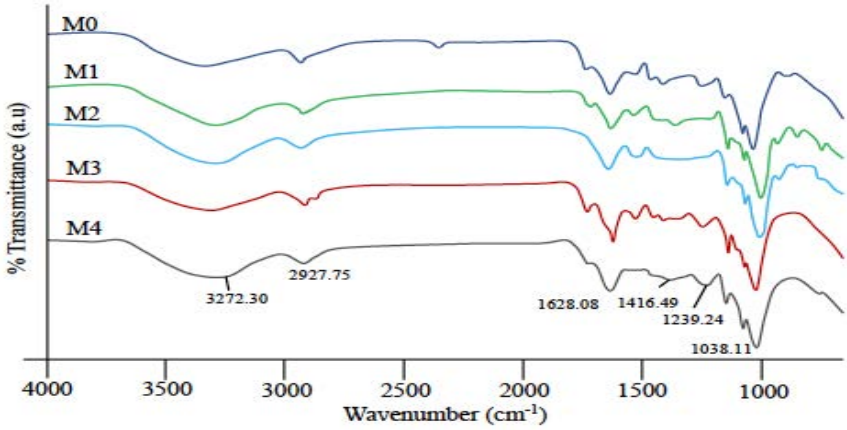

Figure 3.1: Le spectre FTIR de l'hémicellulose

La large bande d'absorption à ~3272 cm^{-1} représente généralement le O-H ou l'absorption d'un grand nombre de molécules individuelles, que l'hydrogène est lié à un composé légèrement différent. En revanche, la bande d'absorption ~2927 cm^{-1} indique la présence d'une vibration d'étirement de la liaison C_{sp3}-H. La bande ~1737 cm^{-1} se réfère à la bande d'étirement C=O conjuguée d'un groupe carbonyle, à attribuer à la présence de la partie acétyle dans l'hémicellulose. L'absorption qui est apparue à ~1628 cm^{-1} est généralement associée à l'eau absorbée. Une forte bande qui est apparue à ~1038 cm^{-1} a été attribuée à la flexion de C-O dans le sucre (Naidu *et al.*, 2018). D'après le spectre FTIR, l'introduction de l'enzyme n'affecte pas la structure du squelette de l'hémicellulose. En outre, on peut conclure que les échantillons de semences optimaux et leurs rapports de cocktail enzymatique pour le HEL1:X7 se sont avérés être de 5:1.25 comme dans M2.

3.2 Les études de la chair des fruits de *M. charantia*

Dans cette étude, l'extrait de n-hexane, d'acétate d'éthyle et de méthanol du fruit de *M. charantia* a fait l'objet d'un dépistage préliminaire in vitro de l'activité anti-dengue. La composition de l'extrait actif a été analysée par GC-MS.

3.2.1 Préparation de l'extrait de chair du fruit de *M. charantia*

La quantité de l'extrait correspond au type de solvants utilisés sur la base de la loi de similitude et d'intermissibilité. Les solvants dont la valeur de la polarité est proche de celle du soluté sont susceptibles d'être plus performants et vice versa. La quantité de matière extractive extraite des fruits de *M. charantia* avec l'utilisation d'un solvant non polaire à polaire implique la variation des composés phytochimiques. Comme les plantes contiennent une variété de composés bioactifs ayant des propriétés de solubilité différentes dans un solvant différent, le solvant optimal utilisé pour l'extraction dépend des matières végétales particulières, et des composés qui doivent être isolés (Truong *et al.*, 2019). L'utilisation d'un solvant non polaire a montré que la plus faible quantité de produit extractif était l'extrait avec un pourcentage de rendement de 0.49 ± 0.03 %, suivi de l'extrait extractif par l'acétate d'éthyle, 1.48 ± 0.11 %, et le méthanol, 3.47 ± 0.04 %, comme présenté dans le tableau 3.2.

Tableau 3.2: Le pourcentage de rendement pour l'extraction des fruits de *M. charantia*

Extract	Percentage of yield (%)
n-hexane	0.49 ± 0.03
Ethyl acetate	1.48 ± 0.11
Methanol	3.47 ± 0.04

Note: The extraction process was triplicated.

$$\text{The percentage of fruits flesh extracted} = \frac{\text{Weight of extract obtained (mg)}}{\text{Weight of dry fruits flesh used (mg)}} \times 100\%$$

3.2.1 a) Screening anti-dengue de l'extrait de chair du fruit de *M. charantia*

Dans l'étude de screening anti-dengue des extraits de chair du fruit de *M. charantia*, les extraits ont été incorporés dans la réaction de protéase à une concentration finale de 200 ppm. Dans cette étude, l'extrait d'acétate d'éthyle a montré une activité d'inhibition maximale. L'extrait de méthanol a montré la moindre activité inhibitrice envers la protéase DENV-2 NS2B/NS3 avec seulement 10.37 ± 1.13 %. L'extrait semi-polaire de *M. charantia* provenant de l'acétate d'éthyle a montré la plus forte activité inhibitrice de la protéase DENV-2 NS2B/NS3 avec 38.11 ± 1.06 %. La différence dans l'activité inhibitrice obtenue a été suggérée en raison du type de composés bioactifs extraits dans un autre type de solvant (Farahmandfar *et al.*, 2019). L'extrait d'acétate d'éthyle ayant la plus grande activité inhibitrice de la protéase

DENV-2 NS2B/NS3 a été soumis à un criblage par GC-MS afin d'identifier ses composants bioactifs.

3.2.1(b) Le screening par GC-MS de l'extrait de chair de fruit de M. charantia

La figure 3.2 montre divers pics indiquant la présence de différents composés dans l'extrait d'acétate d'éthyle du fruit de *M. charantia*. Le profil du chromatogramme GC-MS a révélé la présence de 32 pics différents et a été caractérisé et identifié par comparaison de leurs modèles de fraction de masse avec des données similaires de la bibliothèque du National Institute of Standards and Technology (NIST) ou des données publiées.

Les principaux composés ont été présentés sous forme de tableau dans le tableau 3.3. Les composés ayant une surface de pic de 1 à 2 % étaient le 1,4-bis(triméthylsilyl)benzène (rt. 44.395 min, 1.953 %), l'hexaméthyl-cyclotrisiloxane (rt. 44.288 min, 1. 9 %), 25-désacétoxy cucurbitacine b (rt. 44.670 min, 1.574 %), acide butyl-ester acétique (rt. 2.485 min, 1.539 %), 3,5-bis-triméthylsilyl-2,4,6-cycloheptatriène-1-one (rt. 33.29, 1.434 %), 1,2-bis(triméthylsily)benzène (rt. 44.923 min, 1.433 %), ester bis(2-éthylhexyle) de l'acide décanedioïque (rt. 40.552 min, 1.346 %), phtalate de diisooctyle (rt. 36. 806 min, 1,297 %), N-trifluoroacétyl-1-aminononadécane (rt. 47.265 min, 1.297 %), rétine (rt. 33.660 min, 1.23 %), et 2,6-dihydroxyacétophénone (rt. 47.825, 1.035 %). Les autres composés étaient présents à l'état de traces avec une surface de pic inférieure à 1 %, y compris l'acide gallique (rt. 5.017 min, 0.54 %). Bien que le pic de l'acide gallique ait été observé en moins de 1 %. Jia et son collaborateur (2017), ont indiqué que l'acide gallique était le principal acide phénolique de la chair du fruit de *M. charantia*.

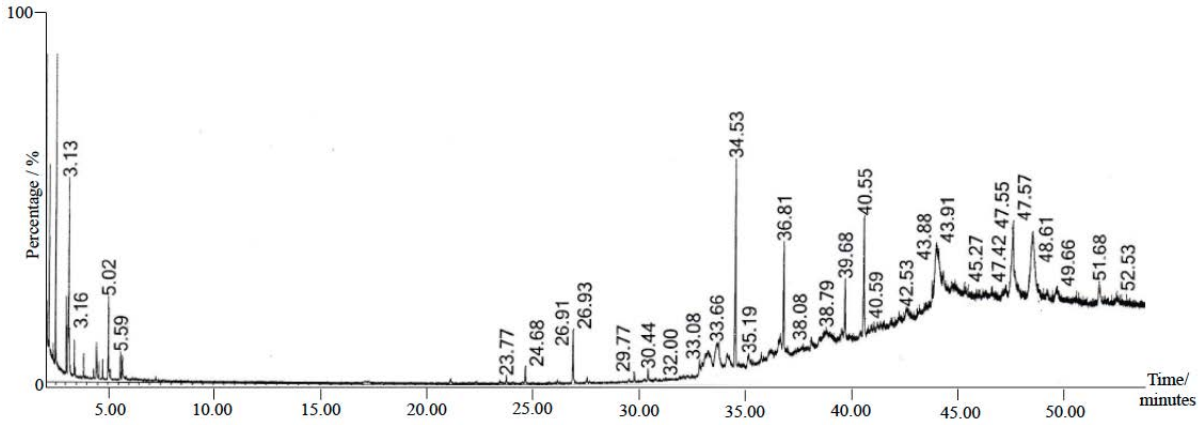

Figure 3.2: Le chromatogramme GC-MS de l'extrait d'acétate d'éthyle du fruit de *M. charantia*.

Tableau 3.3: Les principaux phytochimiques identifiés dans l'extrait d'acétate d'éthyle du fruitde *M. charantia* par GC-MS.

No.	Retention time (min)	Peak total area (%)	Compound name	CAS No.	Library match (%)
1	48.521	5.707	10,12,14-nonacosatriynoic acid	126115-85-3	53.0
2	43.915	5.439	(5α)-3-Ethyl-3-hydroxyandrostan-17-one	57344-99-7	49.1
3	47.573	4.891	(3β,5*S*,22*E*)-3,5-cyclostigmasta-6,22-diene	107304-12-1	56.1
4	34.533	2.111	bis(2-ethylhexyl) ester hexanedioic acid	103-23-1	63.7

3.3 La synthèse de dérivés de benzylidène indanone substitués par un groupe pyrazolyle

Les composés **90a-t** ont permis de synthétiser une quantité appropriée de produit avec un pourcentage de rendement compris entre 40 et 85 % et un point de fusion compris entre 175 et 215 ºC. Les pourcentages de rendement des produits obtenus étaient compris entre 40 et 85 %. Il est possible qu'une partie du produit ait été perdue lors de la récupération de l'échantillon, par exemple lors de la coulée, de la filtration ou de la chromatographie sur colonne, ce qui a entraîné un faible rendement. En outre, le faible pourcentage de rendement des produits pourrait être dû à des réactions incomplètes, dans lesquelles certains réactifs ne réagissent pas pour former le produit.

Il a été observé que le pourcentage de rendement des composés **90h**, **90j**, **90n**, **90s** et **90t** était inférieur à 50 %. D'après les observations, les composés ayant un rendement plus faible ont tendance à avoir un substituant autre que l'hydrogène au niveau de R1, R2 et R3 dans la fraction benzylidène, ce qui en fait des composés en vrac. Les substituants plus volumineux ralentissent considérablement la réaction parce que les groupes plus grands ont effectivement augmenté la répulsion stérique avec le nucléophile entrant. Ainsi, la réaction a pris plus de temps (Liu *et al*., 2010a).

Une des méthodes de surveillance de la formation des dérivés d'indanone pyrazolyle substituée **[90a-t]** consiste à comparer les spectres FTIR des composés **86** et **89a-t**. Cette réaction implique une étape de formation de cycle qui transforme l'amine primaire et secondaire du composé 86 en amine tertiaire du composé 90a-t. Par conséquent, deux bandes d'absorption moyennes -NH et -NH_2 à 3364 cm^{-1} et 3319 cm^{-1} seront absentes du spectre FTIR du composé **90a-t.**

Le spectre FTIR du composé **90b** manifeste une bande d'absorption à 2938 cm^{-1} attribuée à la vibration des liaisons C_{sp2}-H. Dans le composé **90b**, la force d'absorption de C=O à 1697 cm^{-1} a diminué par rapport à la force d'absorption de C=O du composé **89b**. Il est suggéré qu'en raison de la perte de conjugaison d'un côté, la fraction C=O du composé **90b** est située à côté de la fraction amine (Sheat *et al.*, 2018). Alors que la forte flexion hors du plan C-H est apparue à 820 cm^{-1}, elle indique la présence d'un cycle para disubstitué dans le composé **90b** (Lampman *et al.*, 2010). L'analyse LC-MS a indiqué le pic d'ion moléculaire $[MH]^+$, ($^+$ESI) à m/z 459.4460 qui a confirmé la masse moléculaire de la structure.

L'élucidation de la structure des composés 90a-t a été réalisée en utilisant une étude spectroscopique RMN unidimensionnelle et bidimensionnelle. La principale différence entre le spectre RMN ^{1}H des composés 90a-t et le composé réactif **86** était la disparition du décalage N-H et N-H_2. Aucun décalage chimique n'a été observé sur δ_H = 9.744 ppm et δ_H = 4.470, ce qui indique que le succès de la cyclisation des amines de l'amine primaire et secondaire en amine tertiaire.

3.4 Les études in silico vers la DENV-2 protéase NS2B/NS3

Les études in silico ont été menées pour tous les composés synthétisés avec la DENV-2 protéase NS2B/NS3, et son mode de liaison et sa conformation ont été déterminés. Le redécoupage a été effectué avec succès avec une valeur de déviation quadratique moyenne (RMSD) de 1.23 Å. Hevener et son collègue (2009) ont déclaré que les programmes capables de poser la valeur RMSD dans la gamme de 1.5-2 Å, selon la taille du ligand, sont considérés comme ayant réussi. Les paramètres d'amarrage obtenus ont été utilisés dans les études d'amarrage de la DENV-2 protéase NS2B/NS3 du ligand à l'aide des composés synthétisés. La figure 3.3 montre la conformation amarrée par superposition entre le modèle d'homologie de Wichapong et le ligand référencé Bz-Nle-Lys-Arg-Arg-H.

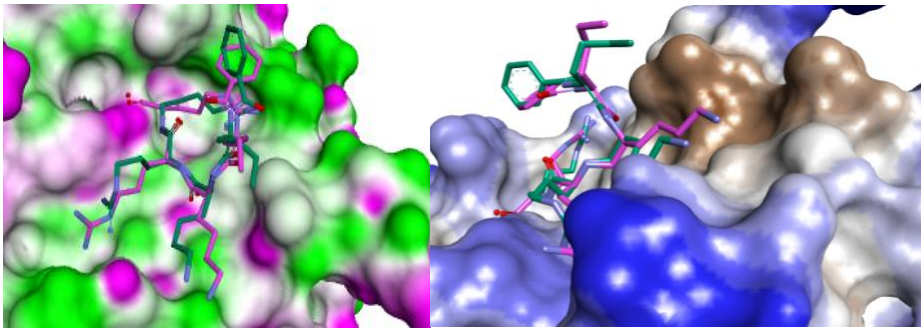

Figure 3.3: La superposition de la conformation ancrée entre le modèle d'homologie de Wichapong et le ligand référencé Bz-Nle-Lys-Arg-Arg-H (- conformation du ligand original; - conformation du ligand ancré)

Au total, 20 composés synthétisés **[90a-t]** et de l'acide gallique ont été retenus, à l'exception de l'inhibiteur peptidique témoin positif. Les résultats de l'amarrage ligand-protéine basés sur les scores d'énergie libre de liaison (FEB) sont présentés dans le tableau 3.4. Les scores ont été classés du plus actif au moins actif. L'activité était basée sur l'interaction de liaison, dans laquelle, plus le score est négatif, plus la liaison est forte. Tous les ligands ancrés ont montré une interaction positive avec la protéase DENV-2 NS2B/NS3 avec une énergie de liaison inférieure à -5.0 kcal/mol. Les composés synthétisés ont montré une bonne interaction de liaison avec la FEB, moins que l'acide gallique et l'inhibiteur peptidique. Cinq composés synthétisés présentaient une FEB inférieure à -7.55 kcal/mol, le composé **90p** présentant la FEB la plus faible, soit -8.12 kcal/mol, et l'interaction de liaison du composé 90p a été sélectionnée pour être examinée plus en détail. La figure 3.4 représente l'illustration de l'interaction de liaison du composé **90p** avec la DENV-2 protéase NS2B/NS3.

Tableau 3.4: Le FEB de l'amarrage ligand-protéine.

Ligand	FEB (kcal/mol)
Positive Control (Peptide Inhibitor)	-6.58
Gallic Acid	-5.73
90p	-8.12
90c	-7.75
90e	-7.71
90g	-7.63
90r	-7.61
90h	-7.53
90o	-7.51
90q	-7.54
90d	-7.36
90j	-7.21
90a	-7.14
90i	-7.13
90t	-7.09
90s	-7.01
90b	-6.99
90k	-6.95
90n	-6.90
90l	-6.87
90m	-6.82
90f	-6.71

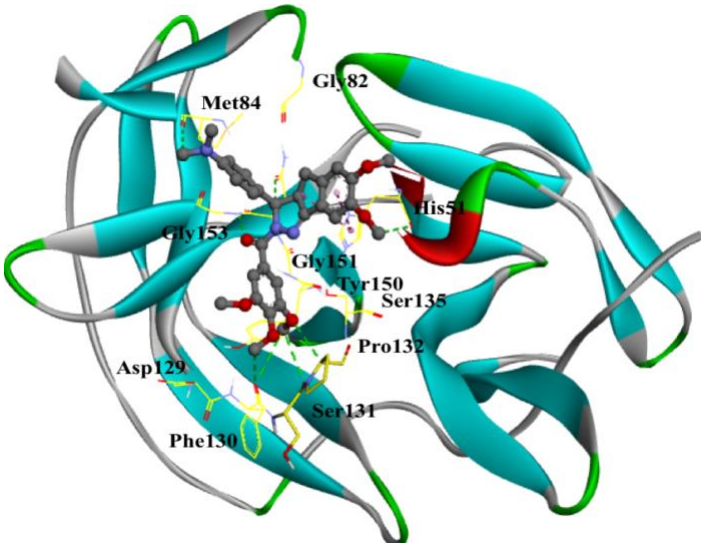

Figure 3.4: L'interaction de liaison de **90p** avec la DENV-2 protéase NS2B/NS3.
(-- hydrogen bond; -- π- π stacking; -- π-alkyl)

Le composé **90p** a montré huit interactions de liaison hydrogène, une interaction d'empilement π-π, et une interaction π-alkyle avec le résidu d'acide aminé dans la protéase DENV-2 NS2B/NS3. Il a été noté que les interactions formées sur ce site provenaient principalement des résidus NS3 avec différents types et forces d'interaction. Le résidu de la protéine NS3 est essentiel pour la réplication virale et la maturation des virions. Par conséquent, une plus grande interaction avec le résidu suggère de donner des résultats plus prometteurs en matière d'activité inhibitrice (Yin *et al.*, 2006).

La présence du groupe aromatique situé au niveau de la fraction benzylidène dans le composé **90p** augmente les possibilités d'interaction de van der Waals. L'interaction par empilement π-π et l'interaction par alkyle π entre le His51 et la fraction benzylidène dans le composé **90p** suggèrent d'affecter la réplication du DENV-2 NS2B/NS3, car le His51 est l'une des triades catalytiques du résidu NS3, qui a nécessité le clivage du résidu NS2B pour les activités de réplication du virus (Noble *et al.*, 2012). La géométrie de cette interaction d'empilement suggère que la localisation du nuage électrostatique joue un rôle dans l'attraction entre les deux systèmes aromatiques (Zhao & Zhang, 2016).

Le composé 90p a formé des liaisons hydrogène avec l'un des résidus d'acides aminés de la triade catalytique qui étaient situés dans la sérine-protéase NS3, His51, ainsi que d'autres résidus d'acides aminés, à savoir Gly153, Asn152, Phe130, Pro132, Ser131 et Phe130. Une seule interaction de liaison hydrogène s'est produite entre le composé **90p** et l'acide aminé du résidu NS2B, qui est Met84. L'atome d'oxygène dans le groupe carbonyle du composé **90p** a suggéré d'agir comme accepteur H, tandis que l'hydrogène attaché à l'atome d'azote présent dans l'acide aminé simple de la glycine a suggéré d'agir comme donneur H (Itoh *et al.*, 2019).

Les cinq composés ayant le plus faible taux de FEB, à savoir **90c**, **90e**, **90g**, **90p** et **90r**, ont été choisis dans les études in silico pour examiner leur activité *in vitro* vis-à-vis de la protéase DENV-2 NS2B/NS3. En général, la différence entre les composés **90c**, **90e**, **90g**, **90p**, et **90r** est le substitut en position para dans le cycle benzénique. La capacité du substituant à former la liaison intermoléculaire avec l'acide aminé dans la protéase NS2B/NS3 détermine l'énergie de liaison. Le composé **90p** a un groupe diméthyl-amino, l'azote pourrait agir comme donneur de liaison hydrogène pour améliorer la liaison intermoléculaire avec l'acide aminé dans la protéase NS2B/NS3.

3.5 Les études in vitro sur la protéase NS2B/NS3 du DENV-2

Le criblage de l'activité des cinq composés les plus actifs vis-à-vis de la protéase DENV-2 NS2B/NS3 en utilisant le substrat peptidique fluorogène Boc-Gly-Arg-7-amino-4-méthylcoumarine a été effectué, et le composé le plus actif a procédé à une analyse des valeurs de la concentration inhibitrice à cinquante pour cent (IC_{50}). La panduratine A a été utilisée comme témoin positif dans cette étude.

Le composé **90p** a montré une activité inhibitrice de la protéase DENV-2 NS2B/NS3 assez élevée (65.61 ± 0.98 %), suivi du composé **90r** avec 53.62 ± 1.05 %, du composé **90g** avec 48.03 ± 1.01 %, de la panduratine A avec 47.59 ± 1.03 %, de l'acide gallique avec 25.11 ± 1.11 %, du composé **90e** avec 20.06 ± 0.99 % et enfin du composé **90c** avec seulement 16.11 ± 0.95 %.

Les composés sélectionnés ont montré une activité prometteuse d'inhibiteur de DENV-2 protéase NS2B/NS3 avec trois composés synthétisés, à savoir le composé **90p**, **90r**, et **90g** ont obtenu un pourcentage d'inhibition supérieur à celui de la panduratine A et de l'acide gallique. Le composé le plus puissant, **90p**, a fait l'objet d'une analyse plus poussée pour déterminer sa valeur IC_{50} et les courbes dose-réponse ont été résumées dans la figure 3.5.
Sur la courbe, la valeur de la IC_{50} pour le composé **90p** a été observée à 42 ppm, ce qui est inférieur à la valeur de 118 ppm pour la panduratine A. Les concentrations obtenues ont été converties en µM à l'aide de l'équation suivante

$$\mu M = \frac{ppm \times 1000}{Molecular\ weight}$$

$$\text{Compound } \mathbf{90p} = \frac{42 \times 1000}{532.48} = 78.87\ \mu M$$

$$\text{panduratin A} = \frac{118 \times 1000}{406.52} = 290.27\ \mu M$$

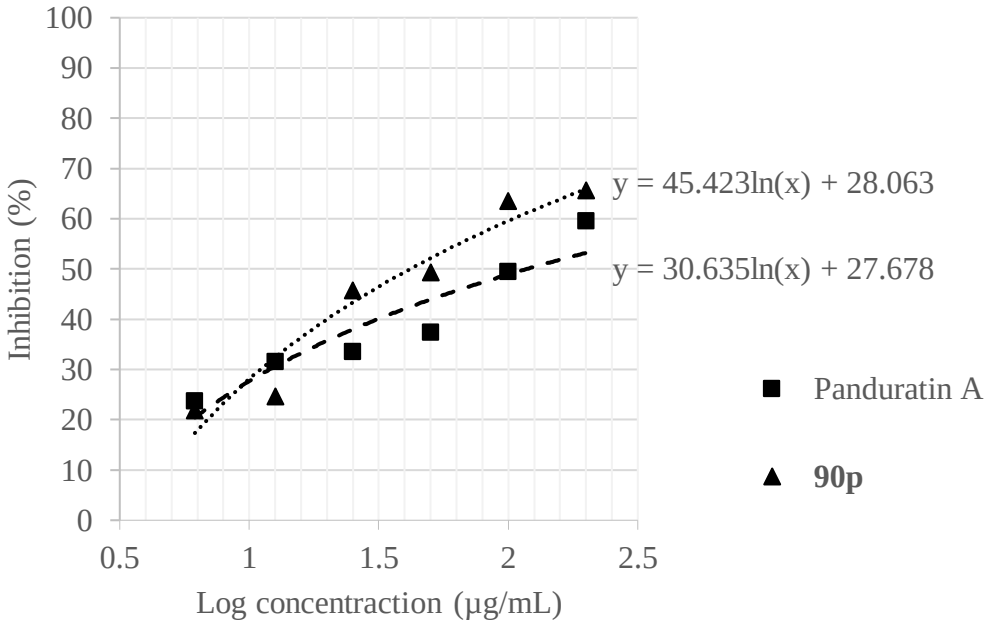

Figure 3.5: Courbes dose-réponse du composé **90p** et de la panduratine A sur les DENV-2 protéases NS2B/NS3.

En résumé, les résultats de cette étude montrent que les résultats sont en accord avec les travaux précédents. Le composé **90p** a montré une bonne activité inhibitrice de la DENV-

2 protéase NS2B/NS3, réalisée selon la méthode de Yusof *et al.* (2000) en utilisant le peptide fluorogène synthétique Boc-Gly-Arg-Arg-AMC. On peut conclure que le composé **90p** pourrait être un puissant inhibiteur de la DENV-2 protéase NS2B/NS3.

4. Conclusion et recommandation

4.1 Conclusion

Cette étude a mis en évidence le potentiel des fruits de *M. charantia*. La partie chair et la partie pépins du fruit ont été utilisées. L'huile des graines de *M. charantia* peut être extraite. On peut conclure que l'extraction assistée par des enzymes peut conduire à une augmentation du rendement en huile et de l'hémicellulose. En outre, de légères modifications des propriétés biochimiques de l'huile extraite ont été détectées. En dehors de cela, la composition de la biomasse lignocellulosique des graines ayant subi une extraction enzymatique aqueuse semble avoir une quantité différente de sucres solubles et d'acides uroniques. L'extrait d'acétate d'éthyle de la chair du fruit de *M. charantia* a montré une activité anti-dengue prometteuse envers la DENV-2 protéase NS2B/NS3. Le profil du chromatogramme GC-MS de l'extrait d'acétate d'éthyle a révélé la présence d'acide gallique, un composé hautement antiviral. L'acide gallique a été choisi pour l'hémisynthèse de l'inhibiteur de la DENV-2 protéase NS2B/NS3. Les dérivés de benzylidène indanone pyrazolyl substitués**, 90a-t**, ont été synthétisés avec succès par la formation d'hétérocycles N à l'aide d'acide acétique. Les composés synthétisés ont montré un inhibiteur de la protéase DENV-2 NS2B/NS3 prometteur, tant en analyse *in silico* qu'*in vitro*. Le composé **90p** a montré une valeur IC_{50} plus faible de 78.87 µM par rapport à la panduratine A, 290.27 µM. On peut conclure que le composé **90p** pourrait être un puissant composé *"hit-to-led"* dans la recherche de l'inhibiteur de protéase NS2B/NS3 du DENV-2.

4.2 Recommandations pour les études futures

L'élargissement de la portée de cette étude produira des contributions de connaissances multidisciplinaires. Les fruits de *M. charantia* pourraient être isolés afin d'identifier le composé qui agit comme inhibiteur de la DENV-2 protéase NS2B/NS3. L'extraction enzymatique aqueuse dans cette étude a utilisé le cocktail d'enzymes HEL1 et X7. Dans les études futures, une seule enzyme telle que la cellulase, l'endocellulase, l'arabinase, la xylanase, la galactanase, l'hémicellulase, la protéinase ou la pectinase pourra être utilisée dans l'extraction enzymatique aqueuse pour obtenir une quantité appropriée d'hémicellulose. En outre, l'utilisation de l'hémicellulose dans la fabrication d'un produit durable tel qu'un plastique biodégradable ou un film mince. Alors que le composé **90p** ayant l'activité inhibitrice de la DENV-2 protéase NS2B/NS3 la plus élevée n'a obtenu qu'un rendement de 63.17 %. Il est possible de lancer une nouvelle optimisation de la méthode pour augmenter le rendement du **90p**. En outre, le composé synthétisé pourrait être soumis à une étude qualitative de la relation structure-activité afin d'obtenir des informations détaillées sur chaque groupe fonctionnel en fonction de sa fonction. D'autres analyses telles que l'étude de toxicité, la CMI et l'analyse *in vivo* peuvent être effectuées pour étudier le potentiel du composé **90p** en tant qu'inhibiteur de DENV-2 protéase NS2B/NS3.

5. Références

Ahmad, N., Fazal, H., Ayaz, M., Abbasi, B. H., Mohammad, I., & Fazal, L. (2011). Dengue fever treatment with *Carica papaya* leaves extracts. *Asian Pacific Journal of Tropical Disease*, **1**, 330–333.

Ali, M. A., Sayeed, M. A., Reza, M. S., Yeasmin, M. S., & Khan, A. M. (2008). Characteristics of seed oils and nutritional compositions of seeds from different varieties of *Momordica charantia Linn*. cultivated in Bangladesh. *Czech Journal of Food Science*, **26(4)**, 275–283.

Atanasov, A. G., Waltenberger, B., Pferschy-Wenzig, E. M., Linder, T., Wawrosch, C., Uhrin, P., Temml, V., Wang, L., Schwaiger, S., Heiss, E. H., Rollinger, J. M., Schuster, D., Breuss, J. M., Bochkov, V., Mihovilovic, M. D., Kopp, B., Bauer, R., Dirsch, V. M., & Stuppner, H. (2015). Discovery and resupply of pharmacologically active plant-derived natural products: A review. *Biotechnology advances*, **33(8)**, 1582–1614.

Baby, K. C., & Ranganathan, T. V. (2016). Effect of enzyme pre-treatment on extraction yield and quality of fennel (*Foeniculum vulgare*) volatile oil. *Biocatalysis and Agricultural Biotechnology*, **8**, 248–256.

Bernama. (2019). Dengue cases up by 89.5% from January to July 2019, says Health Minister. *The Star*. [online] Accessed on 16 September 2019. Available from: https://www.thestar.com.my/news/nation/2019/07/28/dengue-cases-up-by-89pt5pc-from-january-to-july-2019-says-health-minister

Dharmarathna, S. L. C. A., Wickramasinghe, S., Waduge, R. N., Rajapakse, R. P. V. J., & Kularatne, S. A. M. (2013). Does *Carica papaya* leaf-extract increase the platelet count? An experimental study in a murine model. *Asian Pacific Journal of Tropical Biomedicine*, **3(9)**, 720–724.

Farahmandfar, R., Esmaeilzadeh Kenari, R., Asnaashari, M., Shahrampour, D., & Bakhshandeh, T. (2019). Bioactive compounds, antioxidant and antimicrobial activities of Arum maculatum leaves extracts as affected by various solvents and extraction methods. *Food Science and Nutrition*, **7(2)**, 465–475.

Guzman, M. G., & Kouri, G. (2003). Dengue and dengue hemorrhagic fever in the Americas: Lessons and challenges. *Journal of Clinical Virology*, **27(1)**, 1–13.

Hevener, K. E., Zhao, W., Ball, D. M., Babaoglu, K., Qi, J., White, S. W., & Lee, R. E. (2009). Validation of Molecular Docking Programs for Virtual Screening against Dihydropteroate Synthase. *Journal of Chemical Information and Modeling*, **49(2)**, 44–460.

Itoh, Y., Nakashima, Y., Tsukamoto, S., Kurohara, T., Suzuki, M., Sakae, Y., Oda, M., Okamoto, Y., & Suzuki, T. (2019). N+-C-H···O Hydrogen bonds in protein-ligand complexes. *Scientific Reports*, **9(1)**, 1–5.

Jia, S., Shen, M., Zhang, F., & Xie, J. (2017). Recent Advances in *Momordica charantia* : Functional Components and Biological Activities. *International Journal of Molecular Sciences*, **18(2555)**, 1–25.

Kamatou, G. P. P., & Viljoen, A. M. (2017). Comparison of fatty acid methyl esters of palm and palmist oils determined by GCxGC–ToF–MS and GC–MS/FID. *South African Journal of Botany*, **112**, 483–488.

Komakech, R. (2018), Herbs & People. *Momordica charantia:* A unique anti-diabetic plant. *Southworld: Culture,* August 2018. Accessed on 19 September 2020. Available from: https://www.southworld.net/herbs-people-momordica-charantia-a-unique-anti-diabetic-plant/

Korotchenko, V. N., Saydmohammed, M., Vollmer, L. L., Bakan, A., Sheetz, K., Debiec, K. T., & Tsang, M. (2014). In Vivo Structure-Activity Relationship Studies Support Allosteric Targeting of a Dual Specificity Phosphatase. *ChemBioChem*, **15(10)**, 1436–1445

Kumar, K. P. S., & Bhowmik, D. (2010). Traditional medicinal uses and therapeutic benefits of *Momordica charantia Linn*. *International Journal of Pharmaceutical Sciences Review and Research*, ***4*(3)**, 23–28.

Lampman, G., Pavia, D. L., Kriz, G. S., & Vyvyan, J. (2010). Spectroscopy. *Brooks/Cole Cengage Learning***, International edn.**, 15–198.

Latif, S., & Anwar, F. (2011). Aqueous enzymatic sesame oil and protein extraction. *Food Chemistry*, **125(2)**, 679–684.

Li, Y. H., Zhang, B., Yang, H. K., Li, Q., Diao, P. C., You, W. W., & Zhao, P.-L. (2017). Design, synthesis, and biological evaluation of novel alkylsulfanyl-1,2,4-triazoles as cis-restricted combretastatin A-4 analogues. *European Journal of Medicinal Chemistry*, **123**, 1098–1106

Liu, S., Hu, H., & Pedersen, L. G. (2010a). Steric, Quantum, and Electrostatic Effects on SN2 Reaction Barriers in Gas Phase. *Journal of Physical Chemistry A*, **114(18)**, 5913–5918.

Metcalfe, L. D., & Schmitz, A. A. (1961). The rapid preparation of fatty acid esters for gas chromatographic analysis. *Amour Industrial Chemical Co*. **33(3)**, 363–364.

Ministry of Health Malaysia (MoHM). (2015). CPG Management of Dengue Infection In Adults (Third Edition) *2015*. **3rd ed.** *Malaysia Health Technology Assessment Section (MaHTAS)*.

Muniglia, L., Girardin, M., Piffaut, B., & Ricochon, G. (2011). Enzyme method of extracting oils and proteins from vegetable matter in an aqueous medium. *Institut National De La Propriété Industrielle*, 1–18.

Naidu, D. S., Hlangothi, S. P., & John, M. J. (2018). Bio-based products from xylan: A review. *Carbohydrate Polymers*, **179(September 2017)**, 28–41.

Nill, J., Karuna, N., & Jeoh, T. (2018). The impact of kinetic parameters on cellulose hydrolysis rates. *Process Biochemistry*, **74**, 108–117.

Noble, C. G., Seh, C. C., Chao, A. T., & Shi, P. Y. (2012). Ligand-Bound Structures of the Dengue Virus Protease Reveal the Active Conformation. *Journal of Virology*, **86(1)**, 438–446.

Omokhua-Uyi, A. G., & Van Staden, J. (2020). Phytomedicinal relevance of South African *Cucurbitaceae* species and their safety assessment: A review. *Journal of Ethnopharmacology*, **259**, 112967.

Ong, H. C., & Azliza, M. A. (2015). Medicinal Plants for Diabetes by the Orang Asli in Selangor, Malaysia. *Ethano Medicine*, **9(1)**, 77–84.

Perera, S. D., Jayawardena, U. A., & Jayasinghe, C. D. (2018). Potential Use of *Euphorbia hirta* for Dengue: A Systematic Review of Scientific Evidence. *Journal of Tropical Medicine*, **2018**, 1–7.

Rajapakse, S., Rodrigo, C., & Rajapakse, A. (2012). Treatment of dengue fever. *Infection and Drug Resistance*, **5(1)**, 103–112.

Ricochon, G., & Muniglia, L. (2010). Influence of enzymes on the oil extraction processes in aqueous media. *OCL - Oleagineux Corps Gras Lipides*, **17(6)**, 356–359.

Segato, F., Damásio, A. R. L., de Lucas, R. C., Squina, F. M., & Prade, R. A. (2014). Genomics Review of Holocellulose Deconstruction by Aspergilli. *Microbiology and Molecular Biology Reviews*, **78(4)**, 588–613.

Sheat, A. M., Hussein, M. S., & Abood, S. A. (2018). Synthesis and Characterization of Some Spiro Pyrrolidine Compounds. *International Journal of Recent Research and Review*, **10(3)**, 41–47.

Suppiah, J., Ching, S. M., Amin-Nordin, S., Mat-Nor, L. A., Ahmad-Najimudin, N. A., Low, G. K. K., Abdul-Wahid, M. Z., Thayan, R., & Chee, H. Y. (2018). Clinical manifestations of dengue in relation to dengue serotype and genotype in Malaysia: A retrospective observational study. *PLoS Neglected Tropical Diseases*, **12(9)**.

Tan, S. C. (2014). Alternative treatments for dengue fever. *The Star* [Online]. Accessed on 17 September 2019. Available from: https://www.thestar.com.my/lifestyle/health/2014/04/13/alternative-treatments-for-dengue-fever

Truong, D. H., Nguyen, D. H., Ta, N. T. A., Bui, A. V., Do, T. H., & Nguyen, H. C. (2019). Evaluation of the use of different solvents for phytochemical constituents, antioxidants, and in vitro anti-inflammatory activities of *severinia buxifolia*. *Journal of Food Quality*, **2019**, 1–9.

Welker, C. M., Balasubramanian, V. K., Petti, C., Rai, K. M., De Bolt, S., & Mendu, V. (2015). Engineering plant biomass lignin content and composition for biofuels and bioproducts. *Energies*, **8**, 7654–7676.

Wichapong, K., Pianwanit, S., Sippl, W., & Kokpol, S. (2010). Homology modeling and molecular dynamics simulations of Dengue virus NS2B/NS3 protease: Insight into molecular interaction. *Journal of Molecular Recognition*, **23(3)**, 283–300.

World Health Organization (WHO). (2017). Updated Questions and Answers related to information presented in the Sanofi Pasteur press release on 30 November 2017 with regards to the dengue vaccine Dengvaxia® Immunization, Vaccines and Biologicals. Accessed on 2nd September 2020. Available from: https://www.who.int/immunization/diseases/dengue/q_and_a_dengue_vaccine_dengvaxia/en/

World Health Organization (WHO). (2019). Dengue and severe dengue [online]. Accessed on 15 September 2019. Available from: https://www.who.int/news-room/fact-sheets/detail/dengue-and-severe-dengue.

Wu, C., Xiao, Y., Lin, W., Li, J., Zhang, S., Zhu, J., & Rong, J. (2017). Aqueous enzymatic process for cell wall degradation and lipid extraction from *Nannochloropsis sp*. *Bioresource Technology*, **223**, 312–316.

Yin, Z., Patel, S. J., Wang, W. L., Chan, W. L., Ranga Rao, K. R., Wang, G., Ngew, X., Patel, V., Beer, D., Knox, J. E., Ma, N. L., Ehrhardt, C., Lim, S. P., Vasudevan, S. G., & Keller, T. H. (2006). Peptide inhibitors of dengue virus NS3 protease. Part 2: SAR study of tetrapeptide aldehyde inhibitors. *Bioorganic and Medicinal Chemistry Letters*, **16(1)**, 40–43.

Yusof, R., Clum, S., Wetzel, M., & Murthy, H. (2000). Purified NS2B/NS3 Serine Protease of Dengue Virus Type 2 Exhibits Cofactor NS2B Dependence for Cleavage of Substrates with Dibasic Amino Acids in Vitro. *Journal of Biological Chemistry*, **275(14)**, 9963–9969.

Zhao, J., Dong, Z., Li, J., Chen, L., Bai, Y., Jia, Y, & Shao, T. (2018). Ensiling as pretreatment of rice straw: The effect of hemicellulase and *Lactobacillus plantarum* on hemicellulose degradation and cellulose conversion. *Bioresource Tech*nology, **266**, 158–165.

Zhao, R., & Zhang, R. Q. (2016). A new insight into π-π Stacking involving remarkable orbital interactions. *Physical Chemistry Chemical Physics*, **18(36)**, 25452–25457.

Zuorro, A., Malavasi, V., Cao, G., & Lavecchia, R. (2018). Use of cell wall degrading enzymes to improve the recovery of lipids from *Chlorella sorokiniana*. *Chemical Engineering Journal*, **377(November 2018)**, 1–7.

RÉSUMÉ

Il n'existe pas de thérapies curatives ou préventives de la dengue (DF). Seuls des soins médicaux complémentaires et une thérapie par les fluides sont disponibles pour lutter contre la dengue. Certains patients optent pour des mesures de prévention et de traitement utilisées par les peuples anciens ou des remèdes populaires pour traiter la maladie. L'un des remèdes populaires utilisés par les patients atteints de dengue à l'hôpital de Malaisie est la consommation de soupe de viande de grenouille au melon amer (*Momordica charantia*). La chair des fruits et les graines du *Momordica charantia* (*M. charantia*) ont été utilisées dans cette étude. L'huile des graines de *M. charantia* a été extraite par extraction enzymatique aqueuse (AEE) et le rendement en huile a augmenté avec la condition optimale pour extraire l'huile de graines était d'utiliser HEL1:X7 (5:1.25). L'huile de graines ainsi que la teneur en lignine, hémicelullose, sucres solubles et acides uroniques étaient différentes selon le type de cocktail enzymatique. D'autre part, l'extrait d'acétate d'éthyle de la chair du fruit de *M. charantia* a inhibé 38.11±1.06 % de la DENV-2 protéase NS2B/NS3. Sur la base de l'analyse GC-MS, on a trouvé la trace d'acide gallique et on a sélectionné les cadres structurels de base pour la synthèse de l'inhibiteur de protéase DENV-2 NS2B/NS3. Les dérivés de l'indanone substituée par le pyrazolyle, **90a-t**, ont été synthétisés et caractérisés par analyse FTIR, RMN et LC-MS. Un pourcentage approprié de rendement des composés a été obtenu. Les composés **90a-t** ont été soumis à une étude in silico en utilisant AutoDock4.2 pour identifier le mode de liaison et la conformation avec la structure cristalline de la protéine d'homologie de Wichapong. Cinq composés ont obtenu une énergie libre de liaison (FEB) inférieure à -7.55 kcal/mol. Le composé **90p** a montré huit interactions de liaison hydrogène, une interaction d'empilement π-π, et une interaction π-alkyle avec le résidu d'acide aminé dans la DENV-2protéase NS2B/NS3. Enfin, les études in vitro des cinq principaux composés synthétisés par ancrage vers la DENV-2 protéase NS2B/NS3 en utilisant le substrat peptidique fluorogène Boc-Gly-Arg-7-amino-4-méthylcoumarine ont été menées. La panduratine A a été utilisée comme témoin positif. Le composé **90p** a montré une forte activité d'inhibiteur de la DENV-2 protéase NS2B/NS3 (65.61±0.98 %), tandis que la panduratine A (47.59±1.03 %) et l'acide gallique (25.11±1.11 %) ont été utilisés comme témoins positifs. La valeur de la CI_{50} pour le composé **90p** a été observée à 78.87 µM, ce qui est inférieur à la valeur de 290.27 µM pour la panduratine A. Le composé **90p** est considéré comme un puissant composé de type "hit-to-led" dans le développement de l'inhibiteur de DENV-2 protéase NS2B/NS3.

Mots clés: *Momordica charantia*, dérivés de l'indanone substituée par le pyrazolyle, l'inhibiteur de protéase DENV-2 NS2B/NS3

ABSTRACT

There are neither curative nor preventive therapies of dengue fever (DF). Only supplemental medical care and fluid therapy are available to fight DF. Some patients opt for prevention and treatment measure used by the ancient people or folk remedy to treat sickness. One of folk remedy used among patients with dengue fever in the Malaysia hospital is consumption of frog meat soup with bitter melon (*Momordica charantia*). The fruits flesh and seeds of *Momordica charantia* (*M. charantia)* were utilized in this study. The oil of *M. charantia* seeds were extracted via aqueous enzymatic extraction (AEE) and the oil yield increased with optimum condition to extract the seed oil was to use HEL1:X7 (5:1.25). The seeds oil as well as the lignin, hemicelullose, soluble sugars, and uronic acids content were different accordance to the type of enzyme cocktail ratio. On the other hand, the *M. charantia* fruits flesh ethyl acetate extract was found to inhibit 38.11 ± 1.06 % of the DENV-2 NS2B/NS3 protease. Based on the GC-MS analysis the trace of gallic acid was found and was selected the basic structural frameworks for synthesis of the DENV-2 NS2B/NS3 protease inhibitor. The pyrazolyl substituted indanone derivatives, **90a-t** were synthesized and characterized using FTIR, NMR, and LC-MS analysis. An appropriate percentage of yield of the compounds were obtained. The compounds **90a-t** underwent *in silico* study using AutoDock4.2 to identify the binding mode and conformation with the Wichapong homology protein crystal structure. Five compounds were found to obtained free energy of binding (FEB) less than -7.55 kcal/mol. Compound **90p** showed eight hydrogen bond interactions, one π-π stacking interaction, and one π-alkyl interaction with the amino acid residue in the DENV-2 NS2B/NS3 protease. Lastly, the *in vitro* studies of top five docked compoundtowards DENV-2 NS2B/NS3 protease by using fluorogenic peptide substrate Boc-Gly-Arg-7-amino-4-methylcoumarin were conducted. The panduratin A was used as the positive control. Compound **90p** showed a high DENV-2 NS2B/NS3 protease inhibitor activity (65.61 ± 0.98 %), while panduratin A (47.59 ± 1.03 %), and gallic acid (25.11 ± 1.11 %). The IC_{50} value for compound **90p** was observed to be 78.87 µM which is lower compared to the panduratin A, 290.27 µM. The compound **90p** is concluded to be a potent hit-to-led compound in the development of DENV-2 NS2B/NS3 protease inhibitor.

Keywords: *Momordica charantia*, pyrazolyl substituted indanone derivatives, DENV-2 NS2B/NS3 protease inhibitor